Charles University in Prague

First Faculty of Medicine

Study program: Biomedicine

Study field: Biochemistry and Pathobiochemistry

UNIVERZITA KARLOVA
1. lékařská fakulta

Mgr. Jitka Rybová

Patobiochemie lysosomálních střádavých onemocnění: studie Fabryho nemoci a příprava buněčných modelů X-vázaných chorob

Pathobiochemistry of lysosomal storage disorders: study of Fabry disease and generation of cellular models of X-linked disorders

Ph.D. Thesis

Supervisor: RNDr. Jana Ledvinová, CSc.

Consultant: RNDr. Robert Dobrovolný, PhD.

Prague, 2018

Prohlášení:

Prohlašuji, že jsem závěrečnou práci zpracovala samostatně a že jsem řádně uvedla a citovala všechny použité prameny a literaturu. Současně prohlašuji, že práce nebyla použita k získání jiného nebo stejného titulu.

Souhlasím s trvalým uložením elektronické verze mé práce v databázi systému meziuniverzitního projektu Theses.cz za účelem soustavné kontroly podobnosti kvalifikačních prací.

V Praze, 14.6.2018

JITKA RYBOVÁ

Podpis:

Identifikační záznam:

RYBOVÁ, Jitka. Patobiochemie lysosomálních střádavých onemocnění: studie Fabryho nemoci a příprava buněčných modelů X-vázaných chorob [Pathobiochemistry of lysosomal storage disorders: Study of Fabry disease and generation of cellular model of X-linked disorders]. Praha, 2018. 160 s., 6 příl. Dizertační práce (PhD.). Univerzita Karlova, 1. lékařská fakulta, Klinika dětského a dorostového lékařství. Vedoucí práce Ledvinová, Jana

Klíčová slova:

Lysosomální střádavá onemocnění, glykosfingolipidy, Fabryho choroba, mukololysacharidosa typu II, indukované pluripotentní kmenové buňky, diferenciace, inaktivace X chromosomu, neurální buňky.

Key words

Lysosomal storage disorders, glycosphingolipids, Fabry disease, mucopolysaccharidosis type II, induced pluripotent stem cells, differentiation, X chromosome inactivation, neural cells.

Acknowledgment

RNDr. Jana Ledvinová, CSc. my supervisor, for her excellent scientific competence, support and advises throughout this work and the years of my postgraduate studies.

RNDr. Ladislav Kuchař, Ph.D., RNDr. Befekadu Asfaw, Ph.D., RNDr. Robert Dobrovolný, Ph.D., Jakub Sikora, M.D., Ph.D., Ing. Helena Poupětová and Ing. Linda Berná, Ph.D. for their excellent scientific competence, for useful practical advices and interest in my work.

All people at the Research Unit for Rare Diseases for creating a pleasant and friendly working atmosphere, for their help and interest in my research.

I would like to dedicate this work to my family and friends, especially to my boyfriend Jirka, for continuous support, love and understanding during my postgraduate studies.

This work was supported by Charles University Grant Agency (GAUK56214) from Charles University, Prague, Czech Republic, research grant of Medical Research Agency of The Czech Republic AZV ČR 15-33297A, Grant IGA MZ NT14015-3/2013, project RVO-VFN64165 from the Ministry of Health, project PRVOUK-P24/LF1/3 from the Ministry of Education and by Grant SVV 266 504 from the Charles University in Prague.

Abstrakt

Lidské autoptické či bioptické vzorky tkání, myší modely a buněčné kultury různých typů představují nejčastější materiál při zkoumání buněčné patogeneze dědičných chorob. Tato dizertační práce je věnována všem uvedeným přístupům při studiu dvou X-vázaných lysosomálních onemocnění a to Fabryho choroby (FD, deficit α-galaktosidasy A, AGAL) a mukopolysacharidosy typu II (MPSII, deficit iduronát-2-sulfatasy, IDS).

Prvotním cílem práce byla analýza krevních lipidních B-antigenů s terminální α-galaktózou (B-GSL) v pankreatu pacientů s FD a krevní skupinou B (FD-B). B-GSLs představují vedle hlavního glykosfingolipidu (GSL), globotriaosylceramidu (Gb3Cer) další minoritní substrát AGAL. Deposita nedegradovaných B-GSL byla prokázána v autoptických vzorcích pankreatu FD-B pacientů a byla zde výrazně vyšší než u ostatních orgánů jako ledviny a plíce, kde se primárně ukládá Gb3Cer. Vysoká koncentrace lipidních i nelipidních B-antigenů byla u FD-B potvrzena především v exokrinních acinárních epiteliálních buňkách, doprovázená masivní akumulací ceroidu (sekundární znak lysosomálního střádání). Endokrinní část pankreatu zůstala na rozdíl od acinů zcela nepostižena ukládáním substrátů AGAL. Tento zajímavý fenomén buněčné biologie ukazuje, jak může specifická krevní skupina ovlivnit projevy nemoci v orgánech pacientů. Jelikož ledviny představují u FD jeden z nejpostiženějších orgánů, byla v další části práce studována distribuce vybraných GSLs a jejich molekulových typů (isoforem) v řezech ledvin u myšího modelu FD. Pomocí zobrazovací hmotnostní spektrometrie (MSI) bylo identifikováno pět isoforem Gb3Cer zvýšených převážně v kůře ledvin s klesajícím trendem směrem k medule. Zvýšená pozitivita Gb3Cer byla dána zejména depozity v kortikálních tubulech. Tyto výsledky byly v souladu s histochemickými nálezy i s výsledky tandemové hmotnostní spektrometrie, ale MSI ukázala navíc další detaily molekulárního složení nedegradovaného Gb3Cer (i některých dalších lipidů).

Využití buněčných kultur získaných od pacientů představuje klasickou cestu studia chorob. Lidské primární kultury však mají omezení nejen v dostupnosti materiálu ale i v nesnadnosti získat buněčné typy relevantní pro chorobu. Tato omezení z velké části odstraňují indukované pluripotentní kmenové buňky (iPSC). Představují nový směr zkoumání buněčné patologie a patobiochemie dědičných chorob v průběhu časného vývoje a platformu pro testování terapeutických intervencí. Našim důležitým cílem proto bylo vytvoření iPSC linií vybraných lysosomálních chorob, které budou sloužit jako základ pro diferenciaci do vybraných, střádáním postižených, buněčných typů. V rámci této práce byly založeny iPSC linie FD (FD-iPSC) a MPSII (MPSII-iPSC).

Doposud jsou známy dva stavy iPSC lišící se zejména inaktivací X chromosomu (XCI) v samičích buňkách, označované jako primed (buňky po reprogramování s inaktivací jednoho z chromosomů X) a naïve (odvozené od primed iPSC, s oběma aktivními chromosomy). Změna kultivačního media u FD-iPSC a MPSII-iPSC , vedoucí k přechodu primed iPSC do jejich naïve stavu, vedla ke změně morfologie iPSC kolonií u obou nemocí, ale ke změně poměru XCI pouze u FD-iPSC klonu. Vzhledem k tomu že u MPS II dochází také k postižení CNS, byly připravené MPSII-iPSC linie následně diferencovány do směsi neurálních buněk.

Byla potvrzena zvýšená exprese lysosomálních markerů převážně v gliových buňkách a přítomnost abnormálních struktur bez ohraničující membrány. Akumulace glykosaminoglykanů (GAG) byla potvrzena ve směsi terminálně diferencovaných pacientských neurálních buněk. Přídavek rekombinantní IDS v kultivačním mediu měl pouze mírný preventivní efekt. Přetrvávající akumulace GAG je pravděpodobně dána jejich přítomností na plasmatické membráně, kde nemohou být degradovány rekombinantní IDS plně aktivované jen v kyselém prostředí lysosomů.

FD-iPSC linie byly diferencovány do spontánně bijících klastrů kardiomyocytů (CM). Důvodem k jejich přípravě jsou časté kardiomyopatie u pacientů s FD. U FD-CM byla detekována zvýšená koncentrace Gb3Cer i méně početná a dezorganizovaná fibrilární vlákna. Úspěšná internalizace komerčně dostupné rekombinantní AGAL byla potvrzena kolokalizací s lysosomálním markerem Cathepsinem D. Funkční CM budou dále používány k testování terapeutických postupů, např. pomocí farmakologických chaperonů. Dále jsme se zabývali otázkou, zda se na degradaci substrátů AGAL může podílet strukturně příbuzný enzym α-N-acetylgalaktosaminidasa (NAGA), jak upozorňovaly dřívější práce na kožních fibroblastech u FD. Naše metabolické experimenty s radioaktivními substráty na lidských buněčných iPSC modelech s vyřazeným genem pro AGAL, NAGA i obou genů zároveň, však spíše naznačují přítomnost jiné α-galaktosidasy účastnící se degradace B-GSL.

Abstract

Human autopsy or biopsy tissue samples, mouse models and cell cultures of various types represent the most common materials in the investigation of cell pathogenesis of inherited diseases. This dissertation is devoted to all these approaches in the study of two X-linked lysosomal storage diseases, Fabry disease (FD,α-galactosidase A (AGAL) deficiency) and mucopolysaccharidosis type II (MPSII, idunorate-2-sulfatase (IDS) deficiency).

The primary goal of the work was analysis of lipid blood group B antigens with terminal α-galactose (B-GSL) in the pancreas of FD patients with blood group B (FD-B).,In addition to the main glycosphingolipid (GSL) substrate, globotriaosylceramide (Gb3Cer), B-GSLs represent another minor substrate of AGAL. The deposition of undegraded B-GSL has been demonstrated in FD-B pancreas where it was significantly higher than in other organs such as the kidneys and lungs which accumulate mainly Gb3Cer. High concentration of lipid and non-lipid B-antigens was primarily confirmed in exocrine acinar epithelial cells of FD-B, accompanied by massive accumulation of ceroid (secondary sign of lysosomal storage). Unlike acini, the endocrine portion of the pancreas remained unaffected by accumulation of AGAL substrates. This interesting phenomenon of cell biology shows how a specific blood group can influence organ manifestations in patients. Since the kidneys represent the most affected organ in FD, distribution of selected GSLs and their molecular types (isoforms) was examined in the tissue sections of FD mouse model in the next part of this work. Five increased isoforms of Gb3Cer was identified in renal cortex by mass spectrometry imaging with declining trend towards medulla. Increased positivity of Gb3Cer was mainly due to storage in cortical tubules. These results were consistent with both histochemical findings and tandem mass spectrometry but the MSI showed extra details of molecular composition of undegraded Gb3Cer (or other lipids).

The use of cell cultures derived from patients is the classic pathway for the study of disease phenotype. Human primary cultures, however, have limitations not only in material availability but also in difficulty to obtain cell types relevant to disease. Induced pluripotent stem cells (iPSC) remove a large part of these limitations. They represent a new direction for exploring cellular pathology and pathobiochemistry of inherited diseases during early development and a platform to test therapeutic interventions. Therefore, our important goal was to generate iPSC lines for selected lysosomal diseases that will serve as a basis for differentiation into selected cell types affected by storage. In this work, the iPSC lines of FD (FD-iPSC) and MPSII (MPSII-iPSC) were established.

Two states of iPSCs have been identified so far, varying mainly by X chromosome inactivation (XCI) in female cells, referred to as primed (cells after reprogramming with inactivation of one of the X chromosomes) and naïve (derived from the primed cells with both X-chromosomes active). Change of culture media of FD-iPSC and MPSII-iPSC leading to the transition of primed iPSC to their naïve state, led to the change in the morphology of the iPSC colonies in both diseases, but the change in the XCI ratio was recorded in the FD-iPSC clone, only. Since MPS II also affects the CNS, the generated MPSII-iPSC lines were subsequently differentiated into a mixture of neural cells. Increased expression of lysosomal markers and presence of abnormal structures without limiting membrane were largely proven in glial cells. Glycosaminoglycan (GAG) accumulation was confirmed in a mixture of terminally differentiated patient's neural cells. Addition of recombinant IDS to the culture medium had only a mild preventative effect. The persistence of GAG accumulation is probably due to their increased incidence on the plasma membrane, where they cannot be degraded by recombinant IDS fully activated only in acidic environment of lysosomes.

FD-iPSC lines were differentiated into spontaneously beating clusters of cardiomyocytes (CM). The reason of their preparation are frequent cardiomyopathies in FD patients. Increased concentration of Gb3Cer, less numerous and disorganized fibers were detected in FD-CM. Effective internalization of commercially available recombinant AGAL was confirmed by co-localization with lysosomal marker Cathepsin D. Functional CM will be further used for testing of therapeutic approaches, e.g., by pharmacological chaperones. We have further addressed the question of whether a structurally related enzyme α-N-acetylgalactosaminidase (NAGA) can participate on the degradation of AGAL substrates as suggested by earlier work on dermal fibroblasts in the FD. Our metabolic experiments with radiolabeled AGAL substrates in iPSC based lines with knocked-out genes for AGAL, NAGA or both enzymes, rather indicate the presence of another α-galactosidase involved in B-GSL degradation.

CONTENT

Abbreviations

AGAL	α-galactosidase A
ALP	alkaline phosphatase
ATP	adenosine triphosphate
BBB	blood brain barrier
(B)-GSLs	(blood group B) glycosphingolipids
BMP	bone morphogenetic protein
(b)FGF	(basic) fibroblast growth factor
βTubIII	β-Tubulin III
CDH	dihexosylceramides
CM	cardiomyocytes
CMH	monohexosylceramides
CK	ceramide kinase
C-O(A, B)	controls with blood group O (A, B)
CNPase	2',3'-cyclic-nucleotide 3'-phosphodiesterase
CNS	central nervous system
CRISPR/Cas9	clustered regularly interspaced short palindromic repeats/Cas nuclease 9
C1P	ceramide-1-phosphate
D-KO	double knock out of α-galactosidase A and α-N-acetylgalactosaminidase
DSB	double strand break
EB	embryoid bodies
EGF	epidermal growth factor
ESC	embryonic stem cells
(ESI)-MS/MS	tandem mass analyzer (equipped with electrospray ionization)
ER	endoplasmatic reticulum
ERT	enzyme replacement therapy
FD	Fabry disease
FD_$\mathbf{X}^{\mathbf{mut}}$/Y	male hemizygous patients with Fabry disease

FD_$\mathbf{X}^{mut}$/X	female heterozygous patients with Fabry disease
FD-O(B)	Fabry patient with blood group O(B)
FGF-8	fibroblast growth factor 8
FIA-ESI MS/MS	flow injection/electrospray ionization mass spectrometry
FKO	mouse model of Fabry disease
GAG	glycosaminoglycans
Ga2Cer	digalactosylceramide
Gb3Cer	globotriaosylceramide
Gb4Cer	globotetraosylceramide
GFAP	glial fibrillary acidic protein
HPLC-ESI-MS/MS	high-performance liquid chromatography/electrospray ionization tandem mass spectrometry
HR-MS	high-resolution mass spectrometry
HS	heparan sulfate
ICF	immunocytofluorescence
ICM	inner cell mass
IDS	iduronate-2-sulfatase
IDS_$\mathbf{X}^{mut}$/Y	male hemizygous patients with mucopolysaccharidosis type II
IDS_$\mathbf{X}^{mut}$/X	female heterozygous patients with mucopolysaccharidosis type II
IHC	immunohistochemistry
(i)PSC	(induced) pluripotent stem cells
iPSC-D	spontaneously differentiated iPSC into nonspecific adherent cell types
LAMP1	lysosomal-associated membrane protein 1
LAMP2	lysosomal-associated membrane protein 2
LIF	leukemia inhibitory factor
LSD	lysosomal storage disease
MAP2	microtubule-associated protein 2
mEpiSC	mouse epiblast-derived stem cells
MPS	mucopolysaccharidosis
MS	mass spectrometry
NAGA	α-N-acetylgalactosaminidase

NHSM	naïve human stem cell medium
NPC	neural progenitor cells
OXPHOS	oxidative phosphorylation
PBMC	peripheral blood mononuclear cells
P/S	Penicillin-Streptomycin
SCNT	somatic cell nuclear transfer
SRT	substrate reduction therapy
TALEN	transcription activator-like effector nucleases
TGF	transforming growth factor
TH	tyrosine hydroxylase
XCI	X-chromosome inactivation
Xi	inactivated X chromosome
Xist	X-inactive specific transcript
Xm(p)	maternal (paternal) X chromosome
ZFN	zinc-finger nucleases

1. INTRODUCTION

1.1. Sphingolipids and glycosphingolipids

1.1.1. History

The discovery of sphingolipids is attributed to J.L.W Thudichum, chemist and physician, who in 1884 first isolated and named several lipid compounds such as cerebroside, sphingosine, ceramide, sphigomyelin and cephalin (phosphatidylethanolamine) from human brain.

Since then, glycobiology and sphingolipid biology have gained an attention of investigators in different fields and have become the subject of intense studies elucidating the role of sphingolipids and glycosphingolipids and other glycoconjugates in the structural integrity of the cell membrane, their participation in recognition and signaling events and last but not least, their involvement in pathological processes that are at the basis of certain human diseases (Yamakawa 1996; Wennekes et al 2009). This dissertation work deal with one specific group of rare disorders - lysosomal storage diseases (LSD).

1.1.2. Glycoconjugates

Glycoconjugates constitute a large family of substances containing one or more monosaccharide residues. The major types of glycoconjugates are glycoproteins, glycopeptides, peptidoglycans, proteoglycans, glycolipids and lipopolysaccharides.

1.1.2.1. Proteoglycans and glycosaminoglycans

Proteoglycans consist of a core protein and one or more covalently attached glycosaminoglycans (GAG) chains. GAGs such as dermatan sulfate, keratan sulfate, chondroitin sulfate, heparin, and heparan sulfate (HS) are linear polysaccharides that are formed by disaccharide building blocks consisting of an amino sugar (N-acetylated or sulphated glucosamine or N-acetyl galactosamine) and an uronic acid (glucuronic or iduronic acid) or galactose. On the other hand, hyaluronan does not occur covalently linked to proteoglycans but instead interacts with some proteoglycans non-covalently via hyaluronan-binding motifs. Most proteoglycans contain N- and O- links typically found in glycoproteins. The GAG chains are much larger than other types of glycans and typically contain approximately 80 sugar residues (Perrimon and Bernfield 2001).

The protein part of proteoglycans is synthesized by ribosomes and is translocated into the lumen of the rough endoplasmic reticulum. Glycosylation occurs in the Golgi apparatus in multiple enzymatic steps. Different subtypes of sulfated GAGs are attached to their core proteins by unique linkages. For example the biosynthesis of HS is initiated by a formation of a tetrasaccharide linkage region (Xylosa-Galactosa-Galactosa-Glucosamine) which is then attached to a serine side chain of the core protein as a primer for further polysaccharide chain extension. Virtually all mammalian cells produce proteoglycans which are secreted into extracellular matrix, inserted into plasma membrane, or stored in in secretory granules (Lindahl et al 2015).

1.1.2.2. Glycosphingolipids

Glycosphingolipids (GSL) are a group of complex glycolipids containing at least one monosaccharide residue linked by a glycosidic bond to the primary hydroxyl group of sphingoid (or ceramide) (Chester 1998).

Sphingoids (sphingoid bases, sphingosines) are long-chain aliphatic amino alcohols representing the lipid skeleton to which amide-linked fatty acids are attached to form an acylsphingoid. Primary hydroxyl of sphingoid carries a head-group whose complexity ranges from a simple -H, e.g. in ceramide to highly complex glycoconjugates (gangliosides and other sialyl derivates, blood group sphingolipid antigens, etc.). Number of monosaccharide residues in an oligosaccharide chain is indicated by suffixes such as “diosyl”, “triaosyl”, “tetraosyl” etc.

The basic chemical sphingoid structure is represented by the compound originally called “dihydrosphingosine” [(2S,3R)-2-aminooctadecane-1,3-diol] and its homologes, stereoisomers and hydroxyderivatives. Sphingosine [(E)-sphing-4-enine] is the most common unsaturated sphingoid, with a chain length of 18 carbon atoms (Fig.1). Chain-length homologs are named by the root chemical name of the parent hydrocarbon. Substituents such as hydroxy, oxo, methyl, etc. are referred to by appropriate suffixes that denote the position of each substituent (Chester 1998).

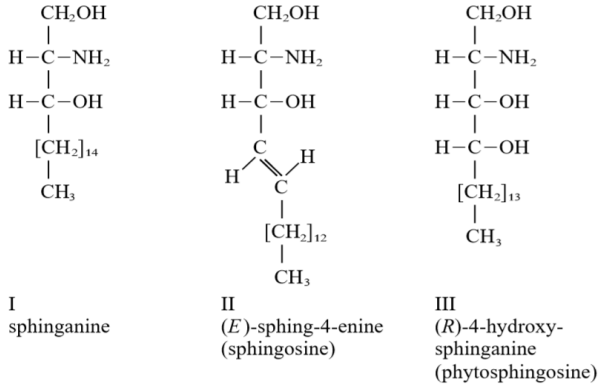

Fig.1: Structural formulas of sphingoid derivatives (Chester 1998).

Ceramides are N-acylated sphingoids. The amide-linked fatty acids of naturally occurring ceramides range in chain length from about C16 to C26. The complete chemical name for a specific ceramide includes the sphingoid and fatty acyl substituent.

GSL are generally divided into two basic groups:

A) Neutral GSL:

- mono-, oligo- and polyglycosylceramides

B) Acid GSL (main groups):

- **sialoglycosphingolipids** (gangliosides, containing one or more sialic acid residues)
- **sulfoglycosphingolipids** (containing one or more carbohydrate-sulfate ester groups)

1.1.2.3. ABO(H) blood group antigens

ABO(H) blood group antigens are complex glycoconjugates composed of carbohydrate chain linked by a glycosidic bond to either the lipid moiety or to the protein backbone. They are widely distributed on erythrocyte membrane but also in body fluids, cells of normal tissues and tumors.

The monosaccharide units in ABH oligosacharides are typically represented by D-galactose, D-glucose, N-acetyl-D-galacto- and -glucosamines, N-acetyl-D-neuraminic acid and L-fucose. These oligosaccharide structures are extremely variable in the chain length, in arrangement of sugar units and may have a dense branching, especially in glycoproteins. ABH active

glycosphingolipids with short carbohydrate chains (5 -10 monosaccharides per molecule) were reported to be present in small quantity in the erythrocyte membranes (about 5% of the total ABH active sites). Polyglycosyl-ceramides which are composed of very complex oligosaccharide structures (megaloglycolipids, up to 60 monosaccharide units), constitute about 20%. Major part of the ABH active determinants is carried by glycoproteins (Schenkel-Brunner 1995).

According to the arrangement of monosaccharides in the chain, they belong to the basic oligosaccharide series defined as lacto, neolacto, globo, muco, isoglobo and ganglio series (Table 1). Specific blood group determinants are formed by three (A or B group) or two (H group) terminal sugar units, one of which is always L-fucose.

Table 1: Series of GSL determined by oligosaccharide chain types.

Series	Symbol	Sugar abbreviation			
		IV	III	II	I
Ganglio-	Gg	Gal(β1→3)	GalNAc(β1→4)	Gal(β1→4)	Glc(β1→Cer)
Lacto-	Lc	Gal(β1→3)	GlcNAc(β1→3)	Gal(β1→4)	Glc(β1→Cer)
Neolacto-	nLc	Gal(β1→4)	GlcNAc(β1→3)	Gal(β1→4)	Glc(β1→Cer)
Globo-	Gb	GalNAc(β1→3)	Gal(α1→4)	Gal(β1→4)	Glc(β1→Cer)
Isoglobo-	iGb	GalNAc(β1→3)	Gal(α1→3)	Gal(β1→4)	Glc(β1→Cer)
Muco-	Mc		Gal(β1→3)	Gal(β1→4)	Glc(β1→Cer)

The H antigen structure is a precursor chain which is synthesized on four main types of oligosaccharide series (Table 1, bold). Type 2 (lacto series) is the major species in erythrocytes glycoproteins and glycolipids. Type 1 is found mostly in milk oligosaccharides and secretory glycoproteins, type 3 in glycoconjugates of epithelial tissues of the gut, lungs and glands. Type 4 is associated preferentially with human kidney. Attachment of L-fucose to β-D-galactose of the precursor chain gives rise to the H-antigen, which, if not further modified, characterizes the blood group O. The A and the B antigens are trisaccharide determinants containing α-N-acetylgalactosamine for the A antigen, and α-D-galactose for the B antigen, both building upon the H antigen. Their synthesis is mediated by α-1,3-N-acetyl-galactosaminyl transferase (A antigen) and α-galactosyl transferase (antigen B) (Fig.2) encoded by corresponding *A* and *B* alleles of *ABO* gene, respectively. This gene is located on chromosome 9q34 (Meloncelli and Lowary 2010; Dean 2012). The inactive *O* allele does not encode any glycosyltransferase and appears to have no function. The biosynthesis of H antigen is controlled by a different gene in locus 19q13.3 (*FUC1* previously known as *H*). The expression of ABH active substances in

secretory tissues and in secretions is controlled by another independent gene (*FUC2* previously known as *Se*) on chromosome 19q13.3 closely linked to the *FUC1* gene.

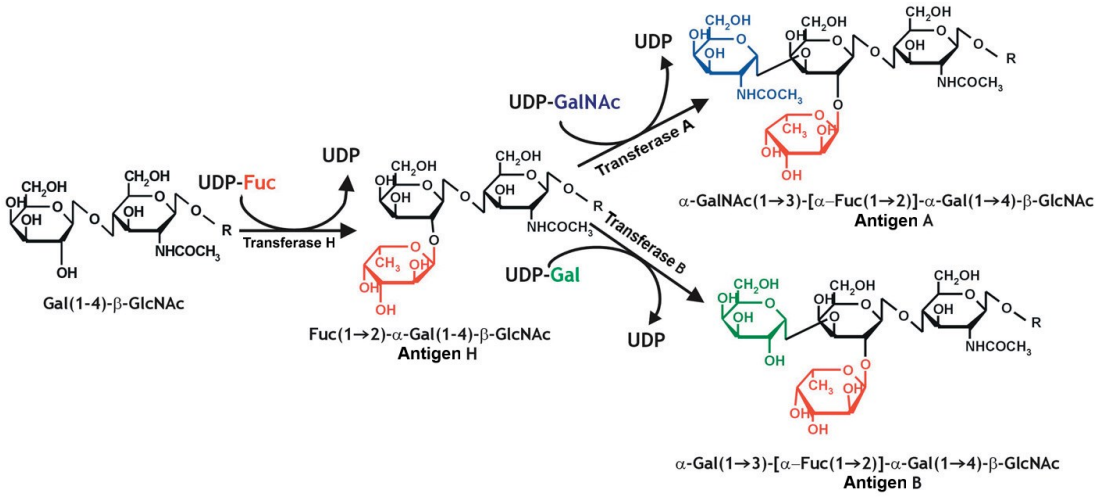

Fig.2: Synthesis of A and B antigens (Smolarek et al 2008).
The biosynthesis starts from the precursor chain type II containing terminal β-galactose on the H antigen. The A and the B antigens are biosynthetized by the attachment of α-N-acetylgalactosamine or D-galactose to the H antigen.

1.1.3. **Chemical a biochemical function of GSL**

GSL are found in all eukaryotes and in some prokaryotes, fungi and viruses as components of membranes and lipoproteins. Their basic function is structural and includes important role in the formation of membrane microdomains (caveolae and rafts) involved in biologically significant cellular processes (Merrill et al 2007).

Biological membranes are mainly composed of phospholipids, sphingolipids, cholesterol, and membrane-associated proteins and serve as a platform for signal transduction, cytoskeletal organization and vesicular trafficking. GSL also cluster to form membrane microdomains (lipid rafts) on plasma membranes. They contain cholesterol and sphingolipids at concentrations up to 50% higher than the rest of the membrane. The lipid rafts are thought to play central role in coordinating key cellular processes such as signal transduction, protein sorting (Gupta and Surolia 2010), intercellular interactions and recognition events (Hakomori and Handa 2002) .

GSL represent various structures depending on the diversity of acyl chains and head group compositions. GSL containing saturated alkyl chains with higher transition temperatures differ from those containing unsaturated chains with a lower transition temperature influencing

membrane fluidity regulation. The transition temperatures of GSL are generally higher than those of other lipids. Long saturated acyl chains enable them to pack together more tightly, which explains why the melting temperatures of sphingolipids are much higher than those of phospholipids (Iwabuchi et al 2010).

Ceramide forms hydrophobic moieties of more complex lipid molecules involved in the formation of micellar and membranous structures (Ulrich-Bott and Wiegandt 1984). Longer fatty acids in ceramides contribute to higher hydrophobicity. Ceramide and related metabolic compounds have been found involved in many cellular events such as induction of programmed cell death or autophagy, phagocytosis or stimulation of DNA synthesis. Saccharide part provides a polar character of the GSL which is increasing with the number of monosaccharide units. Thanks to this saccharide part, GSL are involved in a variety of biological activities including cell adhesion, differentiation, growth processes, initiation of signaling and providing attachment sites for bacteria, viruses and bacterial toxins (Kopitz 2017).

1.1.4. **GSL metabolism**

The endosomal/lysosomal network represents one of the major metabolic regulatory pathways in eukaryotic cells. This includes i) secretory pathway transporting newly synthesized enzymes and other proteins to the lysosomes/endosomes, ii) autophagic pathway delivering intracellular material for lysosomal degradation, and iii) salvage pathway facilitating discharge of lysosomal degradation products to other sites of the cells for reutilization. There are additional mechanisms closely cooperating with these metabolic pathways such as the ubiquitin-proteasome system participating in efficient protein turnover or regulatory network CLEAR (Coordinated Lysosomal Expression and Regulation) which have been shown to be linked at the transcriptional level (Mehta and Winchester 2012).

Biosynthesis of sphingolipids and glycosphingolipids

The amounts and types of complex GSLs are determined by activities of key enzymes in accordance with the relative rate of biosynthesis versus the turnover of the particular molecular type.

De novo biosynthesis begins with condensation of serine and palmitoyl-CoA by serine palmitoyl transferase to form 3-ketosphinganine, which is reduced to sphinganine (dihydrosphingosine), then N-acylated to dihydroceramide and subsequently desaturated to ceramide (Fig.3). In the salvage or recycling pathway, complex GSLs are gradually degraded

by specific exoglycosidases down to ceramide, which is then cleaved by ceramidase. Sphingosine product is mostly re-acylated to ceramide by ceramide synthase (LASS/CerS) (Fig.3) (Novgorodov and Gudz 2011).

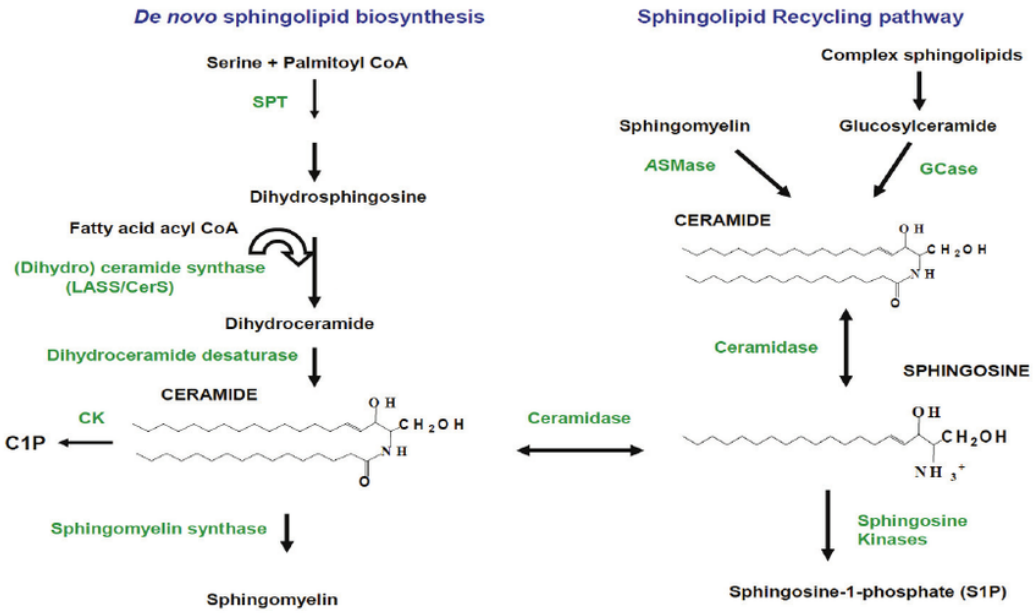

Fig.3: Biosynthesis of ceramide and its conversion into other bioactive sphingolipids (Novgorodov and Gudz 2011).
SPT - serine palmitoyl transferase, CK – ceramide kinase, C1P- ceramide-1-phosphate, ASMase - acid sphingomyelinase, GCase - glucosylceramidase,

Ceramide is precursor of signal molecule ceramide-1-phosphate. Main biosynthetic pathways lead to sphingomyelin and also to glucosylceramide and galactosylceramide which are precursors of more complex sphingolipids (Merrill et al 2007). The subcellular localization of sphingolipids, related metabolic enzymes and transport proteins influence their fate and function. Ceramide is synthetized in the endoplasmatic reticulum (ER) and transported to place of conversion to sphingomyelin via CERT protein transport to both the Golgi and at the plasma membrane. Galactosylceramide is synthesized in the lumen of the ER, whereas glucosylceramide is synthesized on the cytosolic side of the Golgi. For a subsequent step leading to higher-order GSLs, the biosynthesis must be translocated into the Golgi lumen (with participation of FAPP2 and GLTP proteins), where all GSLs are primarily designed for export to the plasma membrane (van Meer et al 2008).

Catabolism of sphingolipids and glycosphingolipids

GSLs of cellular membranes enter the lysosomal compartment by endocytosis, phagocytosis or authophagy and are degraded on the surface of intra-endosomal/intra-lysosomal membrane in a sequential pathway. Monosaccharide units are cleaved off from the non-reducing end of oligosaccharide chain in stepwise manner by specific glycosidases. In case of degradation of saccharide chains of less than four sugars, these enzymes require assistance of small cofactors - activator proteins saposins A-D and GM2 activator. Products of the degradation leave the lysosomes to be processed in different way: either reutilized for the synthesis of more complex molecules, or they are exocytosed or transported to other compartments for further use. In addition to water-soluble hydrolytic enzymes, there are many non-catalytical lysosomal proteins of different functions, e.g. important for intracellular traffic of lipids and cholesterol. NPC1 and 2 proteins are examples of such specific molecules (Kolter and Sandhoff 2010).

1.1.5. **Inherited disorders of sphingolipid catabolism**

When the activities of lysosomal enzymes are impaired, degradation does not proceed normally and undegraded molecules accumulate in the organelle and intracellular membranes. Nowadays, about 50 inherited lysosomal diseases (lysosomal storage disorders - LSD) are known. They are caused by defects in genes encoding lysosomal acid hydrolases, protein activators and/or other lysosomal proteins (Fig.4).

This dissertation is focused on the study of pathobiochemical and biological changes in two of these disorders, Fabry disease and mucopolysaccharidosis type II.

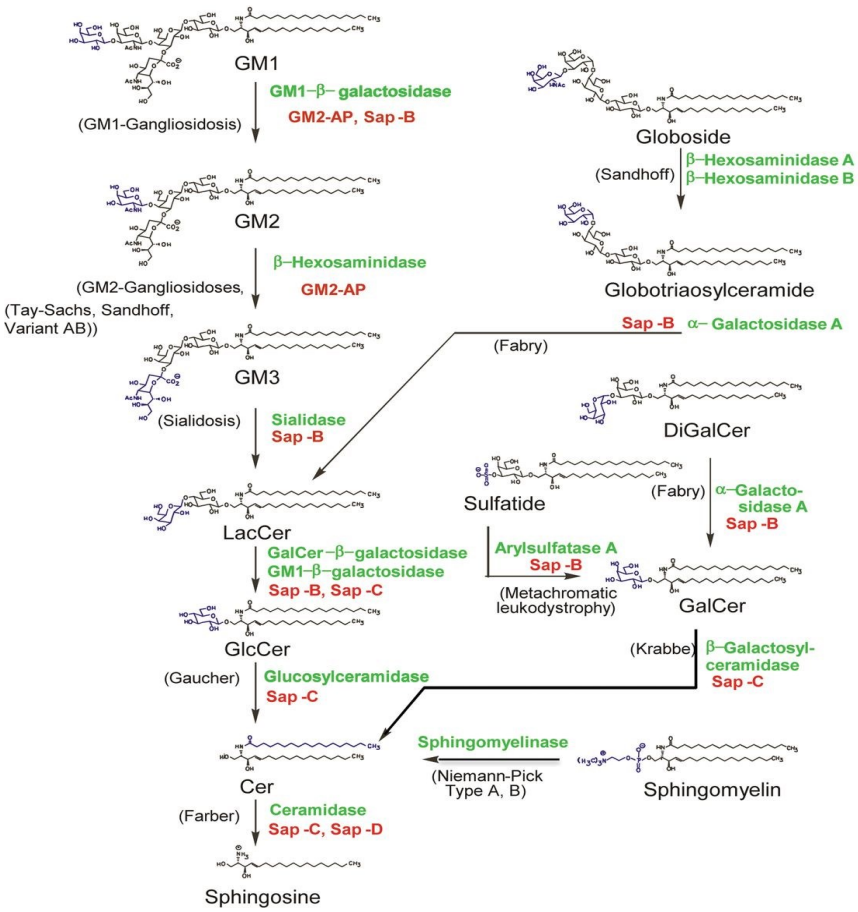

Fig.4: Scheme of lysosomal degradation of selected GSL and enzymes involved in their degradation (Sandhoff 2013).

1.1.5.1. Fabry disease

Fabry disease (FD) is an X-linked recessive lysosomal storage disorder caused by mutations in lysosomal alfa-galactosidase A gene (*GLA*, EC 3.2.1.22). It results in progressive lysosomal accumulation of GSL with terminal alpha-galactosyl moieties, mainly globotriaosylceramide (Gb3Cer), small amount of galabiosylceramide (Ga2Cer) and blood group B GSL substrates in lysosomes of most cells (primarily in endothelial and renal cells, cardiomyocytes and fibroblasts) and body fluids (Fig.5) (Elleder 2010).

Clinical manifestation in classically affected hemizygotes begins in childhood or adolescence and it may exhibit a variety of symptoms, some of which may not be present. They include neurological (pain), cutaneous (angiokeratoma), renal (proteinuria, kidney failure), cardiovascular (cardiomyopathy, arrhythmia), cerebrovascular (ischemic failure, strokes) problems. Heterozygous females may be asymptomatic but they can display symptoms ranging from very mild to severe (Scriver et al 2001).

Confirmation of the clinical diagnosis in hemizygous patients is based on evidence of deficient enzyme activity in plasma, leukocytes, chorionic villi or cultured amniotic cells. Enzyme analysis may occasionally help to detect heterozygous females but due to random X-chromosomal inactivation a mutation analysis of females is mandatory (Scriver et al 2001).

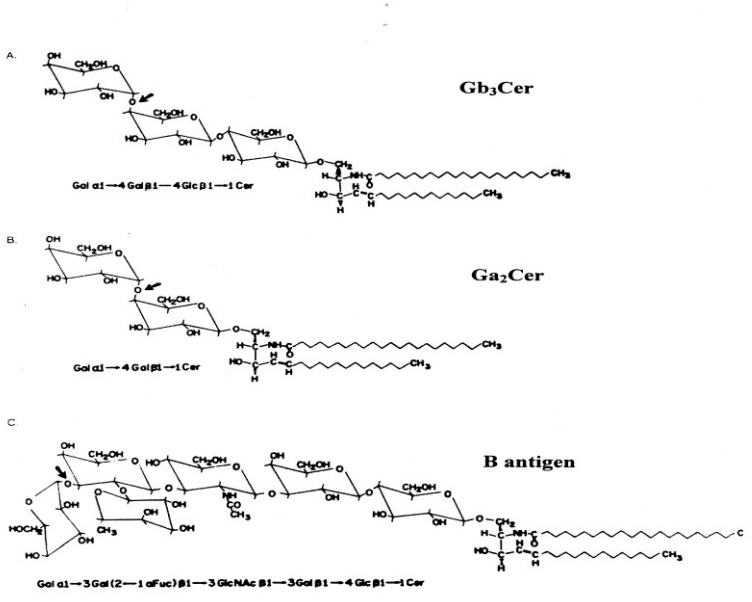

Fig.5: Structures of the main substrates of AGAL (Scriver et al 2001).
The arrow indicates the enzyme cleavage site of AGAL.

1.1.5.2. Mucopolysaccharidosis type II

Mucopolysaccharidosis type II (MPSII, Hunter syndrome) is an X-linked recessive lysosomal storage disorder caused by mutations in the iduronate-2-sulfatase gene (*IDS*, EC 3.1.6.13). The enzymatic defect of IDS leads to an accumulation of two main GAG - dermatan sulfate and heparan sulfate (Fig.6) in tissues throughout the body (Suarez-Guerrero et al 2016).

The Hunter syndrome comprises two recognized clinical entities, mild and severe, but these may represent two ends of a wide spectrum of clinical severity. Severe forms become clinically apparent between 2 and 4 years of age with fatal outcome. Clinical manifestation includes skeletal deformities, hearing loss, airway obstruction, hepatosplenomegaly, cardiomyopathy and progressive neurological impairment. The mild form is with a longer life span and slower progression of somatic deterioration (Scriver et al 2001).

Confirmation of the clinical diagnosis is based on the proof of deficient IDS activity, genetic testing and elevated levels of GAGs in urine samples.

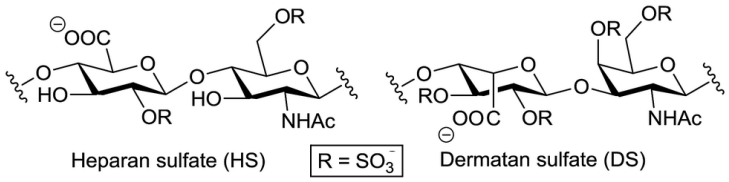

Fig.6: Structure of the repeating disaccharide unit of heparan and dermatan sulfates.

1.1.5.3. Treatment of lysosomal storage disorders

Currently, a number of lysosomal enzymopathies, such as Gaucher and Pompe diseases, FD, MPS type I, II, IV and VI, are treated by FDA (The U.S. Food and Drug Administration) and EMA (European Medicines Agency) - approved enzyme replacement therapies (ERT) which is now a gold standard in the treatment of LSDs.

However, ERT also has some negatives - it requires a weekly or biweekly intravenous infusion of a recombinant enzyme, which is a great burden for the patient. In addition, the large enzyme molecule does not cross blood brain-barrier (BBB) because of its size, and thus treatment is not effective in patients with severe neurological forms. In some patients, the generation of antibodies against enzyme molecule may also complicate the therapy (Ponder 2008).

Another form of the treatment is hematopoietic stem cell and bone marrow transplantation (HSCT / BMT) that allows healthy donor cells to colonize the recipient's deficient bone marrow and provides a constant source of enzyme. The significant benefit is the replacement of neural microglia cells with the healthy cells from the bone marrow precursors after the transplantation. Here too, the efficacy is variable and depends mainly on the progression of the disease (Czechowicz and Weissman 2011).

Consequently, current research is developing new therapeutic approaches geared mainly to gene therapy (Hawkins-Salsbury et al 2011; Macauley 2016). Recombinant viral gene transfer vectors or gene therapy effectively target deficient proteins and enzymes into cells of the affected organs. Long-term gene expression, efficient transduction of disparate cell types, packaging capacity, and low immunogenicity can be achieved not only in the viscera but even in CNS. However, only direct intraventricular, intrathecal, or intraparenchymal injections allow to reach therapeutic levels in CNS though (Macauley 2016). Substrate reduction therapies (SRT) are another approach to LSDs treatment that have achieved success and FDA/EMA approval. Unlike ERT, SRT restores the balance between production and degradation of specific substrates by reducing the total amount of synthesized substrates, and residual

hydolytic activity is then sufficient. Biosynthesis is restricted using small molecules that penetrate the BBB and thus can help to improve CNS function. This approach is actively being studied in preclinical model showing success in Gaucher disease, Fabry disease, Sandhoff disease, Tay Sachs disease, and Niemann-Pick type A/B (Chien et al 2013; Macauley 2016).

As mentioned above, the nervous system is notoriously hard to treat given the presence of the BBB which is an issue of 70% of LSDs. Therefore nanoparticles and other carriers such as the fussion proteins (enzyme – APO proteins) are tested as enzyme transporters. Last but not least, it is chaperon therapy (enzyme enhancement therapy - EET) allowing stabilization of the incorrectly folded proteins with certain amenable mutations and helping to cross quality control check point and express its residual activity in lysosomes. The combination of several treatment methods is another option which is the subject of intensive research (Macauley 2016). However, the above methods cannot yet be considered as optimal.

1.2. iPSC Technology

1.2.1. Classification of cell potency

Stem cells are a type of cells which are unique in two defining capabilities. They are able to self-renew indefinitely as well as they possess potency to give rise to more specialized - differentiated - cells. The most primitive stem cells have the potency to generate all the cell types in an organism but as they divide during embryonic development these cells gradually lose their differentiation potential (Fig.7). Based on this, the stem cells can be divided into following groups:

Totipotent cells

The cells stand at the top of the differentiation potential. They are derived from fertilized egg (zygote/blastomeres) and possess the potential to generate all the embryonic and extra-embryonic cells. Thus, they can give rise to the whole organism (Singh et al 2016).

Pluripotent cells

Pluripotent stem cells (PSCs), descendant of totipotent stem cells, are capable of generating all specialized cells of three germ layers: endoderm, mesoderm, and ectoderm, but lack potential to contribute to the extra-embryonic tissues such as placenta. In humans, this feature is observed only in the blastocyst inner cell mass (ICM) during early embryo development. Identifying the culture conditions required for maintaining of pluripotency led to the derivation of embryonic

stem cells (ESCs) *in vitro* while keeping their self-renewal and differentiation potential. ESCs have opened the door to many novel research applications including modeling normal tissue development *in vitro* or potentially producing suitable cells for regenerative medicine (De Vos et al 2016). However, ESCs have also two main drawbacks: The derivation of human ESC lines is hampered by ethical issues concerning the destruction of human embryos. Moreover, it is exceedingly difficult to derive ESC lines with a specific genotype and almost impossible to obtain an autologous ESC line from a patient to avoid a development of adverse immunological effects after transplantation of the cells or tissues (Kolios and Moodley 2013).

Discovery of induced pluripotent stem cells (iPSCs) seems to have solved these obstacles. The main advantage of iPSC technology is the fact that they are derived from adult specialized cells of the patients who are simultaneously their potential recipients. This avoids ethical issue of acquisition as well as the development of adverse immune-incompatibility effects. However, other problems may arise in connection with reprogramming and cultivation methods. The iPSCs should be reprogrammed without interfering with the host cell genetic material and should be manipulated under xeno-free conditions especially for their application in regenerative medicine (Grabel 2012).

Multipotent cells

Multipotent cells, in contrast with PSCs, have limited differentiation potential. They can be differentiated only within one out of three germ layers they originate from (e.g. neural stem cells that give rise to the cell types of the nervous system: neurons and glial cells). This group includes adult stem cells in the developed organism, where they replenish dying cells and regenerate damaged tissues. Scientific interests in adult stem cells are focused on their ability to help to functionally regenerate the entire organs from few isolated cells (Kolios and Moodley 2013).

Oligopotent / Unipotent cells

The developmental potential of these stem cells is further restricted and they retain ability to give rise to only a very limited or single cell type but they still possess the ability to fully renew themselves. For example, blast forming unit-erythroid which may be differentiated only to erythrocytes (Singh et al 2016).

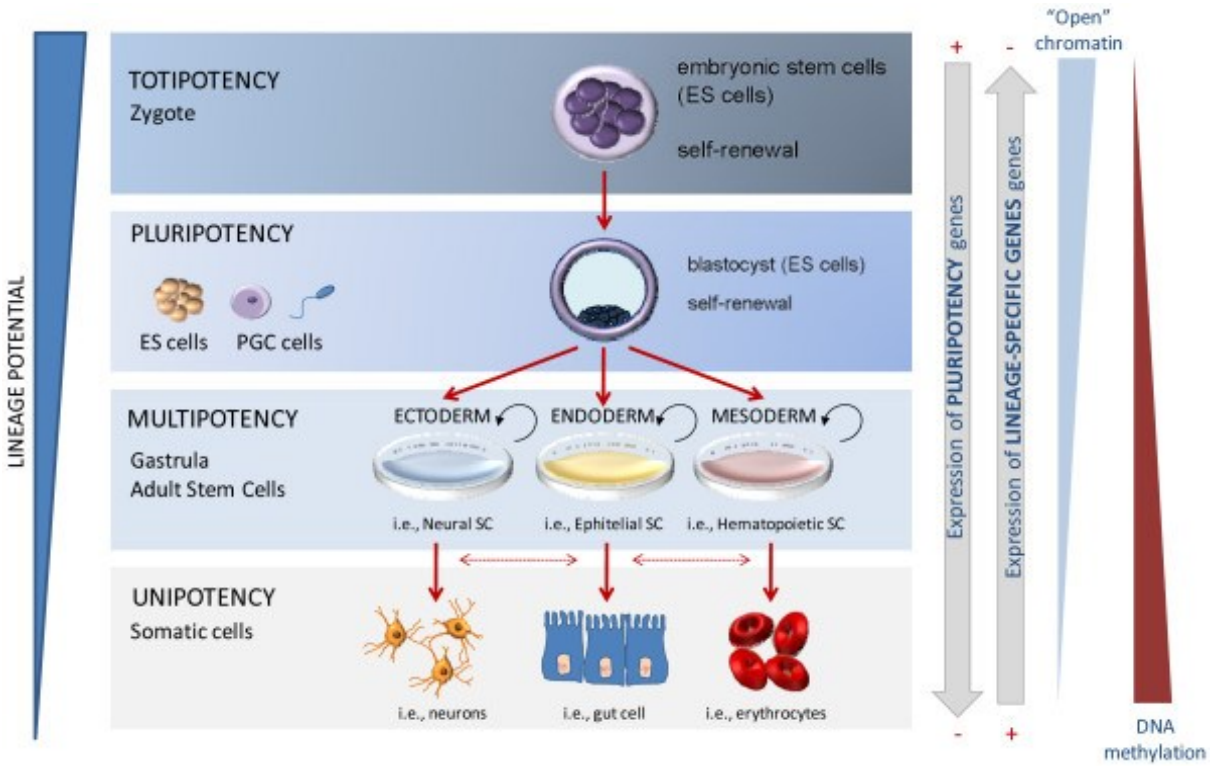

Fig.7: Lineage restriction of human developmental potency (Berdasco and Esteller 2011).
Specific chromatin patterns and epigenetic marks can be observed during human development since they are responsible for controlling transcriptional activation and repression of tissue-specific and pluripotency-related genes, respectively. Global increases of heterochromatin marks and DNA methylation occur during differentiation.

1.2.2. **History of the reprogramming**

The first example of cellular reprogramming was reported by John Gurdon in 1962 during somatic cell nuclear transfer (SCNT): technique in which the nucleus of a somatic cell is transferred to the cytoplasm of an enucleated egg (with nucleus removed) (Gurdon et al 1958). The somatic nucleus is reset by egg cytoplasmic factors and the zygote (fertilized egg) is formed. This zygote can then generate an embryo that is genetically identical to the donor of the somatic cell nucleus. A culture of ESCs can then be established from the inner cell mass of the blastocyst even without complete understanding of nuclear reprograming. SCNT have been used to prepare mouse, monkey and human ESCs with wide potential for applications in medical research.

Martin Evans and Gail Martin introduced the term of ESC for the first time in 1981 when his group established self-renewable cell lines from mouse pre-implantation embryo (Evans and Kaufman 1981; Martin 1981). Around the same time as the first mammalian SCNT efforts appeared, James Thomson derived the first human ESC lines (Thomson et al 1998) possessing and keeping the capacity to generate the cell types of all three germ layers. Practical application

of SCNT have been recorded in the reproductive cloning of animals by implanting an SCNT-derived blastocyst into the uterus of a surrogate mother for development of the embryos into the whole organism. The first mammal animal was sheep Dolly born in 1996 (Wilmut et al 1997).

Due to the ethical and moral issues surrounding the use of ESCs, scientists have searched for ways to reprogram adult somatic cells back to the pluripotent state. In 1983 one group reported that the profile of gene expression in somatic cells can be changed through a fusion with other cell types which leads to their reprogramming (Blau et al 1983). They documented that silenced muscle-specific genes in human amniocytes are activated after cell fusion with muscle cells. Other groups reported that differentiated adult somatic cells grown in culture with ESCs fuse with the stem cells and acquire ESC-like properties and express pluripotency-associated genes. These findings led to the idea that specific genes/reprogramming factors could reprogram differentiated somatic cells. The involvement of reprogramming factors was documented by Davis in 1987 who described conversion of fibroblast to myoblast with a single transcription factor (Davis et al 1987). This process of converting one type of somatic cells into different type of somatic lineages is known as trans-differentiation.

Finally, the works in this area led to the discovery of iPSCs that are (i) derived from somatic cells, (ii) possess self-renewal capacity, (iii) are able to differentiate to all three germ layers and thus are functionally and morphologically similar to ESCs. The pioneers of this technology are Kazutoshi Takahashi and Shinya Yamanaka who in 2006 first described a generation of iPSC from mouse embryonic and adult fibroblast by their reprogramming with retroviral vectors carrying four transcription reprogramming factors (Takahashi and Yamanaka 2006). One year later, two research groups independently reported the generation of iPSC from human fibroblasts (Takahashi et al 2007; Yu et al 2007). Since then, the technology has seen tremendous development in the use of various types of somatic cells as a source material for reprogramming techniques and different combinations of utilized transcription factors. The application of stem cells for drug discovery, disease modeling and regenerative medicine is also in the forefront of interest.

1.2.3. **Mechanism of reprogramming**

Takahashi and Yamanaka selected a minimal set of four main transcription factors (referred to as OSKM or Yamanaka's factors) responsible for reprogramming of mouse and human

fibroblasts among the 24 tested candidates (Takahashi and Yamanaka 2016). They found out that expression of only four genes, encoding Oct3/4, Sox2, Klf4 and c-Myc, reproducibly induced formation of stem cell colonies. The efficiency of this process is quite low and the use of retroviral methods prevent iPSC from being applied in regenerative medicine. Therefore many researchers have attempted to discover alternative methods and new approaches to achieve greater efficiency of the reprogramming and improving iPSC safety.

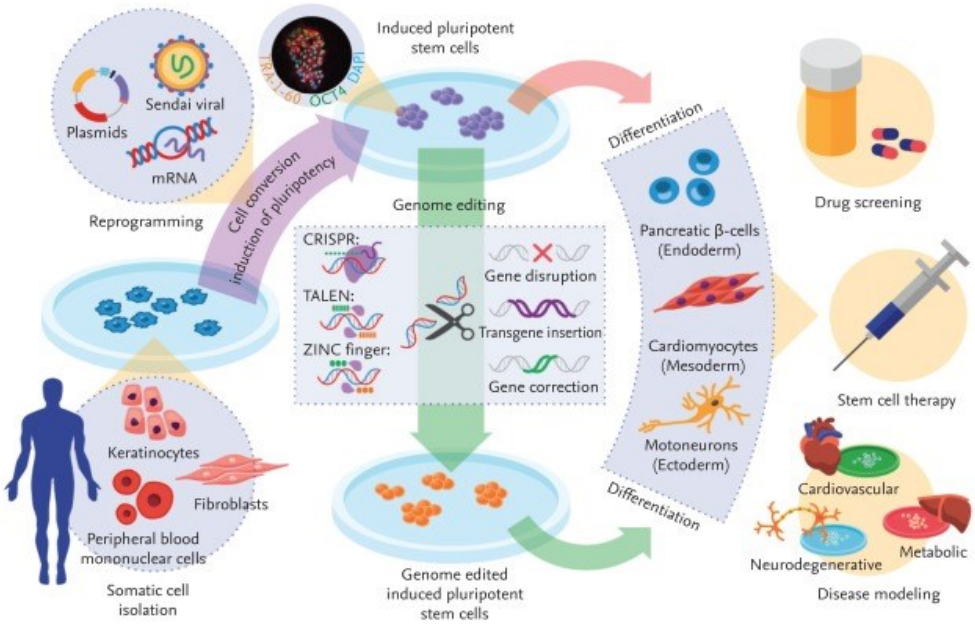

Fig.8: A scheme of iPSC generation and their most common clinical application (Diecke et al 2014). Somatic cells isolated from a patient are reprogramed into iPSC by transduction of reprograming factors. Genetic defects in iPSCs can be corrected (or conversely introduced in heathy iPSC) via gene editing with zinc finger nucleases (ZFNs), activator-like effector nucleases (TALENs), and the clustered regularly interspaced short palindromic repeats (CRISPR) system. Further, stable lines of iPSCs are differentiated into various target cells for disease modeling, drug screening, and stem cell therapy.

1.2.3.1. Reprogramming techniques

The first reprogramming methods were based on retroviral (Takahashi and Yamanaka 2006) or lentiviral vectors (Hotta et al 2009) carrying four genes for reprogramming factors. They integrate into the host genome and thus they are associated with the risk of tumor formation due to the spontaneous reactivation of the viral transgene or aberrant transcriptome due to the integration mutations. Residual transgene expression itself can also influence efficiency of the reprogramming or later differentiation of iPSC into specific lineages.

Therefore, new methods using adenoviral vectors (Stadtfeld et al 2008), plasmids, episomal vectors (Yu et al 2009), Cre/LoxP expressing vectors (Soldner et al 2009) allowing for transient,

high-level expression of exogenous genes without integrated host genome in created stable iPSC lines, have been tested. Although these non-integrating vectors can also successfully generate iPSCs, their main drawback is the relatively low reprogramming efficiency.

Other investigators have tried to move away from genetically based techniques and derived iPSCs using several DNA-free methods. The first reported approach describes the use of recombinant proteins fused with cell-penetrating peptides leading to serial protein transduction (Kim et al 2009; Zhou and Freed 2009). Other reported methods include (i) transgene delivery using RNA-based Sendai virus vector (Fusaki et al 2009), (ii) repeated administration of synthetic messenger RNAs with modifications helping to bypass innate anti-viral responses (Warren et al 2010), (iii) cell permeable and non-immunogenic small chemical compounds or small molecules modulating of the relevant signaling pathways, (iv) chromosomal epigenetic modifications and (v) metabolic processes (Hou et al 2013). Multiple of these protocols are used at this time but the non-integrating ones are preferred for preparing cellular models of inherited disorders or regenerative medicine research.

1.2.3.2. Source of somatic cells for reprogramming

Theoretically, most cells of our body can be used for reprogramming into iPSCs. However, skin fibroblasts, peripheral blood mononuclear cells (PBMC) and urine-derived cells are a “gold standard” so far especially for their relatively good accessibility and less- or non-invasive methods of collection.

1.2.3.3. Characterization of iPSC

iPSCs correspond to the ESC with their morphology, self-renewal capacity, surface and nucleus markers of pluripotency, gene expression, *in vitro* differentiation into all three germ layers, teratoma formation after injection of the cells into immune-deficient mice or their ability to form chimeric organisms after their implantation into developing blastocysts. These characteristics have become the basic methods to evaluate the quality of generated iPSC. The most frequently used methods are based on detection of pluripotency markers such as NANOG, OCT4, SSEA4, LIN28, SOX2 by immunocytofluorescent methods and the ability of iPSC spontaneously differentiate into three germ layers.

1.2.3.4. Epigenetic memory of the iPSC

The so called pluripotency genes in somatic cells are kept in repressed state by chromatin modifications such as DNA methylation of their regulatory regions. During reprogramming, these genes are reactivated and epigenetic repression is removed. Several studies have demonstrated that the iPSC lines still retain background epigenetic memory of source cells which could be limiting factor for the reprogramming and subsequent differentiations.

Analysis of DNA methylation reveals substantial differences between iPSCs and embryo-derived ESCs (Kim et al 2010; Gomes et al 2017) suggesting that low-passage iPSCs conceal residual DNA methylation signatures characteristic of their somatic tissue of origin. The process of effective reprogramming involves a complete remodeling of the existing somatic epigenetic memory. It is also assumed that the residual methylation in generated iPSCs favors their differentiation along lineages related to the donor cell, while restricting alternative cell fates. Demethylation of cytosines in the respective promoter regions is necessary for reactivation of genes and thus inhibition of methylation by enzymes or interfering RNA may be an option to improve the process of reprogramming and thus their self-renew capacity and potency, differentiation and also application in regenerative medicine (Gomes et al 2017).

1.2.3.5. iPSC metabolism

Cellular metabolism is the collection of chemical reactions that capture and release energy from nutrient, break down organic matter and build new substances in order to sustain life and allow the cells to grow, repair damages and respond to environmental changes. It has been demonstrated that cellular metabolism changes during its differentiation (Wu et al 2016). In contrast to somatic cells, PSCs show higher rates of glycolysis and lower levels of mitochondrial metabolism marked by extensive remodeling of the structure and function that appears to be essential for reprogramming and maintenance of pluripotency in iPSCs. Low copy number of mitochondrial DNA, low density of spherical mitochondria without well-developed cristae structures, lower inner mitochondrial membrane potential, all of which is in accordance with down-regulation of their function, are the prominent features of mitochondria in all stem cells (Hsu et al 2016; Wu et al 2016). Further, ESC and iPSCs have low demand for adenosine triphosphate (ATP) synthesis by oxidative phosphorylation (OXPHOS) as well as a strong antioxidant defense system and low level of oxidative stress. During reprogramming of

fibroblasts into iPSCs, the transition from OXPHOS to glycolysis as a major source of ATP has been demonstrated (Varum et al 2011).

1.2.4. *In vitro* disease modeling

The prominent application of the iPSC technology is disease modeling since this technique allows the setting up patient-derived cell lines that carry all genetic variations leading to the particular disease. Especially in case of rare, fatal diseases where biological study material is scarce, iPSCs help to keep the immortal line, produce consistently sufficient amount of material for experiments and obtain disease relevant cell types by their differentiation. Thus, iPSCs provide an experimental *in vitro* system to study pathogenesis of the disease and to possibly develop and test therapeutic strategies (Robinton and Daley 2012). Some of the most remarkable advancements were made in neurodegenerative diseases that are often recapitulated in animal models incompletely.

Trans-differentiation of somatic cells

Trans-differentiation is a process in which one mature somatic cell transforms into another one without undergoing an intermediate pluripotent state and potentially have the same applications as iPSCs in terms of disease modeling, drug discovery and regenerative medicine. Direct reprogramming of somatic cells or trans-differentiation has been developed to directly transform fibroblasts into induced myoblasts (Davis et al 1987; Tapscott et al 1988), neuronal cells (Vierbuchen et al 2010), cardiomyocytes (Ieda et al 2010) and hepatocytes (Huang et al 2011) under the defined conditions or specific factors supplement.

Differentiation of iPSC

Somatic cell formation via the iPSC stage is the leading approach because rapidly dividing iPSC cells serve as an intact cell source for differentiation of multiple cell types of interest without the need for a long-standing reprogramming path during trans-differentiation.

Currently, the major research effort is invested into the development of protocols for the differentiation of iPSCs into cardiomyocytes and neural cells. This is apparently given by the frequent occurrence of cardiovascular (LQT syndrome, diabetic cardiomyopathy, etc.) and neurogenerative (i.e. Alzheimer and Parkinson disease) diseases in population. There have been many attempts to regulate ESC/iPSC differentiation by various factors, including mainly Wnt, activin A, and BMP signaling, which have led to efficient production of cardiomyocytes. On the other hand, the use of retinoic acid with serum-free medium, ascorbic acid, FGF2, epidermal

growth factor (EGF) and neural supplements like B27 or N2 have been shown to play an important role in neural differentiation (Skalova et al 2015).

Disease modeling includes the simultaneous involvement of several cell types. Co-culture experiments of more than one cell type for the study of different cell type interactions, protocols to differentiate PSCs into tissue stem cells and 3D organoid cultures have been made in recent years(Shi et al 2017). Organoids are small functional tissue units comprised of several distinct cell types that can be maintained and used to recapitulate features of tissues rather than that of individual cell types *in vitro* (Sato et al 2011; Lancaster et al 2013). 3D organoids are promising tool for disease modeling enabling the study of disease manifestation and drug testing at the level of an organ. However, limitations of low efficiency and reproducibility compared to traditional 2D cultures still have to be overcome (Shi et al 2017).

1.2.4.1. Genome editing of iPSC

An important issue of iPSC technology is the variability of individual iPSC lines in their ability to differentiate into desired functional cell types. This variation among cell lines is hard to predict and is mostly caused by both genetic background differences and the reprogramming history of a given cell line. Thus, detection of small phenotypic differences between cells differentiated from iPSCs may not reveal a disease-relevant phenotypic difference but rather reflect variation between individual iPSC lines (Hockemeyer and Jaenisch 2016; Shi et al 2017).

Genome editing technologies enable the introduction of genetic changes into iPSCs in a site-specific manner. These are insertion of a specific mutation in healthy control lines or correction of a disease-causing gene mutation in patient-derived iPSCs for generation genetically matched, isogenic iPSC pair. This technology allows to identify an actual pathology connected with the mutation in certain gene without interference by genetic background (Fig10). Genome editing allows to study very rare diseases when it is virtually impossible to obtain patient‘s samples. It is helpful in studies of familial mono-allelic diseases as well as complex idiopathic diseases where phenotypic differences can be very slight. The comparison of pathological state with isogenic control is the most important benefit of these techniques (Hockemeyer and Jaenisch 2016).

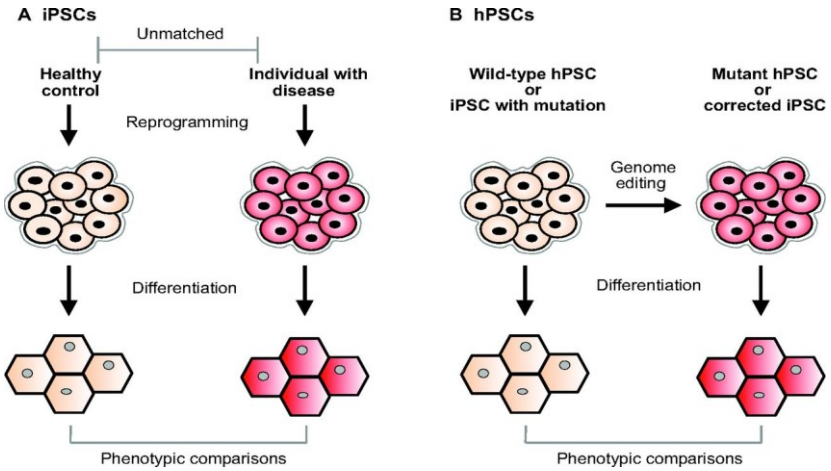

Fig.10: A comparison of two study designs for disease modeling using human pluripotent stem cells (Musunuru 2013).
A) iPSCs are reprogrammed from an individual with the disease and a control individual. The iPSCs are differentiated into a cell type of interest for comparison of relevant phenotypes. (B) hPSCs are modified with genome editing, thereby creating optimally matched cell lines.

Zinc-finger nucleases (ZFN), transcription activator-like effector nucleases (TALEN) and clustered regularly interspaced short palindromic repeats/Cas nuclease 9 (CRISPR/Cas9) system are the three methods used for specific genome editing in human iPSC. They cause DNA double-strand breaks at the desired site of the genome by programmable site-specific nucleases (Carroll 2017). The CRISPR/Cas9 method has come to the fore because of its simplicity in design but appearance of off-target mutations is relatively high. It is using RNA-guided site-specific DNA double strand breaks triggering either non-homologous end joining to create small indels which disrupt the targeted locus or the homology-directed repair pathway allowing for precise sequence modification changes to be made (point mutations, insertions, deletions) (Carroll 2017).

1.2.4.2. Primed and naïve state of iPSC and the study of X-inactivation

Primed and naïve state of iPSCs

Human ESCs (hESCs) were shown to exist in a state of primed pluripotency, while mouse ESCs (mESCs) may display both naïve and primed pluripotent state (Fig.11).Primed mouse epiblast-derived stem cells (mEpiSCs) are establish from the post-implantation epiblast. They are morphologically similar to primed hESCs and iPSCs after reprogramming. These cells display flat, monolayer colony morphology, low single-cell clonogenicity dependence on

TGFb/activing/nodal signaling and show inefficiency to contribute to chimeras (Tesar et al 2007).

Naïve mESCs are derived from the inner cell mass of the preimplantation blastocyst. They show round, dome-shaped cell colony morphology, high single-cell clonogenicity facilitating bulk culture, more homogeneity leading to efficient direct differentiation towards germ layer derivatives, all favoring for future practical applications. They are cultured in serum/leukemia inhibitory factor (LIF) or inhibitors of MEK and GSK3 signaling pathways along with LIF medium (Tesar et al 2007).

Whether naïve state exists in hESCs *in vivo* is unclear but attempts have been made to establish naïve state in cultivated primed iPSC to directly answer this question. Several groups have formulated protocols to induce naïve pluripotency in hESCs/iPSCs mostly by development of special naïve culture media (Gafni et al 2013). These cells show gene expression profiles more closely resembling those of mESCs, but still with certain differences suggesting the role of some epigenetic barriers such as histone modification, DNA methylation and female X-chromosome inactivation (XCI) (Tesar et al 2007).

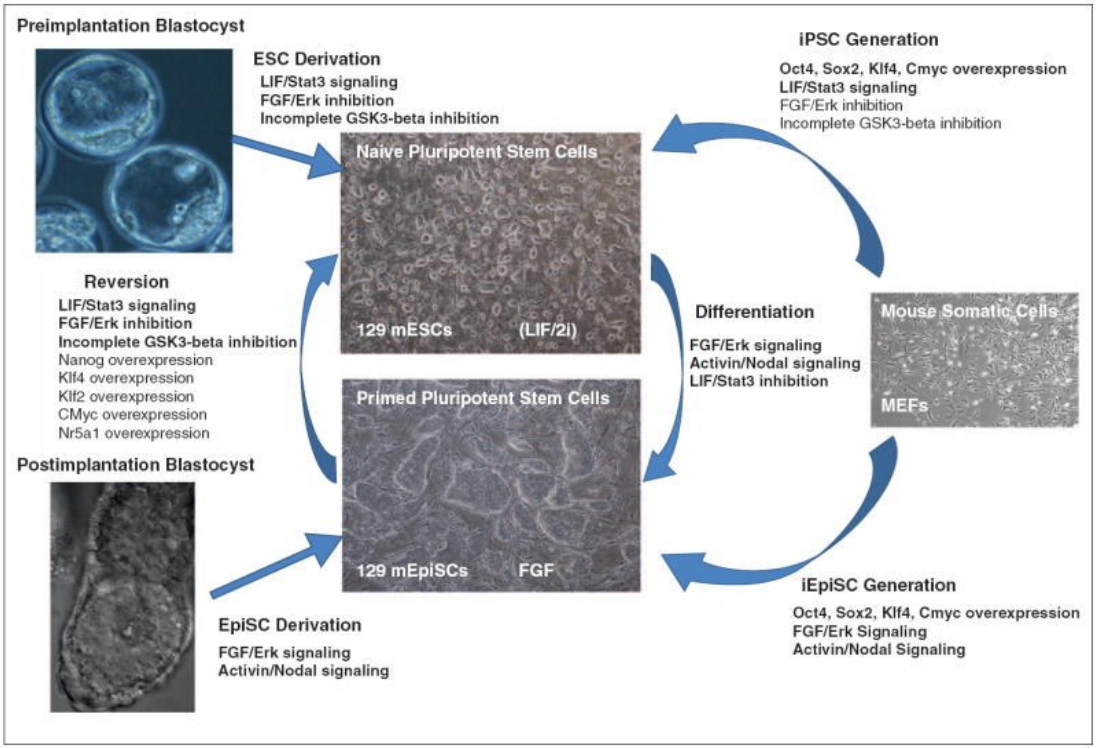

Fig.11: Achievement of mouse naïve pluripotency through three different routes (De Los Angeles et al 2012).

XCI in female iPSCs

Female XCI is established during the early embryogenesis by distinct spatiotemporal regulation. It is a process by which one of the two X chromosomes present in normal female mammalian cells is inactivated and forms a transcriptionally inactive heterochromatin. The particular parental inactivated X chromosome (Xi) retains its inactivation status throughout the lifetime of the cell even after cell divisions.

Mouse cells undergo an early, imprinted inactivation of the paternally-derived X chromosome. During embryogenesis, the extraembryonic tissues (which give rise to the placenta and other tissues supporting the embryo) retain imprinted inactivation of the paternal X chromosome (Xp) which first appears at two-cell to four-cell stage embryos. Only the maternal X chromosome is active in these tissues. The Xp is then reactivated at the blastocyst stage and random XCI occurs, resulting either the maternal X chromosome (Xm) or the Xp being silence (Pinheiro and Heard 2017).

There are four stages associated with XCI, referred to as counting, choosing, initiation, and maintenance. All these stages are mediated by the X-inactivation center, which contains the RNA-encoding X-inactive specific transcript (Xist) locus. Xist RNA is necessary for the initiation of silencing and surrounds the X chromosome selected to be inactivated. Although the exact mechanism involved in counting remains elusive, there is an evidence suggesting that the cell utilizes the ratio between X chromosomes and autosomal chromosome number in order to ensure that only one X chromosome is active. This process is so precise that only one X chromosome is active even in instances where individuals have more than two X chromosomes (e.g. 47, XXX syndrome). Xist forms a "cloud" around the inactivated X chromosome by binding to areas along the length of the chromosome from which Xist is actively transcribed. This results in the loss of RNA polymerase II, initiation factors, and other components necessary for transcription in the areas covered by Xist (Dandulakis et al 2016; Pinheiro and Heard 2017). The chromatin of inactivated chromosome is then modified by CpG methylation and specific histon acetylation and methylation which helps maintaining the XCI status during semiconservative DNA replication.

Some studies suggest that reprogramming of human and mouse somatic cells into iPSCs is accompanied by reactivation of X chromosome in female cells at the very early reprogramming stage (Marchetto et al 2010; Tomoda et al 2012). Later, these cells are subjected to the reverse inactivation of one of the chromosomes during first passages in culture. For mouse fibroblasts, it has been shown that the XCI becomes reactivated during the reprogramming process given

by the presence of H3K27me3 focus and Xist RNA, followed by random XCI upon differentiation of these miPSCs (Maherali et al 2007; Stadtfeld et al 2008). On the other hand, most studies of multiple female human iPSCs/ESCs suggest that the parental origin of inactivated chromosome may be the same as in the original in somatic cell that was reprogrammed (Tchieu et al 2010; Amenduni et al 2011; Ananiev et al 2011). Primed female hPSCs usually feature an inactive X chromosome during following passages of iPSCs, however, a process referred to as erosion was also described which is frequently accompanied by the loss of Xist RNA expression during the later passages of female iPSC cultures (Mekhoubad et al 2012).

Despite intensive research, very little is still known about X chromosome reactivation in human naïve ESCs/iPSCs and thus we focused in this study of XCI state in two female iPSC lines with FD and MPSII.

2. AIMS OF THE STUDY

Autoptic (or bioptic) tissues from patients and tissues from mouse models of certain diseases still represent material of choice for investigation of a wide range of metabolic disorders. Both these sources, however, have some limitations. Examinations of human tissues allow us to study pathogenesis only in the final stages of the disease and availability of appropriate material is very limited. Mouse models - on the other hand, allow monitoring of the disease progression from early stages and testing of various therapeutic possibilities. But, as has been shown multiple times, the mouse model of a particular disease may not reflect its human form entirely, such as in severity of the disease and in various specific phenotypic characteristics.

The technology of induced pluripotent stem cells (iPSC) constitutes modern approach to study rare diseases. The iPSC lines are prepared directly from the patient's cells reflecting the metabolic and genetic basis of the disease. Broad differentiation potential allows studying the disease pathobiochemistry from the initial stage and testing possible therapies targeted to relevant cell types.

This dissertation employs all the above-mentioned sources for monitoring pathological changes in two X-linked lysosomal storage disorders, Fabry disease (FD) and type II mucopolysaccharidosis (MPSII). The design of the study includes following topics:

2.1. Study of human and mouse tissues with biochemical phenotype of FD focused on the nature of storage of undegraded substrates.

2.1.1. Investigation of metabolic fate of glycoconjugates with terminal α-galactosyl moieties in the pancreas of FD patients with blood group B (FD-B):

- Analysis of blood group B antigens and Gb3Cer in the FD pancreas. Comparison of lipid profiles of various tissues (pancreas, kidneys and lungs) in FD patients and controls. Characterization of lysosomal depositions of undegraded substrates in various pancreatic cell types.

2.1.2. Study of renal sphingolipid distribution in the knockout mouse model of FD (FKO):

- Determination of renal sphingolipid profiles in the FKO and WT mouse tissues by MS.
- Distribution of Gb3Cer isoforms in the kidneys of the FKO and WT mice by MS-imaging and by immunohistochemistry.

2.2. Creation of human FD and MPS II cell models using induced pluripotent stem cell technology.

- Generation of stable iPSC lines by reprogramming peripheral blood mononuclear cells of patients with FD, MPSII and of control individuals.

2.2.1. X chromosome inactivation analysis in female patients with FD and MPSII:

- Creation of naïve iPSC from generated primed iPSC of hemizygous patients and analysis of possible X chromosome reactivation during the process.

2.2.2. Neural model of CNS involvement in MPSII:

- Differentiation of MPSII-iPSC and identification of cell types affected by GAG storage.
- Monitoring the efficiency of the recombinant enzyme delivered during neural cell differentiation: ERT testing.

2.2.3. FD cardiomyocytes generated from iPSC as a human model for testing of therapeutic effect of pharmacological chaperones:

- Differentiation of FD-iPSC and description of disease phenotype in FD-CM to assess the suitability of the model for molecular chaperones testing.

2.2.4. CRISPR/Cas9 generation of iPSC models of FD and Schindler disease

- Genome modification in human iPS cells to generate knockout in two lysosomal hydrolases, *GLA* gene, *NAGA* gene and double knockouts of both genes.
- Loading experiments with tritium-labeled glycolipids in spontaneously differentiated control and disease-iPSC to help elucidation of suspected substrate specificity overlap of AGAL and NAGA.

3. METHODS

3.1. Study of human and mouse tissues with biochemical phenotype of FD focused on the nature of storage of undegradable substrates

3.1.1. Investigation of metabolic fate of glycoconjugates with terminal α-galactosyl moieties in the pancreas of FD patients with blood group B (FD-B)

Human tissue samples of all Fabry patients and control individuals were collected at autopsy and all samples were fixed with 4% paraformaldehyde. Detailed information about individual patients, methods of sample processing and methods of individual analyzes are reported in the enclosed publication A (pages: 87-89).

3.1.2. Study of renal sphingolipid distribution in the knockout mouse model of FD (FKO)

The studied Gla C57BL/6 knockout model (FKO) was a 70-week-old male mouse. For a control, a wild-type (WT) isogenic 70-week-old male C57BL/6 mouse was used. Detailed information about methods of sample processing and individual analyzes are reported in the enclosed publication B (pages: 98-99).

3.2. Creation of human FD and MPS II cell models using induced pluripotent stem cell technology

Peripheral blood mononuclear cells used for reprogramming were isolated from collected blood of one male (IDS_$\mathbf{X^{mut}}$/Y with c.[1181-1G>A] *IDS* mutation) and one heterozygous female (IDS_$\mathbf{X^{mut}}$/X with c.[1403G>A] (p.Arg468Gln) *IDS* mutation) MPS II patients, one male ((FD_$\mathbf{X^{mut}}$/Y with c. [277 G>A] *GLA* mutation) and one heterozygous female FD patient (FD_$\mathbf{X^{mut}}$/X with c. [838C>A] (p.Gln280Lys) *GLA* mutation). Four healthy individuals without diagnosis of any lysosomal disease were used as controls. Generation of iPSC lines, and their characterization are reported in the enclosed publications D and E (pages: 131-132 and 148-153).

3.2.1. X chromosome inactivation analysis in female patients with FD and MPSII

Female MPSII-iPSCs and FD-iPSCs were used for examination of XCI status in both primed and naïve state. Methods of achievement of naïve state in primed iPSC after reprograming and further analysis are described in the publication D (pages 131-132).

3.2.2. Neural model of CNS involvement in MPSII

MPSII-iPSCs were used for differentiation into neural lineage cells for study of neural involvement pathology of the disease and testing of ERT. Methods of differentiation and further analysis are described in the publication E (pages 148-153).

3.2.3. FD cardiomyocytes generated from iPSC as a human model for testing of therapeutic effect of pharmacological chaperone

Differentiation of iPSCs into CM

The generated control and FD-iPSCs were differentiated into functional CM based on the previously published protocol using glycogen synthase kinase 3 and Wnt inhibitors (Lian et al 2013). In brief, healthy and FD-iPSCs were cultivated on plates pre-covered with GelTrex™ (ThermoFisher Scientific Inc., USA) in the mTESR1 medium (STEMCELL Technologies, Vancouver, Canada) for two passages necessary for feeder cells removal. 10 μM Y27632 (Tocris Bioscience, UK) was added first day of passage for survival of single cells in the suspension. When the cells were 100% confluent, mixture of 12μM CHIR99021 (STEMCELL Technologies, Vancouver, Canada) in RPMI/B-27-insulin medium consisting of RPMI 1640 medium, 1x B27 Supplement, minus insulin and 100 of U/ml penicillin, 100 μg/ml streptomycin (all from ThermoFisher Scientific Inc.) was added. After 24 hours, the medium was replaced with fresh RPMI/B-27-insulin medium without CHIR99021. After 72 hours, the medium was replaced with combined medium prepared with old medium : fresh RPMI/B-27-insulin medium (1:1), supplemented with IWP2 (Tocris Bioscience, UK) with final concentration of 5 μM. After 5 day, old medium was replaced with fresh RPMI/B-27-insulin medium and was changed every other day until emergence of spontaneously beating clusters of CM.

Characterization of iPSC and iPSC-derived CM by immunostaining

The cells were fixed in 4% paraformaldehyde in PBS for 15 min, permeabilized with 0.2% Triton-X100 in PBS for 5 min, and blocked in 10% goat serum (ThermoFisher Scientific Inc.)

in PBS for 1 hour, all at room temperature. The cells were incubated overnight at 4 °C with primary antibodies against Troponin T (ThermoFisher Scientific Inc., cat# MA5-12960), Troponin I (Santa Cruz Biotechnology, cat# sc-15368), Nkx2.5 (Santa Cruz Biotechnology, cat# sc-14033) and smooth muscle actin (DakoCytomation, Glostrup, Denmark, cat# M0851) for detection of cardiomyocytes. All antibodies were diluted in blocking buffer. Next day, the cells were washed with PBS (5x 5 min) and labeled with Alexa Fluor 488- and Alexa Fluor 568-conjugated species-specific secondary antibodies (ThermoFisher Scientific Inc.) for 1 hour at 37 °C. The cells were then washed with PBS (5x 5 min) and nuclei were counterstained using 4',6-diamidino-2-phenylindole (DAPI, ThermoFisher Scientific Inc.) for 15 min at 37 °C. The sections were mounted on slides using Immu-Mount medium (ThermoFisher Scientific Inc.). Images were taken using either a Nikon Ti80 (Nikon Instruments Europe BV, Netherlands) or a Leica SP8X confocal microscope (Leica Microsystems GmbH, Wetzlar, Germany).

Loading of recombinant AGAL into CM

The recombinant enzyme (Replagal, Shire Pharmaceutical, Lexington, MA, USA), at a final concentration of 1 μg/ml in the RPMI/B-27-insulin medium with antibiotics P/S, was added to spontaneously beating CM (4-weeks old) for 5 days. Control cultures without the recombinant AGAL were prepared in parallel.

3.2.4. CRISPR/Cas9 generation of iPSC models of FD and Schindler disease

Generation of mutant iPSC lines by CRISPR/Cas9 system

The RNA-guided Cas9 nuclease was used for generation of mutant cells with AGAL, NAGA deficiency and with deficiency of both enzymes according to the previously published protocol (Ran et al 2013). In brief, 20-nt target genomic sequences were designed by an online CRISPR Design Tool (http://tools.genome-engineering.org). Top and bottom strands of oligos for each sgRNA design were annealed and phosphorylated with T4 polynucleotide kinase. The sgRNA oligos were cloned into the pSpCas9(BB)-2A-Puro (PX459) vector (Addgene, Cambridge, USA) for co-expression with Cas9. The sgRNA-expressing plasmid was used for transformation of competent E. coli strain: Library Efficiency® DH5α™ (ThermoFisher Scientific Inc., USA) and subsequently purified with QIAGEN Plasmid Maxi Kit (QIAGEN, Hilden, Germany). The sequence of each colony was verified by sequencing from the U6 promoter using a U6-Fwd primer.

Healthy iPSC (25th passage) were cultivated in mTESR1 medium for feeder cells removal as described in paragraph 3.2.3. Transfection was performed with $0.5x10^6$ of the iPSC, 17 µg of the plasmid in 100 µl tips and device setting of 1.05 kV; 2x20 ms by Neon transfection system (ThermoFisher Scientific Inc., USA). The iPSCs were placed onto 6well plate containing feeder cells and cultivated overnight in the mTESR1 medium : HES medium (1:1). 2.5 µg/ml of puromycin dihydrochloride (Sigma-Aldrich Inc., USA) in fresh HES medium was added to the cells on the second day. New feeder cells in HES medium were added after 48 hours of electroporation and medium was changed every other day. Colonies of iPSC began to form after one week. Colonies were picked up to 24well plates containing feeder cells and then propagated to create stable iPSC lines. Mutant cells with enzymes deficiency were verified in cell homogenates by enzyme assay with fluorogenic substrates (Hartree 1972; Voznyi et al 2001).

Loading experiments

iPSCs were seeded in 6 well plates pre-coated with gelatin in DMEM containing 10% of FBS and let to spontaneously differentiate into nonspecific adherent cell types (iPSC-D). iPSC-D were reseeded at least two times before they have been used for loading experiments. Blood group GSL A-6-2, B-6-2 and globotetraosylceramide (Gb4Cer) were isolated and purified from outdated human donor blood concentrates and radioactive labeled as described previously (Asfaw et al 2002)

iPSC-D were cultivated in 6 well plates to near-confluency in DMEM medium with 10% of FBS. The culture medium was replaced with 2 ml of medium with radioactive glycolipid substrate (10^7 dpm) and 0.5mM conduritol -B-epoxide (CBE) and the cells were further cultivated for 4 days. Cultivation of iPSC-D was terminated by removing the medium and washing the cells with PBS (2 ml per well). The cells were harvested with Accutase (200 µl, 37°C, 3 min, ThermoFisher Scientific Inc., USA). The cell suspension was transferred to 1.5 ml Eppendorf tubes with 1 ml of fresh culture medium and centrifuged (300xg, 10 min, RT). After removing the supernatant, the cell pellets were re-suspended in 1 ml of PBS and the centrifugation was repeated.

The cell pellets were homogenated by sonication on ice in 250 µl of ultrapure water (30 seconds, pulse-pause, 20% output cup-horn sonifier). 200 µl of cell homogenates were transferred to glass tubes and mixed vigorously with 800 µl of chloroform: methanol 2:1. The mixtures were centrifuged (300xg, 10 min., RT) and the upper and lower phases carefully aspirated and saved. The inter phases were re-extracted with another 800 µl of chloroform: methanol 2:1 and mixed

with the former extract. The combined extracts were evaporated until dryness under N_2 gas. The residues were re-dissolved in 50 µl of chloroform: methanol 2:1 and applied to HPTLC plate (Merck, Germany).The chromatogram was developed in mobile phase composed of chloroform: methanol: H_2O 70: 30: 5 (v/v/v). The evaluation was performed by TLC-Linear Radioactive Analyzer (Raytest, Straubenhardt, Germany) (Asfaw et al 2002).

4. RESULTS AND DISCUSSION

4.1. Study of human and mouse tissues with biochemical phenotype of FD focused on the nature of storage of undegradable substrates.

4.1.1. Investigation of metabolic fate of glycoconjugates with terminal α-galactosyl moieties in the pancreas of FD patients with blood group B (FD-B).

In 1973, Wherrett and Hakomori first described B-antigens accumulated in the pancreas of a FD patient with blood group B. Since this first report, the possible contribution of non-degraded B-GSL to the pathophysiology of FD pancreas has not been systematically explored. Individual reports have suggested that such defect in degradation does not aggravate the disease phenotype in patients with blood B or AB (Lidove 2002). Although gastrointestinal problems are relatively frequent (Desnick et al 2001), the number of analyzed FD-B patients has never been extensive, also due to low frequency of blood group B individuals in the general population (Garratty et al 2004) . We had a unique opportunity to analyze autopsy material of two male FD patients, blood group B secretors, to confirm previous findings and broaden the knowledge about the consequences of storage process in the FD pancreas. We also used this possibility to compare the biochemical data between secretory (kidneys) and non-secretory (lungs) organs from FD patients with blood B and O groups and from appropriate controls.

Presence of neutral GSLs and B-GSLs in extracts from autopsy tissue samples was examined by HPTLC (with chemical detection and specific immunostaining), HPLC-ESI-MS/MS and FIA-ESI-MS/MS analysis. As expected, orcinol detection of neutral GSL isolated from pancreatic tissue revealed increased accumulation of Gb3Cer in the patients with FD irrespective of blood group (**Fig.12**).

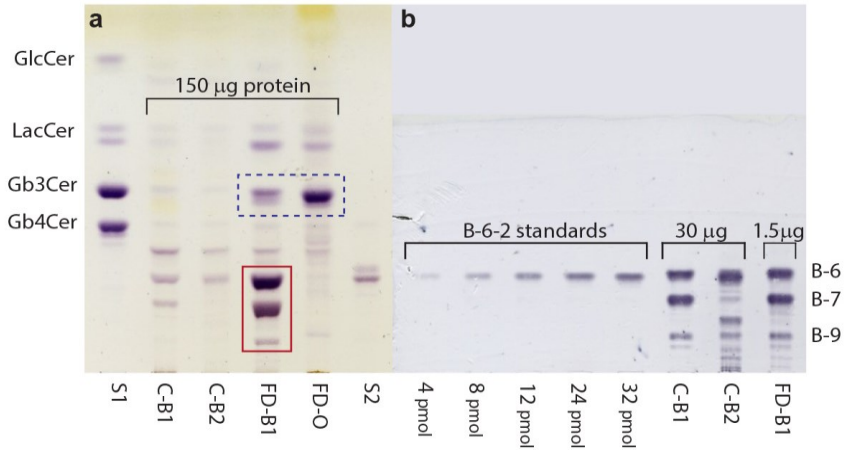

Fig.12: HPTLC analysis of neutral GSLs in the pancreas.
Orcinol detection **(a)** of neutral GSLs in FD pancreas showed increased deposition of Gb3Cer (blue dashed line rectangle). However, in the FD-B1 patient, B-GSLs were identified as additional deposited substances with considerable structural diversity in the carbohydrate moiety, as documented by immunodetection **(b)**.
B-GSLs with 6, 7, or 9 monosaccharides in the chain located in the lower part of the chromatogram (red full line rectangle in (a). **S1** – GSL standards.

However, notable was the massive deposition of complex immunopositive B-GSLs in the pancreas of patient with blood group B in comparison with controls of the same blood group. As for B-GSLs, the immunopositive bands were more pronounced in the kidneys compared to the lungs, but much weaker than in the pancreas. Only trace amounts of B-GSLs were detected in the lung tissue of FD-B patients (**Fig.13**). This variability likely relates to the differences in metabolic turnover of organ-specific cell types as well as subcellular lipid distribution and/or localization.

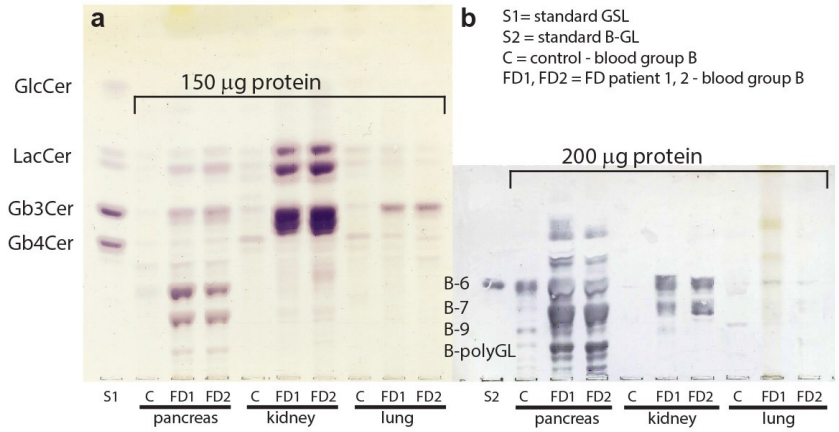

Fig.13: TLC analysis of neutral GSLs and B-GSLs in the pancreas, kidneys and lungs.
Orcinol detection of neutral GSLs revealed the largest deposition of Gb3Cer in the kidneys of both Fabry patients compared to pancreas and lungs. B-GSLs in kidneys were also increased but less than in the pancreas. In contrast, only traces of B-GSLs were detected in the lungs. B-polyGL – B-polyglycosylceramides containing more than 9 monosaccharide units.

Spectrum of B-GSLs in the pancreas was acquired by HR-MS in the m/z range 1425 - 1850 with DataAnalysis 4.0 software and was evaluated by mMass software connected to LipidMAPS. In the selected m/z range, broad representation of various oligosaccharide and lipid structures of blood GSLs were identified in the FD pancreas ranging from 5 to 7 sugars in the oligosaccharide chain. Such B-GSL rich spectrum was not observed in controls (**Fig.14**). A remarkable biochemical finding was that besides the dominant species with six (B-6) and seven (B-7) sugar residues, the whole series of highly complex B-GSLs accumulated in the FD-B pancreas. Although MS cannot distinguish between isobaric compounds (compounds with the same elemental composition), the authenticity of B-positive GSLs was confirmed by HPTLC immunodetection (**Fig. 12b, Fig. 13b**).

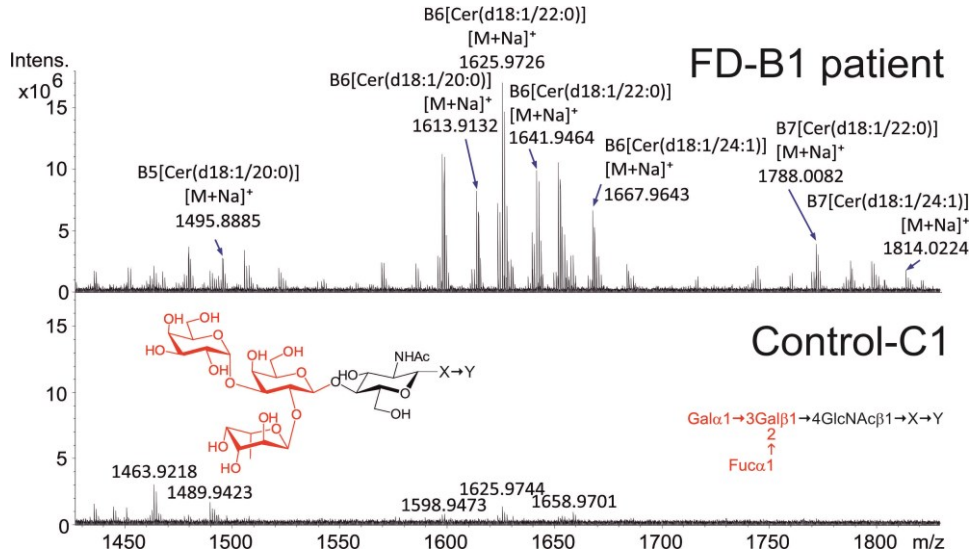

Fig.14: High resolution mass spectra of blood group B-GSLs in the pancreas.
Molecular species of major elevated B6, B7 (and B5) glycolipids are labeled and their ceramide composition is indicated. The structure of the blood group B antigenic determinant comprising three terminal monosaccharides is marked in red. The X in the GSL represents other possible saccharide units in the oligosaccharide structure. The Y indicates the hydrophobic core ceramide structure of glycolipids. Reference to sphingolipids in LipidMAPS database are indicated (LMSP identifiers: http://www.lipidmaps.org/ and http://www.mmass.org/).

Compared to controls, up to a 30-fold increase in the B-6 glycolipid (about 135 vs 4.5 pmol/mg protein) was identified in both FD-B patients by semi-quantitative HPLC-ESI-MS/MS (**Supplementary publication A, page: 90)**. This contrasts with approximately 6-fold elevation of Gb3Cer in FD-B pancreatic homogenates **(Table 2**). The amounts of other neutral GSLs were normal. The only exceptions were the Gb3Cer and ceramidedihexoside (CDH) fractions. The latter contains Ga2Cer, which is another minor AGAL substrate represented in the kidneys and elevated in FD patients **(Table 2**). Interestingly, the massive GSL storage is accompanied

by a distinct decrease in the content of sphingomyelin. This phenomenon was pronounced in all three FD patients irrespective of the blood group.

Table 2: Concentration of neutral GSLs, ceramide and sphingomyelin in the FD and control pancreas, kidneys and lungs.

		Lipid concentrations in nmol/mg protein					
		Cer	CMH	CDH	Gb3Cer	Gb4Cer	SM
Pancreas	*Controls AVG±SD, n=4*	*5.2±1.3*	*3.2±1.2*	*5.4±2.1*	*2.0±0.9*	*0.5±0.2*	*75.9±16.0*
	FD-O	1.5	1.6	8.2	26.2	0.3	26.6
	FD-B1	3.5	5.6	12.8	9.7	0.3	28.4
	FD-B2	7.4	2.4	17.1	11.2	0.5	25.0
Lung	*Controls AVG±SD, n=4*	*4.0±0.9*	*1.6±0.7*	*11.5±4.3*	*2.0±0.7*	*0.9±0.4*	*62.6±15.1*
	FD-O	2.6	1.2	10.8	41.5	0.6	32.9
	FD-B1	3.4	0.7	6.3	14.1	0.5	32.1
	FD-B2	2.5	0.6	3.3	15.0	0.3	32.3
Kidney	*Controls AVG±SD, n=4*	*5.4±1.0*	*2.0±0.6*	*8.4±3.6*	*6.1±1.7*	*2.6±1.0*	*86.8±28.6*
	FD-O	6.1	3.5	157.5	177.0	2.1	59.3
	FD-B1	6.2	6,2	221.1	155.4	0.8	49.9
	FD-B2	5.9	3.4	155.1	108.2	0.6	32.4

Data were obtained by FIA - ESI - MS / MS analysis of lipid extracts of tissues homogenates. The MS/MS does not differentiate between the glucosyl and galactosyl moieties because of the same mass. Therefore, glucosylceramide and galactosylceramide are quantified as monohexosylceramides (CMH), while lactosylceramide and digalactosylceramide as dihexosylceramides (CDH). FD-B1, FD-B2 – Fabry patients, blood group B, FD-O – Fabry patient, blood group O.

The results of the biochemical assays that were performed in de-proteinated homogenates of the whole tissue can not necessarily fully correlate with spatial distribution of lipids in tissue sections due to the heterogeneity of the present cells. This stated, next we aimed to identify the cellular pancreatic populations afflicted by an accumulation of both main substrates, Gb3Cer and blood group B compounds.

B-antigens (both glycoproteins and glycolipids) were immunohistochemically detected in the acini of the exocrine pancreas and in the vascular endothelial cells in both FD-B patients and controls **(Fig.15a - d)**. In the normal tissue, regardless of the blood group, a mosaic pattern of ABH binding sites was clearly visible, suggesting that it is an usual feature of ABH antigens expression (Ito 1992). In FD-B patients however, the expression of all B-antigens in the pancreatic acinar epithelium was uniform and more intense than in controls. Ductal epithelium, endocrine pancreas (islets of Langerhans) and vascular smooth muscle cells were negative for B-antigens (data not shown) which is consistent with report by Raven and Dabelsteen (Ravn

and Dabelsteen 2000). Lipid pre-extraction of tissue sections did not substantially reduce the immunostaining of B-antigens in either FD-B patients or controls (data not shown). This suggests that the positivity of B-antigens also largely appertain to polar non-lipid glycoconjugates with blood group B determinants.

It has been known that lysosomes affected by storage accumulate considerable amounts of autofluorescent lipofuscin-like lipopigment ceroid (Terman and Brunk 1998; Elleder 2010; Hulkova and Elleder 2010). Massive granular autofluorescence of ceroid was also detected in the exocrine parts of the FD-B pancreas (**Fig.15e**, white arrowheads) correlated with the signal for B-antigens. In controls, the autofluorescent material was not detected in any of the listed cell types. Lysosomal localization of B-antigens was confirmed with their co-labeling with lysosomal marker LAMP2 (**Fig.15e**) but not in secretory granules using α-amylase marker (**Fig.15f,** α-amylase positivity). Under normal conditions, Lantini at al (Lantini and Cossu 1997) described specific staining of acinar secretory granules for blood group B antigens with intensive secretion into the pancreatic juice together with digestive enzymes. In our study on FD pancreas, however, neither B-antigens nor Gb3Cer co-localized with secretory granule marker (**Fig.15f, Fig.16f**).

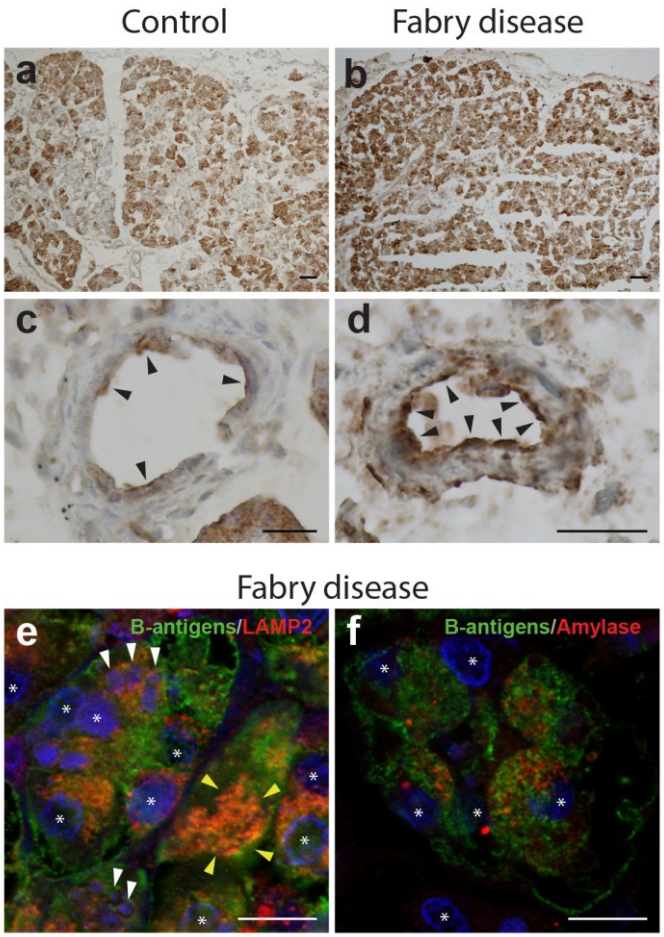

Fig.15: Blood group B antigen immunohistochemistry and confocal microscopy in the pancreas.
(a) Mosaic expression of B-antigens in acinar epithelium in the C-B2 control. **(b)** Intensive and almost homogenous staining for B-antigens in the exocrine part of the FD-B1 pancreas. **(c)** Endothelial cells with the usual expression of B-antigen (black arrowheads). **(d)** Strong positivity for B-antigens in the endothelial cells is suggestive of B-antigen participation in the lysosomal storage in the FD-B1 pancreas (black arrowheads). **(e)** Co-localization of B-antigens (green signal) with LAMP2 (red signal) demonstrates their localization in lysosomes (yellow arrows) accompanied by the increased amount of ceroid (white arrowheads). **(f)** B-antigens signal does not correlate with amylase-positive secretory granules (red signal). DAPI stained nuclei in blue*. Scale bars (a, b) = 50µm, (c, d) = 20µm, (e, f) = 10µm.

Gb3Cer was expressed in vascular endothelial cells as B-antigens and additionally also in vascular smooth muscle cells (**Fig.16a –d**). B-antigens, however, did not contribute to the lysosomal storage in vascular smooth muscle cells in FD-B patients. Importantly, Gb3Cer positivity was more intense in FD-B patients than in controls. Other cell types, including pancreatic acini, were only weakly positive for Gb3Cer but accompanied with increased amount of ceroid **(Fig.16e).**

In smooth muscle cells, but not in endothelial cells, Gb3Cer was partially resistant to lipid extraction (**Fig.16d**), probably reflecting modifications of the lysosomal system by long term storage and intensified by extensive amount of ceroid.

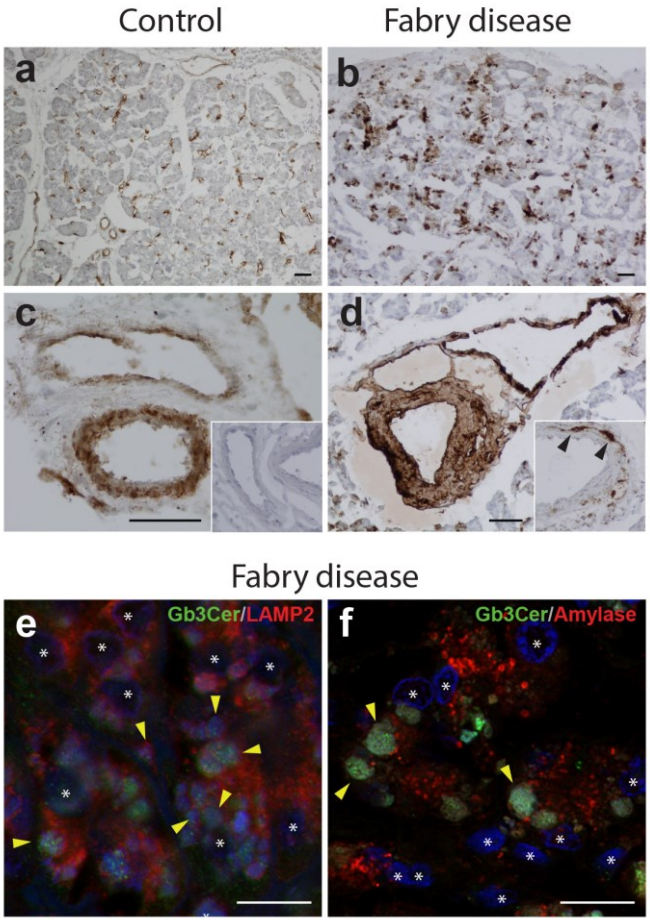

Fig.16: Gb3Cer immunohistochemistry and confocal microscopy in the pancreas. **(a)** Gb3Cer expression is enhanced in blood vessels in the control. **(b)** In Fabry disease, Gb3Cer stains with increased intensity the in pancreatic vessel walls. **(c)** Small vessels display Gb3Cer in the endothelium, however large vessels were positive also in the smooth muscle cells. Staining of Gb3Cer was negative after pre-extraction step of lipids from the tissue (insert) **(d)** Gb3Cer accumulation in the endothelial and smooth muscle cells in the FD-B1 pancreatic vessels is massive. Gb3Cer storage in smooth muscle cells persists after lipid extraction (insert, black arrowheads).
(e) Co-localization of Gb3Cer (week green signal) with LAMP2 (red signal) demonstrates their localization in lysosomes accompanied with the massive accumulation of autofluorescent ceroid (yellow arrowheads). **(f)** Gb3Cer does not correlate with amylase positive secretory granules but correlates exclusively with autofluorescent ceroid (yellow arrowheads). DAPI stained nuclei in blue*. Scale bars (a, b) = 50µm, (c, d) = 20µm, (e, f) = 10µm.

The results clearly show that different, non-degraded, substrates are expressed and stored in lysosomes of distinct pancreatic cellular populations that have different physiological functions. While acinar cells specifically accumulate glycoconjugates of blood group B and only minimally Gb3Cer, the latter AGAL substrate predominates in the blood vessel cells. Importantly, endocrine cells were completely free of storage. Comparison of differences in storage between blood group B and O FD patients provides an explanation for the milder affliction of the pancreas in contrast to other organs in which the accumulation of Gb3Cer predominates. We believe that our results strongly substantiate the need for more detailed clinical studies focused on possible pancreatic (dys)function in FD patients with type B blood group.

Reference: Supplementary publication A

4.1.2. Study of renal sphingolipids distribution in the knockout mouse model of FD (FKO)

As stated, knock-out mice are valuable animal models for exploring the pathophysiology and pathobiochemistry of diseases, including many inherited disorders. Since the kidney is one of the most affected organs in FD, we have focused on the analysis of renal distribution of stored GSL species using histochemical and advanced MS techniques. We used organs from the AGAL knock-out of C57BL/6 mouse serving as a model for the "later onset" phenotypes of FD. Consecutive tissue section of isogenic 70-week old male FKO and wild-type (WT) mice were used for the experiment. Lipids were analyzed by FIA-ESI-MS/MS. The Gb3Cer isoforms were present at 34times higher concentration in FKO mouse compared to WT (**Fig.17A**). The results were more evident when compared to those reported previously on 5- or 12-month- old male or female FKO mice (Durant et al 2011). The second stored lipid in FKO mouse was Ga2Cer which was present in CDH fraction (**Fig.17A**). Its concentration was 2 times higher compared to that in the WT mouse. The individual isoform profiles of the Gb3Cer were also assessed. Molecular species with the C16:0, C20:0, C22:0, C24:0 and C24:1 fatty acids were identified as differently expressed lipid forms in the FKO and WT mice (**Fig.17B**).

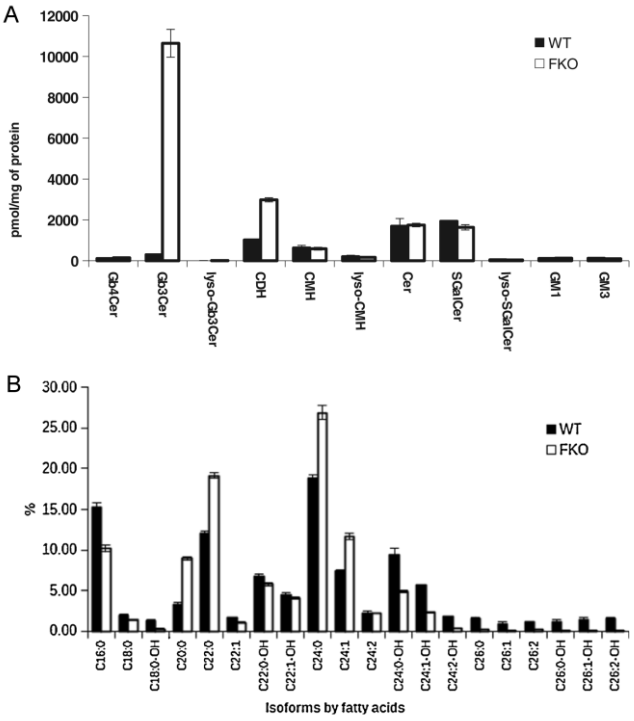

Fig.17: Analysis in FKO and WT kidney samples by FIA-ESI-MS/MS. (A) Renal sphingolipid profiles determined in the FKO (white) and WT (black) murine renal tissues (three technical replicates). (B) Fatty acylation of Gb3Cer in FKO and WT murine renal tissues. C17:0 Gb3 isoform was used as internal standard.

Lipid *in situ* localization was evaluated by mass spectrometry imaging (MSI) and correlated with IHC staining on the consecutive tissue sections. The Gb3Cer concentration calculated using the above-mentioned five major isoforms was almost twice as high as in WT mouse. Higher Gb3Cer accumulation was found in the renal cortex of FD mice, lower concentration was detected in the medulla, which was assessed by both MSI and IHC methods in tissue sections (**Fig.18A**). Cortical tubules were significantly more affected than glomeruli as well as renal tubules in the medulla. In the WT mouse, only a background signal for Gb3Cer was detected (**Fig.18B**). Intensity of Gb3Cer staining was more prominent in the inner part of the medulla in comparison with outer part which is partially based on desquamated epithelium from the upper parts of the nephron in a form of tubular casts (**Fig.18B**).

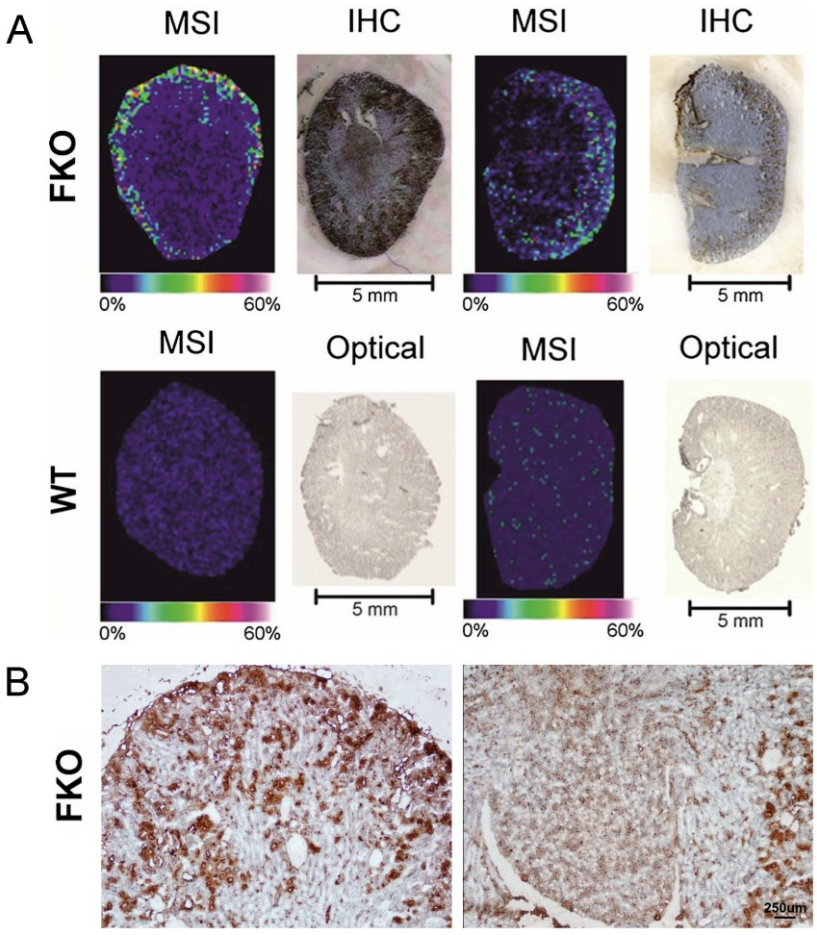

Fig.18: Distribution of Gb3Cer in the kidney tissue section evaluated by IHC and MSI analysis.
(A) Distribution of Gb3Cere (d18:1/24:0) in FKO (top) and WT (bottom) mice. Transversal (all four left) and coronal (all four right) sections show increased accumulation of in the renal cortex. MSI data revealed the sodiated molecules of Gb3Cer at m/z 1158.785. IHC shows Gb3Cer visualized in brown, whereas the cell nuclei counterstained with hematoxylin are blue. (B) IHC details of the transversal section of FKO mouse section demonstrating predominance of Gb3Cer tubular storage in the cortex (left) compared to that in medulla (right). Gb3Cer storage is more pronounced in cortex tubuli compared to glomeruli.

Whereas antibodies-based IHC staining recognized just the saccharide portion of the Gb3Cer molecule, MSI provided a distribution pattern of lipid isoforms in the renal cortex. Thus, the major benefit of MSI is the identification of the spatial distribution of the stored compounds and their molecular species.

In FKO mouse, lysosomal storage of GSLs in the kidneys partially resemble the situation in patients with FD as shown in the previous chapter 4.1.1 (Table 2) and also by other authors (Ohshima et al 1997; Ohshima et al 1999; Ioannou et al 2001). However, unlike humans, storage in FKO mice was higher in proximal tubules but was significantly lower in glomerular mesangial cells and podocytes (Valbuena et al 2011). This corresponds to the absence of renal insufficiency in the mouse model. Our immunohistochemical analyses of accumulated Gb3Cer revealed maximum staining intensity in cortical tubules which correlated well with the MSI results documented by **Fig.18**. MS/MS quantification confirmed that the accumulation of Gb3Cer in the human FD kidneys is several orders higher than in the mouse model which is undoubtedly related to the span of life of both species and to a different degree of damage of specific cell types corresponding to milder mouse phenotype of FD.

These facts led us to attempt to establish human iPSC lines and differentiate them further into defined cell types suitable for investigation of metabolic basis of the disease.

Reference: Supplementary publication B, Supplementary publication C

4.2. Creation of human FD and MPS II cell models using induced pluripotent stem cell technology.

In 2006, Takahashi and Yamanaka first reported the discovery of induced pluripotent stem cells (iPSCs) which were prepared by transcription factor-mediated reprogramming of mouse embryonic fibroblasts. Since then, the field of iPSCs has advanced rapidly and this technology has enabled the modeling of human diseases, followed by the study of pathogenesis at the cellular level and the testing of therapeutic options. Besides disease modeling, potential application of the techniques in regenerative medicine is also experiencing increasing research attention.

We have used the iPSC technology for generation of human iPSC models of selected LSD to investigate the pathology of affected cell types and evaluate the effect of ERT on these cells. For these studies, two X-linked LSD, FD and MPS II, were selected, iPSC lineages were

derived as follows: 1. from one male (IDS_$\mathbf{X^{mut}}$/Y with c.[1181-1G>A] *IDS* mutation) and one heterozygous female (IDS_$\mathbf{X^{mut}}$/X with c.[1403G>A] (p.Arg468Gln) *IDS* mutation) with MPS II; 2. from one male ((FD_$\mathbf{X^{mut}}$/Y with c. [277 G>A] *GLA* mutation) and one heterozygous female (FD_$\mathbf{X^{mut}}$/X with c. [838C>A] (p.Gln280Lys) *GLA* mutation) with FD.

Isolated peripheral blood mononuclear cells of patients and healthy individuals were reprogrammed using non-integrating Sendai virus vectors expressing the reprogramming factors Oct3/4, Sox2, Klf4 and c-Myc and were maintained as co-culture with supporting layer of irradiated mouse embryonic fibroblasts (feeder cells). iPSC colonies typically started forming nine days after viral infection (**Fig.19A, B**). Several colonies were picked from each patient and control cultures and passaged until disappearance of the non-replicating Sendai virus. The iPSCs showed morphology similar to ESC after 3-5 passages and expressed the pluripotency markers OCT3/4, LIN28, SSEA4, TRA-1-81 and ALP (**Fig.19C-F**).

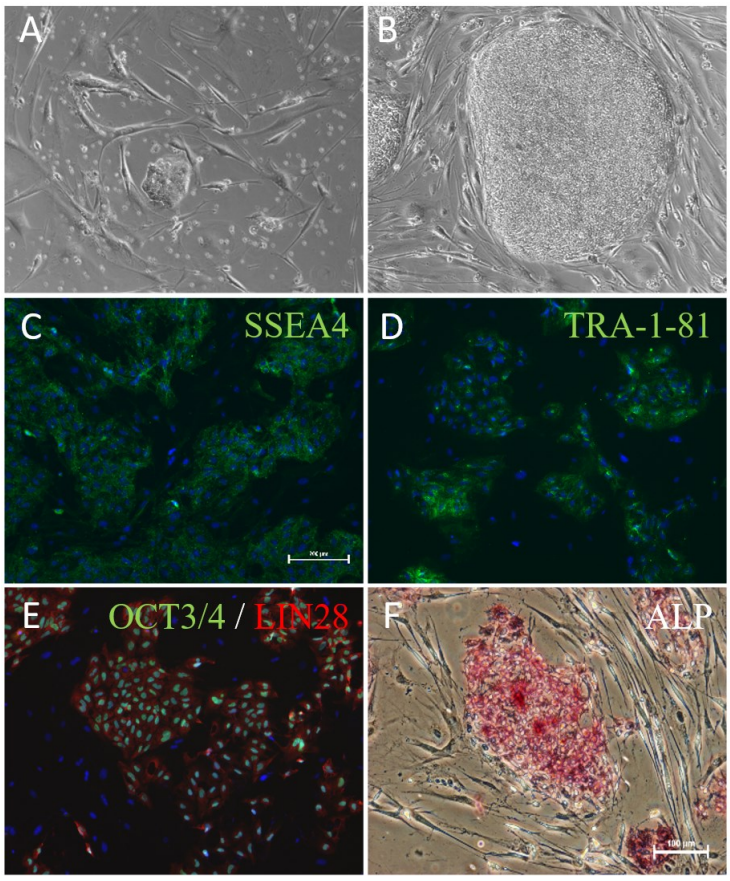

Fig.19: Generation and characterization of iPSC.
The formation of the iPSC colonies were observed at the day 9 (a) and compact colonies at the day 16 (b). Immunofluorescence analysis showing the expression of SSEA4 (green) (c); TRA-1-81 (green) (d); OCT3/4 (green) and LIN28 (red) (e) in iPSC lines. Analyzed iPSC clones were also positive for alkaline phosphatase (f). The nuclei were conterstained with DAPI (blue). The scale bars indicate 100 µm.

Verification of the patient phenotypes was performed by the proof of deficient IDS or AGAL activities in cell homogenates (Skoog and Beck 1956; Hartree 1972) using enzymatic assays (Mayes et al 1981; Voznyi et al 2001) (**Table 3**). β-galactosidase was used as a control enzyme.

The results observed in iPSCs were in accordance with the results measured in leukocytes isolated from blood of the patients.

Table 3: Determination of the enzymes activities in iPSCs and their XCI value.

Sample	IDS activity [nmol/mg.4hod]	AGAL activity + i [nmol/mg.hod]	β-GAL activity* [nmol/mg.hod]	XCI value
IDS_X^{mut}/Y	0.04	-	121.12	-
IDS_X^{mut}/X	7.61	-	476.29	98:2
FD_X^{mut}/Y	-	1.11	243.38	-
FD_X^{mut}/X	-	87.51	214.03	3:97
Control	76.95	99.88	147.24	-

Two selected iPSC clones of each patients and controls showed a weak residual activity of IDS in IDS_$\mathbf{X^{mut}}$/X cells and practically normal activity of αGALA in FD_X^{mut}/X in female cells which is in accordance with the status of X inactivation (XCI ratio 98:2 in IDS_X^{mut}/X favors mutant allele active versus XCI ratio 3:97 in FD_X^{mut}/X favors mutant allele active). Practically no activity was measured in all male patient samples. Values are average of two clones of the same line. *control enzyme.

We did not observe any decline in self-renewal capacity of the generated patient iPSC lines compared to control, unlike other monogenic disease (Chen et al 2016), which is considered as a critical for the practical utility of the models.

Established stable iPSC lines were further used for the study of X-chromosome inactivation status during transition of primed iPSCs to naïve state in heterozygous patient cells and for a study of cell pathology and efficiency of ERT in neural cells derived from MPSII-iPSC and in cardiomyocytes derived from FD-iPSC.

Reference: Supplementary publication D

4.2.1. X chromosome inactivation analysis in female patients with FD and MPSII

There is considerable interest in the use of human induced pluripotent stem cells (hiPSC) for the study of X-linked diseases, not only for the understanding of pathological cellular processes but also for the research of how X-chromosome inactivation (XCI) is regulated during reprogramming and during the long-term culture of female hiPSC lines (Maherali et al 2007; Stadtfeld et al 2008; Marchetto et al 2010; Tchieu et al 2010; Amenduni et al 2011; Ananiev et al 2011; Tomoda et al 2012). The current knowledge of XCI in human female iPSCs

reflected in published reports is contradictory mostly due to sensitivity of experiments to precise definition of conditions, the limitations of XCI research methods as well as subsequent difficulties in interpretation of the results.

Female naïve cells are expected to have two active X chromosomes in both human and mice. Unlike in mouse, however, *Xist* is expressed from one or both active X chromosomes in cells of human inner cell mass (Pinheiro and Heard 2017). Although the existence of naïve state of human PSCs has not yet been demonstrated *in vivo*, several groups have developed "*naïve culture media"* enabling formation of naïve iPSCs/ESCs from the primed PSCs *in vitro*. Naïve state is then accompanied by efficient loss of the XCI specific markers, including XIST RNA and XCI-specific histone modifications, which are re-established upon differentiation (Gafni et al 2013). The possibility of transforming primed iPSCs to naïve state by changing the culture conditions enables further access to the study of XCI in female iPSCs and in fact to the XCI research in general.

We focused on the study of two female patients with FD and MPSII to address the question whether the XCI status of naïve iPSCs is the same as in the source primed cells. Hypothetically, we would be able to detect the condition when both X-chromosomes would be reactivated in whole naïve cellular population. Examination of the methylation status at the AR locus showed extreme skewing in both blood leukocytes and reprogrammed iPSCs in favor of the mutated allele (XCI ration 98:2) in IDS_$\mathbf{X^{mut}}$/X and control allele (XCI ratio 3:97) in FD_$\mathbf{X^{mut}}$/X. Naïve iPSC lines were established by cultivation of iPSCs in naïve human stem cell medium (NHSM) containing LIF and small molecule inhibitors of ERK1/ERK2 and GSK3β signaling inducing conversion of primed iPSCs to naïve pluripotency, as described previously (Gafni et al 2013). After two passages of the iPSCs in the presence of NHSM, the cells showed typical round, dome-shaped cell colony morphology indicating conversion to naïve state. The methylation status at the AR locus did not show a change in XCI ratio in the MPSII clones; however, in case of the FD, the XCI ratio changed from 3:97 to 20:80 (**Fig.20**).

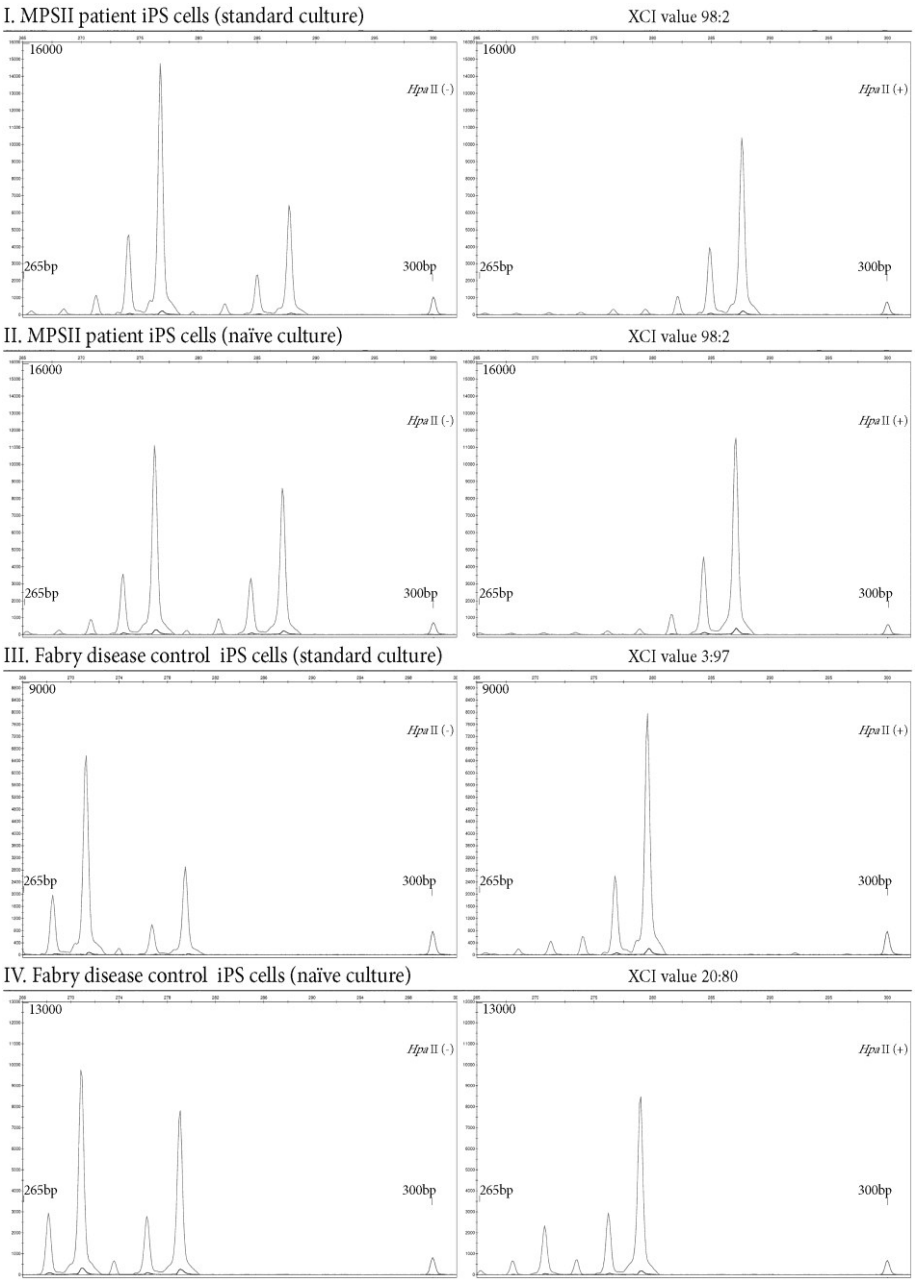

Fig.20: X-chromosome inactivation analysis in the patient's iPSCs generated from the MPS II and FD patients.

Standard culture and naïve culture cells are compared. Methylation status analysis of the *AR* alleles before (Hpa II-) and after (Hpa II+) digestion is shown. The 300-bp peak belongs to the GeneScan 500 ROX size standard. The analysis was conducted using GeneMapper software (Applied Biosystems).

Our results suggest that cultivation of female primed iPSCs in "naïve culture media" can achieve naïve state associated with the reactivation of X chromosomes and that following re-inactivation of X chromosome can be random as it is during embryogenesis. The varying results regarding XCI status obtained for hiPSCs may be explained by different reprogramming techniques and the growth conditions in which hiPSCs are generated and maintained. It is

known that factors like residual DNA methylation signatures characteristic of their somatic tissue of origin (Gomes et al 2017) or mitochondrial metabolism of iPSCs (Varum et al 2011) may affect the quality of individual iPSC lines and thus influence the iPSC transition from primed to naïve state, and also XCI status. Hypothetically, there could be other genomic variants that prevent random XCI in MPSII patient but these variants are often hard to identify conclusively (Di-Battista et al 2016; Mason et al 2018). Another possible explanation of the data can be the fact that HUMARA methylation assay detects only inactivated / methylated allele. If there is present small subpopulation of the cells with incomplete reactivation of X-chromosome, the detection of this methylated allele is interpreted as representative for the whole sample. For all these reasons, further studies are necessary for precise characterization of XCI status in iPSCs and understanding a basic aspect of the epigenetic differences between naïve and primed state. Besides general biological knowledge, these studies are relevant for future medical uses. The iPSC clones from heterozygotes of X-linked disorders with favorable XCI and thus functionally normal can potentially serve as a source of autologous material (hematopoietic progenitors, neurons, cardiomyocytes, etc.) for cell-based therapy in females with severe phenotype of X-linked disorders.

Reference: Supplementary publication D

4.2.2. Neural model of CNS involvement in MPSII

iPSCs of hemizygous and heterozygous MPSII patients and healthy controls were differentiated into neuronal and glial cells using the modified protocols of Stacpoole et al (Stacpoole et al 2011) and All et al (All et al 2015). The differentiation protocols were initiated by generating a suspension of iPSCs to allow formation of multicellular iPSC aggregates, embryonic bodies (EBs), which were later transformed into neurospheres. To demonstrate the differentiation along correct pathway, the neurospheres of neural progenitor cells (NPC) were frozen after two weeks of culture in complete differentiation medium, cryo-sectioned according to publish protocol (Gomes et al 2010) and used for detection of NPC markers Nestin and SOX1 (**Fig.21**). The capacity to form EBs was markedly different between cell lines from MPSII patients and healthy controls. Control iPSCs spontaneously formed compact, spherically shaped EBs after plating a single cell suspension onto ultra-low attachment plates. However, the cultures of patient's iPSCs showed reduced ability to spontaneously form EBs which is analogous to previously reported impaired EB formation in murine MPSVII-iPSC (Meng et al 2014).

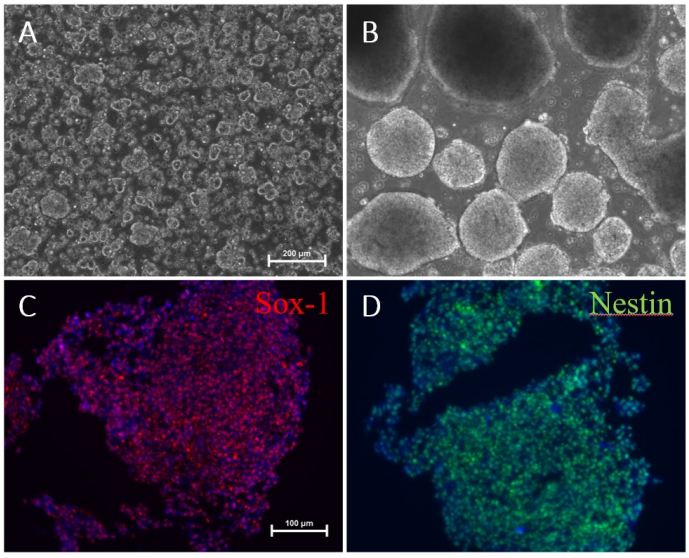

Fig.21: Differentiation of MPSII-iPSCs into neural progenitor cells.
Aggregation of single cell suspension of iPSC was observed one day after neural induction (A) and round, different sized spheres could be detected after 7 days of induction (B). Detection of neural progenitor marker SOX1 (C) and Nestin (D) in controls' and patients' EBs after 14 days of differentiation. Nuclei were counterstained with DAPI (blue signal). Control iPSCs were differentiated in parallel.

The EBs were cultured for additional 2 weeks in complete differentiation medium supplemented with retinoic acid and after adhesion and cultivation in the terminal differentiation medium for an additional 2-8 weeks, we found a heterogenous mixture of neural cells. Immunofluorescence analysis confirmed the presence of vimentin$^+$, β-TubIII$^+$ and MAP2$^+$ neurons, GFAP$^+$ astrocytes and CNPase$^+$ oligodendrocytes (**Fig.22**). While the deficiency in EB forming of MPSII-iPSC was potentially limiting, we showed that by adjusting the differentiation protocol, the MPSII-iPSCs could be differentiated into mixture of neural cells. These observations suggest that IDS deficiency may, similarly to other neurological diseases, partly interfere with the fitness of the neural precursors (Russo et al 2015) but does not represent a fundamental compromise to the differentiation potential of the human MPSII-iPSCs which is in accordance with the results in IDS deficient murine neuronal stem cells (Fusar Poli et al 2013).

Lysosomal membrane marker LAMP1 and lysosomal luminar marker Cathepsin D (CatD) were assayed to determine the impact of IDS deficiency on the lysosomal compartment of the neuronal and glial cells after 6 weeks of terminal differentiation. The increased lysosomal compartment was observed in the perinuclear region of GFAP$^+$ astrocytes and CNPase$^+$ oligodendrocytes and occasionally β-TubIII$^+$ neurons of MPSII patients (**Fig.22**).

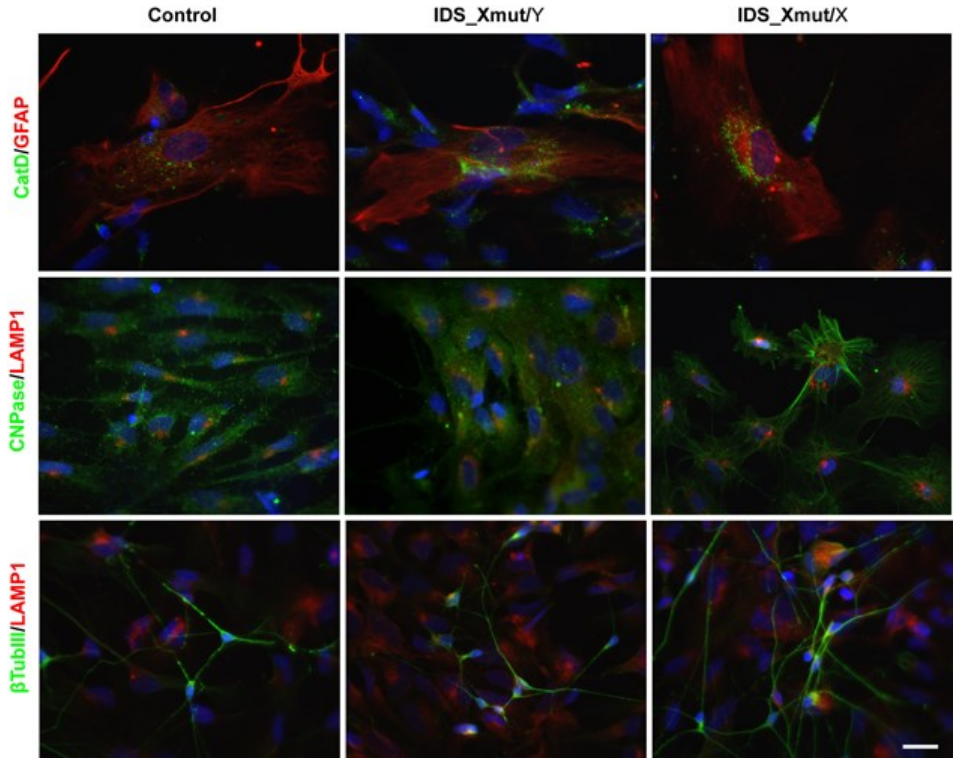

Fig.22: Lysosomal accumulation in iPSC derived neural cells.
Differentiated neural cells were cultured for six weeks and used for immunofluorescence analysis. Increased numbers of $LAMP1^+$ or $CatD^+$ lysosomes were detected mainly in GFAP positive astrocytes and CNPase positive oligodendrocytes and occasionally in βTubIII positive neurons in both hemizygous and heterozygous MPSII patients compared to control(s). Nuclei were counterstained with DAPI (blue signal). Scale bar: 20 μm.

Sub-cellular changes of the neural cells were evaluated by electron microscopy. Contrary to the heterogeneous cellular population evaluated by immuno-cytofluorescence, cells with larger glia-like nuclei prevailed, suggesting relative fragility of neuronal precursors for ultrastructural analysis. All cells formed complex neurosphere structures and developed thin cytoplasmic processes. In comparison to control cells though, patient neural cells contained numerous pleomorphic cytoplasmatic vacuoles containing arranged lamellar or lucent granular material (**Fig.23**).

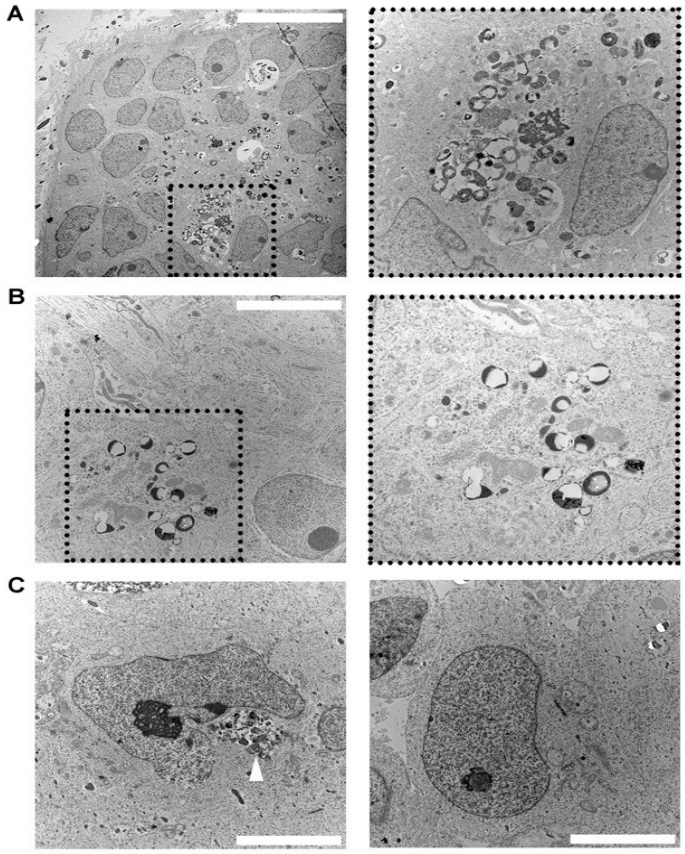

Fig.23: Electron microscopy analysis of iPSC derived neural cells.
Up to 8 weeks-old terminally differentiated neural cells were used for electron microscopy of morphology studies and potential lysosomal storage in patient cells. Similar features were observed in all studied patient samples. (A) edge of a neurosphere with emanating cellular processes and pleomorphic cytoplasmic vacuoles (IDS_X^{mut}/X). (B) comparable cytoplasmic vacuoles in the male patient cells (IDS_X^{mut}/Y). (C) some control cells contained autophagic-like vacuoles (white arrowhead). Scale bar:
(a) 200 μm, (b and c) 5 μm.

Photometric determination of GAG levels was performed in the homogenates of iPSCs, NPCs and terminal differentiated neural cell cultures. No significant increase in GAGs was detected in patient iPSCs and NPCs compared to controls which may be caused by the high proliferative rate of the cells and consecutive dilution of undegraded substrates as have been described in FD-iPSC model (Itier et al 2014). However, GAGs in terminally differentiated neuronal and glial cells, after 8 and 12 weeks of culture, were 1.5-4.3x (hemizygous) and 1.7-4.6x (heterozygous) higher than in controls (**Fig.24A**). Abnormal and progressive accumulation of GAGs became apparent in more differentiated patient cells which was likely caused by decreased proliferation and prolonged cultivation.

The recombinant IDS used for ERT is endocytosed and targeted to the lysosomes via mannose and mannose-6-phosphate receptors on the cell surface (Wraith et al 2008) but its effect on the treatment of the affected CNS is not clear. This is mostly explained by the fact that the recombinant enzyme is too large to cross the blood brain barrier (Boado et al 2013). We tested ERT efficiency in the culture of our iPSC derived neural cells. MPSII and control neural cells were differentiated in media supplemented with recombinant IDS for 10 weeks after reaching the NPC stage when any increase in GAGs was noticeable in patient cells. The recombinant enzymes slightly reduced the levels of elevated GAGs but despite high intracellular enzyme

activity (**Fig.24B**) there was still a gradual increase in accumulated GAGs in patient cells (**Fig.24A**). It is known that heparan sulphate (HS) is present in the cell membrane or in the extracellular matrix where they mediate molecular interactions, bind growth factors, chemokines, enzymes and play a role in signal transduction (Perrimon and Bernfield 2001; Gallagher 2006). Increased amount of HS was immunodetected on the cell surface but not within the lysosomes (**Fig.24C**). This phenomenon was previously described in MPSIII where HS is also one of the main storage compounds (Jakobkiewicz-Banecka et al 2016). We hypothesize that increased amount of IDS substrates in patient cells is given by their presence in extracellular matrix in proximity to the plasma membrane from where they are not transported to lysosomes for degradation nor they are able to be degraded extracellularly by IDS at a neutral pH.

A

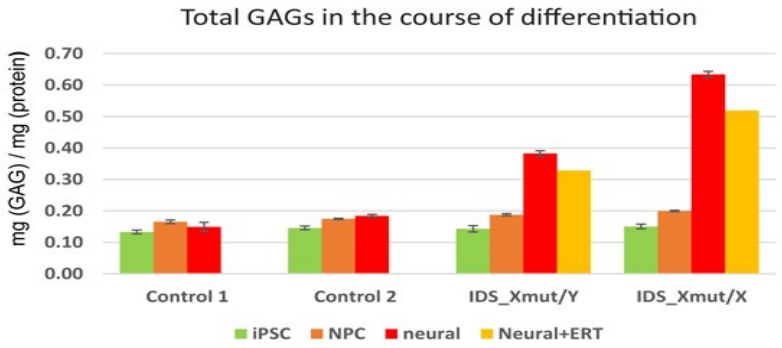

B

Sample	IDS activity [nmol/mg.4hod]
IDS_X^{mut}/Y	9,834
IDS_X^{mut}/Y + ERT	444,378
IDS_X^{mut}/X	5,214
IDS_X^{mut}/X + ERT	285,318
CX5	51,678

C

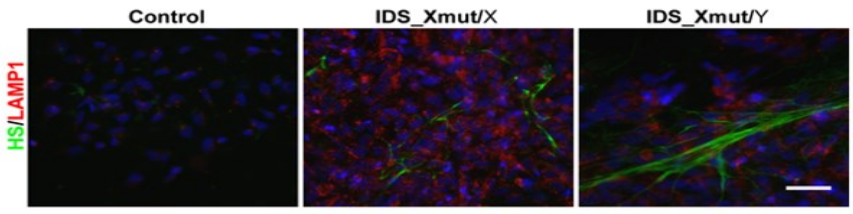

Fig.24: Analysis of GAG accumulation in iPSC, NPC and differentiated neural cells of MPSII patients and controls using a photometric method.
GAG levels were normal in patient iPSC and NPC. Maturation of neural cells was accompanied by an increase in accumulated GAGs. GAG accumulation was reduced by supplementing the deficient IDS (A). Values of enzyme activities measured in neural cells with and without the addition of IDS recombinant enzymes (B). Co-staining of HS and LAMP1 did not shown overlap of the specific signals. HS accumulated in the cytoplasmic membranes from both patients (C).

In conclusion, we created an iPSC model of MPSII which can be differentiated to various neural cell types related to the CNS pathology of the disease. The iPSCs derived terminally differentiated cells accumulate increased amounts of GAGs. HS, one of two substrates affected by the enzyme defect, was localized mostly to the plasma membrane or extracellularly. This biochemical phenotype was not observed in proliferating cells suggesting that longer term cultivation of non-proliferated cells could further emphasize the phenotype. The iPSC lines can be used for future screening of potential therapeutic improvements such as better targeting of recombinant enzymes to neuronal/glial cells, mainly in combination with the iPSC based model of the BBB, which was successfully produced (Canfield et al 2017).

Reference: Supplementary publication E

4.2.3. FD cardiomyocytes generated from iPSC as a human model for testing of therapeutic effect of pharmacological chaperones

Cardiomyocytes (CM) are one of the major cell types affected in FD and therefore we decided to differentiate iPSCs into cardiac cells. We used protocol based on temporal application of a glycogen synthase kinase 3 inhibitor (CHIR99021) combined with chemical Wnt inhibitor (IWP2) and serum-free defined medium to generate functional CM (Lian et al 2013). The presence of cardiac cells could be easily established by visual observation of spontaneously contracting regions. The first beating clusters were observed between differentiation day 8 and 14 in both control and FD cells. Generated FD-CM and control-CM were also positive for typical cardiac marker Nkx2.5, Troponin T a I and SMA (**Fig.25)**.

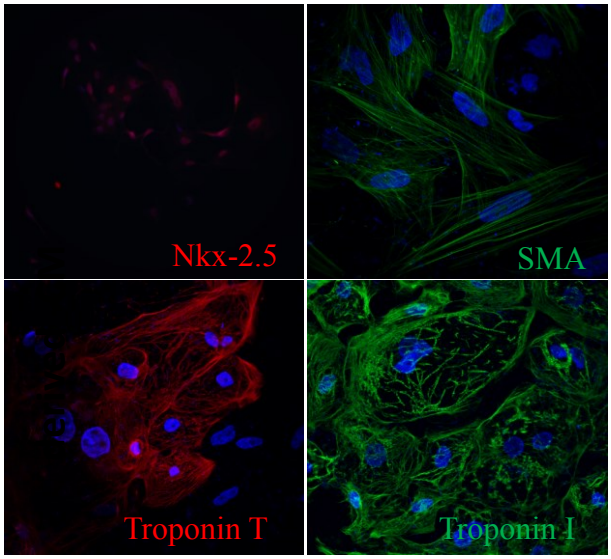

Fig.25: CM generated from human iPSCs. Positivity of beating control-CM for cardiac markers, Nkx2.5, Troponin T and I and smooth muscle actin (SMA)**.**

The efficiency of differentiation, tested by flow cytometry, was significantly smaller for FD-CM compared to control probably due to FD phenotype. Increased accumulation of the main storage compound Gb3Cer was detected by FIA-ESI-MS/MS analysis or ICF (**Fig.26A)** while no accumulation of Gb3Cer was detected in control cells. Its increased level in FD-CM thus may be the reason to an inability to generate functional fibers in these cells (**Fig.26A** right column and also (Itier et al 2014)). Regular intravenous administration of recombinant human AGAL is the most used treatment of LSD, including FD. Recently, an effective clearance of Gb3Cer by the recombinant enzyme in FD-CM has been reported (Itier et al 2014). We tested the trafficking and localization of exogenous enzyme within the cells affected by storage after two months in culture. Its lysosomal internalization was confirmed 5 days after loading the enzyme to the culture media (**Fig.26B**).

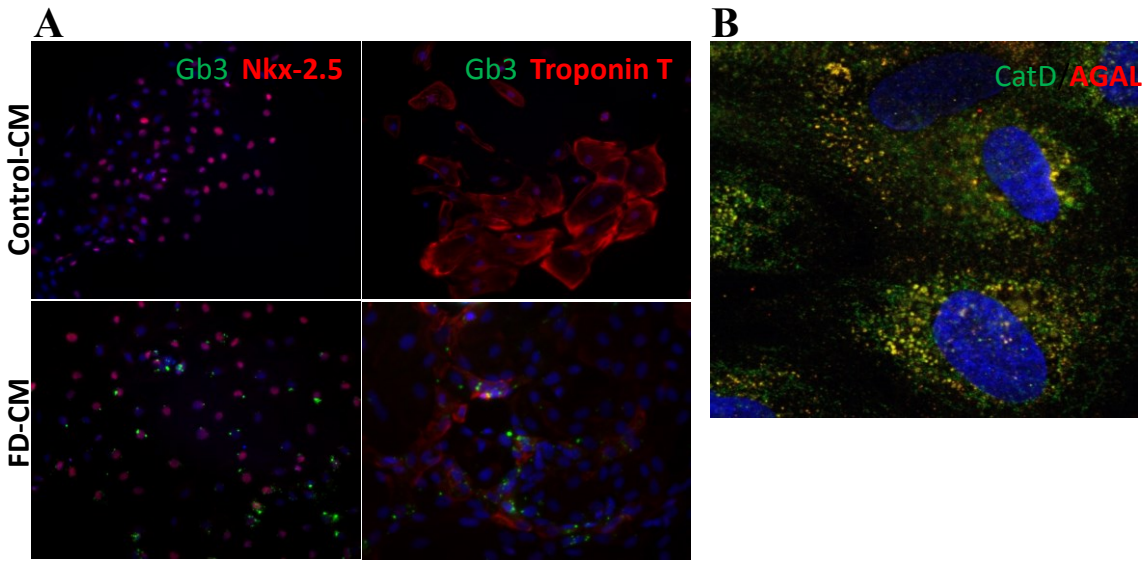

Fig.26: Demonstration of FD phenotype in generated CM.
(A) Significant accumulation of Gb3Cer in FD-CM (bottom line) compared to undetectable one in the control-CM (top line). Functionally organized contractile proteins into fibers in control-CM versus less numerous and disorganized fibers in FD-CM (right column). (B) Internalization of recombinant enzyme (AGAL) into the lysosomes (CatD) of the FD-CM.

In summary, we have created suitable human model of FD-CM which reflect basic phenotypic features typical for FD and can be used for testing of various therapeutic options. Despite the current preference of treatment by recombinant enzymes, other approaches are being developed to overcome some of the negative features of ERT such as need for weekly/biweekly intravenous infusion of the recombinant enzyme or its inability to cross BBB. In the follow up study, prepared cultures of functional human CM will be used for testing small pharmacological chaperones which can stabilize the protein molecule of the enzyme during its synthesis, improve

transport to the lysosomes, and thus achieve significant enzyme activity of selected amenable AGAL mutants.

Reference: Supplementary material F

4.2.4. CRISPR/Cas9 generation of iPSC models of FD and Schindler disease

Phylogenetic analysis of AGAL clearly identifies closely related paralogous α-N-acetyl-galactosaminidase (NAGA) which activity is deficient in patients with Schindler disease (Scriver et al 2001). As NAGA has significant overlap of substrate specificity *in vitro* with AGAL, it has been discussed for a long time how much is NAGA activity contributing to the degradation of AGAL substrates *in vivo*. Previously published results (Asfaw et al 2002) of metabolic experiments in cultures of skin fibroblasts from FD and Schindler disease patients demonstrated that longer AGAL substrates with longer saccharide chain (e.g. B-6-2) are partially degraded even in AGAL activity deficient cells (up to 50%). It has been hypothesized that in contrast with lipophilic Gb3Cer with shorter saccharide chain, more hydrophilic B-6-2 can be degraded to small extent by NAGA that even does not require small activator protein SAP B as in case of Gb3Cer degradation by AGAL. However, at the time of previous experiments, it was not possible to easily and reliably exclude the contribution of NAGA activity in FD cells and thus prove its effect on degradation of AGAL substrate with long carbohydrate chain. Such types of experiments were made possible with recent advances in genome editing tools such as CRISPR/Cas9.

CRISPR/Cas9 is a microbial adaptive immune system that uses RNA-guided nucleases to cleave foreign genetic elements in bacterial genome. Soon after its discovery, this system was exploited as a tool for rapid and highly efficient generation of gene knock-out cell lines particularly useful for genetic disease modeling. Cas9 nuclease induces double strand breaks (DSBs) at desired genomic loci, triggering the endogenous DNA repair machinery. Processing of DSBs by the error-prone nonhomologous end-joining (NHEJ) pathway leads to small insertions and deletions (indels) disrupting the reading frames and leading to loss-of-function mutations (Ran et al 2013).

We successfully applied CRISPR/Cas9 system for efficient genome modification in human iPSCs (Ran et al 2013) to generate gene knock-outs of two studied lysosomal hydrolases, AGAL and NAGA. The set of three model lines, consisting of single knock-outs of *GLA* (AGAL-KO) gene, *NAGA* (NAGA-KO) gene and combined double knock-out (D-KO) of both

genes simultaneously, was prepared to elucidate the supposed overlap of substrate specificities of both evolutionarily related hydrolases (Scriver et al 2001; Asfaw et al 2002).

Deficient activity of particular enzymes in cell homogenates by in vitro enzyme assay (Hartree 1972; Voznyi et al 2001) confirmed the successful generation of knock-out lines (Table 4).

Table 4: Confirmation of the enzyme's deficiencies in iPSCs after genome editing by CRISPR/Cas9.

Sample	NAGA activity [nmol/mg.hod]	AGAL activity [nmol/mg.hod]	β-GAL activity* [nmol/mg.hod]
AGAL-KO	23,436	0,256	124,416
NAGA-KO	0,126	58,368	168,448
D-KO	0,126	0	147,456
Control	17,073	46,848	158,464

*control enzyme

To address the hypothesis that NAGA activity is contributing to degradation of polar AGAL substrates, we performed loading experiments with tritium-labeled natural substrates, globotetraosylceramide (Gb4Cer - precursor of Gb3Cer), A-6-2 (GalNAc(α1→3)[Fuc α1→2]Gal(β1→4)GlcNAc(β1→3)Gal(β1→4)Glc(β1→1')Cer, IV(2)-α-fucosyl-IV(3)-α-N-acetylgalactosaminylneolactotetraosylceramide) and B-6-2 glycolipids (Gal(α1→3)[Fuc α1→2]Gal(β1→4)GlcNAc(β1→3)Gal(β1→4)Glc(β1→1')Cer, IV(2)-α-fucosyl-IV(3)-α-galactosyl-neolactotetraosylceramide) in cultures of the control and all three knock-outs of spontaneously differentiated iPSC lines. All tritium-labeled lipids were re-purified as described previously (Asfaw et al 2002).

As expected these experiments clearly show the block in degradation of Gb3Cer produced *in situ* from loaded Gb4Cer in AGAL-KO and D-KO in contrast with normal degradation of this substrate in control cells and in NAGA-KO (**Fig.27**, first column). The degradation of A-6-2 with terminal α-N-acetylgalactosamine is blocked, as expected, in NAGA-KO and D-KO cells, while this substrate is degraded normally in control cells and in AGAL-KO cells. The degradation pattern of B-6-2 in AGAL-KO is suggesting relatively high residual degradation of this substrate which is in accordance with previously published results (Asfaw et al 2002). However, this residual degradation does not seem to be affected by knocking-out the NAGA

activity which was hypothesized to be responsible for observed degradation of B-6-2 in FD cells. The degradation of B-6-2 in control cell and in NAGA-KO is normal as expected.

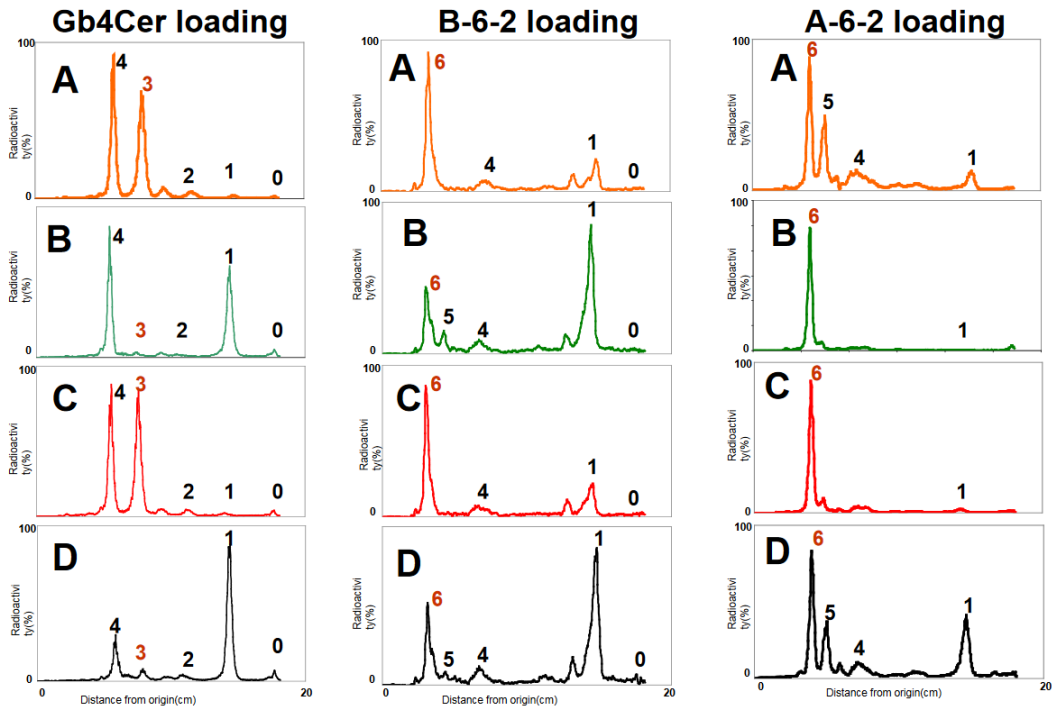

Fig.27: Degradation of tritium-labeled glycolipids Gb4Cer, B-6-2 and A-6-2 by spontaneously differentiated iPSC with knockout of *GLA* and *NAGA* genes and double knockouts of both genes. Lipid pattern of AGAL-KO (A), NAGA-KO (B), D-KO (C) cell lines and of **control cells (D).** The chromatographic positions of substrate and various degradation products are indicated by number of monosaccharide residues in the glycolipid chain: e.g **1** = glucosylceramide, **4** = Gb4Cer. In the cells with AGAL deficiency, a significant block in degradation of glycolipids B-6-2 and Gb3Cer is evident, whereas in NAGA deficient cells, the degradation of A-6-2 is blocked. In double knockout cells none of the three glycolipid substrates was degraded. Conduritol B-epoxide was added to all cultures in order to inhibit glycolipid hydrolysis at the penultimate step catalyzed by β-glucocerebrosidase (peak number 1).

Taken these results together, it seems that there is still another enzyme (or mechanism) that is causing the partial degradation of more polar substrates of AGAL in cells. One of the candidates would be non-lysosomal, neutral α-galactosidase that would partially access these substrates in AGAL deficient cells. The exact identification of this mechanism would be the topic of further studies on these model cellular systems in combination with other advanced techniques (e.g. MS methods).

Reference: Supplementary material G

5. CONCLUSIONS

5.1. Study of human and mouse tissues with biochemical phenotype of FD focused on the nature of storage of undegradable substrates.

5.1.1. Investigation of metabolic fate of glycoconjugates with terminal α-galactosyl moieties in the pancreas of FD patients with blood group B (FD-B), has led to the following findings:

- Examination of the metabolic fate of glycoconjugates with terminal α-galactosyl moieties revealed the massive deposition of complex B-GSL (with more than 5 monosaccharide units) as well as non-lipid B-glycoconjugates in the pancreas of patients with blood group B (FD-B).
- Acinar cells of the exocrine pancreas and vascular endothelial cells were the major sites of increased expression of blood group B-specific antigens accompanied by massive ceroid deposition, whereas the endocrine pancreas (islets of Langerhans) and ductal epithelium were completely free of storage. Co-labeling with the lysosomal marker LAMP2 pointed to lysosomal character of the deposition.
- Interestingly, acini cells were only weakly positive for Gb3Cer, classical storage compound in FD, dominating in the kidneys. The tissue/cell/substrate variability in FD points to differences in metabolic turnover of organ-specific cell types as well as subcellular lipid distribution. We assume that these results could initiate further research of cellular functions influenced by pathological processes in FD.

5.1.2. Study of renal distribution of sphingolipid molecular species in the knockout model of FD (FKO) resulted in the following:

- 34-fold increase of Gb3Cer in the FKO renal tissue has been documented by FIA-ESI-MS/MS analysis. The second stored lipid in FKO mouse was classically Ga2Cer and similar results were obtained by both MALDI mass spectrometry imaging (MSI) and FIA-MS/MS.

- Immunohistochemistry proved higher accumulation of Gb3Cer in renal cortex of the FKO mouse sections compared to the medulla which correlated well with the MSI analysis. Cortical tubules were significantly more affected than glomeruli and renal tubules of the medulla of the FKO mice which evokes pathologically similar human later-onset phenotype of FD.
- The major benefit of MSI in comparison with IHC was the identification of the spatial distribution of sphingolipids and their specific isoforms, which represent true chemical imaging of individual molecular species. Thus, MSI identified five elevated Gb3Cer isoforms and their exact distribution in renal regions of the FKO and WT mice.

5.2. Creation of human FD and MPS II cell models using induced pluripotent stem cell technology.

- We have created human iPSC models of two X-linked LSD- MPSII and FD - expressing the pluripotency markers OCT3/4, LIN28, SSEA4, TRA-1-81 and ALP. These stable iPSC models have been used for further investigation studies.

5.2.1. X chromosome inactivation analysis in female patients with FD and MPSII:

- The cultivation of primed iPSC in naïve culture condition led to the changes of the cell colony morphology indicating a conversion of primed iPSC to naïve state. The methylation status at the AR locus show the change in XCI ratio in the case of the FD but not of the MPSII clones.

5.2.2. Neural model of CNS involvement in MPSII:

- We have succeeded in differentiation of control and MPSII iPSC into the mixture of neural cells (neurons and glial cells). Compared to control, neural cells of MPSII patients accumulated increased amount of GAG with numerous abnormally sized lysosomes.

- The treatment with commercially available recombinant enzyme did not prevent the increase of GAG levels in MPSII cultures. As heparan sulphate was detected mainly on plasma membrane, we hypothesize that increased level of GAG in terminally differentiated neural cells is given by their presence on plasma membrane where recombinant enzyme is not active.

5.2.3. FD cardiomyocytes generated from iPSC as a human model for testing of therapeutic effect of pharmacological chaperones:

- We have successfully differentiated control and FD-iPSC into functional CM exhibiting phenotypic features typical for FD such as increased accumulation of Gb3Cer and reduced ability of functional fibers creation.
- Lysosomal internalization of recombinant enzymes was confirmed. In the follow up study, functional human CM will be used for testing of pharmacological chaperones.

5.2.4. CRISPR/Cas9 generation of iPSC models of FD and Schindler disease:

- We applied CRISPR/Cas9 system for efficient genome modification in human iPSCs and created iPSC knockout models of FD and Schindler disease. Double knockout of both genes encoding particular hydrolases was also formed.
- Loading experiments of tritium-labeled glycolipids did not confirm contribution of NAGA (deficient in Schindler disease) to the degradation of the substrates of AGAL. Due to the limitations of the radiochemical method, other advanced biochemical techniques will be used in the follow up study to identify mechanism of degradation of more polar AGAL substrates.

In summary, the presented work has broadened the knowledge of pathobiochemistry and cell pathology of FD and has successfully dealt with the preparation of cellular model systems applicable not only to LSD but to rare genetic diseases in general. Introduction and mastering the techniques of iPSC models generation is already being used in a number of research projects

at our department. We believe that this work also extends the possibilities of testing therapeutic options for disease-specific cell types.

6. REFERENCES

All AH, Gharibani P, Gupta S, et al (2015) Early intervention for spinal cord injury with human induced pluripotent stem cells oligodendrocyte progenitors. *PLoS One* 10: e0116933.

Amenduni M, De Filippis R, Cheung AY, et al (2011) iPS cells to model CDKL5-related disorders. *Eur J Hum Genet* 19: 1246-1255.

Ananiev G, Williams EC, Li H, Chang Q (2011) Isogenic pairs of wild type and mutant induced pluripotent stem cell (iPSC) lines from Rett syndrome patients as in vitro disease model. *PLoS One* 6: e25255.

Asfaw B, Ledvinova J, Dobrovolny R, et al (2002) Defects in degradation of blood group A and B glycosphingolipids in Schindler and Fabry diseases. *J Lipid Res* 43: 1096-1104.

Berdasco M, Esteller M (2011) DNA methylation in stem cell renewal and multipotency. *Stem Cell Res Ther* 2: 42.

Blau HM, Chiu CP, Webster C (1983) Cytoplasmic activation of human nuclear genes in stable heterocaryons. *Cell* 32: 1171-1180.

Boado RJ, Hui EK, Lu JZ, Sumbria RK, Pardridge WM (2013) Blood-brain barrier molecular trojan horse enables imaging of brain uptake of radioiodinated recombinant protein in the rhesus monkey. *Bioconjug Chem* 24: 1741-1749.

Canfield SG, Stebbins MJ, Morales BS, et al (2017) An isogenic blood-brain barrier model comprising brain endothelial cells, astrocytes, and neurons derived from human induced pluripotent stem cells. *J Neurochem* 140: 874-888.

Carroll D (2017) Genome Editing: Past, Present, and Future. *Yale J Biol Med* 90: 653-659.

Czechowicz A, Weissman IL (2011) Purified hematopoietic stem cell transplantation: the next generation of blood and immune replacement. *Hematol Oncol Clin North Am* 25: 75-87.

Dandulakis MG, Meganathan K, Kroll KL, Bonni A, Constantino JN (2016) Complexities of X chromosome inactivation status in female human induced pluripotent stem cells-a brief review and scientific update for autism research. *J Neurodev Disord* 8: 22.

Davis RL, Weintraub H, Lassar AB (1987) Expression of a single transfected cDNA converts fibroblasts to myoblasts. *Cell* 51: 987-1000.

De Los Angeles A, Loh YH, Tesar PJ, Daley GQ (2012) Accessing naive human pluripotency. *Curr Opin Genet Dev* 22: 272-282.

De Vos J, Bouckenheimer J, Sansac C, Lemaitre JM, Assou S (2016) Human induced pluripotent stem cells: A disruptive innovation. *Curr Res Transl Med* 64: 91-96.

Dean L (2012) ABO Blood Group. In Pratt V, McLeod H, Dean L, Malheiro A, Rubinstein W eds. *Medical Genetics Summaries* Bethesda (MD).

Desnick RJ, Ioannou YA, Eng CM (2001) α-Galactosidase A Deficiency: Fabry Disease. In Scriver CR, Beaudet AL, Sly WS, Valle D eds. *The Metabolic and Molecular Bases of Inherited Disease* New York: McGraw-Hill, 3733-3774.

Di-Battista A, Meloni VA, da Silva MD, Moyses-Oliveira M, Melaragno MI (2016) Unusual X-chromosome inactivation pattern in patients with Xp11.23-p11.22 duplication: Report and review. *Am J Med Genet A* 170: 3271-3275.

Diecke S, Jung SM, Lee J, Ju JH (2014) Recent technological updates and clinical applications of induced pluripotent stem cells. *Korean J Intern Med* 29: 547-557.

Durant B, Forni S, Sweetman L, et al (2011) Sex differences of urinary and kidney globotriaosylceramide and lyso-globotriaosylceramide in Fabry mice. *J Lipid Res* 52: 1742-1746.

Elleder M (2010) Subcellular, Cellular and Organ Pathology of Fabry Disease. In Elstein D, Altarescu G, Beck M eds. *Fabry Disease* Dordrecht: Springer Science+Business Media B.V., 211-243.

Evans MJ, Kaufman MH (1981) Establishment in culture of pluripotential cells from mouse embryos. *Nature* 292: 154-156.

Fusaki N, Ban H, Nishiyama A, Saeki K, Hasegawa M (2009) Efficient induction of transgene-free human pluripotent stem cells using a vector based on Sendai virus, an RNA virus that does not integrate into the host genome. *Proc Jpn Acad Ser B Phys Biol Sci* 85: 348-362.

Fusar Poli E, Zalfa C, D'Avanzo F, et al (2013) Murine neural stem cells model Hunter disease in vitro: glial cell-mediated neurodegeneration as a possible mechanism involved. *Cell Death Dis* 4: e906.

Gafni O, Weinberger L, Mansour AA, et al (2013) Derivation of novel human ground state naive pluripotent stem cells. *Nature* 504: 282-286.

Gallagher JT (2006) Multiprotein signalling complexes: regional assembly on heparan sulphate. *Biochem Soc Trans* 34: 438-441.

Garratty G, Glynn SA, McEntire R (2004) ABO and Rh(D) phenotype frequencies of different racial/ethnic groups in the United States. *Transfusion* 44: 703-706.

Gomes IC, Acquarone M, Maciel Rde M, Erlich RB, Rehen SK (2010) Analysis of pluripotent stem cells by using cryosections of embryoid bodies. *J Vis Exp*.

Gomes KM, Costa IC, Santos JF, Dourado PM, Forni MF, Ferreira JC (2017) Induced pluripotent stem cells reprogramming: Epigenetics and applications in the regenerative medicine. *Rev Assoc Med Bras (1992)* 63: 180-189.

Grabel L (2012) Prospects for pluripotent stem cell therapies: into the clinic and back to the bench. *J Cell Biochem* 113: 381-387.

Gupta G, Surolia A (2010) Glycosphingolipids in microdomain formation and their spatial organization. *FEBS Lett* 584: 1634-1641.

Gurdon JB, Elsdale TR, Fischberg M (1958) Sexually mature individuals of Xenopus laevis from the transplantation of single somatic nuclei. *Nature* 182: 64-65.

Hakomori S, Handa K (2002) Glycosphingolipid-dependent cross-talk between glycosynapses interfacing tumor cells with their host cells: essential basis to define tumor malignancy. *FEBS Lett* 531: 88-92.

Hartree EF (1972) Determination of protein: a modification of the Lowry method that gives a linear photometric response. *Anal Biochem* 48: 422-427.

Hawkins-Salsbury JA, Reddy AS, Sands MS (2011) Combination therapies for lysosomal storage disease: is the whole greater than the sum of its parts? *Hum Mol Genet* 20: R54-60.

Hockemeyer D, Jaenisch R (2016) Induced Pluripotent Stem Cells Meet Genome Editing. *Cell Stem Cell* 18: 573-586.

Hotta A, Cheung AY, Farra N, et al (2009) Isolation of human iPS cells using EOS lentiviral vectors to select for pluripotency. *Nat Methods* 6: 370-376.

Hou P, Li Y, Zhang X, et al (2013) Pluripotent stem cells induced from mouse somatic cells by small-molecule compounds. *Science* 341: 651-654.

Hsu YC, Chen CT, Wei YH (2016) Mitochondrial resetting and metabolic reprogramming in induced pluripotent stem cells and mitochondrial disease modeling. *Biochim Biophys Acta* 1860: 686-693.

Huang P, He Z, Ji S, et al (2011) Induction of functional hepatocyte-like cells from mouse fibroblasts by defined factors. *Nature* 475: 386-389.

Hulkova H, Elleder M (2010) Adipocytes participate in storage in alpha-galactosidase deficiency (Fabry disease). *J Inherit Metab Dis* 33 Suppl 3: S297-300.

Chen J, Riazifar H, Guan MX, Huang T (2016) Modeling autosomal dominant optic atrophy using induced pluripotent stem cells and identifying potential therapeutic targets. *Stem Cell Res Ther* 7: 2.

Chester MA (1998) IUPAC-IUB Joint Commission on Biochemical Nomenclature (JCBN). Nomenclature of glycolipids--recommendations 1997. *Eur J Biochem* 257: 293-298.

Chien YH, Peng SF, Yang CC, et al (2013) Long-term efficacy of miglustat in paediatric patients with Niemann-Pick disease type C. *J Inherit Metab Dis* 36: 129-137.

Ieda M, Fu JD, Delgado-Olguin P, et al (2010) Direct reprogramming of fibroblasts into functional cardiomyocytes by defined factors. *Cell* 142: 375-386.

Ioannou YA, Zeidner KM, Gordon RE, Desnick RJ (2001) Fabry disease: preclinical studies demonstrate the effectiveness of alpha-galactosidase A replacement in enzyme-deficient mice. *Am J Hum Genet* 68: 14-25.

Itier JM, Ret G, Viale S, et al (2014) Effective clearance of GL-3 in a human iPSC-derived cardiomyocyte model of Fabry disease. *J Inherit Metab Dis* 37: 1013-1022.

Ito N (1992) Histochemical localization and analysis of blood group-related antigens in human pancreas using immunostaining with monoclonal antibodies and exoglycosidase digestio. *Prog Histochem Cytochem* 25: 1-85.

Iwabuchi K, Nakayama H, Iwahara C, Takamori K (2010) Significance of glycosphingolipid fatty acid chain length on membrane microdomain-mediated signal transduction. *FEBS Lett* 584: 1642-1652.

Jakobkiewicz-Banecka J, Gabig-Ciminska M, Kloska A, et al (2016) Glycosaminoglycans and mucopolysaccharidosis type III. *Front Biosci (Landmark Ed)* 21: 1393-1409.

Kim D, Kim CH, Moon JI, et al (2009) Generation of human induced pluripotent stem cells by direct delivery of reprogramming proteins. *Cell Stem Cell* 4: 472-476.

Kim K, Doi A, Wen B, et al (2010) Epigenetic memory in induced pluripotent stem cells. *Nature* 467: 285-290.

Kolios G, Moodley Y (2013) Introduction to stem cells and regenerative medicine. *Respiration* 85: 3-10.

Kopitz J (2017) Lipid glycosylation: a primer for histochemists and cell biologists. *Histochem Cell Biol* 147: 175-198.

Lancaster MA, Renner M, Martin CA, et al (2013) Cerebral organoids model human brain development and microcephaly. *Nature* 501: 373-379.

Lantini MS, Cossu M (1997) Ultrastructural localization of blood group antigens in human exocrine pancreas by immunogold labelling. *J Submicrosc Cytol Pathol* 29: 245-251.

Lian X, Zhang J, Azarin SM, et al (2013) Directed cardiomyocyte differentiation from human pluripotent stem cells by modulating Wnt/beta-catenin signaling under fully defined conditions. *Nat Protoc* 8: 162-175.

Lidove O (2002) Influence of blood groups B or AB on phenotype in a population of hemizygous patients with Fabry disease. 439: 124.

Lindahl U, Couchman J, Kimata K, Esko JD (2015) Proteoglycans and Sulfated Glycosaminoglycans. In Varki A, Cummings RD, Esko JD et al eds. *Essentials of Glycobiology* Cold Spring Harbor (NY).

Macauley SL (2016) Combination Therapies for Lysosomal Storage Diseases: A Complex Answer to a Simple Problem. *Pediatr Endocrinol Rev* 13 Suppl 1: 639-648.

Maherali N, Sridharan R, Xie W, et al (2007) Directly reprogrammed fibroblasts show global epigenetic remodeling and widespread tissue contribution. *Cell Stem Cell* 1: 55-70.

Marchetto MC, Carromeu C, Acab A, et al (2010) A model for neural development and treatment of Rett syndrome using human induced pluripotent stem cells. *Cell* 143: 527-539.

Martin GR (1981) Isolation of a pluripotent cell line from early mouse embryos cultured in medium conditioned by teratocarcinoma stem cells. *Proc Natl Acad Sci U S A* 78: 7634-7638.
Mason JA, Aung HT, Nandini A, et al (2018) Demonstration of a novel Xp22.2 microdeletion as the cause of familial extreme skewing of X-inactivation utilizing case-parent trio SNP microarray analysis. *Mol Genet Genomic Med*.
Mayes JS, Scheerer JB, Sifers RN, Donaldson ML (1981) Differential assay for lysosomal alpha-galactosidases in human tissues and its application to Fabry's disease. *Clin Chim Acta* 112: 247-251.
Mehta A, Winchester B (2012) *Lysosomal Stotage Disorders: A Practical Guide*, West Sussex, UK: Wiley-Blackwell, John Wiley & Sons, Ltd. .
Mekhoubad S, Bock C, de Boer AS, Kiskinis E, Meissner A, Eggan K (2012) Erosion of dosage compensation impacts human iPSC disease modeling. *Cell Stem Cell* 10: 595-609.
Meloncelli PJ, Lowary TL (2010) Synthesis of ABO histo-blood group type I and II antigens. *Carbohydr Res* 345: 2305-2322.
Meng Y, Sohar I, Sleat DE, et al (2014) Effective intravenous therapy for neurodegenerative disease with a therapeutic enzyme and a peptide that mediates delivery to the brain. *Mol Ther* 22: 547-553.
Merrill AH, Jr., Wang MD, Park M, Sullards MC (2007) (Glyco)sphingolipidology: an amazing challenge and opportunity for systems biology. *Trends Biochem Sci* 32: 457-468.
Musunuru K (2013) Genome editing of human pluripotent stem cells to generate human cellular disease models. *Dis Model Mech* 6: 896-904.
Novgorodov SA, Gudz TI (2011) Ceramide and mitochondria in ischemic brain injury. *Int J Biochem Mol Biol* 2: 347-361.
Ohshima T, Murray GJ, Swaim WD, et al (1997) alpha-Galactosidase A deficient mice: a model of Fabry disease. *Proc Natl Acad Sci U S A* 94: 2540-2544.
Ohshima T, Schiffmann R, Murray GJ, et al (1999) Aging accentuates and bone marrow transplantation ameliorates metabolic defects in Fabry disease mice. *Proc Natl Acad Sci U S A* 96: 6423-6427.
Perrimon N, Bernfield M (2001) Cellular functions of proteoglycans--an overview. *Semin Cell Dev Biol* 12: 65-67.
Pinheiro I, Heard E (2017) X chromosome inactivation: new players in the initiation of gene silencing. *F1000Res* 6.
Ponder KP (2008) Immune response hinders therapy for lysosomal storage diseases. *J Clin Invest* 118: 2686-2689.
Ran FA, Hsu PD, Wright J, Agarwala V, Scott DA, Zhang F (2013) Genome engineering using the CRISPR-Cas9 system. *Nat Protoc* 8: 2281-2308.
Ravn V, Dabelsteen E (2000) Tissue distribution of histo-blood group antigens. *Apmis* 108: 1-28.
Robinton DA, Daley GQ (2012) The promise of induced pluripotent stem cells in research and therapy. *Nature* 481: 295-305.
Russo FB, Cugola FR, Fernandes IR, Pignatari GC, Beltrao-Braga PC (2015) Induced pluripotent stem cells for modeling neurological disorders. *World J Transplant* 5: 209-221.
Sandhoff K (2013) Metabolic and cellular bases of sphingolipidoses. *Biochem Soc Trans* 41: 1562-1568.
Sato T, Stange DE, Ferrante M, et al (2011) Long-term expansion of epithelial organoids from human colon, adenoma, adenocarcinoma, and Barrett's epithelium. *Gastroenterology* 141: 1762-1772.

Scriver CR, Beaudet AL, Sly WS, Valle D (2001) *The Metabolic and Molecular Bases of Inherited Disease*, New York: McGraw-Hill.
Shi Y, Inoue H, Wu JC, Yamanaka S (2017) Induced pluripotent stem cell technology: a decade of progress. *Nat Rev Drug Discov* 16: 115-130.
Schenkel-Brunner H (1995) *Human blood groups : chemical and biochemical basis of antigen specificity*, Wien ; New York: Springer-Verlag.
Singh VK, Saini A, Kalsan M, Kumar N, Chandra R (2016) Describing the Stem Cell Potency: The Various Methods of Functional Assessment and In silico Diagnostics. *Front Cell Dev Biol* 4: 134.
Skalova S, Svadlakova T, Shaikh Qureshi WM, Dev K, Mokry J (2015) Induced pluripotent stem cells and their use in cardiac and neural regenerative medicine. *Int J Mol Sci* 16: 4043-4067.
Skoog WA, Beck WS (1956) Studies on the fibrinogen, dextran and phytohemagglutinin methods of isolating leukocytes. *Blood* 11: 436-454.
Smolarek D, Krop-Watorek A, Wasniowska K, Czerwinski M (2008) [Molecular background of the ABO blood group system]. *Postepy Hig Med Dosw (Online)* 62: 4-17.
Soldner F, Hockemeyer D, Beard C, et al (2009) Parkinson's disease patient-derived induced pluripotent stem cells free of viral reprogramming factors. *Cell* 136: 964-977.
Stacpoole SR, Bilican B, Webber DJ, et al (2011) Efficient derivation of NPCs, spinal motor neurons and midbrain dopaminergic neurons from hESCs at 3% oxygen. *Nat Protoc* 6: 1229-1240.
Stadtfeld M, Nagaya M, Utikal J, Weir G, Hochedlinger K (2008) Induced pluripotent stem cells generated without viral integration. *Science* 322: 945-949.
Suarez-Guerrero JL, Gomez Higuera PJ, Arias Florez JS, Contreras-Garcia GA (2016) [Mucopolysaccharidosis: clinical features, diagnosis and management]. *Rev Chil Pediatr* 87: 295-304.
Takahashi K, Tanabe K, Ohnuki M, et al (2007) Induction of pluripotent stem cells from adult human fibroblasts by defined factors. *Cell* 131: 861-872.
Takahashi K, Yamanaka S (2006) Induction of pluripotent stem cells from mouse embryonic and adult fibroblast cultures by defined factors. *Cell* 126: 663-676.
Takahashi K, Yamanaka S (2016) A decade of transcription factor-mediated reprogramming to pluripotency. *Nat Rev Mol Cell Biol* 17: 183-193.
Tapscott SJ, Davis RL, Thayer MJ, Cheng PF, Weintraub H, Lassar AB (1988) MyoD1: a nuclear phosphoprotein requiring a Myc homology region to convert fibroblasts to myoblasts. *Science* 242: 405-411.
Terman A, Brunk UT (1998) Ceroid/lipofuscin formation in cultured human fibroblasts: the role of oxidative stress and lysosomal proteolysis. *Mech Ageing Dev* 104: 277-291.
Tesar PJ, Chenoweth JG, Brook FA, et al (2007) New cell lines from mouse epiblast share defining features with human embryonic stem cells. *Nature* 448: 196-199.
Thomson JA, Itskovitz-Eldor J, Shapiro SS, et al (1998) Embryonic stem cell lines derived from human blastocysts. *Science* 282: 1145-1147.
Tchieu J, Kuoy E, Chin MH, et al (2010) Female human iPSCs retain an inactive X chromosome. *Cell Stem Cell* 7: 329-342.
Tomoda K, Takahashi K, Leung K, et al (2012) Derivation conditions impact X-inactivation status in female human induced pluripotent stem cells. *Cell Stem Cell* 11: 91-99.
Ulrich-Bott B, Wiegandt H (1984) Micellar properties of glycosphingolipids in aqueous media. *J Lipid Res* 25: 1233-1245.
Valbuena C, Oliveira JP, Carneiro F, et al (2011) Kidney histologic alterations in alpha-Galactosidase-deficient mice. *Virchows Arch* 458: 477-486.

van Meer G, Voelker DR, Feigenson GW (2008) Membrane lipids: where they are and how they behave. *Nat Rev Mol Cell Biol* 9: 112-124.
Varum S, Rodrigues AS, Moura MB, et al (2011) Energy metabolism in human pluripotent stem cells and their differentiated counterparts. *PLoS One* 6: e20914.
Vierbuchen T, Ostermeier A, Pang ZP, Kokubu Y, Sudhof TC, Wernig M (2010) Direct conversion of fibroblasts to functional neurons by defined factors. *Nature* 463: 1035-1041.
Voznyi YV, Keulemans JL, van Diggelen OP (2001) A fluorimetric enzyme assay for the diagnosis of MPS II (Hunter disease). *J Inherit Metab Dis* 24: 675-680.
Warren L, Manos PD, Ahfeldt T, et al (2010) Highly efficient reprogramming to pluripotency and directed differentiation of human cells with synthetic modified mRNA. *Cell Stem Cell* 7: 618-630.
Wennekes T, van den Berg RJ, Boot RG, van der Marel GA, Overkleeft HS, Aerts JM (2009) Glycosphingolipids--nature, function, and pharmacological modulation. *Angew Chem Int Ed Engl* 48: 8848-8869.
Wilmut I, Schnieke AE, McWhir J, Kind AJ, Campbell KH (1997) Viable offspring derived from fetal and adult mammalian cells. *Nature* 385: 810-813.
Wraith JE, Scarpa M, Beck M, et al (2008) Mucopolysaccharidosis type II (Hunter syndrome): a clinical review and recommendations for treatment in the era of enzyme replacement therapy. *Eur J Pediatr* 167: 267-277.
Wu J, Ocampo A, Izpisua Belmonte JC (2016) Cellular Metabolism and Induced Pluripotency. *Cell* 166: 1371-1385.
Yamakawa T (1996) A reflection on the early history of glycosphingolipids. *Glycoconj J* 13: 123-126.
Yu J, Hu K, Smuga-Otto K, et al (2009) Human induced pluripotent stem cells free of vector and transgene sequences. *Science* 324: 797-801.
Yu J, Vodyanik MA, Smuga-Otto K, et al (2007) Induced pluripotent stem cell lines derived from human somatic cells. *Science* 318: 1917-1920.
Zhou W, Freed CR (2009) Adenoviral gene delivery can reprogram human fibroblasts to induced pluripotent stem cells. *Stem Cells* 27: 2667-2674.

7. SUPPLEMENTARY PUBLICATIONS

Publications in impacted journals related to the topic of this Ph.D. thesis

A – **Rybová** J, Kuchař L, Hůlková H, Asfaw B, Dobrovolný R, Sikora J, Havlíček V, Škultéty L and Ledvinová J: Specific storage of glycoconjugates with terminal α-galactosyl moieties in the exocrine pancreas of Fabry disease patients with blood group B; Glycobiology, 2018 Jun; **28**(6): p. 382-391. **IF 3.112**

B – Kuchar L, Faltyskova H, Krasny L, Dobrovolny R, Hulkova H, Ledvinova J, Volny M, Strohalm M, Lemr K, Kryspinova L, Asfaw B, **Rybová J**, Desnick RJ, Havlicek V: Fabry disease: renal sphingolipid distribution in the α-Gal A knockout mouse model by mass spectrometric and immunohistochemical imaging. Anal Bioanal Chem, 2015 Mar; **407**(8): p. 2283-91. **IF 3.125**

C – Kuchař L, Asfaw B, **Rybová J**, Ledvinová J.: Tandem Mass Spectrometry of Sphingolipids: Applications for Diagnosis of Sphingolipidoses. Adv Clin Chem, 2016; **77**: p. 177-219. **IF 4.722**

D – Řeboun M, **Rybová J**, Dobrovolný R, Včelák J, Veselková T, Štorkánová G, Mušálková D, Hřebíček M, Ledvinová J, Magner M, Zeman J, Pešková K, Dvořáková L.: X-Chromosome Inactivation Analysis in Different Cell Types and Induced Pluripotent Stem Cells Elucidates the Disease Mechanism in a Rare Case of Mucopolysaccharidosis Type II in a Female. Folia Biol (Praha), 2016; **62**(2): p. 82-9. **IF 0.939**

E – **Rybová J**, Ledvinová J, Sikora J, Kuchař L, Dobrovolný R.: Neural cells generated from human induced pluripotent stem cells as a model of CNS involvement in mucopolysaccharidosis type II. J Inherit Metab Dis, 2018 Mar; **41**(2): p. 221-229. **IF 3.970**

Non impacted publications related to topic of this PhD thesis

F – Conference abstract and poster

December 2014 – poster presentation: The 2014 ascb/ifcb meeting, Philadelphia, Pennsylvania; USA: Rybová J, Dobrovolný R, Asfaw B, Sládková J, Hyliš M, Ledvinová J: Fabry cardiomyocytes generated from induced pluripotent stem cells as a human model for morphology and pathobiochemistry studies

G – Conference abstract and poster

October 2015 – poster presentation: ESGLD, Pozzuoly, Italy: Rybova J, Asfaw B, Poupetova H, Kuchar L, Ledvinova J, Dobrovolny R: Crispr/Cas9 Generation Of iPSC Models Of Fabry And Schindler Disease

7.1. Publications in impacted journals related to the topic of this Ph.D. thesis

Supplementary publication A

Rybová J, Kuchař L, Hůlková H, Asfaw B, Dobrovolný R, Sikora J, Havlíček V, Škultéty L and Ledvinová J: Specific storage of glycoconjugates with terminal α-galactosyl moieties in the exocrine pancreas of Fabry disease patients with blood group B; Glycobiology, 2018 Jun; **28**(6): p. 382-391. **IF 3.112**

Glycobiology, 2018, 1–10
doi: 10.1093/glycob/cwy026
Original Article

OXFORD

Chemical Biology

Specific storage of glycoconjugates with terminal α-galactosyl moieties in the exocrine pancreas of Fabry disease patients with blood group B

Jitka Rybová[2], Ladislav Kuchař[2], Helena Hůlková[2,3], Befekadu Asfaw[2], Robert Dobrovolný[2], Jakub Sikora[2,3], Vladimír Havlíček[4], Ľudovít Škultéty[4], and Jana Ledvinová[2,1]

[2]Research Unit For Rare Diseases, Department of Pediatrics and Adolescent Medicine, First Faculty of Medicine, Charles University and General University Hospital, Prague, 12808, Czech Republic, [3]Institute of Pathology, First Faculty of Medicine, Charles University and General University Hospital, Prague 12808, Czech Republic, and [4]Institute of Microbiology of the CAS, v.v.i., Videnska 1083, 14220 Prague 4, Czech Republic

[1]To whom correspondence should be addressed: Tel: +420 224 967 032; Fax: +420 224 967 119; e-mail: jana.ledvinova@lf1.cuni.cz

Received 23 August 2017; Revised 2 February 2018; Editorial decision 10 March 2018; Accepted 13 March 2018

Abstract

Blood group B glycosphingolipids (B-GSLs) are substrates of the lysosomal alpha-galactosidase A (AGAL). Similar to its major substrate–globotriaosylceramide (Gb3Cer)–B-GSLs are not degraded and accumulate in the cells of patients affected by an inherited defect of AGAL activity (Fabry disease—FD).

The pancreas is a secretory organ known to have high biosynthesis of blood group GSLs. Herein, we provide a comprehensive overview of the biochemical and structural abnormalities in pancreatic tissue from two male FD patients with blood group B. In both patients, we found major accumulation of a variety of complex B-GSLs carrying predominantly hexa- and hepta-saccharide structures. The subcellular pathology was dominated by deposits containing B-glycoconjugates and autofluorescent ceroid. The contribution of Gb3Cer to the storage was minor. This abnormal storage pattern was specific for the pancreatic acinar epithelial cells. Other pancreatic cell types including those of islets of Langerhans were affected much less or not at all.

Altogether, we provide evidence for a key role of B-antigens in the biochemical and morphological pathology of the exocrine pancreas in FD patients with blood group B. We believe that our findings will trigger further studies aimed at assessing the potential pancreatic dysfunction in this disease.

Key words: blood group B antigens, ceroid, Fabry disease, Gb3Cer, pancreas

Introduction

Fabry disease (FD, OMIM 301,500) is a rare X chromosome-linked disorder (*Xq22.1*) of glycosphingolipid (GSL) catabolism. FD is caused by deficient activity of the lysosomal enzyme alpha-galactosidase A (AGAL, EC 3.2.1.22) (Desnick et al. 2001). This molecular defect leads to abnormal lysosomal accumulation of GSLs with terminal alpha-galactosyl moiety. Endothelial cells, perivascular smooth muscle cells, fibroblasts and cardiomyocytes are predominantly affected. This abnormal intracellular storage is progressive and substantially affects cardiac and renal functions in FD patients. Although the pancreas is an

organ expected to be functionally and morphologically afflicted in FD, its biochemical and structural pathologies remain understudied.

The main accumulated AGAL substrate in FD is globotriaosylceramide (Gb3Cer), which belongs to the globo-series of glycolipids. Gb3Cer is predominantly expressed in the kidney, aorta, spleen and liver (Elleder 2010).

Blood group B glycosphingolipids (B-GSLs) are additional AGAL substrates. B-GSLs are primarily expressed in the membranes of erythrocytes, though they are also present on the surface of other cell types of blood group B individuals. The blood group B determinant is characterized by the trisaccharide structure Galα1→3(Fucα1→2)Gal, which is usually attached to the lacto- and neolacto-series of glycoproteins or glycolipids (Cartron and Rouger 1995). Importantly, ABH blood group antigens are secreted into various body fluids (e.g., saliva, tears, semen, urine and gastric juice) (Jaff 2010). This release is under a genetic control of allelic secretor genes (*Se* and *se*) and is independent of the *ABO[H]* genes (Schenkel-Brunner 1995; Watkins 2001).

The pancreas consists of two disparate histological and functional compartments. The exocrine part comprises ~90% of the entire gland and is composed of secretory cells organized into acini. Apical portions of the acinar cells are filled with secretory (zymogen) granules that contain precursors of the enzymes of the pancreatic juice (Motta et al. 1997). On the contrary, the endocrine function of the pancreas is carried out by the hormone (e.g., insulin, glucagon, pancreatic polypeptide, somatostatin and ghrelin) producing cells concentrated to the islets of Langerhans (Cao and Wang 2014).

Contrary to insulin-producing β-cells (Buschard et al. 2005; Boslem et al. 2012; Manukyan et al. 2015) roles of sphingolipids and their signaling intermediates to pathologies of pancreatic acinar cells have not yet been extensively studied. The pancreas is rich in fucosylated glycoconjugates with antigenic functions. Ito (1992), Ito et al. (1993) and Uchida et al. (1986) reported that ABH antigens are present on the acinar cells, however, the centroacinar cells, cells of the intercalated pancreatic ducts and islets of Langerhans have been shown to lack these antigens.

Information about the roles and contribution of B-GSLs to the pathogenesis and clinical presentation of FD patients with blood group B (FD-B) is scarce. This is due in part to the relatively low frequency of blood group B in the general population. Abnormal storage of B-GSLs was reported in a single FD patient by Wherrett and Hakomori (1973) who showed that the two major glycolipids with hexasaccharide chains (B-6) and sub-terminal α-galactose, referred to as type 1 (lacto-) and type 2 (neolacto-) chains, could be detected in this patient's pancreas but not in other parenchymatous organs. Electron microscopic studies of FD pancreas are also sporadic. Inclusions in the interstitial fibroblasts, blood vessels and autonomic ganglion cells in FD patient (blood group not specified) were reported by Roth and Roth (1978). Elleder (2010) detected ultrastructural storage in acinar cells of FD patient with blood group B. Last, the analysis of urine sediment of FD patients showed increased excretion of both types of B-6 glycolipid antigens among secretors of blood group B or AB (Ledvinova et al. 1997).

To expand this limited information, we examined the pancreatic tissue collected at autopsy of two male FD patients who were blood group B secretors. Having this unique opportunity we report the biochemical profiles of the accumulated GSLs and also define the most structurally affected pancreatic compartments in this specific patient group.

Materials and methods

Tissue samples (pancreas, kidneys and lungs) were collected at autopsy from two 52-year-old FD male patients—blood group B secretors (FD-B1—AGAL genotype c.[881T > G];[0] (p.L294*), FD-B2—AGAL genotype c.[404C > T];[0] (p.A135V)), one 47-year-old FD male patient—blood group O secretor (FD-O—AGAL genotype c.[277G > A];[0] (p.D93N)), and from four age-matched control individuals without diagnosis of any lysosomal storage disease. All samples were fixed with 4% paraformaldehyde.

All three FD patients presented with a classical FD phenotype with typical clinical symptoms (detailed information is available on request). Gastrointestinal problems or pancreatic dysfunction were not part of the medical history of any of the tested FD patients.

The study was approved by the Ethics Committee (reference number 53/13 Grant GAUK 1.LFUK) of the General Teaching Hospital and the First Faculty of Medicine, Charles University in Prague and was performed in accordance with the guidelines of Declaration of Helsinki.

Thin layer chromatography and immunostaining

Prior to the analyses, tissue samples (pancreas, kidneys and lungs) were washed overnight in water, weighed and homogenized in water using an electric homogenizer. Aliquots were collected to measure protein content (Hartree 1972). Lipid extracts were prepared by repeated extraction of tissue homogenates using mixtures of chloroform:methanol:water (C:M:W) (20:10:1, 10:20:1, 10:10:1, v/v/v) as described previously (Natomi et al. 1988; Kuchar et al. 2012). The dry lipid residue was re-dissolved in C:M (2:1, v/v) in a volume corresponding to the particular protein concentration (in μg/μL) in the original tissue homogenates.

GSLs were separated by high-performance thin layer chromatography (HPTLC) on HPTLC-Alufolien Kieselgel 60 (MERCK, Germany) using C:M:W (65:35:8, v/v/v). Neutral GSLs were detected with orcinol reagent (0.5% in 2 M H_2SO_4 in ethanol) by moderately spraying and heating at 105°C for 3–5 min.

B-GSLs were visualized by TLC immunostaining. After blocking (1% ovalbumin and 1% polyvinylpyrrolidone in PBS, for 1 h at 37°C) the TLC sheets were incubated overnight at 4°C with the mouse primary monoclonal antibody to blood group B (mAb 99-806-L001, Exbio, Czech Republic). On the next day, the sheets were washed six times with PBS, blocked with 1% bovine serum albumin in PBS for 30 min at 37°C and incubated with the secondary peroxidase-conjugated goat anti-mouse IgM (Pierce, USA) for 60 min at 37°C. After six additional washes with PBS, specific staining was developed with chromogenic substrate 4-chloro-1-naphthol (Sigma, USA).

Tandem mass spectrometry and high-resolution mass spectrometry

Quantitative determination of sphingolipids in the lipid extracts of the pancreas, lungs and kidneys was performed according to previously described protocols (Kuchar et al. 2009; Hulkova et al. 2012). Aliquots of lipid extracts that corresponded to 18 μg (pancreas), 9 μg (lungs) and 36 μg (kidneys) of protein were mixed with internal standards. An external calibration point method was used for quantification (Kuchar et al. 2009). Samples were reconstituted in 1 mL of methanol or 1 mL of methanol with 5 mM NH_4COOH for analysis of acidic GSLs or neutral GSLs, respectively.

Measurements were performed using flow injection analysis (FIA) on AB/MDS SCIEX API 4000 triple quadrupole tandem mass spectrometer (MS/MS) equipped with electrospray ionization (ESI) working in the positive (for neutral GSLs) and negative (for acidic GSLs) ion mode. Data were acquired using the single reaction monitoring (SRM) mode. Samples (20 μL) were introduced to the flow of

pure methanol (50 µL/min) via Agilent 1290 UPLC system with autosampler. HR-MS data were acquired using the 12T SolariX FTICR mass spectrometer (Bruker Daltonics, Billerica, MA) equipped with a Smartbeam-II 1 kHz laser (Nd:YAG, 355 nm). α-Cyano-4-hydroxycinnamic acid (Bruker Daltonics, Germany) was used as MALDI matrix. Twenty laser shots per spectrum were collected in the positive ion mode. The acquired data were processed and visualized by DataAnalysis 4.0 software (Bruker Daltonics, Germany). The mass spectra were searched for known lipids using mMass software and LipidMAPS database (http://www.lipidmaps.org/ and http://www.mmass.org/) (Strohalm et al. 2010). B-GSLs were separated and quantified using HPLC–ESI–MS/MS on normal-phase column. SRM pairs were selected according to the data from HR-MS. Cogent Silica-C Column 7.5 cm × 2.1 mm, 4 µm (MicroSolv Technology, Eatontown, NJ) was used for lipid separation. Gradient elution was done in a binary system with mobile phase A consisting of *n*-hexane: 2-propanol:H_2O:acetic acid (68:30:2:1) and mobile phase B consisting of 2-propanol:H_2O:acetic acid (85:15:1); both phases contained 4 mM ammonium acetate for ionization of lipids via protonation. The gradient elution program for HPLC separation started at 100% of mobile phase A and followed a steeping curve to 100% of phase B with increasing flow rate from 50 to 200 µL/min for 60 min.

Because an internal B-GSL standard is not commercially available, B-6 GSL was semi-quantified using C17:0 Gb3Cer internal standard and calculated according to Cifkova et al. (2012). For the same reason, B-7 glycolipid was semi-quantified using peak area ratios as described by others (Fan et al. 2013).

Immunohistochemistry and wide-field light microscopy

Formaldehyde-fixed and paraffin-embedded pancreatic tissues from FD-B patient were used for IHC detection of blood group B antigens. The tissue was cut into 4 µm thick sections and deparaffinized with three xylene washes (5 min each), one acetone wash (2 min), two ethanol washes (2 min each) and two washes in distilled water (2 min each), all at room temperature. Endogenous peroxidase in the tissue sections was blocked with 1% sodium azide and 0.3% H_2O_2 for 30 min and sections were further blocked with 5% fetal bovine serum in PBS. Then the sections were incubated with mouse IgM monoclonal antibodies against blood group B trisaccharide antigenic determinant (mAb 99-806-L001, Exbio, Czech Republic) diluted 1:25 at 4°C overnight. After four PBS washes, anti-mouse EnVision+ System-HRP and diaminobenzidine (DAB)+ Substrate Chromogen system (both DakoCytomation, Glostrup, Denmark) were used for detection of the primary antibodies. Last, the sections were counterstained with Harris hematoxylin, dehydrated and mounted in Solacryl BMX (Penta, Czech Republic).

Cryostat sections prepared from the fixed pancreas were used for lipid immunohistochemistry (IHC). Formaldehyde-fixed tissue blocks were frozen in liquid nitrogen and 5 µm thick sections were cut with cryostat microtome (Leica Biosystems, Nussloch GmbH). Sections were air dried, blocked as described above and incubated with primary mAb overnight at 4°C. Mouse IgG2b anti-Gb3Cer antibody (370,680, Seikagaku, Japan) and mouse IgM antibody against blood group B were diluted 1:50 and 1:20, respectively. Parallel sections were stained before and after the total extraction of lipids with the following procedure: 50% ethanol (10 min), mixture consisting of C:M:W(4:8:3, v/v/v, 6 h), mixture consisting of C:M (2:1, v/v, overnight), and final washing in 50% ethanol (5 min) and in distilled water (5 min), all at room temperature. Primary antibodies were detected with anti-mouse EnVision+ System-HRP with DAB as a chromogen, the sections were counterstained with Harris hematoxylin and mounted in Immu-Mount medium (Shandon, Pittsburgh, PA).

Confocal microscopy—co-localization studies of blood group B antigens in the pancreas

The co-localization studies of blood group B antigens with other markers (see below) were performed in paraffin-embedded tissue sections of the FD-B1 pancreas. Sections were washed with a series of solvents and distilled water as described above. The primary antibodies against α-Amylase (rabbit, A8273, Sigma, USA), Cathepsin D (rabbit, ab75852, Abcam, UK) and lysosomal-associated membrane protein type 2 (LAMP2, rabbit, NBP1-02965, Novus Biologicas, Littleton, CO) were chosen to specifically detect secretory granules (anti-amylase) and lysosomes (anti-cathepsin D and anti-LAMP2). Secondary detection of the primary antibodies used Alexa Fluor 488-conjugated goat anti-rabbit IgG and Alexa Fluor 568-conjugated goat anti-mouse IgG (Molecular Probes, Invitrogen/ThermoScientific, Carlsbad, CA). Primary antibodies were incubated for 1 h at 37°C. Secondary antibodies were incubated for 1 h at 37°C. Nuclei were visualized using DAPI (4′, 6-diamidino-2-phenylindole, dihydrochloride, Invitrogen/ThermoScientific, Carlsbad, CA) for 15 min at 37°C.

The sections were scanned with Laser Scanning Confocal Microscope Leica SP8X (Leica Microsystems GmbH, Wetzlar, Germany). All confocal images were acquired with HC PL APO 63x/1.40 OIL CS2 objective. DAPI, Alexa Fluor 488 and Alexa Fluor 568 were excited with 405 nm, 499 nm and 577 nm, respectively. The detector emission wavelengths were set to 410–489 nm, 505–582 nm and 589–726 nm, respectively. Alexa Fluor dyes were detected with HybridDetectors using counting mode in 12 bits per channel and gated detection (0.3–12 ns). The Nyquist resolution used for image acquisitions was 41 nm/px. The individual channels were deconvolved by Maximum likelihood estimation algorithm using HuygensPro software (Scientific Volume Imaging b.v., Hilversum, the Netherlands). Cropping, final resolution adjustments and conversion to 8 bits per channel was done in LAS X (Leica Microsystems) and Adobe Photoshop CS6 (Adobe Systems, Inc., San Jose, CA).

Detection of the autofluorescent ceroid

Ceroid was detected by its autofluorescence in both paraffin and cryostat sections. For wide-field epi-fluoresce, Nikon E800 Microscope (Nikon Instruments, Inc., Melville, NY) equipped with the UV-2A filter cube (Ex355/50DM400Em420LP) and Olympus DP70 Digital Camera (Olympus Corporation, Shinjuku, Tokyo, Japan) were used. The resultant images (Figure 3C and D, and Supplementary data, Figure S4A and S4B) contain the autofluorescent signal coded in yellow–green.

In the confocal setup, autofluorescence of ceroid can be detected in all three channels with the maximum being in the 410–489 nm channel. As a result, ceroid autofluorescence is coded in blue in Figures 4E, F and 5E, F. DAPI labeled nuclei were discriminated from the autofluorescent signal of ceroid by their specific morphology.

Results

Lipid analysis of pancreatic tissue revealed a striking accumulation of variety of B-GSLs

Neutral GSLs and B-GSLs in lipid extracts of the pancreas, lungs and kidneys were analyzed by HPTLC, HPLC–ESI–MS/MS and FIA–ESI MS/MS. Orcinol detection of neutral GSLs from the pancreatic tissue revealed accumulation of Gb3Cer in all three FD patients irrespective

of their blood group (Figure 1). Remarkable though was the massive deposition of a multitude of various immunopositive B-GSLs in the FD-B1 pancreas in comparison to control blood group B samples (C-B1 and C-B2). The spectrum of the FD-O pancreatic GSLs displayed no distinct bands in the area corresponding to TLC mobility of the blood group lipid antigens (Figure 1). Gb3Cer was substantially less accumulated in the lungs and pancreas than in the kidneys (Table II).

As for B-GSLs, the immunopositive bands were more pronounced in the kidneys compared with the lungs but were much weaker than in the pancreas. Only trace amounts of B-GSLs were detected in lungs of FD-B patients (Supplementary data, Figure S1).

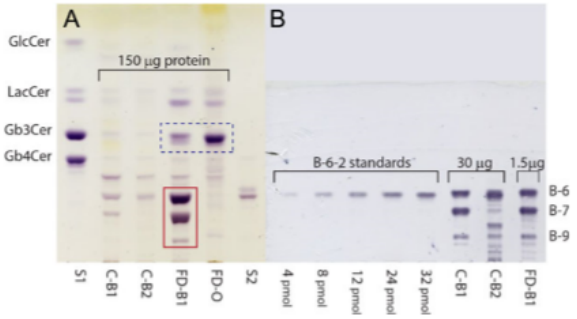

Fig. 1. HPTLC analysis of neutral GSLs in the pancreas. Tissue extracts corresponding to identical protein amounts were applied as indicated. Orcinol detection (**A**) of neutral GSLs in FD pancreas showed increased deposition of Gb3Cer (blue dashed line rectangle). However, in the FD-B1 patient, B-GSLs were identified as additional deposited substances with considerable structural diversity in the carbohydrate moiety, as documented by immunodetection (**B**). Specific immunodetection with blood group B mouse monoclonal antibody revealed B-GSLs with 6, 7 or 9 monosaccharides in the chain located in the lower part of the chromatogram (red full line rectangle in a). S1 – GSL standards; FD-B2 patient not shown. Details of both detection procedures are given in the Methods.

HR-MS spectrum (in the m/z range 1425–1850) of the pancreatic B-GSLs is shown in Figure 2. Interestingly, a broad array of various oligosaccharides and lipid structures of blood GSLs ranging from 5 to 7 carbohydrate units in the oligosaccharide chain were identified in both FD-B patients. Such a B-GSL rich spectrum was not observed in controls as documented in Figure 2 (Control C-B1 sector of the MS spectra vs the Fabry sector FD-B1).

Because of the technical limits of the MS instrumentation to detect ions with higher m/z than 1800 kDa, only two major B-GSLs containing six (B-6) and seven (B-7) sugar residues were semi-quantitatively evaluated by HPLC–ESI–MS/MS. Compared with controls, up to a 30-fold increase in the B-6 glycolipid was identified in both FD-B patients (Table I). This contrasts with ~6-fold elevation of Gb3Cer in FD-B pancreatic homogenates (Table II).

Massive augmentation of B-GSL antigens in both FD-B patients was confirmed by semi-quantitative densitometry after immunodetection of chromatograms (data not shown). The amounts of other neutral GSLs were normal. The only exception was the Gb3Cer and ceramidedihexoside (CDH) fractions. The latter contains Ga2Cer, which is another minor AGAL substrate represented in the kidneys and elevated in FD patients (Table II).

Interestingly, the massive GSL storage is accompanied by a distinct decrease in the content of sphingomyelin. This phenomenon was pronounced in all three FD patients irrespective of the blood group (Table II). On the contrary, a substantial storage of Gb3Cer and CDH fractions was detected in the kidneys and reached a 2–3-fold increase in the concentration of total GSLs in this organ (Supplementary data, Figure S2).

Accumulation of blood group B glycoconjugates in pancreatic acinar cells is massive

Increased amounts of the lysosomal marker Cathepsin D was found in the entire exocrine pancreas of FD-B patient compared with weaker staining in control (Figure 3A and B). Signal for Cathepsin D did not correlate

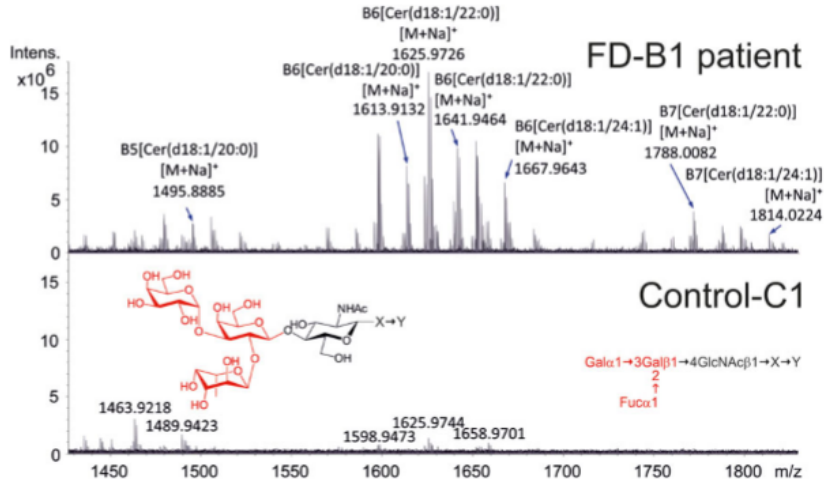

Fig. 2. High-resolution mass spectra of blood group B-GSLs in the pancreas. Differences in lipid spectra between FD-B1 (upper part) and C-B1 (lower part) are in regions corresponding to sphingolipids containing complex carbohydrate structures with 5 and more monosaccharides. Molecular species of major elevated B-6, B-7 (and B5) glycolipids are labeled and their ceramide composition is indicated. The structure of the blood group B antigenic determinant comprising three terminal monosaccharides linked to the oligosaccharide chain type 2 (neolacto-series) is marked in red. Although MS cannot distinguish between isobaric compounds (compounds with the same elemental composition), the authenticity of B-positive GSLs is confirmed by TLC immunodetection, where the peaks of B-6 and B-7 molecular species correspond to immuno-specific bands (Figure 1 and Supplementary data, Figure S1). The X in the GSL represents other possible saccharide units in the oligosaccharide structure. The Y indicates the hydrophobic core ceramide structure of glycolipids.

with amylase-positive secretory granules. In the exocrine parts of the FD-B pancreas, massive granular autofluorescence of ceroid was detected. Such an extensive presence of this abnormal intracellular pigment is known in a plethora of lysosomal storage diseases and can be used to spatially identify the storage-affected lysosomes (Figure 3C and D).

B-antigens (both glycoproteins and glycolipids) were detected in the acini of the exocrine pancreas and in the vascular endothelial cells in both FD-B patients and controls. Ductal epithelium, endocrine pancreas (islets of Langerhans) and vascular smooth muscle cells were negative for B-antigens (Figures 3E, F and 4A–D) both in controls and FD-B patients. In contrast with the mosaic expression pattern seen in the controls, B-antigens were uniformly expressed in acinar epithelial cells of the patients.

Lipid pre-extraction did not substantially reduce the immunostaining of B-antigens in either FD-B patients or controls (Supplementary data, Figure S3). This suggests that the positivity of B-antigens largely corresponds to polar nonlipid glycoconjugates with blood group B determinants.

Similar to B-antigens, Gb3Cer was expressed in vascular endothelial cells. Vascular smooth muscle cells were also positive. Importantly, Gb3Cer positivity was more intense in both FD-B patients than in controls (Figure 5A–D). Lipid pre-extraction interfered with Gb3Cer immunostaining in endothelial cells both in FD-B patients and controls. Smooth muscle cells in the FD-B patients remained, unlike in the controls, partially Gb3Cer positive (Figure 5C and D insert). Other cell types, including pancreatic acinar cells, were only weakly positive for Gb3Cer (Figure 5A and B).

When compared with the intracellular accumulation of the autofluorescent ceroid, which is thought to correspond to the lysosomal storage compartment, Gb3Cer and B-antigens positive vascular endothelial cells were devoid of this abnormal pigment (Supplementary data, Figure S4B). On the contrary, lysosomal storage in vascular smooth muscle cells was characterized by accumulation of both Gb3Cer and ceroid (Figure 5D and Supplementary data, Fig. S4B). B-antigen(s) did not contribute to the lysosomal storage in vascular smooth muscle cells in FD-B patients (Figure 4D). Pancreatic acinar cells were affected by accumulation of B-GSL (Figures 3F and 4E) and by massive load of autofluorescent ceroid in combination with a minor amount of nondegraded Gb3Cer (Figure 5E). In controls, the autofluorescent material was not detected in any of the listed cell types (Figure 3C and Supplementary data, Figure S4A).

While B-antigens were predominantly expressed in the apical parts of the cytoplasm of acinar cells (Figure 3F), the signal did not co-localize with the signal of secretory granules, (Figure 4F). Gb3Cer also did not co-localize with the signal of the secretory granules (Figure 5F). Lastly, though lysosomal localization of B-antigens was confirmed by the overlap with the LAMP2 signal (Figure 4E).

Table I. Blood group B glycosphingolipids in FD and control pancreas and kidneys

Patients	Pancreas pmol/mg protein		Kidneys pmol/mg protein	
	B-6	B-7	B-6	B-7
FD-B1	115.0 ± 2.6	334.5 ± 17.2	20.7 ± 1.6	27.2 ± 1.4
FD-B2	154.7 ± 0.2	137.1 ± 14.6	36.6 ± 1.1	76.4 ± 6.6
C-B1	4.6 ± 0.2	6.8 ± 2.1	2.1 ± 0.2	0.0
FD-O	0.0	0.0	0.0	0.0
C-O	6.6 ± 0.2	0.0	0.0	0.0

Data were obtained by HPLC–ESI–MS/MS analysis of lipid extracts of tissues homogenates. B-glycosphingolipids were semi-quantified with C17:0 Gb3Cer internal standard and by application of methods by Cifkova et al. (2012) and Fan et al. (2013). For details see Methods. AVG ± SD from technical doublets. FD-B1, FD-B2—Fabry patients, blood group B; FD-O—Fabry patient, blood group O; C-B1—control, blood group B and C-O—control, blood group O.

Discussion

The possible contribution of nondegraded B-GSLs to pancreatic pathophysiology of FD has not been systematically explored since 1973 (Wherrett and Hakomori 1973). Individual reports have suggested that the defect in degradation of AGAL substrates did not influence the disease phenotype in patients with blood group B or AB (Lidove 2002). However, the number of analyzed FD-B patients has never been extensive, also due to low frequency of blood group B individuals in the general population (Garratty et al. 2004).

Table II. Concentration of neutral GSLs, ceramide and sphingomyelin in the FD and control pancreas, kidneys and lungs

		Lipid concentrations in nmol/mg protein					
		Cer	CMH	CDH	Gb3Cer	Gb4Cer	SM
Pancreas	*Controls AVG ± SD, n = 4*	*5.2 ± 1.3*	*3.2 ± 1.2*	*5.4 ± 2.1*	*2.0 ± 0.9*	*0.5 ± 0.2*	*75.9 ± 16.0*
	FD-O	1.5	1.6	8.2	26.2	0.3	26.6
	FD-B1	3.5	5.6	12.8	9.7	0.3	28.4
	FD-B2	7.4	2.4	17.1	11.2	0.5	25.0
Lung	*Controls AVG ± SD, n = 4*	*4.0 ± 0.9*	*1.6 ± 0.7*	*11.5 ± 4.3*	*2.0 ± 0.7*	*0.9 ± 0.4*	*62.6 ± 15.1*
	FD-O	2.6	1.2	10.8	41.5	0.6	32.9
	FD-B1	3.4	0.7	6.3	14.1	0.5	32.1
	FD-B2	2.5	0.6	3.3	15.0	0.3	32.3
Kidney	*Controls AVG ± SD, n = 4*	*5.4 ± 1.0*	*2.0 ± 0.6*	*8.4 ± 3.6*	*6.1 ± 1.7*	*2.6 ± 1.0*	*86.8 ± 28.6*
	FD-O	6.1	3.5	157.5	177.0	2.1	59.3
	FD-B1	6.2	6,2	221.1	155.4	0.8	49.9
	FD-B2	5.9	3.4	155.1	108.2	0.6	32.4

Data were obtained by FIA–ESI–MS/MS analysis of lipid extracts of tissues homogenates. Sphingolipids were quantified using appropriate internal standards and external calibration point method (Kuchar et al. 2009). For further details see Methods. The MS/MS does not differentiate between the glucosyl and galactosyl moieties because of the same mass. Therefore, glucosylceramide and galactosylceramide are quantified as monohexosylceramides (CMH), while lactosylceramide and digalactosylceramide as dihexosylceramides (CDH). FD-B1, FD-B2—Fabry patients, blood group B and FD-O—Fabry patient, blood group O.

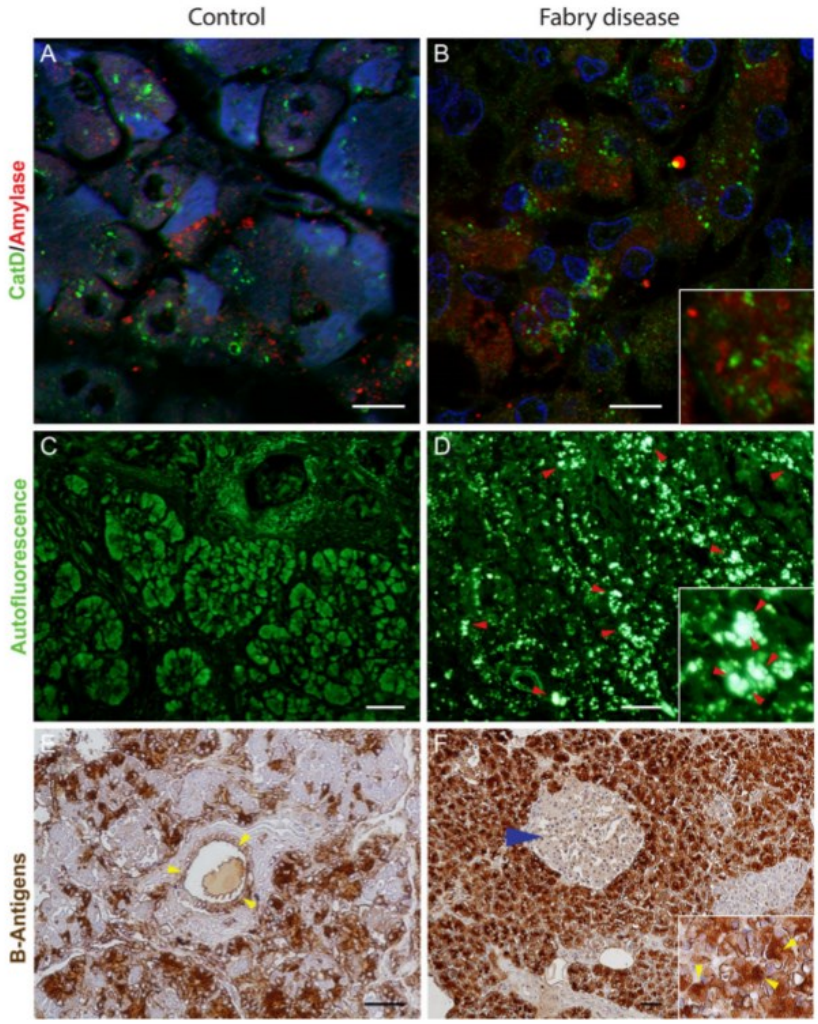

Fig. 3. Lysosomal storage pattern in the FD-B1 pancreas compared with control. **(A, B)** Immunofluorescent detection of lysosomal marker CatD (green signal) in the pancreas reveals increased amount of the lysosomes in the FD-B1 patient compared with the C-B2 control. The signal of CatD does not correlate with that of secretory granules (amylase, red signal) in either the pancreas of **(A)** C-B2 control or **(B)** FD-B1 patient. **(A, B)** DAPI stained nuclei (blue signal). **(C)** C-B2 control without ceroid accumulation. **(D)** Ceroid storage characterized by typical autofluorescent signal (red arrowheads) displays distribution across the whole pancreas of the FD-B1 patient in contrast to C-B2 control **(E)** Blood group B antigens are not expressed in the ductal epithelium, (yellow arrowheads) and endocrine portion of pancreas **(F,** blue arrowhead) in contrast to the surrounding acinar cells in the FD-B1 pancreas. Strong positivity of B-antigens was detected mainly in the apical parts of the cytoplasm of acinar cells in FD-B1 **(F,** yellow arrowheads in the insert). Scale bars (a, b) = 10 μm and (c–f) = 50 μm.

Gastrointestinal symptoms are relatively frequent (33%) and appear early in life of FD patients (Desnick et al. 2001). Recent clinical studies have not associated these symptoms with pancreatic disease, however, the blood group status of these patients was not considered (Vujasinovic et al. 2015).

This stated we aimed to (i) biochemically characterize the pancreatic storage patterns and (ii) specify the cellular pancreatic populations afflicted by an accumulation of Gb3Cer and/or blood group B compounds.

To compare the spectrum of accumulated metabolites in pancreas of FD-B patients to other tissues, we analyzed GSLs in the kidneys and lungs as representatives of secretory and nonsecretory organs, respectively. In contrast to the previous work (Wherrett and Hakomori 1973) and to a lesser extent than in the pancreas, our current report demonstrates increased amounts of B-GSLs also in the kidneys. The smallest, barely detectable amounts of GSLs were present in the lungs of FD-B patients.

Interestingly, Gb3Cer accumulated less in the pancreas and the lungs than in the kidneys where it dominated (together with Ga2Cer containing CDH fraction). This variability likely relates to differences in metabolic turnover of organ-specific cell types as well as subcellular lipid distribution and/or localization. A remarkable biochemical finding was that besides the dominant species with six (B-6) and seven (B-7) sugar residues, the whole series of highly complex B-GSLs accumulated in the FD-B pancreas (Supplementary data, Figure S1).

Under normal conditions, ABH active GSLs with shorter carbohydrate chains (5–15 monosaccharide units per molecule) have been reported at ~5% of the total number of ABH sites on erythrocyte

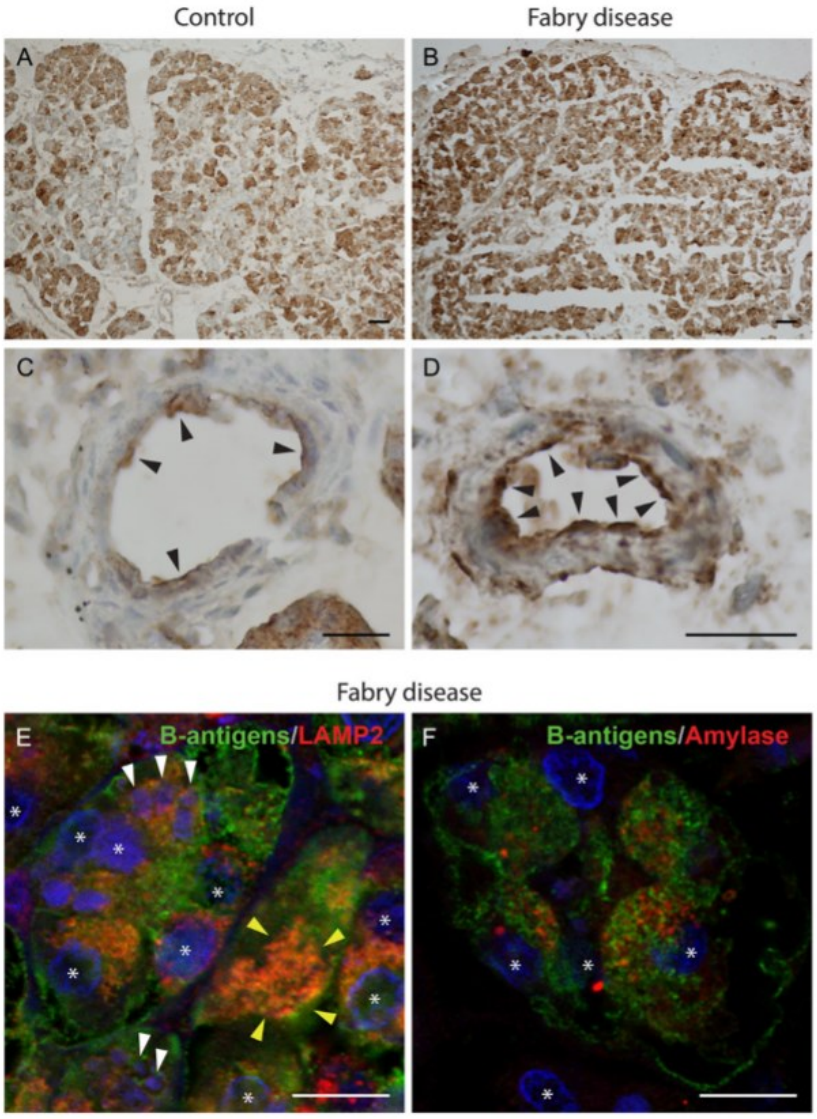

Fig. 4. Blood group B antigen immunohistochemistry and confocal microscopy in the pancreas. **(A)** Mosaic expression of B-antigens in acinar epithelium in the C-B2 control. **(B)** Intensive and almost homogenous staining for B-antigens in the exocrine part of the FD-B1 pancreas. Acinar epithelium with coarsely granular positivity. **(C)** Endothelial cells with the usual expression of B-antigen (black arrowheads) in the control. **(D)** Strong positivity for B-antigens in the endothelial cells is suggestive of B-antigen participation in the lysosomal storage in the FD-B1 pancreas (black arrowheads). **(E)** Co-localization of B-antigens (green signal) with LAMP2 (red signal) demonstrates their localization in lysosomes (yellow arrows). Massive accumulation of B-antigens in acinar cells is accompanied by the increased amount of ceroid (white arrowheads). The autofluorescent ceroid can be visually distinguished from DAPI stained nuclei (marked by *) by specific fluorescence and morphology. **(F)** B-antigens signal does not correlate with amylase-positive secretory granules (red signal). Scale bars (a, b) = 50 μm, (c, d) = 20 μm and (e, f) = 10 μm.

membranes. Approximately 75% of compounds carrying ABH active determinants are nonlipid compounds such as glycoproteins (Schenkel-Brunner 1995).

As such, the results of the biochemical assays that were performed in deproteinated tissue homogenates may not necessarily fully correlate with spatial distribution studies in lipid-extracted tissue sections.

This stated, we next aimed to identify the cellular pancreatic populations afflicted by an accumulation of both Gb3Cer and blood group B compounds. We show that pancreatic vascular endothelial, smooth muscle cells and acinar epithelial cells represent the cell types prominently affected by the lysosomal storage. Importantly, the abnormal acinar deposits consisted mainly of B-glycoconjugates (both GSLs and glycoproteins). In contrast to acinar cells, ductal epithelium and cells of the endocrine part of pancreas were free of storage. This is consistent with report by Ravn and Dabelsteen (2000), who also failed to detect ABH antigens in the ductal system of the normal exocrine pancreas. In the normal tissue, regardless of the blood group, a mosaic pattern of ABH binding sites was clearly visible, suggesting that it is a usual feature of ABH antigen expression (Ito 1992). In FD-B patients, however, the expression of all

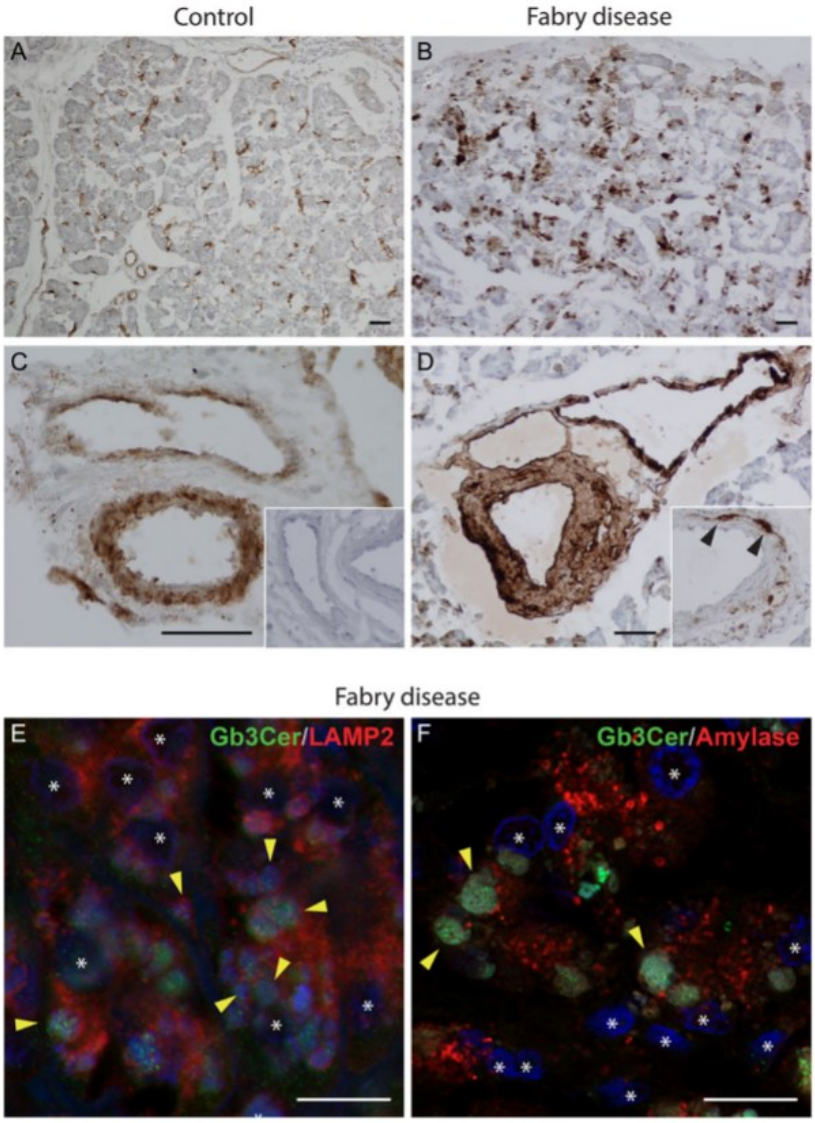

Fig. 5. Gb3Cer immunohistochemistry and confocal microscopy in the pancreas. **(A)** Gb3Cer expression is enhanced in blood vessels in the control. **(B)** In Fabry disease, Gb3Cer stains with increased intensity the in pancreatic vessel walls. **(C)** Small vessels display Gb3Cer in the endothelium, however, large vessels were positive also in the smooth muscle cells. Staining of Gb3Cer was negative after pre-extraction step of lipids from the tissue (insert) **(D)** Gb3Cer accumulation in the endothelial and smooth muscle cells in the FD-B1 pancreatic vessels is massive. Gb3Cer storage in smooth muscle cells persists after lipid extraction (insert, black arrowheads). **(E)** Co-localization of Gb3Cer (green signal) with LAMP2 (red signal) demonstrates their localization in lysosomes of Fabry pancreas which is accompanied by the massive accumulation of autofluorescent ceroid (yellow arrowheads). The ceroid can be visually distinguished from DAPI stained nuclei (marked by *) by specific fluorescence and morphology **(F)** Gb3Cer does not correlate with amylase-positive secretory granules but correlates exclusively with autofluorescent ceroid (yellow arrowheads). Scale bars (a–d) = 50 μm and (e, f) = 10 μm.

B-antigens in the pancreatic acinar epithelium was uniform and more intense than in controls suggesting a defect in the catabolic pathway of B-glycoconjugates, previously confirmed by metabolic experiments in fibroblast cultures (Asfaw et al. 2002). Lipid extraction of the tissue sections eliminated B-polyglycosylceramides and partially reduced the intensity of IHC staining in acinar cells. The residual strong IHC positivity of B-antigens suggested substantial presence of B-active nonlipid glycoconjugates in the pancreas.

Lantini and Cossu (1997) demonstrated blood group substances both as cell surface-bound antigens and contents of the secretory granules of acinar and interlobular duct cells. These authors presented specific staining of acinar secretory granules for blood group B antigens with intensive secretion into the pancreatic juice together with digestive enzymes. In our study, however, neither B-antigens nor Gb3Cer co-localized with secretory granule marker.

It has been known that storage-affected lysosomes accumulate considerable amounts of autofluorescent lipofuscin-like lipopigment ceroid (Terman and Brunk 1998; Elleder 2010; Hulkovaand Elleder 2010). This material has been defined as a that arises from different pathological conditions of organism, including storage disorders,

malnutrition, cell stress, etc. (Seehafer and Pearce 2006; Goebel and Muller 2013). In FD, ceroid is a major secondary storage component. Storage in pancreatic acinar epithelial cells of our FD-B patients was prominent and characterized by massive B-antigens and autofluorescent ceroid deposition in combination with a small amount of nondegraded Gb3Cer. Lysosomal localization of these compounds was confirmed by co-labeling with lysosomal marker LAMP2.

In contrast to other cell types, moderate Gb3Cer deposition observed in endothelial cells of FD pancreas was not associated with accumulation of ceroid in lysosomes. On the other hand, storage in vascular smooth muscle cells that normally accumulate only minor amounts of Gb3Cer was dominated by substantial deposition of both Gb3Cer and ceroid. In these cells, but not in endothelial cells, Gb3Cer was partially resistant to lipid extraction, probably reflecting modifications of the lysosomal system by long-term storage and intensified by extensive stock of ceroid.

Changes in the lysosomal system were previously shown to interfere with therapeutic protocols. In FD, *continuous storage in some cells* leads to inefficient clearing of accumulated substrates by the enzyme replacement therapy (Keslova-Veselikova et al. 2008). As such, long-term accumulation of B- glycoconjugates in FD-B patients may theoretically worsen their lysosomal pathology. To conclude, our work provides novel and detailed biochemical and morphological data on lysosomal storage in the pancreas of FD-B patients. The results clearly show that different, nondegraded, substrates are expressed and stored in lysosomes of distinct pancreatic cellular populations that have different physiological functions. While acinar cells specifically accumulate glycoconjugates of blood group B and only minimally Gb3Cer, the latter AGAL substrate predominates in the blood vessel cells. Importantly, endocrine cells were completely free of storage. Comparisons of findings between blood group B and O FD patients provide an explanation for the milder affliction of the pancreas in contrast to other organs in which the accumulation of Gb3Cer predominates. We believe that our results strongly substantiate the need for more detailed clinical studies focused on pancreatic (dys)function in FD patients with type B blood group.

Supplementary data

Supplementary data is available at *GLYCOBIOLOGY* online.

Funding

This work was supported by Grant Agency of Charles University (GAUK 56214), Prague, Czech Republic and in part by the Ministry of Education, Youth, and Sports of the Czech Republic (LO1509) and by Ministry of Health of the Czech Republic (grant no. 15-33297A).

Acknowledgements

The authors thank Helena Poupětová for her expertize in enzymology, Marie Kolářová and Michala Fialová for excellent technical assistance and Dr Cristin Davidson for critical discussions and proofing of the English usage. We thank Dr Tomáš Koblas (IKEM, Prague), for providing the anti-pancreatic amylase antibody.

Conflict of interest statement

None declared.

Abbreviations

C-O(A, B), controls with blood group O (A, B); CDH, dihexosylceramides; CMH, monohexosylceramides; (ESI)-MS/MS, tandem mass analyzer (equipped with electrospray ionization); FD-O(B), Fabry patient with blood group O (B); FBS, fetal bovine serum; FD, Fabry disease; Ga2Cer, digalactosylceramide; Gb3Cer, globotriaosylceramide; (B)-GSLs, (blood group B) glycosphingolipids; IHC, immunohistochemistry; LAMP2, lysosomal-associated membrane protein 2; PBS, phosphate-buffered saline

References

Asfaw B, Ledvinova J, Dobrovolny R, Bakker HD, Desnick RJ, van Diggelen OP, de Jong JG, Kanzaki T, Chabas A, Maire I et al. 2002. Defects in degradation of blood group A and B glycosphingolipids in Schindler and Fabry diseases. *J Lipid Res*. 43:1096–1104.

Boslem E, Meikle PJ, Biden TJ. 2012. Roles of ceramide and sphingolipids in pancreatic beta-cell function and dysfunction. *Islets*. 4:177–187.

Buschard K, Blomqvist M, Osterbye T, Fredman P. 2005. Involvement of sulfatide in beta cells and type 1 and type 2 diabetes. *Diabetologia*. 48:1957–1962.

Cao Z, Wang X. 2014. The endocrine role between beta cells and intra-islet endothelial cells. *Endocr J*. 61:647–654.

Cartron J-P, Rouger P. 1995. *Molecular basis of human blood group antigens*. New York: Plenum Press.

Cifkova E, Holcapek M, Lisa M, Ovcacikova M, Lycka A, Lynen F, Sandra P. 2012. Nontargeted quantitation of lipid classes using hydrophilic interaction liquid chromatography–electrospray ionization mass spectrometry with single internal standard and response factor approach. *Anal Chem*. 84:10064–10070.

Desnick RJ, Ioannou YA, Eng CM. 2001. α-Galactosidase A deficiency: Fabry disease. In: Scriver CR, Beaudet AL, Sly WS, Valle D, editors. *The Metabolic and Molecular Bases of Inherited Disease*. New York: McGraw-Hill. p. 3733–3774.

Elleder M. 2010. Subcellular, cellular and organ pathology of Fabry disease. In: Elstein D, Altarescu G, Beck M, editors. *Fabry Disease*. Dordrecht: Springer Science+Business Media B.V. p. 211–243.

Fan M, Sidhu R, Fujiwara H, Tortelli B, Zhang J, Davidson C, Walkley SU, Bagel JH, Vite C, Yanjanin NM et al. 2013. Identification of Niemann-Pick C1 disease biomarkers through sphingolipid profiling. *J Lipid Res*. 54:2800–2814.

Garratty G, Glynn SA, McEntire R. 2004. ABO and Rh(D) phenotype frequencies of different racial/ethnic groups in the United States. *Transfusion*. 44: 703–706.

Goebel HH, Muller HD. 2013. Storage diseases: diagnostic position. *Ultrastruct Pathol*. 37:19–22.

Hartree EF. 1972. Determination of protein: a modification of the Lowry method that gives a linear photometric response. *Anal Biochem*. 48:422–427.

Hulkova H, Elleder M. 2010. Adipocytes participate in storage in alpha-galactosidase deficiency (Fabry disease). *J Inherit Metab Dis*. 33(Suppl 3): S297–S300.

Hulkova H, Ledvinova J, Kuchar L, Smid F, Honzikova J, Elleder M. 2012. Glycosphingolipid profile of the apical pole of human placental capillaries: the relevancy of the observed data to Fabry disease. *Glycobiology*. 22:725–732.

Ito N. 1992. Histochemical localization and analysis of blood group-related antigens in human pancreas using immunostaining with monoclonal antibodies and exoglycosidase digestion. *Prog Histochem Cytochem*. 25:1–85.

Ito N, Tabata S, Kawahara S, Hirano Y, Nakajima K, Uchida K, Hirota T. 1993. Histochemical analysis of blood-group antigens in human sublingual glands and pancreas—an application of high-performance liquid-chromatography to estimate the quantity of galactose liberated from tissue-sections by alpha-galactosidase digestion. *Histochem J*. 25:242–249.

Jaff MS. 2010. Higher frequency of secretor phenotype in O blood group—its benefits in prevention and/or treatment of some diseases. *Int J Nanomedicine*. 5:901–905.

Keslova-Veselikova J, Hulkova H, Dobrovolny R, Asfaw B, Poupetova H, Berna L, Sikora J, Golan L, Ledvinova J, Elleder M. 2008. Replacement

of alpha-galactosidase A in Fabry disease: effect on fibroblast cultures compared with biopsied tissues of treated patients. *Virchows Arch*. 452: 651–665.

Kuchar L, Asfaw B, Ledvinova J. 2012. Tandem Mass Spectrometry of Sphingolipids: Application in Metabolic Studies and Diagnosis of Inherited Disorders of Sphingolipid Metabolism. In: Prasain JK, editor. *Tandem Mass Spectrometry - Applications and Principles*. Rijeka: InTech. p. 739–768.

Kuchar L, Ledvinova J, Hrebicek M, Myskova H, Dvorakova L, Berna L, Chrastina P, Asfaw B, Elleder M, Petermoller M et al. 2009. Prosaposin deficiency and saposin B deficiency (activator-deficient metachromatic leukodystrophy): report on two patients detected by analysis of urinary sphingolipids and carrying novel PSAP gene mutations. *Am J Med Genet A*. 149A:613–621.

Lantini MS, Cossu M. 1997. Ultrastructural localization of blood group antigens in human exocrine pancreas by immunogold labelling. *J Submicrosc Cytol Pathol*. 29:245–251.

Ledvinova J, Poupetova H, Hanackova A, Pisacka M, Elleder M. 1997. Blood group B glycosphingolipids in alpha-galactosidase deficiency (Fabry disease): influence of secretor status. *Biochim Biophys Acta*. 1345: 180–187.

Lidove O. 2002. Influence of blood groups B or AB on phenotype in a population of hemizygous patients with Fabry disease. *Acta Paediatr Suppl*. 439:124.

Manukyan L, Ubhayasekera SJ, Bergquist J, Sargsyan E, Bergsten P. 2015. Palmitate-induced impairments of beta-cell function are linked with generation of specific ceramide species via acylation of sphingosine. *Endocrinology*. 156: 802–812.

Motta PM, Macchiarelli G, Nottola SA, Correr S. 1997. Histology of the exocrine pancreas. *Microsc Res Tech*. 37:384–398.

Natomi H, Sugano K, Iwamori M, Takaku F, Nagai Y. 1988. Region-specific distribution of glycosphingolipids in the rabbit gastrointestinal tract: preferential enrichment of sulfoglycolipids in the mucosal regions exposed to acid. *Biochim Biophys Acta*. 961:213–222.

Ravn V, Dabelsteen E. 2000. Tissue distribution of histo-blood group antigens. *APMIS*. 108:1–28.

Roth J, Roth H. 1978. Electron-microscopic observations in internal organs in Morbus Fabry. *Virchows Arch A*. 378:75–90.

Schenkel-Brunner H. 1995. *Human blood groups: chemical and biochemical basis of antigen specificity*. Wien; New York: Springer-Verlag.

Seehafer SS, Pearce DA. 2006. You say lipofuscin, we say ceroid: defining autofluorescent storage material. *Neurobiol Aging*. 27:576–588.

Strohalm M, Kavan D, Novak P, Volny M, Havlicek V. 2010. mMass 3: a cross-platform software environment for precise analysis of mass spectrometric data. *Anal Chem*. 82:4648–4651.

Terman A, Brunk UT. 1998. Ceroid/lipofuscin formation in cultured human fibroblasts: the role of oxidative stress and lysosomal proteolysis. *Mech Ageing Dev*. 104:277–291.

Uchida E, Steplewski Z, Mroczek E, Buchler M, Burnett D, Pour PM. 1986. Presence of two distinct acinar cell populations in human pancreas based on their antigenicity. *Int J Pancreatol*. 1:213–225.

Vujasinovic M, Tepes B, Vujkovac B, Vujkovac AC, Tretjak M, Korat V. 2015. Exocrine pancreatic insufficiency is not a cause of abdominal complaints in patients with Fabry disease. *Wien Klin Wochenschr*. 127: 931–934.

Watkins WM. 2001. The ABO blood group system: historical background. *Transfus Med*. 11:243–265.

Wherrett JR, Hakomori SI. 1973. Characterization of a blood group B glycolipid, accumulating in the pancreas of a patient with Fabry's disease. *J Biol Chem*. 248:3046–3051.

Publications in impacted journals related to the topic of this Ph.D. thesis

Supplementary publication B

Kuchar L, Faltyskova H, Krasny L, Dobrovolny R, Hulkova H, Ledvinova J, Volny M, Strohalm M, Lemr K, Kryspinova L, Asfaw B, **Rybová J**, Desnick RJ, Havlicek V: Fabry disease: renal sphingolipid distribution in the α-Gal A knockout mouse model by mass spectrometric and immunohistochemical imaging. Anal Bioanal Chem, 2015 Mar; **407**(8): p. 2283-91. **IF 3.125**

Anal Bioanal Chem (2015) 407:2283–2291
DOI 10.1007/s00216-014-8402-7

RESEARCH PAPER

Fabry disease: renal sphingolipid distribution in the α-Gal A knockout mouse model by mass spectrometric and immunohistochemical imaging

Ladislav Kuchar · Helena Faltyskova · Lukas Krasny · Robert Dobrovolny · Helena Hulkova · Jana Ledvinova · Michael Volny · Martin Strohalm · Karel Lemr · Lenka Kryspinova · Befekadu Asfaw · Jitka Rybová · Robert J. Desnick · Vladimir Havlicek

Received: 22 October 2014 / Revised: 3 December 2014 / Accepted: 8 December 2014 / Published online: 27 December 2014

Abstract Fabry disease is an X-linked lysosomal storage disease due to deficient α-galactosidase A (α-Gal A) activity and the resultant lysosomal accumulation of globotriaosylceramide (Gb3) and related lipids primarily in blood vessels, kidney, heart, and other organs. The renal distribution of stored glycolipid species in the α-Gal A knockout mouse model was compared to that in mice to assess relative distribution and absolute amounts of accumulated sphingolipid isoforms. Twenty isoforms of five sphingolipid groups were visualized by mass spectrometry imaging (MSI), and their distribution was compared with immunohistochemical (IHC) staining of Gb3, the major stored glycosphingolipid in consecutive tissue sections. Quantitative bulk lipid analysis of tissue sections was assessed by electrospray ionization with tandem mass spectrometry (ESI-MS/MS). In contrast to the findings in wild-type mice, all three analytical techniques (MSI, IHC, and ESI-MS/MS) revealed increases in Gb3 isoforms and ceramide dihexosides (composed mostly of galabiosylceramides), respectively. To our knowledge, this is the first report of the distribution of individual molecular species of Gb3 and galabiosylceramides in kidney sections in Fabry disease mouse. In addition, the spatial distribution of ceramides, ceramide monohexosides, and sphingomyelin forms in renal tissue is presented and discussed in the context of their biosynthesis.

Keywords Fabry disease · Kidney · Glycosphingolipids · Mass spectrometry imaging · Quantitation

Published in the topical collection *Mass Spectrometry Imaging* with guest editors Andreas Römpp and Uwe Karst.

Ladislav Kuchar and Helena Faltyskova contributed equally to this work.

Electronic supplementary material The online version of this article (doi:10.1007/s00216-014-8402-7) contains supplementary material, which is available to authorized users.

L. Kuchar · R. Dobrovolny · H. Hulkova · J. Ledvinova · L. Kryspinova · B. Asfaw · J. Rybová
Institute of Inherited Metabolic Disorders, Charles University in Prague, Ke Karlovu 2, 128 08 Prague 2, Czech Republic

H. Faltyskova · L. Krasny · M. Volny · M. Strohalm · K. Lemr · V. Havlicek
Institute of Microbiology, ASCR, v.v.i, Videnska 1083, 14220 Prague 4, Czech Republic

L. Krasny
Institute of Chemical Technology in Prague, Technicka 5, 16228 Prague 6, Czech Republic

K. Lemr · V. Havlicek (✉)
Regional Centre of Advanced Technologies and Materials, Department of Analytical Chemistry, Faculty of Science, Palacky University, 17.listopadu 12, 771 46 Olomouc, Czech Republic
e-mail: vlhavlic@biomed.cas.cz

R. J. Desnick
Department of Genetics and Genomics Sciences, Icahn School of Medicine at Mount Sinai, New York, NY 10029, USA

Introduction

Fabry disease (OMIM 301500) is a rare X-linked lysosomal storage disease [1]. Mutations in the α-Gal A gene (*GLA*) result in the deficient activity of α-Gal A and the resultant accumulation of its glycosphingolipid substrates with terminal alpha-galactosyl moieties, particularly globotriaosylceramide (Gb3Cer, Gb3, also called CTH, GL3, CD77) and, to a lesser extent, galabiosylceramide (digalactosylceramide, Ga2Cer, Ga2, CDH, or GL2) and blood group B substances in lysosomes of cells throughout the body [2]. Also, the deacylated derivative, globotriaosylsphingosine (lyso-globotriaosylceramide, lyso-Gb3), accumulates in some cells and body fluids [3]. There

are two major phenotypes. Affected males with the "classic" phenotype have essentially no α-Gal A enzymatic activity, marked vascular endothelial Gb3 accumulation and present in childhood or adolescence with angiokeratoma, acroparesthesias, hypohidrosis, and corneal opacities. They develop renal failure, cardiac hypertrophy, and/or cerebrovascular disease that lead to their premature demise. Newborn screening studies reveal an incidence of classic males of 1 in 25,000 to 40,000. In contrast, affected males with the "later-onset" phenotype (cardiac variant) have residual α-Gal A activity and lack the microvascular endothelial Gb3 accumulation [4]. The clinical diagnosis is confirmed by demonstrating the deficient enzyme activity in males and by identifying the family's gene mutation in the heterozygous females [2].

Large amounts of globotriaosylceramides (Fig. 1) and galabiosylceramide isoforms are excreted in the urine of affected males and heterozygous females with the classic disease phenotype [5–9], where it may vary according to the level of the X-chromosome inactivation [10]. The major sphingoid base is sphingosine (d18:1), and the minor bases are dihydrosphingosine (d18:0) and sphingadienine (d18:2). Fatty acylation varies from C16:0 to C24:0 although there are no supporting exact measurements. A recent report noted that accumulated lyso-Gb3 may serve as a plasma and urine biomarker [11]. This metabolite was more abundant in classically affected males (94.4 pmol/mL), with less accumulation in heterozygous females from families with the classic phenotype (9.6 pmol/mL), and essentially undetectable in healthy controls (0.4 pmol/mL plasma) [11]. Notably, these glycosphingolipids are not elevated in males with the *GLA* "pseudodeficient" mutation D313Y, which is not pathogenic [12].

The first attempt to detect Fabry-related biomarkers by mass spectrometry imaging (MSI) was made on skin and kidney biopsies using secondary ion mass spectrometry (SIMS) and matrix-assisted laser desorption/ionization (MALDI) time-of-flight mass spectrometry in 2007 [13]. Subsequently, there was only one short report on heart tissue using low mass resolution MALDI mass spectrometry [14].

As renal complications represent a major site of glycolipid accumulation and organ dysfunction [15], efforts were directed to investigate the lipid distribution in the kidney of the murine model of Fabry disease [16] by accurate mass spectrometry imaging and immunohistochemistry to determine molecular species of the major accumulated glycolipids, to compare their distribution in tissue sections with immunochemical localization (IHC), and to assess whether MALDI MSI Gb3 signal intensities are comparable with quantitative data from flow injection electrospray ionization tandem mass spectrometry (FIA-ESI-MS/MS).

These studies were performed on Fabry knockout (FKO) and wild-type (WT) mouse as pilot studies to determine and compare the relative merits of MS and IHS in evaluating the renal sphingolipids and particularly the glycosphingolipids accumulated in GLA knockout Fabry disease model. These efforts represent a prerequisite for the future evaluation of human Fabry tissues by accurate mass spectrometry imaging.

Experimental

The studied *Gla* C57BL/6 knockout model (FKO) was a 70-week-old male mouse [16]. This mouse lacks the microvascular endothelial involvement and, therefore, serves as a model of the "later-onset" phenotype. For a control, a wild-type (WT) isogenic 70-week-old male C57BL/6 mouse was used.

Gb3 immunohistochemistry and MSI were performed on 6- and 12-μm consecutive kidney cryosections, respectively. The sections for IHC were briefly fixed with 4 % buffered paraformaldehyde exposed to standard blocking procedures and incubated for 60 min at 37 °C with monoclonal mouse anti-Gb3 antibody (Seikagaku, Japan) diluted 1:100. Antigen detection was carried out with anti-mouse EnVision + System-HRP (Dako, Denmark) with diaminobenzidine as chromogen, and sections were counterstained with Harris hematoxylin [17]. Additionally, polar glycosphingolipids were detected using periodic acid-Schiff (PAS) staining. Both Gb3 immunohistochemistry and PAS stains were additionally verified after two sequential lipid pre-extraction steps with 50 % ethanol for 10 min, chloroform/methanol/water (C/M/W,4:8:3, *v*/*v*/*v*) for 6 h, chloroform/methanol (C/M, 2:1, *v*/*v*/*v*)

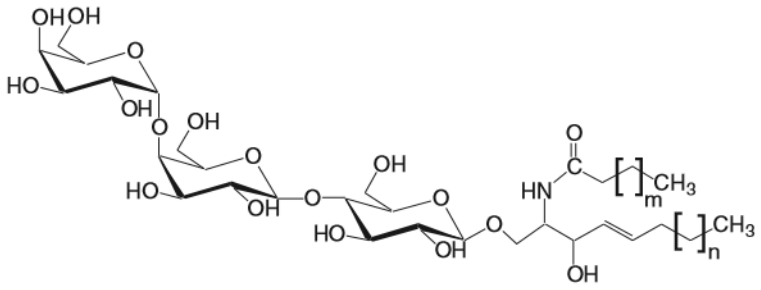

Fig. 1 General structure of globotriaosylceramides (Gb3) (*m*=13–23, *n*=11). Globotriaosylsphingosines (lyso-Gb3) are lacking the fatty acid chain. Sphingosine is d(18:1) in all isoforms

overnight, and then rinsing with 50 % ethanol; all steps at room temperature.

Sections for mass spectrometry imaging were obtained with a cryomicrotome CM1950 (Leica, Germany) at −15 °C, placed on indium-tin oxide-coated glass slides (Bruker Daltonics, Bremen, Germany), and then dried in a desiccator (30 min). α-Cyano-4-hydroxycinnamic acid was used as the MALDI matrix (7 mg/ml in 50 % acetonitrile/0.1 % trifluoroacetic acid) and was applied by the ImagePrep (Bruker Daltonics). An APEX-Q Ultra 9.4 FTICR (Bruker Daltonics) mass spectrometer equipped with an Apollo II ESI/MALDI dual ion source and a Smartbeam I laser (200 Hz) was used for mass spectral data collection. For all experiments, ion cooling and time of flight were set to 0.1 s and 0.4 ms, respectively. Mass spectra were collected over a mass range of *m/z* 300–1500 with 512 k data points and with a spatial resolution of 150 μm, acquiring 100 shots/pixel. MSI raw data were processed both by FlexImaging 3.0 (Bruker Daltonics) and in-house software mMass designed for direct lipid identification [18]. Individual spectra were also interrogated using DataAnalysis v4.1 (Bruker Daltonics).

In parallel, Folch liquid-liquid extraction with chloroform/methanol (2:1, *v/v*) was performed on consecutive tissue sections. Low mass resolution FIA-ESI-MS/MS bulk analyses were performed on AB/MDS SCIEX API 3200 or 4000 triple-quadrupole mass spectrometers. Three analytical replicates were evaluated in this study, and three fragments were monitored in multiple reaction monitoring (MRM) mode: sphingosine base fragment of positive ion *m/z* 264 for neutral glycosphingolipids, negative ion *m/z* 97 for sulfatides (SGalCer), and negative-ion *m/z* 291 for GM1 and GM3 gangliosides. Lipid quantitation was assayed with in-house synthesized C17:0 GM1 ganglioside and commercial lipid standards (e.g., C17:0 Gb3, Matreya LLC, PA, USA) as described elsewhere [19, 20].

Glucosyl- and galactosylceramides (GlcCer and GalCer, respectively) were quantified as ceramide monohexosides (CMH) because they are isobaric (have the same mass and product ions) and therefore are indistinguishable by MS. For the same reason, Ga2 (dominating in Fabry disease) and lactosylceramide (LacCer) were both evaluated as ceramide dihexosides (CDH). Results were normalized to 50 μg total protein in each sample.

Results and discussion

Murine renal glycolipids relevant in Fabry disease

Twelve different lipid classes in the knockout mouse model of Fabry disease (FKO) and control mouse (WT) were compared. Quantitative data were obtained in three technical replicates from FIA-ESI-MS/MS measurements which revealed essential identical lipid profiles with two important distinctions. The statistical significance of the results was validated with a *t* test (see the *p* values in the Electronic Supplementary Material (ESM) Table S1). In the 70-week-old FKO mouse, the Gb3 isoforms were present at 34 times higher concentrations compared to those in the control mouse (Fig. 2), reaching 10 nmol Gb3/mg tissue protein. This striking difference was even more evident when compared to previously reported glycolipid determinations in younger C57B16/SVJ129 *Gla* knockout Fabry mice [21]. In that report, the Gb3 accumulation was only three or five times higher in 5- or 12-month-old male mice, respectively. In addition, the increment of Gb3 levels in female Fabry mice was even more statistically significant [21].

Galabiosylceramides (Ga2), measured in the ceramide dihexoside fraction, represented the second lipid class increased in the FKO mouse and displayed an about 3-fold higher concentration (2.98 nmol/mg protein) compared to that in the wild-type mouse (1.02 nmol/mg protein). In agreement with the literature [21], none or very low amounts of lyso-Gb3 biomarkers were found in WT and FKO mice, respectively. Other lipid classes examined by us, i.e., globoside (Gb4), CMH, lyso-CMH, ceramides (Cer), sphingomyelin (SM), SGalCer, lyso-SGalCer, GM1, and GM3 gangliosides, remained comparable in both the disease and healthy mice. The detailed quantitation results are reported in ESM Table S1.

In addition to global glycosphingolipid analyses, the individual isoform profiles of the Gb3 fraction were assessed (Fig. 3). The C16:0, C20:0, C22:0, C24:0, and C24:1 fatty acylations were identified as the differently expressed lipid forms in the Fabry model and further selected for lipid visualization in mass spectrometry imaging experiments (see below). Interestingly, the isoform pattern in the FKO mouse was not exactly similar to that observed in the WT. It is worth mentioning that “higher” or “different” isoform content indicated in Fig. 3 is related to relative intensities only. On the contrary, the imaging mass spectrometry data show absolute intensities relevant to quantitation of actual lipid classes.

Isoforms in CDH, CMH, Cer, and SGalCer are depicted in ESM Figure S1. In all four lipid groups, comparable profiles were obtained with a single exception. In the ceramide dihexoside fraction, the C22:0-OH isoform was markedly elevated and the C24:0-OH was slightly elevated in FKO tissue.

Gb3 distribution in murine renal tissue

The lipid profiles in the kidney of FKO and WT mice were compared by bimodal visualization. Lipid localization was assessed by mass spectrometry imaging and correlated with immunohistochemical staining on consecutive sections. In the FKO mouse, the Gb3 concentrations of the five most

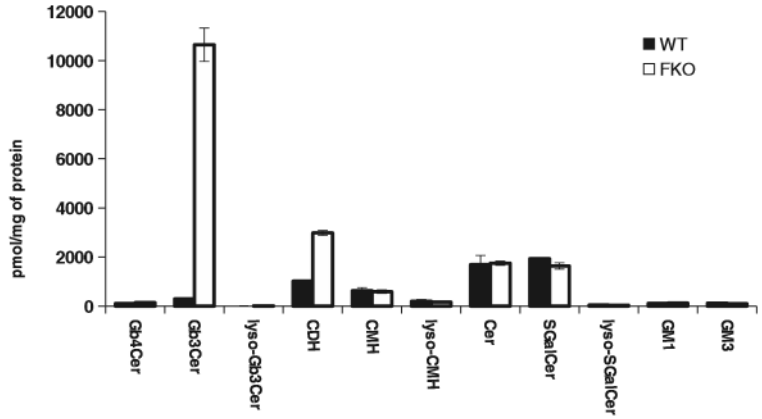

Fig. 2 Renal sphingolipid profiles determined in the FKO (*white*) and WT (*black*) murine renal tissue (three technical replicates). Abbreviated names *Gb4Cer*, *Gb3Cer*, *lyso-Gb3Cer*, *CDH*, *CMH*, *lyso-CMH*, *Cer*, *SGalCer*, *lyso-SGalCer*, *GM1*, and *GM3* are used for globotetraosylceramide (globoside), globotriaosylceramide, lyso-globotriaosylceramide, ceramide dihexoside, ceramide monohexoside, lyso-ceramide monohexoside, ceramide, sulfogalactosylceramide, lyso-sulfogalactosylceramide, monosialotetraglycosylceramide (GM1 ganglioside), and monosialodiglycosylceramide (GM3 ganglioside), respectively

abundant isoforms were 1–2 orders of magnitude higher compared to those in the WT mouse. This was in agreement with bulk ESI-MS/MS quantitation in lipid extracts from the whole sections. Specifically, the absolute intensities in MALDI signals of potassiated Gb3 (d18:1/C24:0) averaged over the whole tissue slice were ~588,000 and ~12,800 counts for the FKO and WT samples, respectively (Fig. 4). This 45-fold increase is consistent with the more precise ESI-MS/MS measurements reported above (~34-fold increase for the total Gb3 fraction). Our results reveal the dominating storage of five Gb3 species in the FKO kidney (ESM Figure S2). The same distributions were obtained in both coronal and transversal sectioning planes (Fig. 4).

In the FKO mouse, the IHC data confirmed the higher accumulation of Gb3 in renal cortex compared to the medulla. In both coronal (longitudinal) and transversal (cross) sections, the highest Gb3 concentration was observed in the subcapsular region of the renal cortex. In the WT mouse, only a background signal for Gb3 was detected in the renal interstitium (Fig. 4). The maximum Gb3 storage was in the renal cortical tubules of the FKO mouse, which exceeded the Gb3 accumulation in the FKO glomeruli. Renal tubules in the medulla had less Gb3 storage in contrast to their cortical counterparts. Gb3 staining intensity was more prominent in the inner part of the medulla in comparison with the outer part, being partially based on desquamated epithelium from the upper parts of the nephron in a form of tubular casts (Fig. 5). PAS staining of the renal glycosphingolipids resulted in a pattern similar to that obtained by immunohistochemistry (data not shown).

Whereas the antibodies recognized just the saccharidic region of the Gb3 molecule, mass spectrometry imaging provided a distribution pattern of lipid isoforms in the renal cortex. By MALDI MSI, Gb3 isoforms were present as sodiated and potassiated species exclusively. The observed

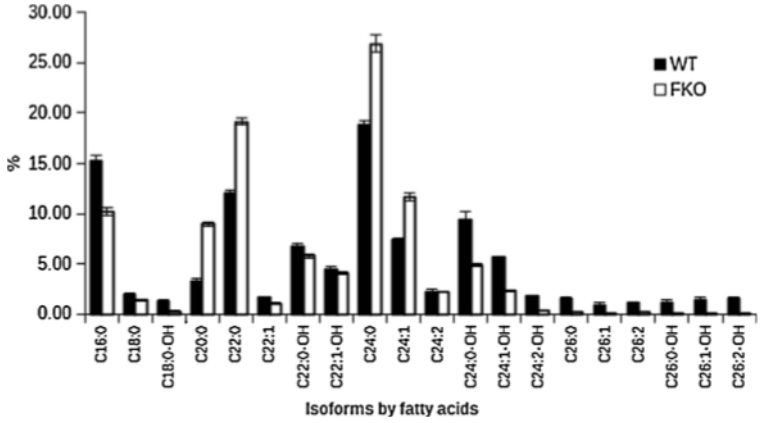

Fig. 3 Fatty acylation of globotriaosylceramides in murine FKO and WT renal tissues. C17:0 Gb3 isoform was used as internal standard

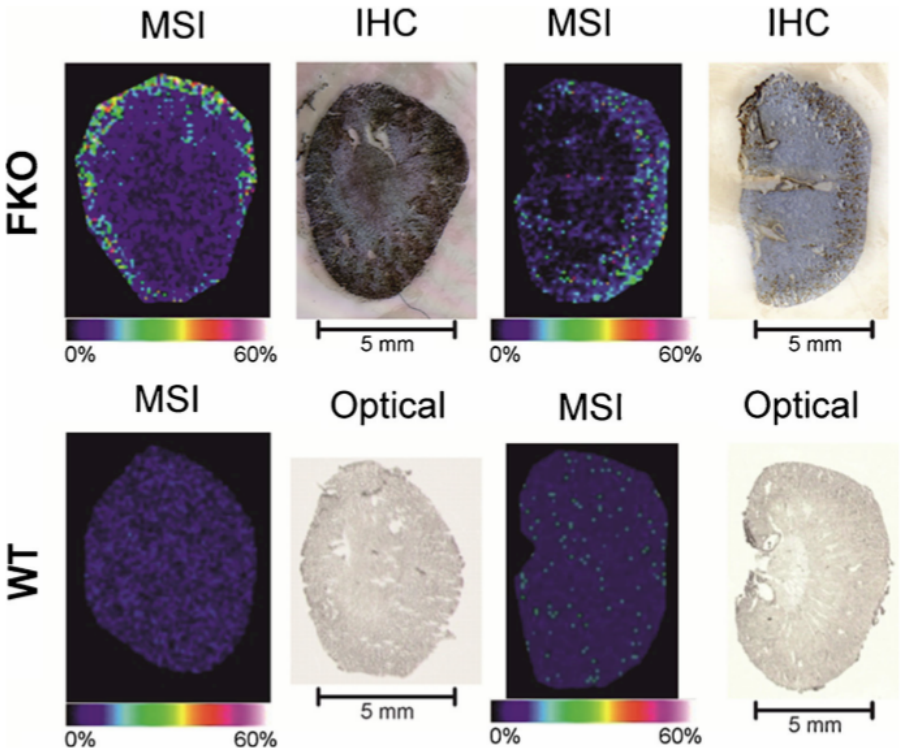

Fig. 4 Distribution of globotriaosylceramide (d18:1/24:0) in FKO (*top*) and WT (*bottom*) mice. Transversal (*all four left*) and coronal (*all four right*) sections show preferential accumulation of globotriaosylceramides in the renal cortex. MSI data revealed the sodiated molecules of Gb3 (d18:1/C24:0) at *m/z* 1158.785. IHC shows Gb3 visualized in *brown*, whereas the cell nuclei counterstained with hematoxylin are *blue*

Gb3 selectivity to Na^+ ions was higher. Some other lipid classes were also present in protonated forms (data not shown).

Possible MALDI matrix effects and chemical interferences were considered. The importance of accurate mass spectrometry imaging was illustrated on a potassiated Gb3 (d18:1/C24:1) example. With a low mass resolution instrument, its potassiated signal at *m/z* 1172.7439 would be undistinguishable from a component having a smaller mass defect and high abundance (ESM Figure S2). Similar signal complexity was also apparent in the Gb3 (d18:1/C24:0) mass spectrum (Fig. 4). In the mixture of different analytes, the MALDI ionization efficiencies could be potentially different for saturated and unsaturated fatty acids [22]. However, this behavior was not observed in our MALDI imaging experiments as evidenced by quantitative ESI-MS/MS control analyses.

All major Gb3 isoforms show similar mass distribution in the FKO renal tissue supporting the IHC data. No differences in storage capacity directly correlating with fatty acyl chain length or saturation in Gb3 were observed (Fig. 6). Isoform profiles dissected to distribution of $[M+Na]^+$ and $[M+K]^+$ are shown in ESM Table S2. Elevated Gb3 levels were also apparent in the FKO mouse tissue and were in agreement with ESI-MS/MS quantitative data (ESM Table S1).

The spatial distribution of Gb3 and Ga2 in the kidney reflects the expected lysosomal storage pattern of Fabry disease which is characterized by the lysosomal accumulation of both glycosphingolipids. The lysosomal storage pattern in the kidney of Fabry disease males with the classic phenotype has been described in detail with marked storage in glomerular podocytes and lesser amounts in glomerular endothelial and mesangial cells as well as in collecting tubules and loops of Henle [23]. Tubular glycosphingolipid storage with the exception of the cortical tubules and prominent deposition in the medullary portion of the nephron as well as in the system of collecting tubules with a decreasing gradient from the outer medulla to the papilla has been described by Vylet'al et al. [24]. The Gb3 accumulation in males with the later onset phenotype (cardiac variant) differs from that of males with the classic phenotype. Later onset males have little, if any, mesangial, interstitial, or vascular endothelial accumulation, while the major site of glomerular accumulation is in the podocytes. Also, there was little Gb3 accumulation in tubular epithelial cells [25].

In the FKO mouse, lysosomal glycosphingolipid storage partially resembling that observed in patients with Fabry disease has been described [26, 27, 16]. However, in the FKO mouse, the storage was greater in proximal tubules and

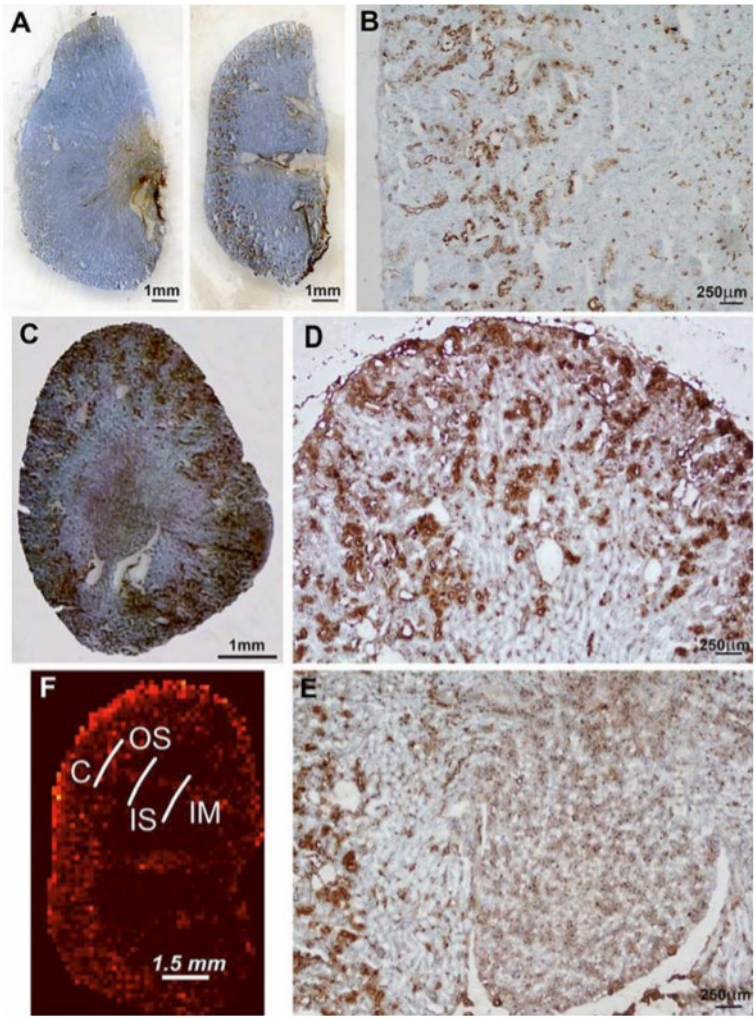

Fig. 5 IHC detection of globotriaosylceramides in FKO kidney in longitudinal (*upper line*) and cross (*bottom line*) sections. **A** Survey of the Gb3 staining pattern in FKO kidney (*right scan*) showing a strong spotted signal with a maximum intensity in renal cortex. WT kidney (*left scan*) is Gb3 negative in the cortex displaying a background signal in the renal papilla. **B** Detail of the previous section of FKO kidney (see **A**, *right scan*) focused on the renal cortex and corticomedullary junction shows that the signal for Gb3 is based on intensive storage in a portion of the cortical tubules. Note the decreasing positivity towards the medulla. **C** Survey of the Gb3 in the FKO kidney in a cross-section. The same Gb3 distribution observed in the longitudinal section with maximum staining intensity in the cortex, weak positivity in the inner medulla, and even less intensity in the outer medulla. **D**, **E** Details of the previous section demonstrating predominance of Gb3 tubular storage in the **D** cortex compared to that in **E** medulla. Note also the marked less Gb3 storage in glomeruli in **D** and Gb3-positive epithelial cells in the form of tubular casts in the medulla in **E. F** Histological profile of mouse kidney. MSI of a longitudinal section of FKO kidney. *C* cortex consisting of glomeruli, proximal convoluted and straight tubules, distal convoluted tubules, thick ascending limb of Henle's loop (TALH), cortical collecting ducts, and connecting tubules. *OS* outer strip of the outer medulla consisting of proximal straight tubules, TALH, and collecting ducts (CD). *IS* inner strip of outer medulla consisting of TALH, thin descending limb of Henle's loop, and CD. *IM* inner medulla consisting of thin descending and ascending limbs of Henle's loop and of the large CD

was markedly less in glomerular mesangial cells and podocytes [28] which correspond with the absence of proteinuria and renal insufficiency. Our immunohistochemical analyses of stored Gb3 revealed maximum staining intensity in cortical tubules (Fig. 5) which correlated well with the MSI results.

Cer, CMH, and SM distribution in murine renal tissue

Interestingly, the spatial distribution was detected of the other sphingolipids which are not generally accumulated in Fabry disease, including ceramides, ceramide monohexosides, and sphingomyelins (ESM Table S2). Their spatial distribution

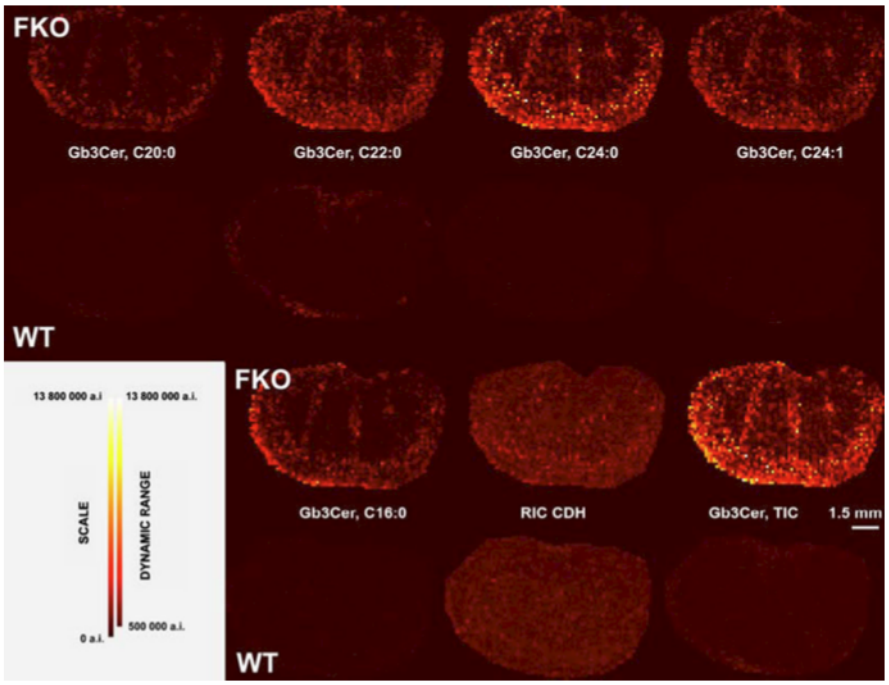

Fig. 6 Distribution of the major cationized molecules of Gb3 (d18:1) in FKO and in WT mouse and total ion chromatogram (TIC) of ceramide dihexoside. The specific Gb3 isoform as well as TIC images were constructed as the sum of sodiated and potassiated species. Reconstructed ion chromatogram (RIC) of CDH with dominating Ga2 was scaled to be comparable to Gb3 TIC

was compared to detect any unique distribution or amount in the FKO kidney. Generally, the distribution of Gb3 was compared to the distribution of two basic lipids, ceramide - the key structure and precursor of all sphingolipids - and sphingomyelin - a metabolically related and the most abundant representative of sphingolipid molecules. C16:0 sphingomyelin, the most prominent isoform, was colocalized with its biosynthetic precursor C16:0 ceramide, and analogously, the C24:0 isoform colocalized partially with C24:0 ceramide. Also, C24:0 Gb3 and the galabiosylceramide isoform (which was dominating in the CDH fraction) colocalized to a large extent with the corresponding ceramide isoforms, although ceramides are not the direct biosynthetic precursors of these lipids (ESM Table S2). This observation suggests that the ceramide distribution in the cortical region of the kidney - the site with high concentrations of sphingolipids - may reflect the ceramide's role in the biosynthesis or degradation of these complex sphingolipids. These observations suggest that the spatial distribution of the different isoforms and different types of sphingolipids differ in certain regions of the kidney and that the FKO mice are more similar pathologically to the human later-onset phenotype.

The detection of sphingomyelin on the MSI scan was similar in both the FKO and WT kidney and displayed a lamellar pattern with remarkable zonal differences between its short- and long-chain isoforms which were concentrated differently in the kidney (ESM Table S2). The C16:0, C18:0, C20:0, and C22:0 isoforms were prevalent in the outer medulla, whereas the signals for C24:0 and C24:1 sphingomyelin had showed maximal intensities in the cortex. The switch between shorter and longer sphingomyelin isoforms gradually progressed from the outer medulla to the subcapsular cortex, which may reflect a different tubular composition of the renal zones (Fig. 5F). Also, the development of the nephron and collecting ducts, as well as the high rate of cell turnover in these structures, should be considered.

C16:0 sphingomyelin is the major sphingomyelin isoform in extraneural tissues [29, 30]. It also was the major isoform in the WT and FKO mouse kidney which is consistent with the outer medulla being especially rich in sphingomyelin (ESM Figure S1, Table S2). The next most abundant sphingomyelins, the C24 sphingomyelin isoforms, were localized preferentially in the subcapsular cortex. The functions of the different sphingomyelin isoforms presumably relate to their physico-chemical properties in biological membranes. For example, sphingomyelin protects cholesterol from an aqueous environment with its large phosphocholine polar head group. The C16:0 sphingomyelin isoform optimally binds cholesterol structurally and is most abundant in the outer medulla [29].

The C24:0 sphingomyelin isoform can penetrate into the inner leaflet of the lipid bilayer where it may affect the diffusion rates in the membrane as do other longer lipids with asymmetric hydrophobic chains [29]. Another important function of sphingomyelin is its involvement in cell signaling processes and membrane modulation by its enzymatic conversion in situ in the membrane to ceramide by different sphingomyelinases [30, 31]. The assessment of physiological

activities of ceramide structures, which are important membrane components and second messengers, is increasingly focused on their chain length-specific effects [29–31]. The isoforms with shorter chains, like C16:0, are pro-apoptotic and are produced in the endoplasmic reticulum regions related to mitochondria and interact with Bak/Bax proteins [31]. On the other hand, the longer C24:0 isoforms may have pro-proliferative effects by stabilization of membrane domains. Although such lipid functions were not addressed by these studies, they indicate the important role of the spatial distribution of specific sphingolipid isoforms in the cell membranes of the murine kidney.

Conclusion

The analysis of the dynamic range and relative signal intensities of the Gb3 isoforms by MALDI mass spectrometry imaging provided similar trends to that of the FIA-ESI-MS/MS analysis. Whereas the Gb3 increase in the FKO renal tissue was 34-fold greater than that in the WT mouse in a calibrated FIA experiment, a similar increase was observed in MSI. As expected, the MSI also revealed a 3-fold increase of the ceramide dihexoside fraction primarily due to the Ga2 accumulation in the FKO kidney compared to that in the WT mouse, which presumably had little, if any, Ga2. These results are similar to the values obtained by ESI-MS/MS, which is prone to be compromised by chemical interferences. As an example, see the potassiated signal of Ga2 (C24:0) in the CDH fraction in Table S2 in the ESM.

The major benefit of MSI was the identification of the spatial distribution of the sphingolipids and their isoforms, which represent true chemical imaging. Contrary to IHC visualization that uses an anti-Gb3 monoclonal antibody for localization and provides a density map, mass spectrometry imaging identified five elevated Gb3 isoforms and their detailed distribution in renal regions of the FKO and WT mice. The differential comparison of averaged or projected [32] MSI data of the cortical and medullary regions provides new information about the spatial distribution and colocalization of metabolically related sphingolipids, especially when other ionization techniques or sample handling steps, which discriminate by polarity and/or mass, are used. Distinct renal functions of the subcapsular cortex and outer medulla in relation to the SFL distribution have been suggested and may stimulate further investigations.

Authors' contributions The manuscript was written through contributions of all authors. All authors have given their approval to the final version of the manuscript. RJD generated the FKO mouse. RD participated in mouse colony management, sample collection, preparation, and coordination of the study. LKr and HF were responsible for the MSI data acquisition; LKu collected and evaluated the quantitative MS data. JR and BA participated in preparation of lipid samples and protein analysis. MS and MV analyzed and evaluated the MSI data. HH was responsible for the IHC and in situ studies. LKry performed the immunohistochemical analyses. JL, LKu, HH, KL, RJD, and VH wrote the paper.

Funding sources The authors acknowledge the major direct support from the Ministry of Education, Youth and Sports of the Czech Republic (COST-CZ-LD13038, PRVOUK-P24/LF1/3, COST-CZ-LD13005 and UNCE 204011), Ministry of Health of the Czech Republic (Grant IGA MZ NT14015-3/2013), and Czech Science Foundation (P206/12/1150). Access to instrumental and other facilities was also supported by EU (COST BM1104, Operational Program Prague—Competitiveness project CZ.2.16/3.1.00/24023) and IMIC institutional research concept RVO61388971.

Conflict of interest RJD serves as a consultant to Amicus Therapeutics and Genzyme Corp, holds shares of Amicus Therapeutics, receives grants from Genzyme Corp., and receives royalties from Genzyme Corp. and Shire HGT.

References

1. Poupetova H, Ledvinova J, Berna L, Dvorakova L, Kozich V, Elleder M (2010) The birth prevalence of lysosomal storage disorders in the Czech Republic: comparison with data in different populations. J Inherit Metab Dis 33:387–396
2. Desnick RJ, Ioannou YA, Eng CM (eds) (2001) Alpha-galactosidase A deficiency: Fabry disease. The metabolic and molecular bases of inherited disease. McGraw-Hill, New York
3. Rombach SM, Dekker N, Bouwman MG, Linthorst GE, Zwinderman AH, Wijburg FA, Kuiper S, Weerman MAB, Groener JEM, Poorthuis BJ, Hollak CEM, Aerts JMFG (2010) Plasma globotriaosylsphingosine: diagnostic value and relation to clinical manifestations of Fabry disease. Biochim Biophys Acta-Mol Basis Dis 1802:741–748
4. Elleder M, Bradova V, Smid F, Budesinsky M, Harzer K, Kustermannkuhn B, Ledvinova J, Belohlavek, Kral V, Dorazilova V (1990) Cardiocyte storage and hypertrophy as a sole manifestation of Fabry disease—report on a case simulating hypertrophic nonobstructive cardiomyopathy. Virchows Archiv A: Pathol Anat Histopathol 417:449–455
5. Touboul D, Roy S, Germain D, Baillet A, Brion F, Prognon P, Chaminade P, Laprevote O (2005) Fast fingerprinting by MALDI-TOF mass spectrometry of urinary sediment glycosphingolipids in Fabry disease. Anal Bioanal Chem 382:1209–1216
6. Kuchar L, Ledvinova J, Hrebicek M, Myskova H, Dvorakova L, Berna L, Chrastina P, Asfaw B, Elleder M, Petermoeller M, Mayrhofer H, Staudt M, Kraegeloh-Mann I, Paton BC, Harzer K (2009) Prosaposin deficiency and saposin B deficiency (activator-deficient metachromatic leukodystrophy): report on two patients detected by analysis of urinary sphingolipids and carrying novel PSAP gene mutations. Am J Med Genet A 149A:613–621
7. Fuller M, Sharp PC, Rozaklis T, Whitfield PD, Blacklock D, Hopwood JJ, Meikle PJ (2005) Urinary lipid profiling for the identification of Fabry hemizygotes and heterozygotes. Clin Chem 51: 688–694
8. Kitagawa T, Ishige N, Suzuki K, Owada M, Ohashi T, Kobayashi M, Eto Y, Tanaka A, Mills K, Winchester B, Keutzer J (2005) Non-invasive screening method for Fabry disease by measuring globotriaosylceramide in whole urine samples using tandem mass spectrometry. Mol Genet Metab 85:196–202

of alpha-galactosidase A in Fabry disease: effect on fibroblast cultures compared with biopsied tissues of treated patients. *Virchows Arch*. 452: 651–665.

Kuchar L, Asfaw B, Ledvinova J. 2012. Tandem Mass Spectrometry of Sphingolipids: Application in Metabolic Studies and Diagnosis of Inherited Disorders of Sphingolipid Metabolism. In: Prasain JK, editor. *Tandem Mass Spectrometry - Applications and Principles*. Rijeka: InTech. p. 739–768.

Kuchar L, Ledvinova J, Hrebicek M, Myskova H, Dvorakova L, Berna L, Chrastina P, Asfaw B, Elleder M, Petermoller M et al. 2009. Prosaposin deficiency and saposin B deficiency (activator-deficient metachromatic leukodystrophy): report on two patients detected by analysis of urinary sphingolipids and carrying novel PSAP gene mutations. *Am J Med Genet A*. 149A:613–621.

Lantini MS, Cossu M. 1997. Ultrastructural localization of blood group antigens in human exocrine pancreas by immunogold labelling. *J Submicrosc Cytol Pathol*. 29:245–251.

Ledvinova J, Poupetova H, Hanackova A, Pisacka M, Elleder M. 1997. Blood group B glycosphingolipids in alpha-galactosidase deficiency (Fabry disease): influence of secretor status. *Biochim Biophys Acta*. 1345: 180–187.

Lidove O. 2002. Influence of blood groups B or AB on phenotype in a population of hemizygous patients with Fabry disease. *Acta Paediatr Suppl*. 439:124.

Manukyan L, Ubhayasekera SJ, Bergquist J, Sargsyan E, Bergsten P. 2015. Palmitate-induced impairments of beta-cell function are linked with generation of specific ceramide species via acylation of sphingosine. *Endocrinology*. 156: 802–812.

Motta PM, Macchiarelli G, Nottola SA, Correr S. 1997. Histology of the exocrine pancreas. *Microsc Res Tech*. 37:384–398.

Natomi H, Sugano K, Iwamori M, Takaku F, Nagai Y. 1988. Region-specific distribution of glycosphingolipids in the rabbit gastrointestinal tract: preferential enrichment of sulfoglycolipids in the mucosal regions exposed to acid. *Biochim Biophys Acta*. 961:213–222.

Ravn V, Dabelsteen E. 2000. Tissue distribution of histo-blood group antigens. *APMIS*. 108:1–28.

Roth J, Roth H. 1978. Electron-microscopic observations in internal organs in Morbus Fabry. *Virchows Arch A*. 378:75–90.

Schenkel-Brunner H. 1995. *Human blood groups: chemical and biochemical basis of antigen specificity*. Wien; New York: Springer-Verlag.

Seehafer SS, Pearce DA. 2006. You say lipofuscin, we say ceroid: defining autofluorescent storage material. *Neurobiol Aging*. 27:576–588.

Strohalm M, Kavan D, Novak P, Volny M, Havlicek V. 2010. mMass 3: a cross-platform software environment for precise analysis of mass spectrometric data. *Anal Chem*. 82:4648–4651.

Terman A, Brunk UT. 1998. Ceroid/lipofuscin formation in cultured human fibroblasts: the role of oxidative stress and lysosomal proteolysis. *Mech Ageing Dev*. 104:277–291.

Uchida E, Steplewski Z, Mroczek E, Buchler M, Burnett D, Pour PM. 1986. Presence of two distinct acinar cell populations in human pancreas based on their antigenicity. *Int J Pancreatol*. 1:213–225.

Vujasinovic M, Tepes B, Vujkovac B, Vujkovac AC, Tretjak M, Korat V. 2015. Exocrine pancreatic insufficiency is not a cause of abdominal complaints in patients with Fabry disease. *Wien Klin Wochenschr*. 127: 931–934.

Watkins WM. 2001. The ABO blood group system: historical background. *Transfus Med*. 11:243–265.

Wherrett JR, Hakomori SI. 1973. Characterization of a blood group B glycolipid, accumulating in the pancreas of a patient with Fabry's disease. *J Biol Chem*. 248:3046–3051.

Publications in impacted journals related to the topic of this Ph.D. thesis

Supplementary publication C

Kuchař L, Asfaw B, **Rybová J**, Ledvinová J.: Tandem Mass Spectrometry of Sphingolipids: Applications for Diagnosis of Sphingolipidoses. Adv Clin Chem, 2016; **77**: p. 177-219. **IF 4.722**

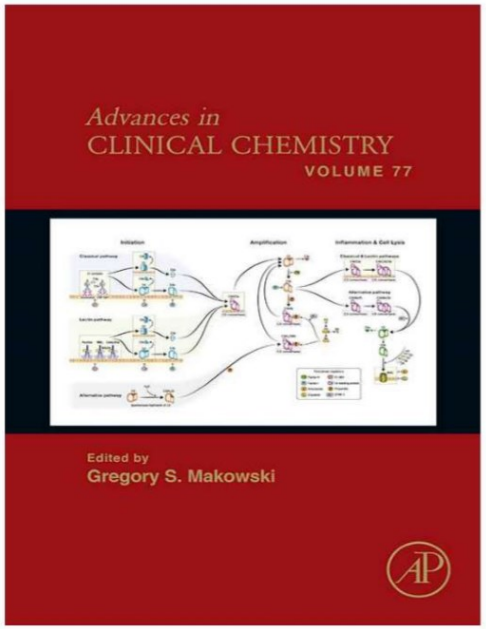

From L. Kuchař, B. Asfaw, J. Rybová and J. Ledvinová, Tandem Mass Spectrometry of Sphingolipids: Applications for Diagnosis of Sphingolipidoses. In: Gregory S. Makowski, editor, *Advances in Clinical Chemistry, Vol. 77*, Burlington: Academic Press, 2016, pp. 177-219.
ISBN: 978-0-12-804686-9

Academic Press

CHAPTER FIVE

Tandem Mass Spectrometry of Sphingolipids: Applications for Diagnosis of Sphingolipidoses

L. Kuchař[1], B. Asfaw, J. Rybová, J. Ledvinová[1]
Charles University in Prague and General University Hospital, Prague, Czech Republic
[1]Corresponding authors: e-mail address: ladislav.kuchar@lf1.cuni.cz; jana.ledvinova@lf1.cuni.cz

Contents

Abstract

In recent years, mass spectrometry (MS) has become the dominant technology in lipidomic analysis. It is widely used in diagnosis and research of lipid metabolism disorders including those characterized by impairment of lysosomal functions and storage of nondegraded–degraded substrates. These rare diseases, which include sphingolipidoses, have severe and often fatal clinical consequences. Modern MS methods have contributed significantly to achieve a definitive diagnosis, which is essential in clinical practice to begin properly targeted patient care.

Here we summarize MS and tandem MS methods used for qualitative and quantitative analysis of sphingolipids (SL) relative to the diagnostic process for sphingolipidoses and studies focusing on alterations in cell functions due to these disorders.

This review covers the following topics:

- Overview of the biochemistry of SL under normal and pathological conditions (lysosomal storage disorders, LSD)
- Overview of MS and its applications to the analysis of SL: evidence of pathological storage of nondegraded SL in cells and body fluids focused on a laboratory diagnosis of LSD, isoform profiles and deacylated forms of SL as new biomarkers, applications in enzymology and metabolic experiments in living cells using mass-labeled substrates.

Tandem MS is sensitive and robust in determining the composition of sphingolipid classes in various biological materials. Its ability to establish SL metabolomic profiles using MS bench-top analyzers, significantly benefits the first stages of a diagnosis as well as metabolic studies of these disorders. It can thus contribute to a better understanding of the biological significance of SL.

ABBREVIATIONS

BMP bis(monoacylglycerol)phosphate/lyso-bisphosphatidic acid
CerS ceramide synthase(s)
CID collision-induced dissociation
DBS dried blood spots
EET enzyme enhancement therapy/chaperone therapy
ERT enzyme replacement therapy
ESI electrospray ionization
FIA flow injection analysis
Gb3Cer globotriaosylceramide
HPLC high-performance/high-pressure liquid chromatography
HRMS high-resolution mass spectrometry
IMS ion mobility separation
LC liquid chromatography
LSD lysosomal storage disorder(s)
lyso-SL lyso-sphingolipid(s) (deacylated form of sphingolipid(s))
m/z mass to charge ratio
MALDI matrix-assisted laser desorption ionization
MLD metachromatic leukodystrophy
MS mass spectrometry
MS/MS tandem mass spectrometry
NP Niemann–Pick
NP-A/B Niemann–Pick type A or B
NP-C Niemann–Pick type C
NPC1 cholesterol transport protein NPC1
NPC2 cholesterol transport protein NPC2
Ppm parts per million
pSap-d prosaposin deficiency
SapB-d saposin B deficiency
Saps A–D saposins A, B, C, and D
SL sphingolipid(s)
SM sphingomyelin
SPC sphingosylphosphorylcholine—lyso-sphingomyelin
SPC509 sphingosylphosphorylcholine with 50 *m/z*
TLC thin layer chromatography
UPLC ultraperformance/ultrapressure liquid chromatography

1. INTRODUCTION

Sphingolipids (SL) are an amazing and diverse group of lipids found in all eukaryotes, some prokaryotes, and viruses. The early history of SL is connected with the German biochemist J.L.W. Thudichum and his famous book "*A Treatise on the Chemical Constitution of the Brain*" (Bailliere, Tindall and Cox, London, 1884).

Thudichum's work started research in the field of SL, a class of lipids originally isolated from human brains. The structure of the basic component, sphingosine was elucidated in 1947 by Carter [1], which resulted in significant progress in the field of sphingolipid biochemistry in the next years [2–7]. This research continues now as part of the field of lipidomics (http://www.lipidmaps.org).

The first clinical and pathological findings in patients suffering from diseases associated with deposition of various SL were reported in the late 19th and early 20th centuries (W. Tay, 1881, B. Sachs 1887, P. Gaucher 1882, J. Fabry 1897/1898, W. Anderson 1897, K. Krabbe 2016, A. Niemann 1914, L. Pick 1927) [8–10]. Many other types of these diseases, which now belong to the group of lysosomal storage disorders (LSD), started to be recognized long before the discovery of the lysosome by Christian de Duve in 1955 [11]. The nature of the accumulated products was often demonstrated long after the first description of the disease, eg, glucocerebroside in Gaucher and sphingomyelin (SM) in Niemann–Pick (NP) diseases were biochemically identified in 1934 [12].

A link between storage products and defective enzyme function was first demonstrated by Hers based on observations made in type II glycogenosis (Pompe diseases) in 1963 [13]. Shortly thereafter, defects in other lysosomal enzymes were identified and this led to the basic classification of different

types of LSD. A good example is Gaucher disease, the metabolic basis of which was not described until 1965 when Brady and collaborators reported evidence of acid beta-glucosylceramidase deficiency [14].

The history of NP disease is also interesting. It was originally viewed as one unit with several variant subtypes (A, B, C, and D). However, further investigations based on observations of multiple lipid storage and somatic cell hybridization studies suggested that Niemann–Pick type C (NP-C) was a separate entity. In 1982, The International Symposium on NP disease in Prague declared NP-C to be a separate disease [15], while Niemann–Pick types A and B (NP-A/B) have retained their original classification as an acid sphingomyelinase deficiency. Indeed, the next stage of research confirmed that the genetic defects in NP-C involved lysosomal cholesterol transporters, NPC1 and NPC2 proteins [16–18], which was accompanied by secondary accumulation of certain SL, especially SM.

Progress in research and diagnosis of sphingolipidoses required systematic development of modern, sophisticated methods and instruments to optimally separate and characterize lipids from diverse biological samples. Analytical separation techniques have gradually developed from thin layer and liquid chromatography (LC) [6] to sophisticated new methodologies based on the principles of mass spectrometry (MS) [19–21].

One of the most commonly used MS analytical methods is tandem mass spectrometry (MS/MS), which meets the requirements of both, high selectivity and sensitivity, even when analyzing crude lipid samples. Therefore, this overview will focus on the contribution of MS/MS to the development of sphingolipidomics and its use in diagnostics of inherited disorders of sphingolipid catabolism.

2. STRUCTURE AND FUNCTION OF SL

SL are a ubiquitous lipid category with unique biophysical properties that are important in the formation of membranes and their domains. Hydrophobic ceramide represents the core structure of complex SL and consists of a sphingoid base backbone and a long-chain fatty acid attached by an amide bond (linkage) to the 2-amino group of the base [22]. This hydrophobic core is responsible for SL participation in the generation or modulation of membranous structures. Fatty acids bound in the ceramide are also responsible for the shape and diverse functions of the molecule [23–27].

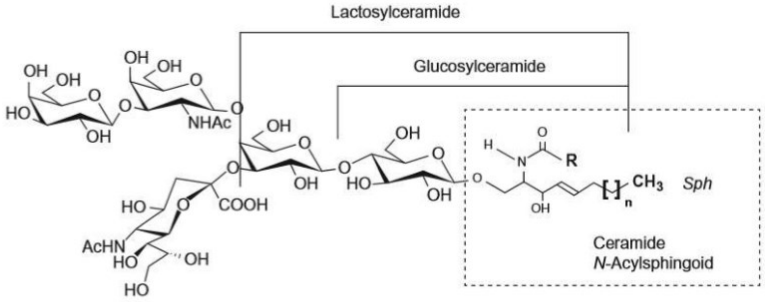

GM1 ganglioside (Galβ1-3GalNAcβ1-4(NeuAcα2-3)Galβ1-4Glcβ-Cer)

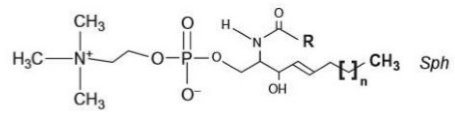

Sphingomyelin (*N*-acyl-sphing-4-enine-1-phosphocholine)

Fig. 1 Structure of sphingolipids: GM1a ganglioside as a representative of glycosphingolipids, sphingomyelin as a representative of phosphosphingolipids. Different molecular species (isoforms) of sphingolipids are represented by fatty acids having different carbon chain length (R) in the range of C14–C24 carbons, mostly in saturated (or monounsaturated) forms. Some of them can be hydroxylated. The most common sphingoid base (Sph) backbone has 18 carbons in the chain with a *trans* 4–5 double bond (major extraneutral form). Sphingoid bases containing 20 carbons are present in a significant quantity in the nervous tissue.

Hydrophilic structures can be bound to ceramide (Fig. 1) via glycosidic or ester bonds. They protrude away from the membrane and play important roles in adhesion, recognition, differentiation, antigenic functions, signaling, and immunity [28–39].

2.1 Biosynthesis of SL

De novo biosynthesis of ceramides begins in the lumen of the endoplasmic reticulum with condensation of L-serine and palmitoyl-CoA to 3-ketosphinganine, which is catalyzed by serine palmitoyl-CoA transferase. 3-Ketosphinganine is then reduced by reductase and NADPH+H to sphinganine. Ceramide synthase (CerS) produces dihydroceramide from sphinganine and Acyl-CoA, which is then processed by dihydroceramide

desaturase to ceramide [34,40–43]. In the recycling pathway, the ceramide is directly produced from sphing-4-enine and Acyl-CoA [44].

CerS are an important group of enzymes that regulate the biosynthesis of molecular species of ceramides. So far, six different CerS with different tissue expression and substrate specificity have been reported [41,45].

Biosynthesis of galactosylceramides and sulfatides takes place in the endoplasmatic reticulum, whereas glucosylceramides and other more complex SL are synthesized (after ceramide transport) in the Golgi apparatus, eg, SM synthesis is located in the lumen of the trans-Golgi [40,43,46–48].

2.2 Degradation of SL

Catabolism of SL (Fig. 2) takes place in the endolysosomal compartment of the cell. Degradation products then enter lipid recycling pathways, which are important regulatory mechanisms for cell homeostasis [49,50].

Lysosomal degradation of SL is going on the surface of intralysosomal membranous vesicles originating from endosomal intraluminal vesicles. High concentrations of bis(monoacylglycerol)phosphate (BMP) and to some extent, also phosphatidylinositol-3,5-bisphosphate, generate the negative charge required for docking of positively charged acidic hydrolases. The low internal pH of lysosomes, which is needed for proper function of acidic hydrolases, is maintained by a specific V-ATPase. A thick glycocalyx layer protects intralysosomal membranes from self-degradation [49,50].

Glycosphingolipids with short oligosaccharide chains (having four or less saccharide units) require protein activators (saposins A, B, C, and D, and the GM2 activator) for their mobilization from the hydrophobic membrane and activation of catabolic reactions [50–52].

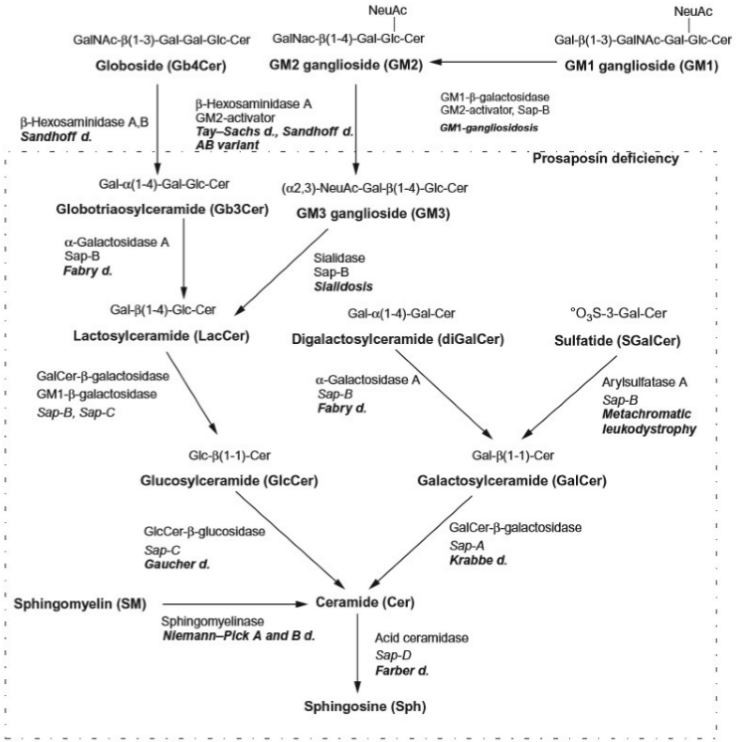

Fig. 2 Degradation pathways of sphingolipids with participating enzymes and activator proteins (*Saps A–D* and *GM2 activator; in italics*). Diseases caused by impairment of specific catabolic steps are indicated.

2.3 Lysosomal Storage Disorders

Defects in genes encoding lysosomal hydrolases and several nonlysosomal proteins involved in lysosomal biogenesis and functions characterize a group of inherited diseases known as LSD. They currently encompass more than 50 diseases [10,53]. Impaired lysosomal processing of specific substrates leads to intralysosomal accumulation and failure of the respective cellular functions, eg, calcium homeostasis, oxidative stress, autophagy, inflammation, and lipid trafficking [54]. Defects in lysosomal processing of SL belong to the category of sphingolipidoses [50,51,55] as shown in Fig 2.

LSD are considered to be rare diseases with a combined prevalence from 7 to 14 per 100,000 live births in the majority of Caucasian populations [53,56–58]; however, the frequency estimate of specific disorders differs between countries and can be higher in some geographically isolated areas or in certain ethnicities [59,60]. Sphingolipidoses are the most prevalent group with an approximate proportion 50% of all LSD [58]. The numbers of patients with late-onset disorders are constantly increasing, which suggests that LSD have apparently been under diagnosed. Diagnostic procedures have traditionally been based mainly on clinical symptomatology, which can miss attenuated forms of LSD as well as asymptomatic individuals. In recent years, newborn screening programs have demonstrated much higher incidences of some selected LSD, compared with previous studies, because screening programs can reveal even mild forms of these diseases [61,62].

Screening programs were made possible thanks to the introduction of advanced technologies such as MS/MS and the ability to perform analyses of acid hydrolases on dry blood spots (DBS) [63–68]. Continued development in these techniques, however, has exposed some ethical problems because neither enzymological results nor determination of the type of mutation can accurately predict disease progression and the need for therapeutic intervention especially in the late-onset variants of LSD. This is a frustrating fact for both patients and doctors when deciding on treatment. Large natural history studies and longitudinal monitoring of the course of early identified late-onset variants with or without treatment are becoming crucial [69,70].

Current trends in the treatment of these diseases are based on three main strategies: (1) enzyme replacement therapy (ERT), which is the most widely used, (2) substrate reduction therapy, and (3) enzyme enhancement/chaperone therapy (EET) [71,72]. Due to the hematoencephalic barrier, ERT has limitations in the treatment of neurological disorders; therefore, it is typically used for nonneurological types of LSD, such as Fabry and Gaucher type 1 diseases. Bone marrow transplantation has been found efficient in *the presymptomatic stage* of some neurological LSD, eg, Krabbe disease [73]. Therapeutic outcomes require monitoring on the biochemical level to evaluate therapy efficiency [74–78]. However, for many of these diseases suitable biomarkers still need to be found in order to better monitor the course of treatment. This is also one of the most important challenges for MS technologies.

3. MASS SPECTROMETRY OF SPHINGOLIPIDS

3.1 Theoretical Background

MS is an analytical method based on measurement of the mass to charge ratio (m/z) of ions in a gaseous state [19,79]. Mass spectrometers consist of an ion source, a mass to charge analyzer, and a detector. Ion sources can be differentiated according to specific criteria [19,79] of which two soft methods of ionization—electrospray and matrix-assisted laser desorption ionization (MALDI), clearly dominate in MS instruments used in clinical laboratories.

3.1.1 Electrospray Ionization

Electrospray ionization (ESI) generates gaseous ions from polar compounds in liquid solvents passing through a capillary tip on which a strong electric field is applied [19,79–81]. The main advantages of ESI are (1) the ability to directly infuse a sample, usually a crude lipid extract, into the ion source [20] and (2) direct coupling to LC [82]. Direct infusion of the sample (shotgun analysis) or flow injection analysis (FIA-ESI) technique commonly suffers from matrix effects associated with coextracted compounds [83,84]; however, they are fast and simple and can utilize solvents providing the best yields of ions.

3.1.2 LC Coupled to ESI-MS/MS

This combination uses different solid phases for LC separation based on the requirements of the analysis. Normal phase LC (eg, on a silica gel column) separates SL into classes according to the hydrophilic part of the molecule. In contrast, reverse phase LC of lipids is based on the different properties of hydrophobic part of their molecules [82].

LC separation is also important for analysis of isobaric compounds, such as glucosyl- and galactosylceramide, which cannot be resolved using shotgun MS [85].

The key advantages of LC are the reduction of the matrix effect of coextracted impurities, increased sensitivity, and improved identification of mutually interfering compounds [83,84]. Retention time adds another parameter that improves the specificity of analysis. However, these benefits are effective only under well-tuned LC operating conditions with specific demands for ESI. Properties of the mobile phase (pH, composition of the organic phase, etc.) may affect the efficacy of ESI and formation of product ion spectra [86–88]. Additionally, retention time is partly dependent on the composition of the matrix [89]. All these factors demonstrate that coupling of LC to ESI–MS/MS requires the conditions to be thoroughly balance for optimal ESI efficiency with optimal LC separation of analytes.

3.1.3 MALDI

The second most widespread ionization method is MALDI. Gaseous ions are generated when a matrix, with dissolved analytes, absorbs the energy of a laser beam causing ionization of the surface layer during ablation of the sample [19]. The generation of single charged ions dominates in MALDI whereas ESI generates both single- and multiple-charged ions. Another difference is that MALDI cannot be directly coupled to LC. To achieve good reproducibility is also more complicated [90,91] and requires thorough sample preparation and application of standards, eg, due to the heterogeneous distribution of lipids that results from sample crystallization [92,93].

On the other hand, MALDI has some advantages over other methods like the ability to aim the laser beam at specific sites on the surface and

evaluate the spatial distribution of compounds. This is perfectly exploited in mass spectrometry imaging, which has the potential to specifically locate biomarkers in exact tissue regions [94].

3.1.4 MS/MS: With Low-Resolution Analyzers

MS/MS is a methodical approach using several common processes in the following order: ionization of sample molecules, precursor ions selection, fragmentation of precursors, and formation and selection of product ions and their detection. This system couples two mass analyses and can be carried out either in time (eg, quadrupolar ion traps) or in space (eg, triple quadrupole mass spectrometry) [79,95,96].

For MS/MS with *triple quadrupole MS/MS instruments*, the MS analysis of precursor and product ions (in the form of ion beam) takes place in different physical regions of MS/MS instrument. This instrumental arrangement is called tandem-in-space. In *quadrupole ion trap MS/MS instruments*, the precursor ions are trapped in the one cell. The analysis of precursor ions, generation, and analysis of product ions are performed in the same physical space (ion trap cell) and occur sequentially at different time periods. Such MS/MS analysis is called tandem-in-time. Generally, both instrumental arrangements can produce essentially the same mass spectra for the analyzed compounds [95,97].

Bench-top instruments that are currently used for MS/MS are typically equipped with low-resolution quadrupole mass filters and are able to exactly measure the nominal mass of gaseous ions. The major advantage of these instruments is high dynamic range and reproducible spectra measurements, which makes them the instrument of choice for quantitative analysis of lipids and other metabolites in clinical praxis. Besides quantitative analysis, these instruments are also used for other analyses that require accurate and reproducible measurements of the lipid signals, eg, evaluation of the ratios of molecular species.

The resolution (R) is an important parameter of the device and is defined as the ability to distinguish between two peaks of slightly different m/z:

$$R = \frac{m/z_2}{m/z_1 - m/z_2} \Rightarrow \frac{m/z \text{ of second peak}}{\Delta m/z \rightarrow \text{difference between two separated peaks}}.$$

Fragmentation of precursor ions can be achieved in different ways [19]. One example uses a collision-induced dissociation (CID), which is the most commonly used fragmentation method in MS/MS sphingolipidomics [79,96,98] (Fig. 3). The most common sphingolipid fragments are derived

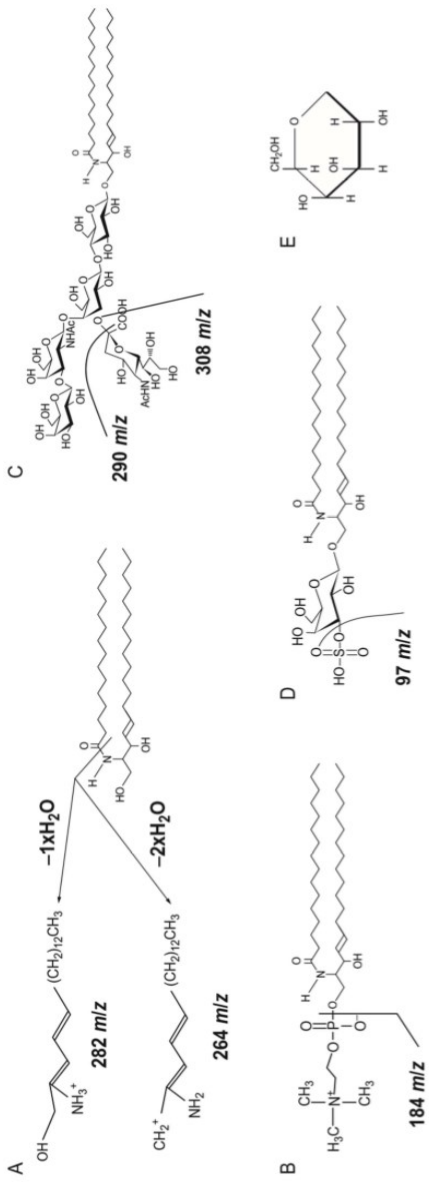

Fig. 3 Fragmentation reaction after collision-induced dissociation (CID): (A) general ceramide fragmentation reaction, (B) sphingomyelin, (C) ganglioside, (D) sulfatide, (E) neutral saccharide fragments generated during neutral loss scan, and (F) fragmentation of glycosphingolipids having sphinganine in a ceramide core.

from ceramide (d18:1 base) with m/z 264 and 282 [21,99–101]. The 282 m/z fragment is used as a specific fragmentation product of deacylated derivatives of SL (lyso-SL) [99,101–103]. The following examples include other useful fragments: phosphocholine—m/z 184 [21,104,105], sialic acid—m/z 290 and 308 [106,107], and the sulfate group—m/z 97 [108,109]. A neutral loss scan of saccharides derived from oligosaccharide chains of glycosphingolipids (Fig. 3) represents another fragmentation reaction that is particularly preferred for those containing dihydroceramide or sphinganine [101,106,110,111].

3.1.5 High-Resolution Mass Spectrometry

High-resolution mass spectrometry (HRMS) provides the highest possible precision of m/z measurement using different analyzers such as time of flight, Orbitrap [112], or Fourier transform ion cyclotron resonance. Standard resolution is usually at least 20 times higher than in low-resolution MS systems [95].

Compounds with the same nominal mass are discriminated via an exactly measured *specific mass defect*, which represents the difference between the exact and nominal mass of a particular compound [113].

The ability of HRMS to exactly identify compounds according to summary equations is limited because the required resolution is m/z dependent. The number of possible combinations of elements having the same nominal mass in the molecule increases with m/z, eg, for 118 m/z accuracy only 34 ppm is enough but for 750 m/z 0.018 ppm is necessary [114]. Accuracy of m/z measurement, defined as parts per million (ppm), is expressed by the equation:

$$\mathrm{ppm}_{\text{error of the mesurement}} = \frac{\text{calculated exact mass} - \text{measured mass}}{\text{calculated exact mass}} \times 10^6.$$

To summarize the previous two sections, two main distinct families of mass spectrometers have evolved. *Low-resolution MS instruments*, usually in the MS/MS setup excel in dynamic range of signal response and reproducibility of analysis. This makes them particularly suitable for quantitative analysis and other similar applications, eg, evaluation of precise ratios of molecular species of analyzed metabolites. They are usually constructed as a bench-top apparatus, which allows for routine use. *HRMS instruments* are, on the contrary, leaders in resolution and accuracy of m/z determination. This allows them to separate peaks of compounds with close m/z and measure their m/z with standard 1 ppm accuracy. The enormous amount of data produced from samples makes HRMS suitable for use in nontargeted metabolomic/lipidomic analyses. They are usually operated as research instruments.

3.1.6 MS: Limits and Progress in the Field

HRMS evaluates the elemental composition but cannot reveal anything about the structure, which in turn can be exposed using MS/MS. Conversely, in MS/MS analysis, it is impossible to precisely select precursor ions. This is caused, in general, by the fact that precursor ions are selected by quadrupole mass analyzers with nominal (low) mass resolution and thus the precursor m/z window may include more than one compound. Fragments are then produced from all compounds with the same nominal mass, and interpretation of such a spectrum is not based on an accurately measured m/z at high resolution. Specificity and selectivity of analysis depends on precursor and product ion pairs, which are also called transition pairs. This is partially solved by measuring ratios of three transitions pairs for the same precursor ion to identify a compound. Sensitivity is thus determined by the fragment with the lowest signal. Separations of analytes greatly helps in solving these problems, therefore LC–MS/MS coupling is the much preferred technique.

Another limitation is that neither MS/MS nor HRMS can distinguish isobaric compounds but, on a positive note, these methodical problems stimulate further development in the field.

A promising new method for separating compounds is *ion mobility*, which also has the potential to separate isobaric molecules. Ion mobility separation (IMS) is based on different speeds of ions in an electromagnetic field, ultimately depending on the size and shape of the measured ion. Principles of IMS can be found in the works of McLukey [95], Buryakov [115], and Giles [116].

Speed of ion movement through IMS unit is a matrix independent characteristic, and one of the most stable parameters which in combination with HRMS can gradually improve analyte identification [89]. IMS can also be combined with LC separation and with mass spectrometry imaging [117].

These technological improvements have had a major impact on metabolomics including lipidomic analyses and their clinical applications [89,117–121]. *Nontargeted analysis* using HRMS is going to become the method of choice in metabolomic analysis due to its capability of measuring all ions in the whole mass range (high-resolution full spectrum analysis). It produces huge amounts of data that must be statistically processed and could lead to the discovery of new biomarkers [122–124]; however, they will still need to be verified by *targeted analysis* using highly quantitative and reproducible MS methods, mostly exploiting low-resolution mass spectrometers [125]. When solving complicated cases in the clinical practice, the global analysis of metabolites should include HRMS as the first step of testing to assess changes in the MS spectrum.

Revealed changes must be then verified and quantitatively confirmed by precise MS quantitative methods. This complex approach can only be performed in well-equipped laboratories. In the simplified scheme, it is also possible to evaluate panels of biomarkers for selected groups of diseases using low-resolution mass spectrometers.

It should be noticed that new analytical procedures should be implemented using unified strategies and conceptions, together with the establishment of open access libraries of biomarkers.

3.2 Sample Preparation: Lipid Extraction

SL are usually extracted using mixtures of organic solvents with different polarities to enrich their content in the sample. The most widespread methods of lipid extraction using mixtures of chloroform and methanol are described by Folch *et al.* [126], and Bligh and Dyer [127]. Recently, the *Shevcenko* method using methyl-*terc*-butyl ether has become increasingly popular [128]. Exhaustive extraction of various hydrophobically different lipid classes from biological material always requires repeated use of organic solvent mixtures with different polarities [129]. The methods of extraction and purification of SL from different categories were extensively reviewed in several volumes of *Methods in Enzymology* [130–132] as well as in other publications [133,134]. DBS are also usually extracted prior MS analysis using off-line solid–liquid extraction with organic solvents in tubes or wells. A second and less common option is the online extraction using special instruments that are coupled directly to the ion source. The advantages and disadvantages of various methods of DBS processing, prior MS analysis, are summarized in a comprehensive review by Wagner *et al.* [135].

3.3 Quantitative Analysis of Lipids

For quantitative analyses, a linear relationship between the relative intensity of pseudo-molecular ions and the mass is required. From the ion sources, the ESI provides a 10,000-fold dynamic range in the low concentration regime of individual lipids. It achieves excellent reproducibility of measurements in one identical sample [20,136]. This has made ESI the ion source of choice for quantitative lipid analysis using specific internal standards, which compensates for various errors caused by sample preparation and by variable signal suppression due to coeluted matrix compounds. Internal standards are either structural analogs labeled with stable isotopes, structural homologues, or compounds from the same chemical family. Quantitative MS generally uses three major approaches: external standard method (using an external calibration curve), internal standard method, and the isotopic dilution method, described in detail by de Hoffman and Stroobant [79].

A large number of lipid internal standards are already commercially available but some specific compounds must be prepared in the laboratory by chemical [137,138] or enzymatic semisynthesis [137,139–142]. However, there are specific quantitative methods which enable to overcome this lack. One of the most universal and simple method was described by Cifkova *et al.* [143]. Concentrations are calculated via class specific response factors related to the single internal standard, which is used as a common reference for all analyzed lipids.

ESI requires mass analyzers with a good reproducibility and high dynamic range. Quadrupole mass analyzers meet these needs, their maintenance is easy and operational conditions are compatible with routine clinical laboratory environments. This leads to the dominant position of ESI–MS/MS instruments in the quantitative analysis of lipids in clinical biochemistry.

4. SPHINGOLIPIDOMICS AND LSD DIAGNOSIS

Sphingolipidoses, as do all LSD, have remarkably variable symptom presentations, which may include a spectrum of neurological and/or visceral components, eg, slow development, visceromegaly, cardiac and kidney involvement, dysmorphic features (facial dysmorphism), skeletal deformities, dermatological, and ocular findings. Also the age of the onset can range from newborn to late adult, even with the same disease (although, usually caused by a different gene mutation), which, in general classifies LSD into clinical subtypes (eg, infantile, juvenile, and adult forms). Diagnosis is often complicated, because universal diagnostic tests do not exist. An excellent concise review of current diagnostic approaches at the clinical, pathological, and laboratory level, together with the classification and description of relevant storage diseases and potential treatments are provided in a book by Mehta and Winchester [144].

Initial investigations include urine and blood, occasionally cultured skin fibroblasts (NPC, mucolipidosis I) or exceptionally a tissue biopsy.

Definitive confirmation of a suspected diagnosis is based, in most cases, on the evidence of deficient activity of a particular lysosomal enzyme in white blood cells and a description of mutation in the respective gene.

Today, the use of DBS is increasing especially in those LSD with a deficiency of a specific lysosomal enzyme function because it simplifies blood sample collection and processing and particularly transportation. Using MS/MS for DBS enzymology accelerated the pathway to a definitive diagnosis in large-scale population screening programs, which included newborns.

The preliminary laboratory indication regarding the type of the disease can be obtained from screening tests on blood and urine samples by detection of storage products or increased levels of some plasma enzymes (eg, chitotriosidase, lysosomal hydrolases in I-cell disease).

For sphingolipidoses, TLC and high-performance/high-pressure liquid chromatography (HPLC) have traditionally been the basic methods used to establish the storage of nondegraded SL in the first stage of the biochemical investigation. In recent years the importance of MS/MS in the diagnosis of LSD has increased significantly. This method has considerable advantages over the chromatographic procedures—the analysis is quantitative and much more sensitive, fast, and less laborious.

However, for many SL it is the coupling of chromatography with MS (eg, HPLC–MS/MS, UPLC–MS/MS) that achieves the best results, since it benefits from both methodological approaches.

4.1 Primary Stored Sphingolipid Substrates

Currently, MS has become the most important method for SL analysis suitable for measurement of both absolute and relative metabolite quantities. Its tremendous advantage is its ability to examine molecular types of SL relative to the spectrum of different fatty acids and sphingoid bases.

Evidence of lysosomal storage of nondegraded SL is useful supporting information for making a diagnosis. Increased amounts of SL in tissues and body fluids have traditionally been part of the basic biochemical characteristics of different types of sphingolipidoses, and they are still valuable diagnostic indicators [74,109,111,145,146]. Laboratory diagnosis is currently being more and more targeted at utilization of noninvasively obtained material, and therefore this chapter will focus primarily on urine, blood, and blood plasma as sources for first-tier analysis to establish LSD status.

Urine samples are easily acquired and are preferable for the first stage of laboratory diagnosis in many suspected LSD cases, often with indefinite clinical symptoms. However, in lipidoses, this analysis is still facing the problem how best to normalize lipid concentrations. In clinical chemistry, it is creatinine that reflects dilution of urine and is a commonly used parameter for normalization of urinary metabolites. The main sources of urinary lipids, however, are desquamated cells of the urinary tract, mainly from the loop of Henle and distal tubules, which are without any direct metabolic relation to creatinine.

Despite that, creatinine is still used as a normalizer in many publications [147–149], although some authors have pointed out the risk of false positive results [150]. It is obvious that the concentration of SL standardized to urinary creatinine should be artificially increased when its concentration is less than 1 mmol per liter of urine, which is a creatinine value quite frequently observed in neonates and infants and this might lead to an incorrect diagnosis in some suspected cases (eg, metachromatic leukodystrophy (MLD), Fabry and Farber diseases, pSap-d and SapB-d) [111]. It is therefore essential to take into account that samples from patients should be age- and creatinine matched to controls [149,151]. In cases with extremely low levels of creatinine, it is useful to employ other methods for normalizing urinary lipids, such as a lipid/lipid ratio [109,146,152,153], or to relate lipid concentrations to the volume of urine [111,150]. However, even these methods are not fully rational since the latter ignores diuresis, and the former faces the problem that urine can have a very heterogeneous composition of cells in the sediment and hence different concentrations of reference lipids. However, it may be helpful in some questionable cases.

Percentage composition of the main urinary SL [146] provides a relevant picture of their relative proportions and may also indicate a direction for further investigation in the absence of reference parameters, which is the advantage over other methods (see Fig. 4 for details). In any case, confirmation of a diagnosis by enzymology (in lysosomal enzymopathies, eg, MLD and Fabry disease) and DNA analysis must follow as the final step.

Another way to bypass this problem is profiling molecular species of lipids characterized by different long-chain fatty acids [154], which enables monitoring changes in their relative representation in respect to the nature of the disease.

In MLD, the urinary sulfatide profile has shifted in favor of sulfatides with higher fatty acids [83]. In urine from MLD patients, the ratio of five major elevated sulfatide isoforms (C22 to C24) to C18:0 isoform was defined as isoform profile number (IPN) and introduced as new biomarker (Fig. 5). This approach does not require specifically labeled lipid standards or any additional standardizing parameter, such as creatinine.

Apart from classic MLD cases, urine analysis can be extremely useful in detection of pseudodeficiency status where in vitro arylsulfatase

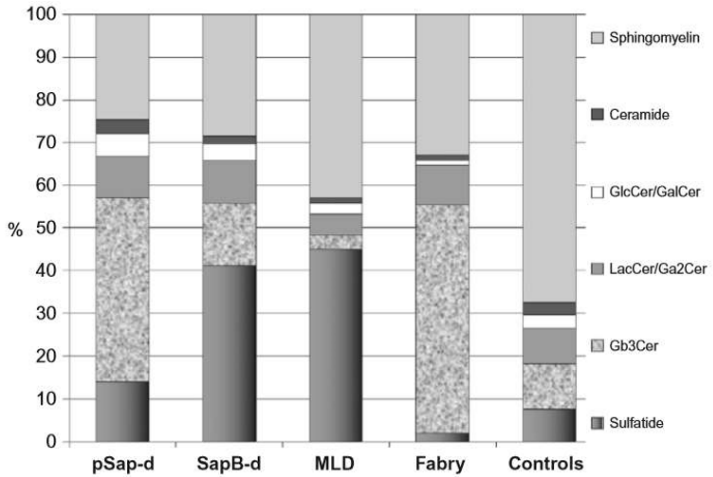

Fig. 4 Distribution of the major urinary sphingolipids. Order of column sections from bottom to top: sulfatide (*right edge dark*), Gb3Cer (*sand-like*), dihexosylceramides (lactosyl-/digalactosylceramide; LacCer/Ga2Cer) (*gray*), monohexosylceramides (glucosyl-/galactosylceramide; GlcCer/GalCer) (*light*), ceramide (*black*), sphingomyelin (*light gray*). Columns: pSap-d patient; SapB-d patient; MLD, metachromatic leukodystrophy group ($n=6$); Fabry, Fabry disease group (males, classical phenotype, $n=10$); controls ($n=28$). Interestingly, the proportion of sphingomyelin in the spectrum of urinary sphingolipids accounted for about 60% in controls ($n=28$, mean $\pm$ SD $= 64.3 \pm 10.6\%$) and this value decreases considerably in sphingolipidoses due to the predominance of other sphingolipids with respect to the level of the lysosomal storage [146]. The highest percentage decrease of sphingomyelin is evident in diseases with multiple sphingolipid storage pSAP-d (24.6%) and Sap B deficiencies (28.3%). The percentage of sphingomyelin in the group of MLD patients was $40 \pm 8.1\%$ ($n=6$), while in classically affected Fabry hemizygotes it was $33.4 \pm 12.3\%$ ($n=10$). *Modified from L. Kuchar, J. Ledvinova, M. Hrebicek, H. Myskova, L. Dvorakova, L. Berna, P. Chrastina, B. Asfaw, M. Elleder, M. Petermoller, H. Mayrhofer, M. Staudt, I. Krageloh-Mann, B.C. Paton, K. Harzer, Prosaposin deficiency and saposin B deficiency (activator-deficient metachromatic leukodystrophy): report on two patients detected by analysis of urinary sphingolipids and carrying novel PSAP gene mutations, Am. J. Med. Genet. A 149A (2009) 613–621.*

A activity has pathological values but the lipid substrates are degraded normally [78,109,155].

The hypothesis explaining changes in isoform profiles was based on a comparison of sulfatide profiles in the kidneys and urine of patients and controls. Tissue specific patterns indicated that isoform profile changes are caused by increased amounts of desquamated renal tubular cells in the urine of patients with sulfatidoses [83].

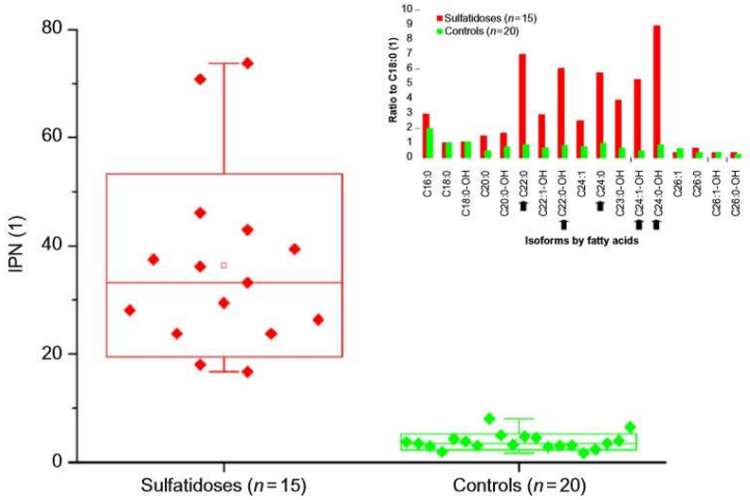

Fig. 5 IPN (isoform profile number), a new biomarker for diagnosis of MLD (also prosaposin and Sap B deficiencies). IPN reflects changes of the molecular profile of urinary sulfatides and is defined as a ratio of the summed intensities of five major elevated urinary sulfatide isoforms (C22:0, C:22:0-OH, C24:0, C24:1-OH, and C24:0-OH marked with *black arrows* in the inserted picture) to the C18:0 isoform which value is relatively stable.

In Fabry disease, changed molecular pattern of urinary globotriaosylceramide (Gb3Cer), a key substrate for the missing α-galactosidase, was reported [111,156,157]. A biomarker representing the ratio of Gb3Cer C24:0/C18:0 isoforms was found to be robust and reliable for screening for Fabry disease even in unselected cohorts with chronic kidney disease. The diagnostic potential of the MS/MS quantification of the Gb3Cer isoforms in urine from Fabry patients (including females) related to the sensitivity, specificity, predictive value, etc., was evaluated by Paschke *et al.* [158]. They found that the ratio of C24:0/C18:0 isoforms could provide a simple and effective improvement in methodology with independence from the conventional reference parameters (urinary creatinine, sphingomyelin, etc.) which were reported as sources of errors. Moreover, the Gb3Cer C24:0/C18:0 ratio was found to be unaffected by potential variables such as urinary leukocytes, erythrocytes, bacteria, or higher protein content, thereby improving the original method for testing total Gb3Cer excretion [157].

Additionally, pSap-d and SapB-d are examples of rare diseases in which lipid analysis in urine is of utmost importance since routine "in vitro"

enzymology is not informative. Dysfunction of several sphingolipid hydrolases leads to increased concentration of hydrophobic SL, ceramides, and GSL with shorter oligosaccharide chains (mono- and dihexosylceramides, Gb3Cer, and sulfatides) producing a characteristic urinary pattern that can provide important information for a differential diagnosis, as shown in Fig. 4 and discussed in Kuchar *et al.* [146].

Blood plasma is another valuable diagnostic material for preliminary testing of circulating metabolites in suspected LSD. One example is Gb3Cer, the major storage glycolipid in Fabry disease, found to be elevated in the plasma of hemizygous males having the classic phenotype, and for a long time had been considered as a suitable Fabry disease marker [159–161]. However, males with variant forms of the disease and many female heterozygotes are not necessarily identified by Gb3Cer levels in plasma, which are often within normal range, thus its predicative value for disease manifestation is poor [162–165]. Therefore because of its low diagnostic sensitivity, Gb3Cer is not regarded as an ideal plasma marker for monitoring disease progression and therapeutic interventions [159,166,167]. Its diagnostic importance was recently surpassed by discovery of its deacetylated product [74], which is currently considered to be an effective plasma biomarker and a hallmark of Fabry disease (see the following Section 4.2).

Plasma sphingolipidomics has also become popular in diagnosis of other LDS such as Gaucher disease [76,168,169], GM2 gangliosidosis [170,171], and more recently NP-C [77,125]. In MLD, quantification of sulfatides in DBS and dried urine spots has also been reported and has been suggested as feasible for newborn screening because the development of a direct arylsulfatase A assay in DBS is still problematic and needs further investigation [155,172,173].

Finally, it is worth mentioning that new sophisticated UPLC–MS/MS methods enabled detection of rare GM3 synthase deficiencies, by determination of changes in ganglioside pattern in patient blood plasma [174]. This has contributed to the expansion of laboratory diagnostics also into the area of neurodegenerative diseases caused by disturbances of biosynthetic glycosphingolipid pathways. Molecular basis of a whole range of these disorders is still enigmatic [175] and therefore involvement of MS in this newly developing field of research is to be expected.

4.2 Deacylated SL and Their Analogs

Participation of lyso-SL in the pathological process of LSD has been studied for many years, but their utilization in the diagnostics only began quite recently, and paralleled the development of new and sensitive triple–quadrupole instruments [122,176]. Originally it was psychosine (galactosylsphingosine), another substrate of missing β-galactosylceramidase, and its cytotoxicity that was considered responsible for selective and complete destruction of oligodendrocytes and the unusual pathobiochemistry of Krabbe disease [177–179]. Later, this "psychosine hypothesis" was expanded to other sphingolipidoses in order to explain pathogenic mechanisms associated with the toxicity of deacylated primary substrates of the relevant defective hydrolases.

It was primarily Gaucher disease, where the existence of neuronopathic and nonneuronopathic clinical forms were attributed to the level of glucosylsphingosine (glucosyl-psychosine) in the brain [180,181]. In vitro examination confirmed its toxicity by demonstration of alterations in cellular morphology and suppression of neurite outgrowth in cultures, which supports the view that glucosylsphingosine contributes to neuronal destruction in neuronopathic forms of Gaucher disease [182]. The particular role of lyso-SL in the development of pathological processes was the impetus for their use as biomarkers in the diagnosis of several important LSD. Storage macrophages (Gaucher cells) in visceral organs are probably the main sources of glucosylsphingosine in the plasma, levels of which seem to correlate with disease severity. A marked, up to 300-fold increase of glucosylsphingosine was observed in the plasma of symptomatic patients with type 1 of Gaucher disease, providing another convenient biochemical marker of the disease, alongside chitotriosidase and CCL18. These findings offer an opportunity to monitor disease progression as well as the effect of therapeutic interventions [76,168,183].

Interestingly, in Fabry disease, plasma globotriaosylsphingosine was described in 2008 after having been overlooked for decades as an important factor [74] that appears to contribute significantly to the pathology due to its considerable inhibitory effect on the residual activity of α-galactosidase A. Furthermore, globotriaosylsphingosine also acts as a stimulator of smooth muscle cell growth in culture, and this feature is thought to be the cause of vascular pathologies typical for Fabry disease [74,168]. A potential role of lyso-derivatives and sphingoid bases, in cell signaling, has also been hypothesized as one of the most important functions of these biomolecules [184,185]. In this regard, there have been several studies attempted to explain the origin and functions of deacylated SL in terms of both biosynthesis and degradation [74,76,182,186,187]. Although final resolving this question is still pending, last work of Ferraz *et al.* [188] brought a new experimental evidence about the involvement of acid ceramidase (EC 3.5.1.23) into direct intralysosomal deacylation of glycosphingolipids due to its

broaden substrate specificity induced by deficiencies of glycohydrolases. This alternate metabolic pathway deserves further studies which would examine the possible existence of other metabolic ways of production of deacylated glycosphingolipids and would elucidate the role of these compounds in the pathophysiological process in LSD.

Some studies have compared urine and plasma to determine which material is diagnostically preferable for analysis of lyso-SL. Regarding Fabry disease, Gold *et al.* [189] found about 40- to 480-fold higher concentrations of globotriaosylsphingosine in the plasma, the processing of which, in the preanalytical phase, was considered easier and more practical than urine. In urine samples of Gaucher type 1 patients, Mirzaian *et al.* [183] demonstrated markedly elevated glucosylsphingosine. However, because of the complexity of the urinary pattern, plasma with one prominent form of glucosylsphingosine was given priority in the diagnosis of Gaucher disease. Interestingly, glucosylceramide, a key substrate of the missing enzyme, was not found to be increased. Therefore, in both Fabry and Gaucher disease, plasma was evaluated as the preferable material in terms of high levels of the respective lyso-derivative, easier processing, and for better discrimination between patients and controls [183,189].

Smid *et al.* [190] investigated the value of plasma globotriaosylsphingosine to distinguish between subjects with classical, nonclassical, and uncertain phenotypes of Fabry disease. They documented a clear distinction between classical Fabry patients and subjects without the disease, including females. In individuals presenting with nonspecific Fabry signs, but without characteristic clinical or biochemical features of classical Fabry disease, modest increase in globotriaosylsphingosine merely offers a suspicion of Fabry disease, not evidence. On the other hand, in females, normal globotriaosylsphingosine cannot exclude Fabry disease [190]. Data from a Dutch cohort of subjects with an uncertain diagnosis revealed that for subjects with the *GLA* gene variant, individual assessment of all other risk factors that could potentially cause the symptoms must be carefully examined [188,190,191].

Plasma globotriaosylsphingosine was found as a reliable biomarker of late-onset variant of Fabry disease with a particularly high incidence in Taiwan (*GLA* mutation c.936 + 919G → A), where increased levels have been documented at birth, ie, in the presymptomatic stage [192].

Publications indicating other lyso-SL as biomarkers for LSD are listed next. Examples include sphingosylphosphorylcholine (SPC) in NP-B [193] and in NP-C [194] or lyso-GM2 ganglioside in Tay–Sachs and Sandhoff diseases [171]. In certain LSD, however, analysis of plasma lyso-derivatives was not diagnostically successful, as in the case of MLD [149].

The initial focus on blood plasma was followed by determination of these metabolites in urine and DBS [75,193]. Globotriaosylsphingosine in Fabry disease and SPC in NP-B were also demonstrated in DBS, which expanded the availability of screening and facilitated transportation of samples. Although globotriaosylsphingosine is reliably measurable in DBS of hemizygous males with classical Fabry disease, its application for newborn screening is still very problematic due to its extremely low levels in most newborns [195]. A modest (fivefold) increase of SPC was found in DBS from 27 NP-B patients compared with controls [193], but further investigation in the group of milder forms is needed.

An indisputable advantage of MS analysis is the potential to measure profiles for lyso-SL isoforms comprising *various analog structures* of sphingoid bases (see Table 1). According to recent literature, it is apparent that d18:1 sphingoid is the prevailing component of lyso-SL in the plasma, while in the urine, there is considerable heterogeneity of its structural forms [183,196,197]. In the plasma of Fabry patients, these structures represent relatively low percentage against globotriaosylsphingosine which is the most prominent plasma biomarker of classical and some later-onset variants of Fabry disease [198]. In contrast, the percentage of structural analogs in urine is much higher than that of regular globotriaosylsphingosine and therefore analysis of the complete "panel of biomarkers" is recommended for diagnosis efficiency and better monitoring of treated patients [196]. The diagnostic value of such structural analogs seems to be significant, particularly for some atypical clinical variants (eg, cardiac variants p.N215S or p.R301Q in children), which might be difficult to recognize in the first stage of a diagnostic investigation[196].

A recently published work reported a novel potential biomarker for the primary diagnosis of NP-C, "sphingosylphosphorylcholine 509" (SPC m/z 509; SPC509) that has a structure similar to the regular SPC (SPC m/z 465), but which has not yet been precisely determined. The SPC509 analog was primarily detected using nontargeted lipidomic analysis and then quantified in plasma samples of 110 NP-C patients and 21 NP-A/B (acid sphingomyelinase deficiency) patients and seems to be specific for both groups. NP-C patients were well differentiated by SPC509 plasma concentrations from healthy controls as well as from the acid sphingomyelinase deficiency group, where the concentration of this metabolite was highest [125]

Table 1 Core Structures of Deacylated Sphingolipids and Their Structural Analogs: Mass Shifts, Structure Modifications, and Related References

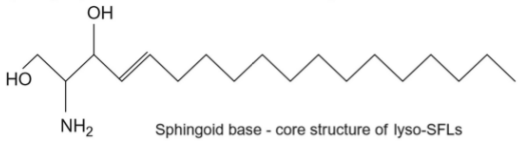

Sphingoid base - core structure of lyso-SFLs

Initial Structure	lyso-SFL Analogue	Mass Shift	Predicted Modification of Sphingoid Base	Source
lyso-GlcCer [183] Glucosylpsychosine *m/z* 462	lyso-GlcCer 434	−28	$-C_2H_4$	Urine
	lyso-GlcCer 450	−12	$-C_2H_4 + (O \rightarrow OH)$	
	lyso-GlcCer 460	−2	Di-ene	
	lyso-GlcCer 476	+14	Di-ene + $(O \rightarrow OH)$ or CH_2	
	lyso-GlcCer 478	+16	$+O \rightarrow OH$	
lyso-Gb3Cer [196–199] Globotriaosylsphingosine *m/z* 786	lyso-Gb_3Cer 758	−28	$-C_2H_4$	Urine
	lyso-Gb_3Cer 774	−12	$-C_2H_4 + (O \rightarrow OH)$	Urine
	lyso-Gb_3Cer 784	−2	Di-ene	Urine/plasma [198]
	lyso-Gb_3Cer 800	+14	Di-ene + $(O \rightarrow OH)$ or CH_2	Urine
	lyso-Gb_3Cer 802	+16	$+O \rightarrow OH$	Urine
	lyso-Gb_3Cer 820	+34	$+H_2O_2$	Urine
	lyso-Gb_3Cer 836	+50	$+H_2O_3$	Urine
lyso-SM [125] Sphingosylphosphorylcholine *m/z* 465	lyso-SM 509	+44	$+CO_2$	Plasma

(L. Kuchar, unpublished observation). MS/MS plasma analysis of SPC509 is a promising screening method for NP-C disease, the biochemical detection of which is still difficult task in contrast to NP-A/B where enzyme analysis is available. Interestingly, in NPC patients and also in the mouse model of NPC, a moderate increase in plasma glucosylsphingosine has also been found, which was more pronounced than that of glucosylceramide [194,200].

Despite the promising role of lyso-derivative analogs in the diagnosis, monitoring, and therapy effectiveness in certain LSD, considerable effort is still needed to resolve detailed structures and to map out metabolic pathways of these biomolecules, which are still more or less enigmatic [183,196,199].

In conclusion, the main advantage of measuring lyso-SL is the higher diagnostic sensitivity and specificity in comparison to their acylated SL counterparts. This was demonstrated in cases with mild mutations and some cases in the presymptomatic stage of the disease. Highly sensitive MS analysis also allowed for the incorporation of newly described lyso-SL analogs into the spectrum of biomarkers. Such an approach allows evaluation of a wider spectrum of mutations associated with the defective enzyme protein in various sphingolipidoses. Plasma is the preferred material for analysis due to the relatively high concentration of lyso-SL and ease of processing. At present, this practice can be recommended as the standard in the diagnostic approach to the relevant sphingolipidoses (eg, Fabry and Gaucher diseases). The analog compounds, due to their heterogeneity, different associations to various mutations and higher relative concentration compared to basic deacylated molecules should be analyzed in the urine in one panel comprising their whole spectrum. However, interpretation of such complex results is still rather complicated and requires further clinical investigation and consensus on their applications.

4.3 Secondarily Altered Metabolites

Another group of lipid molecules, which has been gaining importance in the diagnostic process as well as in monitoring the therapeutic effectiveness in certain LSD are called secondary altered molecules [77,78,201,202]. These compounds are not substrates or ligands of deficient enzymes or other nonenzymatic proteins and thus they are not directly related to the disease. Concentrations of these molecules are secondarily changed due to a primary defect and have been reported in different LSD. In NP-C, MS analysis of oxysterols became popular in laboratory diagnoses and is widely used as a practical screening test, using the plasma of suspected NP-C patients [201–203]. However, it is necessary to take into account that the

test is not strictly specific for NP-C, since similar changes may also be present in other diseases (NP-B, Smith–Lemli–Opitz syndrome, acid lipase deficiency, etc.) [18]. For these reasons and for better monitoring of disease progression and therapeutic interventions, Fan *et al.* [77] recommended testing a wider MS panel of all sphingolipid circulating biomarkers that are elevated in the plasma and cerebrospinal fluid of patients suspected of NP-C disease. Such a procedure could be useful in the context of complex metabolic medical consultations, where it is advantageous to evaluate a set of biomarkers.

Another lipid molecule associated with lysosomal storage is BMP, acidic phospholipid, and structural isomer of phosphatidylglycerol. It is located almost solely in the internal vesicles of endosomal/lysosomal compartments in the subpopulation of internal membranes where it helps to create a favorable environment for the interaction of hydrophobic sphingolipid substrates with corresponding hydrolases and protein activators [55]. Its origin is mainly derived from macrophages, which are also the primary sites of storage processes for a number of LSD [33,204–206]. In addition to cells and tissues, increased concentrations of BMP have been reported in plasma from patients with LSD characterized by storage macrophages and/or hepatomegaly. The highest elevation of specific BMP C18:1/C18:1 species has been found in NP-A/B, NP-C, and Gaucher diseases, which suggests that it may be useful as another biomarker for certain subgroups of LSD [207].

Although great progress has been made in the field of lipid biomarkers in recent years, further studies are needed to select the optimal set of molecules useful for diagnosis of particular LSD, which could also distinguish their clinical phenotypes and monitor therapeutic responses.

4.4 Enzymology

Determination of activity of the respective lysosomal hydrolase is still the gold standard for confirmation of diagnosis in the majority of cases suspected of lysosomal enzymopathies since it directly verifies the functionality of the gene product. That is why MS became involved in the investigation of lysosomal enzymology. The first stage was focused on the development of appropriate enzymological methods using newly designed artificial substrates and cell lysates as enzyme sources. Subsequent analysis of the reaction products was performed by FIA–ESI–MS/MS [138,208]. Natural SL with shorter acyl chains were also used as substrates in enzyme assays as reported, eg, for Gaucher fibroblasts and DBS [111,209] or for DBS samples in NP-A/B and Krabbe diseases [209].

The need to simplify the collection and transport of material and also to speed up the analyses applicable for newborn screening has resulted in extensive development of methods for analysis in DBS [64–67,210,211]. Soon after that, the individual MS/MS methodologies of various lysosomal enzymes were combined in multiplex programs [68,209–212]. These multiplexed methods have been used in large studies in various countries around the world based on the specific requirements for nationwide newborn screening, such as in Korea [213] or Austria [62] or targeted at high-risk populations [214] or small populations [215].

An overview of worldwide screening activities is currently available on the CDC's homepage, including a list of participants from different countries (Centers for Disease Control and Prevention, http://www.cdc.gov/nbslabbulletin/bulletin.html).

Coupling of MS/MS with HPLC instrumentation enabled separation and purification of reaction products prior to MS analysis. This led to simplification and speeding up of the process, which allowed incorporation of these methods into population wide screening programs [216]. Development of new, more sensitive [217], and versatile [218] substrates is still in progress.

Screening programs running in different countries have revealed some interesting facts. A Korean screening program compared DBS and leukocytes and found a correlation of results using both enzyme sources [213]. Kumar *et al.* [219] compared MS and fluorimetry in evaluation of reaction products using double-labeled substrates containing both 4 MU and mass labels. MS detection revealed 1–2 orders of magnitude higher analytical performance over fluorimetric measurements, which was due to the intrinsic fluorescence of the 4 MU substrate increasing the background and reducing the analytical range.

An exceedingly important phase of these analyses is preanalytical preparation of DBS exhaustively reviewed by Wagner *et al.* [135]. The review demonstrated many factors that may affect the quality of DBS, eg, incorrect application of the blood sample to the filter paper or utilization of different filter paper types that could adversely affect measured enzyme activity due to differences in the paper saturation. Principles of good management of the preanalytical phase and control of factors that can negatively influence results are valid for DBS analysis in general.

Nevertheless, these in vitro methods need detergents to solubilize lipid substrates, and this fact complicates the diagnostics of protein activator deficiencies. In such cases, only loading experiments on living cells [220]

provide reliable function tests of enzyme reactions, which in combination with MS/MS analysis of SL in urine may lead to a final diagnosis confirmed by DNA analysis [83,111,146].

4.5 Metabolic Experiments in Living Cells

Application of MS/MS lipidomic technologies to monitoring the metabolic fate of mass-labeled precursor molecules in living cells has become an important objective.

Such studies were traditionally performed using radioactively labeled natural lipids precursors, exogenously added to cell cultures, to follow, after a specified incubation period, their uptake and metabolic products. This model has been successfully utilized for decades in studies of metabolic pathways of SL including degradation defects in LSD [220–223]. Degradation products were usually separated using TLC and then traced using radioactivity scanning or liquid scintillation. Utilization and scientific contribution of these chemical-biology tools in the investigation of sphingolipid metabolism are discussed in an excellent review by Schwarzmann *et al.* [224].

Recently, the development of efficient and sensitive MS/MS technology has shown the potential to replace radioactive tracers in some experiments using stable isotopes [225] or atypical nonradioactive analogs as described for GM1 gangliosidosis [111]. These mass-labeled compounds can be traced and quantified using MS, which also provides data regarding lipid molecular species. Zeng *et al.* [226] studied alternation of sulfatide metabolism associated with Alzheimer disease and MLD on neuroblastoma cells and primary neuron cultures supplemented with bovine brain sulfatides and d_{35}-$C_{18:0}$-galactosylceramide. They found that abnormal sulfatide metabolism characterized by increased ceramide and sphingosine content induced neuronal cell apoptosis due to accelerated ceramide generation in endosomes and lysosomal storage of toxic lipids. Recently, glucosylceramide labeled with the $^{13}C_5$-stable isotope in the sphingosine moiety was used for loading experiments in fibroblast cultures to demonstrate the direct deacylation of glucosylceramide to glucosylsphingosine in Gaucher disease ([188], see also Section 4.2) as alternate catabolic pathway in LSD.

Additionally, MS-based evaluation of loading experiments with stable isotope-labeled cholesterol (eg, $^{13}C_3$-cholesterol or d_7-cholesterol) opened new possibilities for monitoring free cholesterol and cholesterol esters in metabolic studies on living cells [227,228]. These studies also have relevance for many LSD (eg, NP-A/B, NP-C, cholesterol esters storage disease).

A comprehensive overview of the utilization of stable isotopes for investigation of metabolism and transport of lipid species (including SL) and selection of mass-labeled precursors that might also have relevance for clinical utilization was recently published by Ecker and Liebisch [229].

5. CONCLUSION

The tremendous diversity of lipid structures, encompassing thousands molecular subtypes, poses a challenge to new analytical technologies such as MS/MS. Mass-labeled SL have become the tools for studies of SL metabolism, transportation, and interactions, and they might come to replace radioactive substrates in a number of experiments. The ability to establish metabolomic profiles of SL under normal and pathological conditions, in cells, tissues, and body fluids contributes to a better understanding of the biological significance of SL molecules and aids in the search for new specific biomarkers. MS lipidomics have also great potential for monitoring the therapeutic interventions. At present, it is mainly investigation in the field of deacylated SL, and their analogs, which appears to offer new avenues for laboratory diagnostics in a number of sphingolipidoses.

ACKNOWLEDGMENTS

This work was supported by Grant IGA MZ NT14015-3/2013 from the Grant Agency of the Ministry of Health, Czech Republic. This chapter also summarizes the topics and main results of this grant project, involving the development and exploitation of new mass spectrometry techniques in the diagnosis of LSD.

Compliance with Ethics Guidelines: This chapter does not contain any studies that used human or animal subjects.

Conflict of Interest: L.K., B.A., J.R., and J.L. declare that they have no conflicts of interest.

REFERENCES

[1] H.E. Carter, F.J. Glick, W.P. Norris, G.E. Phillips, Biochemistry of the sphingolipides. 3. Structure of sphingosine, J. Biol. Chem. 170 (1947) 285–294.
[2] E. Klenk, [Contribution to the concept of gangliosides], Hoppe Seylers Z. Physiol. Chem. 288 (1951) 216–220.
[3] R. Kuhn, H. Wiegandt, Die Konstitution Der Ganglio-N-Tetraose Und Des Gangliosids Gi, Chem. Ber. Recl. 96 (1963) 866.
[4] L. Svennerholm, On the isolation and characterization of N-acetyl-sialic acid, Acta Soc. Med. Ups. 61 (1956) 74–85.
[5] L. Svennerholm, Composition of gangliosides from human brain, Nature 177 (1956) 524–525.
[6] T. Yamakawa, A reflection on the early history of glycosphingolipids, Glycoconj. J. 13 (1996) 123–126.

[7] T. Yamakawa, N. Kiso, S. Handa, A. Makita, S. Yokoyama, On the structure of brain cerebroside sulfuric ester and ceramide dihexoside of erythrocytes, J. Biochem. 52 (1962) 226–227.
[8] J.N. Kanfer, The sphigolipidoses, in: J.N. Kanfer, S.-I. Hakomori (Eds.), Sphingolipid Biochemistry, Springer US, New York, ISBN: 978-0-306-41092-5, 1983, pp. 167–325.
[9] F.M. Platt, S.U. Walkley, Lysosomal defects and storage, in: F.M. Platt, S.U. Walkley (Eds.), Lysosomal Disorders of the Brain, Oxford University Press, Oxford, ISBN: 978-0-198-50878-6, 2004, pp. 32–49.
[10] C.R. Scriver, A.L. Beaudet, W.S. Sly, D. Valle, The Metabolic and Molecular Bases of Inherited Disease, in: eighth ed., vol. 3, McGraw-Hill, New York, ISBN: 0-07-136321-1, 2001.
[11] C. de Duve, Lysosomes, a new group of cytoplasmic particles, in: T. Hayashi (Ed.), Subcellular Particles; A Symposium Held During the Meeting of the Society of General Physiologists at the Marine Biological Laboratory, Woods Hole, Massachusetts, June 9–11, 1958, Ronald Press, New York, ISBN: 978-1-296-83268-1, 1959, pp. 128–159.
[12] E. Klenk, Uber die natur der phosphatide der milz bei Niemann-Pickchen Krankheit, Z. Physiol. Chem. 229 (1934) 151–156.
[13] H.G. Hers, Alpha-glucosidase deficiency in generalized glycogen-storage disease (Pompes disease), Biochem. J. 86 (1963) 11–16.
[14] R.O. Brady, J.N. Kanfer, D. Shapiro, Metabolism of glucocerebrosides. II. Evidence of an enzymatic deficiency in Gaucher's disease, Biochem. Biophys. Res. Commun. 18 (1965) 221–225.
[15] M. Elleder, A. Jirasek, Niemann-Pick disease. Report on a symposium held in Hlava's Institute of Pathology, Charles University, Prague 2nd–3rd September, Acta Univ. Carol. Med. (Praha) 29 (1983) 259–267.
[16] S. Naureckiene, D.E. Sleat, H. Lackland, A. Fensom, M.T. Vanier, R. Wattiaux, M. Jadot, P. Lobel, Identification of HE1 as the second gene of Niemann-Pick C disease, Science 290 (2000) 2298–2301.
[17] M.C. Patterson, M.T. Vanier, K. Suzuki, J.A. Morris, E. Carstea, E.B. Neufeld, J.E. Blanchette-Mackie, P.G. Pentchev, Niemann-Pick disease type C: a lipid trafficking disorder, in: C.R. Scriver, et al. (Eds.), The Metabolic and Molecular Bases of Inherited Disease, McGraw-Hill, New York, ISBN: 0-07-136321-1, 2001,pp. 3589–3633.
[18] M.T. Vanier, Complex lipid trafficking in Niemann-Pick disease type C, J. Inherit. Metab. Dis. 38 (2015) 187–199.
[19] R.B. Cole, Electrospray and MALDI mass spectrometry, in: Fundamentals, Instrumentation, Practicalities, and Biological Applications, second ed., John Wiley & Sons, New Jersey, ISBN: 978-0-471-74107-7, 2010.
[20] X. Han, R.W. Gross, Shotgun lipidomics: electrospray ionization mass spectrometric analysis and quantitation of cellular lipidomes directly from crude extracts of biological samples, Mass Spectrom. Rev. 24 (2005) 367–412.
[21] R.C. Murphy, J. Fiedler, J. Hevko, Analysis of nonvolatile lipids by mass spectrometry, Chem. Rev. 101 (2001) 479–526.
[22] M.A. Chester, IUPAC-IUB joint commission on biochemical nomenclature (JCBN). Nomenclature of glycolipids—recommendations 1997, Eur. J. Biochem. 257 (1998) (1997) 293–298.
[23] F.M. Goni, A. Alonso, Biophysics of sphingolipids I. Membrane properties of sphingosine, ceramides and other simple sphingolipids, Biochim. Biophys. Acta 1758 (2006) 1902–1921.
[24] S. Grosch, S. Schiffmann, G. Geisslinger, Chain length-specific properties of ceramides, Prog. Lipid Res. 51 (2012) 50–62.
[25] M. Masserini, D. Ravasi, Role of sphingolipids in the biogenesis of membrane domains, Biochim. Biophys. Acta 1532 (2001) 149–161.
[26] B. Ulrich-Bott, H. Wiegandt, Micellar properties of glycosphingolipids in aqueous media, J. Lipid Res. 25 (1984) 1233–1245.
[27] B. Westerlund, J.P. Slotte, How the molecular features of glycosphingolipids affect domain formation in fluid membranes, Biochim. Biophys. Acta 1788 (2009) 194–201.
[28] D.I. Godfrey, J. Rossjohn, New ways to turn on NKT cells, J. Exp. Med. 208 (2011) 1121–1125.
[29] S. Hakomori, Glycosphingolipids in cellular interaction, differentiation, and oncogenesis, Annu. Rev. Biochem. 50 (1981) 733–764.
[30] S. Hakomori, Cancer-associated glycosphingolipid antigens: their structure, organization, and function, Acta Anat. (Basel) 161 (1998) 79–90.
[31] S.I. Hakomori, Structure and function of glycosphingolipids and sphingolipids: recollections and future trends, Biochim. Biophys. Acta 1780 (2008) 325–346.
[32] J.L. Kanter, S. Narayana, P.P. Ho, I. Catz, K.G. Warren, R.A. Sobel, L. Steinman, W.H. Robinson, Lipid microarrays identify key mediators of autoimmune brain inflammation, Nat. Med. 12 (2006) 138–143.
[33] T. Kolter, K. Sandhoff, Principles of lysosomal membrane digestion: stimulation of sphingolipid degradation by sphingolipid activator proteins and anionic lysosomal lipids, Annu. Rev. Cell Dev. Biol. 21 (2005) 81–103.
[34] S. Lahiri, A.H. Futerman, The metabolism and function of sphingolipids and glycosphingolipids, Cell. Mol. Life Sci. 64 (2007) 2270–2284.
[35] M. Maceyka, K.B. Harikumar, S. Milstien, S. Spiegel, Sphingosine-1-phosphate signaling and its role in disease, Trends Cell Biol. 22 (2012) 50–60.
[36] M. Maceyka, S. Milstien, S. Spiegel, Sphingosine-1-phosphate: the Swiss army knife of sphingolipid signaling, J. Lipid Res. 50 (Suppl.) (2009) S272–S276.
[37] R.L. Schnaar, A. Suzuki, P. Stanley, Glycosphingolipids, in: A. Varki, et al. (Eds.), Essentials of Glycobiology, Cold Spring Harbor Laboratory Press, New York, ISBN: 978-0-879-69770-9, 2009.
[38] C.E. Stevenson, K. Takabe, M. Nagahashi, S. Milstien, S. Spiegel, Targeting sphingosine-1-phosphate in hematologic malignancies, Anticancer Agents Med. Chem. 11 (2011) 794–798.
[39] K. Takabe, S.W. Paugh, S. Milstien, S. Spiegel, "Inside-out" signaling of sphingosine-1-phosphate: therapeutic targets, Pharmacol. Rev. 60 (2008) 181–195.
[40] A.H. Futerman, Intracellular trafficking of sphingolipids: relationship to biosynthesis, Biochim. Biophys. Acta 1758 (2006) 1885–1892.
[41] M. Levy, A.H. Futerman, Mammalian ceramide synthases, IUBMB Life 62 (2010) 347–356.
[42] S. Neumann, G. van Meer, Sphingolipid management by an orchestra of lipid transfer proteins, Biol. Chem. 389 (2008) 1349–1360.
[43] T. Wennekes, R.J. van den Berg, R.G. Boot, G.A. van der Marel, H.S. Overkleeft, J.M. Aerts, Glycosphingolipids—nature, function, and pharmacological modulation, Angew. Chem. Int. Ed. Engl. 48 (2009) 8848–8869.
[44] K. Kitatani, J. Idkowiak-Baldys, Y.A. Hannun, The sphingolipid salvage pathway in ceramide metabolism and signaling, Cell. Signal. 20 (2008) 1010–1018.
[45] E.L. Laviad, L. Albee, I. Pankova-Kholmyansky, S. Epstein, H. Park, A.H. Merrill Jr., A.H. Futerman, Characterization of ceramide synthase 2: tissue distribution, substrate specificity, and inhibition by sphingosine 1-phosphate, J. Biol. Chem. 283 (2008) 5677–5684.
[46] G. D'Angelo, E. Polishchuk, G. Di Tullio, M. Santoro, A. Di Campli, A. Godi, G. West, J. Bielawski, C.C. Chuang, A.C. van der Spoel, F.M. Platt,

Y.A. Hannun, R. Polishchuk, P. Mattjus, M.A. De Matteis, Glycosphingolipid synthesis requires FAPP2 transfer of glucosylceramide, Nature 449 (2007) 62–67.
[47] G. D'Angelo, L.R. Rega, M.A. De Matteis, Connecting vesicular transport with lipid synthesis: FAPP2, Biochim. Biophys. Acta 1821 (2012) 1089–1095.
[48] T.P. Levine, A lipid transfer protein that transfers lipid, J. Cell Biol. 179 (2007) 11–13.
[49] J. Huotari, A. Helenius, Endosome maturation, EMBO J. 30 (2011) 3481–3500.
[50] T. Kolter, K. Sandhoff, Lysosomal degradation of membrane lipids, FEBS Lett. 584 (2010) 1700–1712.
[51] T. Kolter, A view on sphingolipids and disease, Chem. Phys. Lipids 164 (2011) 590–606.
[52] K. Sandhoff, T. Kolter, K. Harzer, Sphingolipid activator proteins, in: C.R. Scriver, et al. (Eds.), The Metabolic and Molecular Bases of Inherited Disease, McGraw-Hill, New York, ISBN: 0-07-136321-1, 2001, pp. 3371–3388.
[53] M. Filocamo, A. Morrone, Lysosomal storage disorders: molecular basis and laboratory testing, Hum. Genomics 5 (2011) 156–169.
[54] E.B. Vitner, F.M. Platt, A.H. Futerman, Common and uncommon pathogenic cascades in lysosomal storage diseases, J. Biol. Chem. 285 (2010) 20423–20427.
[55] H. Schulze, K. Sandhoff, Sphingolipids and lysosomal pathologies, Biochim. Biophys. Acta 1841 (2014) 799–810.
[56] S.D. Kingma, O.A. Bodamer, F.A. Wijburg, Epidemiology and diagnosis of lysosomal storage disorders; challenges of screening, Best Pract. Res. Clin. Endocrinol. Metab. 29 (2015) 145–157.
[57] B.J. Poorthuis, R.A. Wevers, W.J. Kleijer, J.E. Groener, J.G. de Jong, S. van Weely, K.E. Niezen-Koning, O.P. van Diggelen, The frequency of lysosomal storage diseases in the Netherlands, Hum. Genet. 105 (1999) 151–156.
[58] H. Poupetova, J. Ledvinova, L. Berna, L. Dvorakova, V. Kozich, M. Elleder, The birth prevalence of lysosomal storage disorders in the Czech Republic: comparison with data in different populations, J. Inherit. Metab. Dis. 33 (2010) 387–396.
[59] F. Al Jasmi, A novel mutation in an atypical presentation of the rare infantile Farber disease, Brain Dev. 34 (2012) 533–535.
[60] M. Hult, N. Darin, U. von Dobeln, J.E. Mansson, Epidemiology of lysosomal storage diseases in Sweden, Acta Paediatr. 103 (2014) 1258–1263.
[61] D. Matern, D. Gavrilov, D. Oglesbee, K. Raymond, P. Rinaldo, S. Tortorelli, Newborn screening for lysosomal storage disorders, Semin. Perinatol. 39 (2015) 206–216.
[62] T.P. Mechtler, S. Stary, T.F. Metz, V.R. De Jesus, S. Greber-Platzer, A. Pollak, K.R. Herkner, B. Streubel, D.C. Kasper, Neonatal screening for lysosomal storage disorders: feasibility and incidence from a nationwide study in Austria, Lancet 379 (2012) 335–341.
[63] M.H. Gelb, F. Turecek, C.R. Scott, N.A. Chamoles, Direct multiplex assay of enzymes in dried blood spots by tandem mass spectrometry for the newborn screening of lysosomal storage disorders, J. Inherit. Metab. Dis. 29 (2006) 397–404.
[64] N.A. Chamoles, M. Blanco, D. Gaggioli, Fabry disease: enzymatic diagnosis in dried blood spots on filter paper, Clin. Chim. Acta 308 (2001) 195–196.
[65] N.A. Chamoles, M. Blanco, D. Gaggioli, Diagnosis of alpha-L-iduronidase deficiency in dried blood spots on filter paper: the possibility of newborn diagnosis, Clin. Chem. 47 (2001) 780–781.
[66] N.A. Chamoles, M.B. Blanco, D. Gaggioli, C. Casentini, Hurler-like phenotype: enzymatic diagnosis in dried blood spots on filter paper, Clin. Chem. 47 (2001) 2098–2102.
[67] N.A. Chamoles, M.B. Blanco, S. Iorcansky, D. Gaggioli, N. Specola, C. Casentini, Retrospective diagnosis of GM1 gangliosidosis by use of a newborn-screening card, Clin. Chem. 47 (2001) 2068.
[68] Z. Spacil, H. Tatipaka, M. Barcenas, C.R. Scott, F. Turecek, M.H. Gelb, High-throughput assay of 9 lysosomal enzymes for newborn screening, Clin. Chem. 59 (2013) 502–511.
[69] L.F. Ross, Newborn screening for lysosomal storage diseases: an ethical and policy analysis, J. Inherit. Metab. Dis. 35 (2012) 627–634.
[70] R.Y. Wang, O.A. Bodamer, M.S. Watson, W.R. Wilcox, Lysosomal storage diseases: diagnostic confirmation and management of presymptomatic individuals, Genet Med. 13 (2011) 457–484.
[71] F.M. Platt, R.H. Lachmann, Treating lysosomal storage disorders: current practice and future prospects, Biochim. Biophys. Acta 1793 (2009) 737–745.
[72] H. Sakuraba, M. Sawada, F. Matsuzawa, S. Aikawa, Y. Chiba, Y. Jigami, K. Itoh, Molecular pathologies of and enzyme replacement therapies for lysosomal diseases, CNS Neurol. Disord. Drug Targets 5 (2006) 401–413.
[73] M.L. Escolar, M.D. Poe, J.M. Provenzale, K.C. Richards, J. Allison, S. Wood, D.A. Wenger, D. Pietryga, D. Wall, M. Champagne, R. Morse, W. Krivit, J. Kurtzberg, Transplantation of umbilical-cord blood in babies with infantile Krabbe's disease, N. Engl. J. Med. 352 (2005) 2069–2081.
[74] J.M. Aerts, J.E. Groener, S. Kuiper, W.E. Donker-Koopman, A. Strijland, R. Ottenhoff, C. van Roomen, M. Mirzaian, F.A. Wijburg, G.E. Linthorst, A.C. Vedder, S.M. Rombach, J. Cox-Brinkman, P. Somerharju, R.G. Boot, C.E. Hollak, R.O. Brady, B.J. Poorthuis, Elevated globotriaosylsphingosine is a hallmark of Fabry disease, Proc. Natl. Acad. Sci. U.S.A. 105 (2008) 2812–2817.
[75] C. Auray-Blais, A. Ntwari, J.T.R. Clarke, D.G. Warnock, J.P. Oliveira, S.P. Young, D.S. Millington, D.G. Bichet, S. Sirrs, M.L. West, R. Casey, W.L. Hwu, J.M. Keutzer, X.K. Zhang, R. Gagnon, How well does urinary lyso-Gb(3) function as a biomarker in Fabry disease? Clin. Chim. Acta 411 (2010) 1906–1914.
[76] N. Dekker, L. van Dussen, C.E. Hollak, H. Overkleeft, S. Scheij, K. Ghauharali, M.J. van Breemen, M.J. Ferraz, J.E. Groener, M. Maas, F.A. Wijburg, D. Speijer, A. Tylki-Szymanska, P.K. Mistry, R.G. Boot, J.M. Aerts, Elevated plasma glucosylsphingosine in Gaucher disease: relation to phenotype, storage cell markers, and therapeutic response, Blood 118 (2011) e118–e127.
[77] M. Fan, R. Sidhu, H. Fujiwara, B. Tortelli, J. Zhang, C. Davidson, S.U. Walkley, J.H. Bagel, C. Vite, N.M. Yanjanin, F.D. Porter, J.E. Schaffer, D.S. Ory, Identification of Niemann-Pick C1 disease biomarkers through sphingolipid profiling, J. Lipid Res. 54 (2013) 2800–2814.
[78] M.A. Tan, M. Fuller, Z.A. Zabidi-Hussin, J.J. Hopwood, P.J. Meikle, Biochemical profiling to predict disease severity in metachromatic leukodystrophy, Mol. Genet. Metab. 99 (2010) 142–148.
[79] E. de Hoffman, V. Stroobant, Mass Spectrometry, Principles and Applications, second ed., John Wiley & Sons, Ltd., Chichester, ISBN: 0-471-48566-7, 2002.
[80] T. Dulcks, R. Juraschek, Electrospray as an ionisation method for mass spectrometry, J. Aerosol Sci. 30 (1999) 927–943.
[81] P. Kebarle, A brief overview of the present status of the mechanisms involved in electrospray mass spectrometry, J. Mass Spectrom. 35 (2000) 804–817.
[82] R.L. Shaner, J.C. Allegood, H. Park, E. Wang, S. Kelly, C.A. Haynes, M.C. Sullards, A.H. Merrill Jr., Quantitative analysis of sphingolipids for lipidomics using triple quadrupole and quadrupole linear ion trap mass spectrometers, J. Lipid Res. 50 (2009) 1692–1707.
[83] L. Kuchar, B. Asfaw, H. Poupetova, J. Honzikova, F. Turecek, J. Ledvinova, Direct tandem mass spectrometric profiling of sulfatides in dry urinary samples for screening of metachromatic leukodystrophy, Clin. Chim. Acta 425C (2013) 153–159.

[84] P.J. Taylor, Matrix effects: the Achilles heel of quantitative high-performance liquid chromatography-electrospray-tandem mass spectrometry, Clin. Biochem. 38 (2005) 328–334.
[85] M.C. Sullards, J.C. Allegood, S. Kelly, E. Wang, C.A. Haynes, H. Park, Y. Chen, A.H. Merrill Jr., Structure-specific, quantitative methods for analysis of sphingolipids by liquid chromatography-tandem mass spectrometry: "inside-out" sphingolipidomics, Methods Enzymol. 432 (2007) 83–115.
[86] J. Liigand, A. Kruve, I. Leito, M. Girod, R. Antoine, Effect of mobile phase on electrospray ionization efficiency, J. Am. Soc. Mass Spectrom. 25 (2014) 1853–1861.
[87] M.J. Ruiz-Angel, S. Carda-Broch, M.C. Garcia-Alvarez-Coque, A. Berthod, Effect of ionization and the nature of the mobile phase in quantitative structure-retention relationship studies, J. Chromatogr. A 1063 (2005) 25–34.
[88] J. Wang, A. Aubry, M.S. Bolgar, H. Gu, T.V. Olah, M. Arnold, M. Jemal, Effect of mobile phase pH, aqueous-organic ratio, and buffer concentration on electrospray ionization tandem mass spectrometric fragmentation patterns: implications in liquid chromatography/tandem mass spectrometric bioanalysis, Rapid Commun. Mass Spectrom. 24 (2010) 3221–3229.
[89] G. Paglia, J.P. Williams, L. Menikarachchi, J.W. Thompson, R. Tyldesley-Worster, S. Halldorsson, O. Rolfsson, A. Moseley, D. Grant, J. Langridge, B.O. Palsson, G. Astarita, Ion mobility derived collision cross sections to support metabolomics applications, Anal. Chem. 86 (2014) 3985–3993.
[90] T.W. Jaskolla, K. Onischke, J. Schiller, 2,5-Dihydroxybenzoic acid salts for matrix-assisted laser desorption/ionization time-of-flight mass spectrometric lipid analysis: simplified spectra interpretation and insights into gas-phase fragmentation, Rapid Commun. Mass Spectrom. 28 (2014) 1353–1363.
[91] Z. Wang, L. Russon, L. Li, D.C. Roser, S.R. Long, Investigation of spectral reproducibility in direct analysis of bacteria proteins by matrix-assisted laser desorption/ionization time-of-flight mass spectrometry, Rapid Commun. Mass Spectrom. 12 (1998) 456–464.
[92] P. Horka, V. Vrkoslav, R. Hanus, K. Peckova, J. Cvacka, New MALDI matrices based on lithium salts for the analysis of hydrocarbons and wax esters, J. Mass Spectrom. 49 (2014) 628–638.
[93] G. Li, R. Hu, Y. Kamijo, T. Nakajima, T. Aoyama, T. Inoue, K. Node, R. Kannagi, M. Kyogashima, A. Hara, Establishment of a quantitative, qualitative, and high-throughput analysis of sulfatides from small amounts of sera by matrix-assisted laser desorption ionization-time of flight mass spectrometry, Anal. Biochem. 362 (2007) 1–7.
[94] L. Kuchar, H. Faltyskova, L. Krasny, R. Dobrovolny, H. Hulkova, J. Ledvinova, M. Volny, M. Strohalm, K. Lemr, L. Kryspinova, B. Asfaw, J. Rybova, R.J. Desnick, V. Havlicek, Fabry disease: renal sphingolipid distribution in the alpha-Gal A knockout mouse model by mass spectrometric and immunohistochemical imaging, Anal. Bioanal. Chem. 407 (2015) 2283–2291.
[95] S.A. McLuckey, J.M. Wells, Mass analysis at the advent of the 21st century, Chem. Rev. 101 (2001) 571–606.
[96] L. Sleno, D.A. Volmer, Ion activation methods for tandem mass spectrometry, J. Mass Spectrom. 39 (2004) 1091–1112.
[97] J.V. Johnson, R.A. Yost, P.E. Kelley, D.C. Bradford, Tandem-in-space and tandem-in-time mass-spectrometry—triple quadrupoles and quadrupole ion traps, Anal. Chem. 62 (1990) 2162–2172.
[98] K.R. Jennings, The changing impact of the collision-induced decomposition of ions on mass spectrometry, Int. J. Mass Spectrom. 200 (2000) 479–493.
[99] M. Gu, J.L. Kerwin, J.D. Watts, R. Aebersold, Ceramide profiling of complex lipid mixtures by electrospray ionization mass spectrometry, Anal. Biochem. 244 (1997) 347–356.
[100] G. Liebisch, W. Drobnik, M. Reil, B. Trumbach, R. Arnecke, B. Olgemoller, A. Roscher, G. Schmitz, Quantitative measurement of different ceramide species from crude cellular extracts by electrospray ionization tandem mass spectrometry (ESI-MS/MS), J. Lipid Res. 40 (1999) 1539–1546.
[101] A. Olling, M.E. Breimer, E. Peltomaa, B.E. Samuelsson, S. Ghardashkhani, Electrospray ionization and collision-induced dissociation time-of-flight mass spectrometry of neutral glycosphingolipids, Rapid Commun. Mass Spectrom. 12 (1998) 637–645.
[102] B. Lieser, G. Liebisch, W. Drobnik, G. Schmitz, Quantification of sphingosine and sphinganine from crude lipid extracts by HPLC electrospray ionization tandem mass spectrometry, J. Lipid Res. 44 (2003) 2209–2216.
[103] M. Scherer, K. Leuthauser-Jaschinski, J. Ecker, G. Schmitz, G. Liebisch, A rapid and quantitative LC-MS/MS method to profile sphingolipids, J. Lipid Res. 51 (2010) 2001–2011.
[104] F.F. Hsu, J. Turk, Structural determination of sphingomyelin by tandem mass spectrometry with electrospray ionization, J. Am. Soc. Mass Spectrom. 11 (2000) 437–449.
[105] J.L. Kerwin, A.R. Tuininga, L.H. Ericsson, Identification of molecular species of glycerophospholipids and sphingomyelin using electrospray mass spectrometry, J. Lipid Res. 35 (1994) 1102–1114.
[106] B. Domon, C.E. Costello, Structure elucidation of glycosphingolipids and gangliosides using high-performance tandem mass spectrometry, Biochemistry 27 (1988) 1534–1543.
[107] T. Ii, Y. Ohashi, Y. Nagai, Structural elucidation of underivatized gangliosides by electrospray-ionization tandem mass spectrometry (ESIMS/MS), Carbohydr. Res. 273 (1995) 27–40.
[108] F.F. Hsu, A. Bohrer, J. Turk, Electrospray ionization tandem mass spectrometric analysis of sulfatide. Determination of fragmentation patterns and characterization of molecular species expressed in brain and in pancreatic islets, Biochim. Biophys. Acta 1392 (1998) 202–216.
[109] P.D. Whitfield, P.C. Sharp, D.W. Johnson, P. Nelson, P.J. Meikle, Characterization of urinary sulfatides in metachromatic leukodystrophy using electrospray ionization-tandem mass spectrometry, Mol. Genet. Metab. 73 (2001) 30–37.
[110] F. Boscaro, G. Pieraccini, G. la Marca, G. Bartolucci, C. Luceri, F. Luceri, G. Moneti, Rapid quantitation of globotriaosylceramide in human plasma and urine: a potential application for monitoring enzyme replacement therapy in Anderson-Fabry disease, Rapid Commun. Mass Spectrom. 16 (2002) 1507–1514.
[111] L. Kuchar, B. Asfaw, J. Ledvinova, Tandem mass spectrometry of sphingolipids: application in metabolic studies and diagnosis of inherited disorders of sphingolipid metabolism, in: J.K. Prasain (Ed.), Tandem Mass Spectrometry—Applications and Principles, InTech, Rijeka, ISBN: 978-953-51-0141-3, 2012, pp. 739–768.
[112] Q. Hu, R.J. Noll, H. Li, A. Makarov, M. Hardman, R. Graham Cooks, The Orbitrap: a new mass spectrometer, J. Mass Spectrom. 40 (2005) 430–443.
[113] L. Sleno, The use of mass defect in modern mass spectrometry, J. Mass Spectrom. 47 (2012) 226–236.
[114] M.L. Gross, Accurate masses for structure confirmation, J. Am. Soc. Mass Spectrom. 5 (1994) 57.
[115] I.A. Buryakov, E.V. Krylov, E.G. Nazarov, U.K. Rasulev, A new method of separation of multi-atomic ions by mobility at atmospheric-pressure using a high-frequency

amplitude-asymmetric strong electric-field, Int. J. Mass Spectrom. Ion Process. 128 (1993) 143–148.
[116] K. Giles, S.D. Pringle, K.R. Worthington, D. Little, J.L. Wildgoose, R.H. Bateman, Applications of a travelling wave-based radio-frequency-only stacked ring ion guide, Rapid Commun. Mass Spectrom. 18 (2004) 2401–2414.
[117] G. Paglia, M. Kliman, E. Claude, S. Geromanos, G. Astarita, Applications of ion-mobility mass spectrometry for lipid analysis, Anal. Bioanal. Chem. 407 (2015) 4995–5007.
[118] P.R. Baker, A.M. Armando, J.L. Campbell, O. Quehenberger, E.A. Dennis, Three-dimensional enhanced lipidomics analysis combining UPLC, differential ion mobility spectrometry, and mass spectrometric separation strategies, J. Lipid Res. 55 (2014) 2432–2442.
[119] S. Kmoch, J. Majewski, V. Ramamurthy, S. Cao, S. Fahiminiya, H. Ren, I.M. MacDonald, I. Lopez, V. Sun, V. Keser, A. Khan, V. Stranecky, H. Hartmannova, A. Pristoupilova, K. Hodanova, L. Piherova, L. Kuchar, A. Baxova, R. Chen, O.G. Barsottini, A. Pyle, H. Griffin, M. Splitt, J. Sallum, J.L. Tolmie, J.R. Sampson, P. Chinnery, E. Banin, D. Sharon, S. Dutta, R. Grebler, C. Helfrich--Foerster, J.L. Pedroso, D. Kretzschmar, M. Cayouette, R.K. Koenekoop, Mutations in PNPLA6 are linked to photoreceptor degeneration and various forms of childhood blindness, Nat. Commun. 6 (2015) 5614.
[120] T.P. Lintonen, P.R. Baker, M. Suoniemi, B.K. Ubhi, K.M. Koistinen, E. Duchoslav, J.L. Campbell, K. Ekroos, Differential mobility spectrometry-driven shotgun lipidomics, Anal. Chem. 86 (2014) 9662–9669.
[121] G. Paglia, P. Angel, J.P. Williams, K. Richardson, H.J. Olivos, J.W. Thompson, L. Menikarachchi, S. Lai, C. Walsh, A. Moseley, R.S. Plumb, D.F. Grant, B.O. Palsson, J. Langridge, S. Geromanos, G. Astarita, Ion mobility-derived collision cross section as an additional measure for lipid fingerprinting and identification, Anal. Chem. 87 (2015) 1137–1144.
[122] C. Auray-Blais, M. Boutin, R. Gagnon, F.O. Dupont, P. Lavoie, J.T. Clarke, Urinary globotriaosylsphingosine-related biomarkers for Fabry disease targeted by metabolomics, Anal. Chem. 84 (2012) 2745–2753.
[123] M. Boutin, C. Auray-Blais, Metabolomic discovery of novel urinary galabiosylceramide analogs as Fabry disease biomarkers, J. Am. Soc. Mass Spectrom. 26 (2015) 499–510.
[124] V. Manwaring, M. Boutin, C. Auray-Blais, A metabolomic study to identify new globotriaosylceramide-related biomarkers in the plasma of Fabry disease patients, Anal. Chem. 85 (2013) 9039–9048.
[125] A.K. Giese, H. Mascher, U. Grittner, S. Eichler, G. Kramp, J. Lukas, D. te Vruchte, N. Al Eisa, M. Cortina-Borja, F.D. Porter, F.M. Platt, A. Rolfs, A novel, highly sensitive and specific biomarker for Niemann-Pick type C1 disease, Orphanet J. Rare Dis. 10 (2015) 78.
[126] J. Folch, M. Lees, G.H. Sloane Stanley, A simple method for the isolation and purification of total lipides from animal tissues, J. Biol. Chem. 226 (1957) 497–509.
[127] E.G. Bligh, W.J. Dyer, A rapid method of total lipid extraction and purification, Can. J. Biochem. Physiol. 37 (1959) 911–917.
[128] V. Matyash, G. Liebisch, T.V. Kurzchalia, A. Shevchenko, D. Schwudke, Lipid extraction by methyl-tert-butyl ether for high-throughput lipidomics, J. Lipid Res. 49 (2008) 1137–1146.
[129] H. Natomi, K. Sugano, M. Iwamori, F. Takaku, Y. Nagai, Region-specific distribution of glycosphingolipids in the rabbit gastrointestinal tract: preferential enrichment of sulfoglycolipids in the mucosal regions exposed to acid, Biochim. Biophys. Acta 961 (1988) 213–222.
[130] R.W. Ledeen, R.K. Yu, Gangliosides: structure, isolation, and analysis, Methods Enzymol. 83 (1982) 139–191.
[131] R.L. Schnaar, Isolation of glycosphingolipids, Methods Enzymol. 230 (1994) 348–370.
[132] G. van Echten-Deckert, Sphingolipid extraction and analysis by thin-layer chromatography, Methods Enzymol. 312 (2000) 64–79.
[133] S.J. Iverson, S.L. Lang, M.H. Cooper, Comparison of the Bligh and Dyer and Folch methods for total lipid determination in a broad range of marine tissue, Lipids 36 (2001) 1283–1287.
[134] Y. Lee do, T. Kind, Y.R. Yoon, O. Fiehn, K.H. Liu, Comparative evaluation of extraction methods for simultaneous mass-spectrometric analysis of complex lipids and primary metabolites from human blood plasma, Anal. Bioanal. Chem. 406 (2014) 7275–7286.
[135] M. Wagner, D. Tonoli, E. Varesio, G. Hopfgartner, The use of mass spectrometry to analyze dried blood spots, Mass Spectrom. Rev. 35 (2014) 361–438.
[136] X. Han, R.W. Gross, Global analyses of cellular lipidomes directly from crude extracts of biological samples by ESI mass spectrometry: a bridge to lipidomics, J. Lipid Res. 44 (2003) 1071–1079.
[137] M. Gantner, G. Schwarzmann, K. Sandhoff, T. Kolter, Partial synthesis of ganglioside and lysoganglioside lipoforms as internal standards for MS quantification, J. Lipid Res. 55 (2014) 2692–2704.
[138] X. Zhou, F. Turecek, C.R. Scott, M.H. Gelb, Quantification of cellular acid sphingomyelinase and galactocerebroside beta-galactosidase activities by electrospray ionization mass spectrometry, Clin. Chem. 47 (2001) 874–881.
[139] M. Ito, K. Kita, T. Kurita, N. Sueyoshi, H. Izu, Enzymatic N-deacylation of sphingolipids, Methods Enzymol. 311 (2000) 297–303.
[140] M. Ito, T. Kurita, K. Kita, A novel enzyme that cleaves the N-acyl linkage of ceramides in various glycosphingolipids as well as sphingomyelin to produce their lyso forms, J. Biol. Chem. 270 (1995) 24370–24374.
[141] K. Kita, T. Kurita, M. Ito, Characterization of the reversible nature of the reaction catalyzed by sphingolipid ceramide N-deacylase. A novel form of reverse hydrolysis reaction, Eur. J. Biochem. 268 (2001) 592–602.
[142] L. Kuchar, J. Rotkova, B. Asfaw, J. Lenfeld, D. Horak, L. Korecka, Z. Bilkova, J. Ledvinova, Semisynthesis of C17:0 isoforms of sulphatide and glucosylceramide using immobilised sphingolipid ceramide N-deacylase for application in analytical mass spectrometry, Rapid Commun. Mass Spectrom. 24 (2010) 2393–2399.
[143] E. Cifkova, M. Holcapek, M. Lisa, M. Ovcacikova, A. Lycka, F. Lynen, P. Sandra, Nontargeted quantitation of lipid classes using hydrophilic interaction liquid chromatography-electrospray ionization mass spectrometry with single internal standard and response factor approach, Anal. Chem. 84 (2012) 10064–10070.
[144] A. Mehta, B. Winchester (Eds.), Lysosomal Storage Disorders: A Practical Guide, first ed., John Wiley & Sons, Ltd., Chichester, ISBN: 978-0-470-67087-3, 2012.
[145] M. Fuller, P.C. Sharp, T. Rozaklis, P.D. Whitfield, D. Blacklock, J.J. Hopwood, P.J. Meikle, Urinary lipid profiling for the identification of fabry hemizygotes and heterozygotes, Clin. Chem. 51 (2005) 688–694.
[146] L. Kuchar, J. Ledvinova, M. Hrebicek, H. Myskova, L. Dvorakova, L. Berna, P. Chrastina, B. Asfaw, M. Elleder, M. Petermoller, H. Mayrhofer, M. Staudt, I. Krageloh-Mann, B.C. Paton, K. Harzer, Prosaposin deficiency and saposin B deficiency (activator-deficient metachromatic leukodystrophy): report on two patients detected by analysis of urinary sphingolipids and carrying novel PSAP gene mutations, Am. J. Med. Genet. A 149A (2009) 613–621.

[147] C. Auray-Blais, D. Cyr, A. Ntwari, M.L. West, J. Cox-Brinkman, D.G. Bichet, D.P. Germain, R. Laframboise, S.B. Melancon, T. Stockley, J.T. Clarke, R. Drouin, Urinary globotriaosylceramide excretion correlates with the genotype in children and adults with Fabry disease, Mol. Genet. Metab. 93 (2008) 331–340.
[148] C. Auray-Blais, D.S. Millington, C. Barr, S.P. Young, K. Mills, J.T. Clarke, Gb(3)/creatinine biomarkers for Fabry disease: issues to consider, Mol. Genet. Metab. 97 (2009) 237.
[149] M. Mirzaian, G. Kramer, B.J. Poorthuis, Quantification of sulfatides and lysosulfatides in tissues and body fluids by liquid chromatography-tandem mass spectrometry, J. Lipid Res. 56 (2015) 936–943.
[150] S. Forni, X. Fu, R. Schiffmann, L. Sweetman, Falsely elevated urinary Gb3 (globotriaosylceramide, CTH, GL3), Mol. Genet. Metab. 97 (2009) 91.
[151] C. Barr, J.T. Clarke, A. Ntwari, R. Drouin, C. Auray-Blais, Fabry disease urinary globotriaosylceramide/creatinine biomarker evaluation by liquid chromatography-tandem mass spectrometry in healthy infants from birth to 6 months, Mol. Genet. Metab. 97 (2009) 278–283.
[152] L. Berna, B. Asfaw, E. Conzelmann, B. Cerny, J. Ledvinova, Determination of urinary sulfatides and other lipids by combination of reversed-phase and thin-layer chromatographies, Anal. Biochem. 269 (1999) 304–311.
[153] K. Mills, P. Morris, P. Lee, A. Vellodi, S. Waldek, E. Young, B. Winchester, Measurement of urinary CDH and CTH by tandem mass spectrometry in patients hemizygous and heterozygous for Fabry disease, J. Inherit. Metab. Dis. 28 (2005) 35–48.
[154] A.D. Postle, Phospholipid profiling, in: W.J. Griffiths (Ed.), Metabolomics, Metabonomics and Metabolite Profiling, Royal Society of Chemistry, Cambridge, ISBN: 978-0-85404-299-9, 2008, pp. 116–133.
[155] Z. Spacil, A. Babu Kumar, H.C. Liao, C. Auray-Blais, S. Stark, T.R. Suhr, C.R. Scott, F. Turecek, M.H. Gelb, Sulfatide analysis by mass spectrometry for screening of metachromatic leukodystrophy in dried blood and urine samples, Clin. Chem. 62 (2016) 279–286.
[156] G. Fauler, G.N. Rechberger, D. Devrnja, W. Erwa, B. Plecko, P. Kotanko, F. Breunig, E. Paschke, Rapid determination of urinary globotriaosylceramide isoform profiles by electrospray ionization mass spectrometry using stearoyl-d35-globotriaosylceramide as internal standard, Rapid Commun. Mass Spectrom. 19 (2005) 1499–1506.
[157] M. Gaggl, M. Hofer, S. Weidner, J. Kleinert, G. Fauler, M. Wallner, P. Kotanko, E. Paschke, G. Sunder-Plassmann, Interfering parameters in the determination of urinary globotriaosylceramide (Gb3) in patients with chronic kidney disease, J. Nephrol. 28 (2015) 679–689.
[158] E. Paschke, G. Fauler, H. Winkler, A. Schlagenhauf, B. Plecko, W. Erwa, F. Breunig, W. Urban, B. Vujkovac, G. Sunder-Plassmann, P. Kotanko, Urinary total globotriaosylceramide and isoforms to identify women with Fabry disease: a diagnostic test study, Am. J. Kidney Dis. 57 (2011) 673–681.
[159] S. Bekri, O. Lidove, R. Jaussaud, B. Knebelmann, F. Barbey, The role of ceramide trihexoside (globotriaosylceramide) in the diagnosis and follow-up of the efficacy of treatment of Fabry disease: a review of the literature, Cardiovasc. Hematol. Agents Med. Chem. 4 (2006) 289–297.
[160] K. Mills, A. Johnson, B. Winchester, Synthesis of novel internal standards for the quantitative determination of plasma ceramide trihexoside in Fabry disease by tandem mass spectrometry, FEBS Lett. 515 (2002) 171–176.
[161] B.C. Nelson, T. Roddy, S. Araghi, D. Wilkens, J.J. Thomas, K. Zhang, C.C. Sung, S.M. Richards, Globotriaosylceramide isoform profiles in human plasma by liquid chromatography-tandem mass spectrometry, J. Chromatogr. B Analyt. Technol. Biomed. Life Sci. 805 (2004) 127–134.
[162] R. Kruger, K. Bruns, S. Grunhage, H. Rossmann, J. Reinke, M. Beck, K.J. Lackner, Determination of globotriaosylceramide in plasma and urine by mass spectrometry, Clin. Chem. Lab. Med. 48 (2010) 189–198.
[163] T. Togawa, T. Kodama, T. Suzuki, K. Sugawara, T. Tsukimura, T. Ohashi, N. Ishige, K. Suzuki, T. Kitagawa, H. Sakuraba, Plasma globotriaosylsphingosine as a biomarker of Fabry disease, Mol. Genet. Metab. 100 (2010) 257–261.
[164] A.C. Vedder, V.E. Gerdes, B.J. Poorthuis, M. Helmond, M.D. Trip, J.M. Aerts, C.E. Hollak, Failure to detect Fabry patients in a cohort of prematurely atherosclerotic males, J. Inherit. Metab. Dis. 30 (2007) 988.
[165] A.C. Vedder, G.E. Linthorst, M.J. van Breemen, J.E. Groener, F.J. Bemelman, A. Strijland, M.M. Mannens, J.M. Aerts, C.E. Hollak, The Dutch Fabry cohort: diversity of clinical manifestations and Gb3 levels, J. Inherit. Metab. Dis. 30 (2007) 68–78.
[166] J.M. Aerts, W.W. Kallemeijn, W. Wegdam, M. Joao Ferraz, M.J. van Breemen, N. Dekker, G. Kramer, B.J. Poorthuis, J.E. Groener, J. Cox-Brinkman, S.M. Rombach, C.E. Hollak, G.E. Linthorst, M.D. Witte, H. Gold, G.A. van der Marel, H.S. Overkleeft, R.G. Boot, Biomarkers in the diagnosis of lysosomal storage disorders: proteins, lipids, and inhibodies, J. Inherit. Metab. Dis. 34 (2011) 605–619.
[167] E. Young, K. Mills, P. Morris, A. Vellodi, P. Lee, S. Waldek, B. Winchester, Is globotriaosylceramide a useful biomarker in Fabry disease? Acta Paediatr. Suppl. 94 (2005) 51–54. discussion 37–58.
[168] M.J. Ferraz, W.W. Kallemeijn, M. Mirzaian, D. Herrera Moro, A. Marques, P. Wisse, R.G. Boot, L.I. Willems, H.S. Overkleeft, J.M. Aerts, Gaucher disease and Fabry disease: new markers and insights in pathophysiology for two distinct glycosphingolipidoses, Biochim. Biophys. Acta 1841 (2014) 811–825.
[169] P.J. Meikle, P.D. Whitfield, T. Rozaklis, D. Blacklock, S. Duplock, D. Elstein, A. Zimran, E. Mengel, P. Cannell, J.J. Hopwood, M. Fuller, Plasma lipids are altered in Gaucher disease: biochemical markers to evaluate therapeutic intervention, Blood Cells Mol. Dis. 40 (2008) 420–427.
[170] M. Fuller, S. Duplock, L.K. Hein, B.A. Rigat, D.J. Mahuran, Liquid chromatography/electrospray ionisation-tandem mass spectrometry quantification of GM2 gangliosides in human peripheral cells and plasma, Anal. Biochem. 458 (2014) 20–26.
[171] T. Kodama, T. Togawa, T. Tsukimura, I. Kawashima, K. Matsuoka, K. Kitakaze, D. Tsuji, K. Itoh, Y. Ishida, M. Suzuki, T. Suzuki, H. Sakuraba, Lyso-GM2 ganglioside: a possible biomarker of Tay-Sachs disease and Sandhoff disease, PLoS One 6 (2011) e29074.
[172] M. Barcenas, T.R. Suhr, C.R. Scott, F. Turecek, M.H. Gelb, Quantification of sulfatides in dried blood and urine spots from metachromatic leukodystrophy patients by liquid chromatography/electrospray tandem mass spectrometry, Clin. Chim. Acta 433 (2014) 39–43.
[173] M. Han, S.H. Jun, S.H. Song, H.D. Park, K.U. Park, J. Song, Ultra-performance liquid chromatography/tandem mass spectrometry for determination of sulfatides in dried blood spots from patients with metachromatic leukodystrophy, Rapid Commun. Mass Spectrom. 28 (2014) 587–594.
[174] Q. Huang, X. Zhou, D. Liu, B. Xin, K. Cechner, H. Wang, A. Zhou, A new liquid chromatography/tandem mass spectrometry method for quantification of gangliosides in human plasma, Anal. Biochem. 455 (2014) 26–34.
[175] L. Astudillo, F. Sabourdy, N. Therville, H. Bode, B. Segui, N. Andrieu-Abadie, T. Hornemann, T. Levade, Human genetic disorders of sphingolipid biosynthesis, J. Inherit. Metab. Dis. 38 (2015) 65–76.

[176] P.D. Whitfield, P.C. Sharp, R. Taylor, P. Meikle, Quantification of galactosylsphingosine in the twitcher mouse using electrospray ionization-tandem mass spectrometry, J. Lipid Res. 42 (2001) 2092–2095.
[177] T. Miyatake, K. Suzuki, Globoid cell leukodystrophy—additional deficiency of psychosine galactosidase, Biochem. Biophys. Res. Commun. 48 (1972) 538–543.
[178] K. Suzuki, Twenty five years of the "psychosine hypothesis": a personal perspective of its history and present status, Neurochem. Res. 23 (1998) 251–259.
[179] L. Svennerholm, M.T. Vanier, J.E. Mansson, Krabbe disease: a galactosylsphingosine (psychosine) lipidosis, J. Lipid Res. 21 (1980) 53–64.
[180] O. Nilsson, L. Svennerholm, Accumulation of glucosylceramide and glucosylsphingosine (psychosine) in cerebrum and cerebellum in infantile and juvenile Gaucher disease, J. Neurochem. 39 (1982) 709–718.
[181] E. Orvisky, J.K. Park, M.E. LaMarca, E.I. Ginns, B.M. Martin, N. Tayebi, E. Sidransky, Glucosylsphingosine accumulation in tissues from patients with Gaucher disease: correlation with phenotype and genotype, Mol. Genet. Metab. 76 (2002) 262–270.
[182] U.H. Schueler, T. Kolter, C.R. Kaneski, J.K. Blusztajn, M. Herkenham, K. Sandhoff, R.O. Brady, Toxicity of glucosylsphingosine (glucopsychosine) to cultured neuronal cells: a model system for assessing neuronal damage in Gaucher disease type 2 and 3, Neurobiol. Dis. 14 (2003) 595–601.
[183] M. Mirzaian, P. Wisse, M.J. Ferraz, H. Gold, W.E. Donker-Koopman, M. Verhoek, H.S. Overkleeft, R.G. Boot, G. Kramer, N. Dekker, J.M. Aerts, Mass spectrometric quantification of glucosylsphingosine in plasma and urine of type 1 Gaucher patients using an isotope standard, Blood Cells Mol. Dis. 54 (2015) 307–314.
[184] D. Meyer zu Heringdorf, H.M. Himmel, K.H. Jakobs, Sphingosylphosphorylcholine-biological functions and mechanisms of action, Biochim. Biophys. Acta 1582 (2002) 178–189.
[185] C. O'Sullivan, K.K. Dev, Galactosylsphingosine (psychosine)-induced demyelination is attenuated by sphingosine 1-phosphate signalling, J. Cell Sci. 128 (2015) 3878–3887.
[186] D.A. Wenger, P. Luzi, M.A. Rafi, Lysosomal storage diseases: heterogeneous group of disorders, Bioimpacts 3 (2013) 145–147.
[187] Y. Yamaguchi, N. Sasagasako, I. Goto, T. Kobayashi, The synthetic pathway for glucosylsphingosine in cultured fibroblasts, J. Biochem. 116 (1994) 704–710.
[188] M.J. Ferraz, A.R. Marques, M.D. Appelman, M. Verhoek, A. Strijland, M. Mirzaian, S. Scheij, C.M. Ouairy, D. Lahav, P. Wisse, H.S. Overkleeft, R.G. Boot, J.M. Aerts, Lysosomal glycosphingolipid catabolism by acid ceramidase: formation of glycosphingoid bases during deficiency of glycosidases, FEBS Lett. 590 (2016) 716–725.
[189] H. Gold, M. Mirzaian, N. Dekker, M. Joao Ferraz, J. Lugtenburg, J.D. Codee, G.A. van der Marel, H.S. Overkleeft, G.E. Linthorst, J.E. Groener, J.M. Aerts, B.J. Poorthuis, Quantification of globotriaosylsphingosine in plasma and urine of Fabry patients by stable isotope ultraperformance liquid chromatography-tandem mass spectrometry, Clin. Chem. 59 (2013) 547–556.
[190] B.E. Smid, L. van der Tol, M. Biegstraaten, G.E. Linthorst, C.E. Hollak, B.J. Poorthuis, Plasma globotriaosylsphingosine in relation to phenotypes of Fabry disease, J. Med. Genet. 52 (2015) 262–268.
[191] B.E. Smid, C.E. Hollak, B.J. Poorthuis, M.A. van den Bergh Weerman, S. Florquin, W.E. Kok, R.H. Lekanne Deprez, J. Timmermans, G.E. Linthorst, Diagnostic dilemmas in Fabry disease: a case series study on GLA mutations of unknown clinical significance, Clin. Genet. 88 (2015) 161–166.
[192] H.C. Liao, Y.H. Huang, Y.J. Chen, S.M. Kao, H.Y. Lin, C.K. Huang, H.C. Liu, T.R. Hsu, S.P. Lin, C.F. Yang, C.S. Fann, P.C. Chiu, K.S. Hsieh, Y.C. Fu, Y.Y. Ke, C.Y. Lin, F.J. Tsai, C.H. Wang, M.C. Chao, W.C. Yu, C.C. Chiang, D.M. Niu, Plasma globotriaosylsphingosine (lysoGb3) could be a biomarker for Fabry disease with a Chinese hotspot late-onset mutation (IVS4+919G>A), Clin. Chim. Acta 426 (2013) 114–120.
[193] W.L. Chuang, J. Pacheco, S. Cooper, M.M. McGovern, G.F. Cox, J. Keutzer, X.K. Zhang, Lyso-sphingomyelin is elevated in dried blood spots of Niemann-Pick B patients, Mol. Genet. Metab. 111 (2014) 209–211.
[194] R.W. Welford, M. Garzotti, C. Marques Lourenco, E. Mengel, T. Marquardt, J. Reunert, Y. Amraoui, S.A. Kolb, O. Morand, P. Groenen, Plasma lysosphingomyelin demonstrates great potential as a diagnostic biomarker for Niemann-Pick disease type C in a retrospective study, PLoS One 9 (2014) e114669.
[195] B. Johnson, H. Mascher, D. Mascher, E. Legnini, C.Y. Hung, A. Dajnoki, Y.H. Chien, L. Marodi, W.L. Hwu, O.A. Bodamer, Analysis of lyso-globotriaosylsphingosine in dried blood spots, Ann. Lab. Med. 33 (2013) 274–278.
[196] C. Auray-Blais, C.M. Blais, U. Ramaswami, M. Boutin, D.P. Germain, S. Dyack, O. Bodamer, G. Pintos-Morell, J.T. Clarke, D.G. Bichet, D.G. Warnock, L. Echevarria, M.L. West, P. Lavoie, Urinary biomarker investigation in children with Fabry disease using tandem mass spectrometry, Clin. Chim. Acta 438 (2015) 195–204.
[197] S. Ferreira, C. Auray-Blais, M. Boutin, P. Lavoie, J.P. Nunes, E. Martins, S. Garman, J.P. Oliveira, Variations in the GLA gene correlate with globotriaosylceramide and globotriaosylsphingosine analog levels in urine and plasma, Clin. Chim. Acta 447 (2015) 96–104.
[198] H. Sueoka, J. Ichihara, T. Tsukimura, T. Togawa, H. Sakuraba, Nano-LC-MS/MS for quantification of Lyso-Gb3 and its analogues reveals a useful biomarker for Fabry disease, PLoS One 10 (2015) e0127048.
[199] P. Lavoie, M. Boutin, C. Auray-Blais, Multiplex analysis of novel urinary lyso-Gb3-related biomarkers for Fabry disease by tandem mass spectrometry, Anal. Chem. 85 (2013) 1743–1752.
[200] M.J. Ferraz, A.R. Marques, P. Gaspar, M. Mirzaian, C. van Roomen, R. Ottenhoff, P. Alfonso, P. Irun, P. Giraldo, P. Wisse, C. Sa Miranda, H.S. Overkleeft, J.M. Aerts, Lyso-glycosphingolipid abnormalities in different murine models of lysosomal storage disorders, Mol. Genet. Metab. 117 (2016) 186–193.
[201] F.D. Porter, D.E. Scherrer, M.H. Lanier, S.J. Langmade, V. Molugu, S.E. Gale, D. Olzeski, R. Sidhu, D.J. Dietzen, R. Fu, C.A. Wassif, N.M. Yanjanin, S.P. Marso, J. House, C. Vite, J.E. Schaffer, D.S. Ory, Cholesterol oxidation products are sensitive and specific blood-based biomarkers for Niemann-Pick C1 disease, Sci. Transl. Med. 2 (2010) 56ra81.
[202] J. Reunert, A.S. Lotz-Havla, G. Polo, F. Kannenberg, M. Fobker, M. Griese, E. Mengel, A.C. Muntau, P. Schnabel, O. Sommerburg, I. Borggraefe, A. Dardis, A.P. Burlina, M.A. Mall, G. Ciana, B. Bembi, A.B. Burlina, T. Marquardt, Niemann-Pick type C-2 disease: identification by analysis of plasma cholestane-3beta, 5alpha,6beta-triol and further insight into the clinical phenotype, JIMD Rep. 23 (2015) 17–26.
[203] X. Jiang, R. Sidhu, F.D. Porter, N.M. Yanjanin, A.O. Speak, D.T. te Vruchte, F.M. Platt, H. Fujiwara, D.E. Scherrer, J. Zhang, D.J. Dietzen, J.E. Schaffer, D.S. Ory, A sensitive and specific LC-MS/MS method for rapid diagnosis of Niemann-Pick C1 disease from human plasma, J. Lipid Res. 52 (2011) 1435–1445.
[204] Z. Akgoc, S. Iosim, T.N. Seyfried, Bis(monoacylglycero)phosphate as a macrophage enriched phospholipid, Lipids 50 (2015) 907–912.
[205] C. Luquain-Costaz, E. Lefai, M. Arnal-Levron, D. Markina, S. Sakai, V. Euthine, A. Makino, M. Guichardant, S. Yamashita, T. Kobayashi, M. Lagarde, P. Moulin, I. Delton-Vandenbroucke, Bis(monoacylglycero)phosphate accumulation in

macrophages induces intracellular cholesterol redistribution, attenuates liver-X receptor/ATP-binding cassette transporter A1/ATP-binding cassette transporter G1 pathway, and impairs cholesterol efflux, Arterioscler. Thromb. Vasc. Biol. 33 (2013) 1803–1811.
[206] M. Scherer, G. Schmitz, Metabolism, function and mass spectrometric analysis of bis(monoacylglycero)phosphate and cardiolipin, Chem. Phys. Lipids 164 (2011) 556–562.
[207] P.J. Meikle, S. Duplock, D. Blacklock, P.D. Whitfield, G. Macintosh, J.J. Hopwood, M. Fuller, Effect of lysosomal storage on bis(monoacylglycero)phosphate, Biochem. J. 411 (2008) 71–78.
[208] S.A. Gerber, C.R. Scott, F. Turecek, M.H. Gelb, Direct profiling of multiple enzyme activities in human cell lysates by affinity chromatography/electrospray ionization mass spectrometry: application to clinical enzymology, Anal. Chem. 73 (2001) 1651–1657.
[209] F. Turecek, C.R. Scott, M.H. Gelb, Tandem mass spectrometry in the detection of inborn errors of metabolism for newborn screening, Methods Mol. Biol. 359 (2007) 143–157.
[210] Y. Li, K. Brockmann, F. Turecek, C.R. Scott, M.H. Gelb, Tandem mass spectrometry for the direct assay of enzymes in dried blood spots: application to newborn screening for Krabbe disease, Clin. Chem. 50 (2004) 638–640.
[211] Y. Li, C.R. Scott, N.A. Chamoles, A. Ghavami, B.M. Pinto, F. Turecek, M.H. Gelb, Direct multiplex assay of lysosomal enzymes in dried blood spots for newborn screening, Clin. Chem. 50 (2004) 1785–1796.
[212] Z. Spacil, S. Elliott, S.L. Reeber, M.H. Gelb, C.R. Scott, F. Turecek, Comparative triplex tandem mass spectrometry assays of lysosomal enzyme activities in dried blood spots using fast liquid chromatography: application to newborn screening of Pompe, Fabry, and Hurler diseases, Anal. Chem. 83 (2011) 4822–4828.
[213] M. Han, S.H. Jun, S.H. Song, K.U. Park, J.Q. Kim, J. Song, Use of tandem mass spectrometry for newborn screening of 6 lysosomal storage disorders in a Korean population, Korean J. Lab. Med. 31 (2011) 250–256.
[214] C.D. Castilhos, J. Mezzalira, M.P. Goldim, V.V. Daitx, S. Garcia Cda, C.V. Andrade, A.C. Breier, J. Ce, A.S. Mello, J.C. Coelho, Determination of the lysosomal hydrolase activity in blood collected on filter paper, an alternative to screen high risk populations, Gene 536 (2014) 344–347.
[215] J.J. Orsini, M.M. Martin, A.L. Showers, O.A. Bodamer, X.K. Zhang, M.H. Gelb, M. Caggana, Lysosomal storage disorder 4 + 1 multiplex assay for newborn screening using tandem mass spectrometry: application to a small-scale population study for five lysosomal storage disorders, Clin. Chim. Acta 413 (2012) 1270–1273.
[216] D.C. Kasper, J. Herman, V.R. De Jesus, T.P. Mechtler, T.F. Metz, B. Shushan, The application of multiplexed, multi-dimensional ultra-high-performance liquid chromatography/tandem mass spectrometry to the high-throughput screening of lysosomal storage disorders in newborn dried bloodspots, Rapid Commun. Mass Spectrom. 24 (2010) 986–994.
[217] B.J. Wolfe, F. Ghomashchi, T. Kim, C.A. Abam, M. Sadilek, R. Jack, J.N. Thompson, C.R. Scott, M.H. Gelb, F. Turecek, New substrates and enzyme assays for the detection of mucopolysaccharidosis III (Sanfilippo Syndrome) types A, B, C, and D by tandem mass spectrometry, Bioconjug. Chem. 23 (2012) 557–564.
[218] N.K. Chennamaneni, A.B. Kumar, M. Barcenas, Z. Spacil, C.R. Scott, F. Turecek, M.H. Gelb, Improved reagents for newborn screening of mucopolysaccharidosis types I, II, and VI by tandem mass spectrometry, Anal. Chem. 86 (2014) 4508–4514.
[219] A.B. Kumar, S. Masi, F. Ghomashchi, N.K. Chennamaneni, M. Ito, C.R. Scott, F. Turecek, M.H. Gelb, Z. Spacil, Tandem mass spectrometry Has a larger analytical range than fluorescence assays of lysosomal enzymes: application to newborn screening and diagnosis of mucopolysaccharidoses types II, IVA, and VI, Clin. Chem. 61 (2015) 1363–1371.
[220] K. Harzer, B.C. Paton, A. Poulos, B. Kustermannkuhn, W. Roggendorf, T. Grisar, M. Popp, Sphingolipid activator protein-deficiency in a 16-week-old atypical Gaucher disease patient and his fetal sibling—biochemical signs of combined sphingolipidoses, Eur. J. Pediatr. 149 (1989) 31–39.
[221] H. Kihara, C.K. Ho, A.L. Fluharty, K.K. Tsay, P.L. Hartlage, Prenatal diagnosis of metachromatic leukodystrophy in a family with pseudo arylsulfatase A deficiency by the cerebroside sulfate loading test, Pediatr. Res. 14 (1980) 224–227.
[222] L. Riboni, P. Viani, G. Tettamanti, Estimating sphingolipid metabolism and trafficking in cultured cells using radiolabeled compounds, Methods Enzymol. 311 (2000) 656–682.
[223] G. Schwarzmann, Uptake and metabolism of exogenous glycosphingolipids by cultured cells, Semin. Cell Dev. Biol. 12 (2001) 163–171.
[224] G. Schwarzmann, C. Arenz, K. Sandhoff, Labeled chemical biology tools for investigating sphingolipid metabolism, trafficking and interaction with lipids and proteins, Biochim. Biophys. Acta 1841 (2014) 1161–1173.
[225] P. Wisse, H. Gold, M. Mirzaian, M.J. Ferraz, G. Lutteke, R.J.B.H.N. van den Berg, H. van den Elst, J. Lugtenburg, G.A. van der Marel, J.M.F.G. Aerts, J.D.C. Codee, H.S. Overkleeft, Synthesis of a panel of carbon-13-labelled (glyco)sphingolipids, Eur. J. Org. Chem. (2015) 2661–2677.
[226] Y. Zeng, H. Cheng, X. Jiang, X. Han, Endosomes and lysosomes play distinct roles in sulfatide-induced neuroblastoma apoptosis: potential mechanisms contributing to abnormal sulfatide metabolism in related neuronal diseases, Biochem. J. 410 (2008) 81–92.
[227] R.J. Brown, F. Shao, A. Baldan, C.J. Albert, D.A. Ford, Cholesterol efflux analyses using stable isotopes and mass spectrometry, Anal. Biochem. 433 (2013) 56–64.
[228] G. Liebisch, M. Binder, R. Schifferer, T. Langmann, B. Schulz, G. Schmitz, High throughput quantification of cholesterol and cholesteryl ester by electrospray ionization tandem mass spectrometry (ESI-MS/MS), Biochim. Biophys. Acta 1761 (2006) 121–128.
[229] J. Ecker, G. Liebisch, Application of stable isotopes to investigate the metabolism of fatty acids, glycerophospholipid and sphingolipid species, Prog. Lipid Res. 54 (2014) 14–31.

Publications in impacted journals related to the topic of this Ph.D. thesis

Supplementary publication D

Řeboun M, **Rybová J**, Dobrovolný R, Včelák J, Veselková T, Štorkánová G, Mušálková D, Hřebíček M, Ledvinová J, Magner M, Zeman J, Pešková K, Dvořáková L.: X-Chromosome Inactivation Analysis in Different Cell Types and Induced Pluripotent Stem Cells Elucidates the Disease Mechanism in a Rare Case of Mucopolysaccharidosis Type II in a Female. Folia Biol (Praha), 2016; **62**(2): p. 82-9. **IF 0.939**

Original Article

X-Chromosome Inactivation Analysis in Different Cell Types and Induced Pluripotent Stem Cells Elucidates the Disease Mechanism in a Rare Case of Mucopolysaccharidosis Type II in a Female

(mucopolysaccharidosis II / Hunter syndrome / iduronate sulphatase deficiency / X-chromosome inactivation / induced pluripotent stem cells)

M. ŘEBOUN[1], J. RYBOVÁ[1], R. DOBROVOLNÝ[1], J. VČELÁK[3], T. VESELKOVÁ[1], G. ŠTORKÁNOVÁ[1], D. MUŠÁLKOVÁ[1], M. HŘEBÍČEK[1], J. LEDVINOVÁ[1], M. MAGNER[2], J. ZEMAN[2], K. PEŠKOVÁ[1], L. DVOŘÁKOVÁ[1]

[1]Institute of Inherited Metabolic Disorders, [2]Department of Paediatrics and Adolescent Medicine, First Faculty of Medicine, Charles University in Prague and General University Hospital in Prague, Czech Republic
[3]Institute of Endocrinology, Prague, Czech Republic

Abstract. Mucopolysaccharidosis type II (MPS II) is an X-linked lysosomal storage disorder resulting from deficiency of iduronate-2-sulphatase activity. The disease manifests almost exclusively in males; only 16 symptomatic heterozygote girls have been reported so far. We describe the results of X-chromosome inactivation analysis in a 5-year-old girl with clinically severe disease and heterozygous mutation p.Arg468Gln in the *IDS* gene. X inactivation analysed at three X-chromosome loci showed extreme skewing (96/4 to 99/1) in two patient's cell types. This finding correlated with exclusive expression of the mutated allele. Induced pluripotent stem cells (iPSC) generated from the patient's peripheral blood demonstrated characteristic pluripotency markers, deficiency of enzyme activity, and mutation in the *IDS* gene. These cells were capable of differentiation into other cell types (cardiomyocytes, neurons). In MPS II iPSC clones, the X inactivation ratio remained highly skewed in culture conditions that led to partial X inactivation reset in Fabry disease iPSC clones. Our data, in accordance with the literature, suggest that extremely skewed X inactivation favouring the mutated allele is a crucial condition for manifestation of MPS II in females. This suggests that the X inactivation status and enzyme activity have a prognostic value and should be used to evaluate MPS II in females. For the first time, we show generation of iPSC from a symptomatic MPS II female patient that can serve as a cellular model for further research of the pathogenesis and treatment of this disease.

Received December 22, 2015. Accepted February 16, 2016.

This study was supported by the Ministry of Health, Czech Republic (IGA MZ CR NT14015-3/2013, MZ CR – RVO VFN 64165, MZ CR – RVO EÚ, 00023761) and by project reg. No. CZ.2.16/3.1.00/24012 from OP Prague Competitiveness.

Corresponding author: Lenka Dvořáková, Institute of Inherited Metabolic Disorders, Laboratory of DNA Diagnostics, bldg E1a, Ke Karlovu 455/2, 128 08 Prague 2, Czech Republic. Phone: (+ 420) 224 967 701; Fax: (+420) 224 967 168; e-mail: lenka.dvorakova@lf1.cuni.cz

Abbreviations: DMB – dimethylmethylene blue, DMSO – dimethyl sulphoxide, ERT – enzyme replacement therapy, FBS – foetal bovine serum, IDS – iduronate-2-sulphatase, iPSC – induced pluripotent stem cells, LIF – leukaemia inhibitory factor, MPS II – mucopolysaccharidosis type II, PBMC – peripheral blood mononuclear cells, SNP – single-nucleotide polymorphism, XCI – X-chromosome inactivation.

Introduction

Mucopolysaccharidosis II (Hunter syndrome, MPS II, OMIM 309900) is an X-linked lysosomal storage disorder caused by deficiency of iduronate-2-sulphatase activity (IDS, EC 3.1.6.13). Iduronate-2-sulphatase encoded by the *IDS* gene (Xq27-q28) catalyses the first step in the sequential degradation of heparan sulphate and dermatan sulphate, and its deficiency leads to the lysosomal accumulation of these glycosaminoglycans (Neufeld and Muenzer, 2001).

Children with MPS II have a normal appearance at birth and the disease manifests usually in late infancy or toddler age. The signs and symptoms include coarse facial features, short stature with joint stiffness, dysostosis multiplex, hepatosplenomegaly, and cognitive decline. The prognosis depends on the severity of the disease,

and is poor especially in children with severe form associated with death in the second decade of life (Neufeld and Muenzer, 2001).

Enzyme replacement therapy improves the visceral disease; however, it has no effect on the CNS. The first study on intrathecal idursulfase-IT in children has been published recently (Muenzer et al., 2016) and lentiviral isogeneic haematopoietic stem cell gene therapy was described as a promising approach for correction of neuronal manifestation in MPS II mice by ameliorating lysosomal storage and autophagic dysfunction in the brain (Wakabayashi et al., 2015).

Recently, the possibility of using autologous induced pluripotent stem cells (iPSC) instead of haematopoietic stem cells for cell-based therapy received a great deal of attention. In female heterozygotes with X-linked diseases, individual cells are either functionally normal or deficient based on the origin of inactivated X chromosome (mutant or normal), and the X-chromosome inactivation (XCI) remains conserved in daughter cells. Selected iPSC clones or differentiated cells with favourable XCI skewing could possibly serve as suitable material for cell therapy without the need for gene manipulations (Bhatnagar et al., 2014).

The prevalence of MPS II is estimated to be 0.43–1.09 per 100,000 live births in five different countries (Poupetova et al., 2010). The vast majority of MPS II patients are males, while only 16 symptomatic MPS II female patients have been reported in the literature so far.

Three of these affected females had structural abnormality of the X chromosome impairing *IDS* expression of the wild-type allele, while two others had both *IDS* alleles defective. In the remaining 11 patients, the cause of MPS II manifestation was the presence of one mutated *IDS* allele in combination with highly skewed XCI leaving only the mutated allele active (Jurecka et al., 2012; Pina-Aguilar et al., 2013; Lonardo et al., 2014); other cases are reviewed in Tuschl et al. (2005) and Scarpa et al. (2011).

Here, we describe the first MPS II female patient in the Czech Republic. We show extremely skewed XCI favouring the mutated allele as the apparent epigenetic cause of the clinical manifestation. For the first time we demonstrate iPSC generated from the MPS II patient cells. This cellular model will serve for future research into the pathogenesis and treatment of MPS II.

Material and Methods

Ethics

The study was approved by the ethics committee of the General University Hospital in Prague (The Ethics Committee Approval number 41/12) and was conducted in agreement with institutional guidelines. Written informed consent was obtained from both adult study participants. On behalf of the patient, written informed consent was obtained from her parents.

Molecular analyses

Genomic DNA was extracted from whole blood and from the urinary sediment using a QIAamp DNA Blood Mini Kit (Qiagen, Valencia, CA). DNA from buccal swabs and total RNA were isolated using a QIAamp DNA Micro Kit (Qiagen) and a BiOstic Blood Total RNA Isolation Kit (MO BIO Laboratories, Inc., Carlsbad, CA), respectively. Reverse transcription of RNA to cDNA was performed using a High Capacity RNA to cDNA Kit (Applied Biosystems, Carlsbad, CA).

PCR and reverse transcription PCR (RT-PCR) products of the *IDS* (GenBank NC_000023.11, NM_000202.6) and *LAMP2* (NM_002294.2) genes were generated according to standard PCR protocols using primers shown in Table 1. The genotypes were analysed by Sanger sequencing using a Big Dye Terminator v3.1 Cycle Sequencing Kit and a 3500xL Genetic Analyzer (Applied Biosystems).

For amplicon-based deep sequencing, singleplex PCR and RT-PCR products were pooled and prepared under standard protocols using the NexteraXT kit and the MiSeq reagent kit (2×250), respectively. Paired-end sequence reads were generated using the MiSeq platform (Illumina, San Diego, CA). Sequencing data were demultiplexed and trimmed for low quality and duplicates using MiSeq reporter v.2.4. Secondary analysis of the cDNA data was performed using TopHat v2.0.13 (Kim

Table 1. Primer sequences used for PCR amplification

Gene		Fragment/ Exon	Sequence
IDS	cDNA	Fr. 4 U	TAATACGACTCACTATAG GGACCTTGTGGAACTTGTGT
		Fr. 4 L	TGAAACAGCTATGACCATG AAACGACCAGCTCTAACTCC
	gDNA	ex. 9a U	TAATACGACTCACTATAG TCCTGCTATTTGATTGGATG
		ex. 9a L	TGAAACAGCTATGACCATG GTCTATGGTGCGTATGGAAT
		ex. 9b U	TAATACGACTCACTATAG CGATTCCGTGACTTGGA
		ex. 9b L	TGAAACAGCTATGACCATG ATGGGTAATCACAAAACGAC
LAMP2	cDNA	Fr.1 U	GGTCGGTGGTCATCAGTGCT
		Fr.1 L	ATTCTGATGGCCAAAAGTTCAT
	gDNA	ex.2 U	TAATACGACTCACTATAG TTTAGAGCTGGTTGAACTTC
		ex.2 L	TGAAACAGCTATGACCATG TCTAAAGGATAAAGTCAATTAAA

Upper (U) and lower (L) primers (excepting LAMP2 cDNA) contain a T7 and an RP sequence, respectively, at the 5′ end.

et al., 2013). The human hg19 genome sequence was used as a reference.

X-chromosome inactivation analysis

Two independent methods were used to determine the XCI pattern: a DNA methylation-based assay and a transcript expression analysis. The methylation status of polymorphic repeat regions was examined at two loci, *AR* and *CNKSR2*, using digestion with methylation-sensitive enzyme *Hpa*II, as described elsewhere (Racchi et al., 1998; Musalkova et al., 2015). The DNA of the patient's father was used as a male control.

The transcriptional assay was performed similarly as described previously (Mossner et al., 2013). The RT-PCR product containing the single-nucleotide polymorphism (SNP) was used for quantification of SNP allele frequencies, which reflected the XCI ratios. The *LAMP2* gene polymorphism c.156A>T (rs12097) was selected for the assay as *LAMP2* is subject to XCI (Cotton et al., 2013), and the patient is heterozygous for this polymorphism. Instead of pyrosequencing (Mossner et al., 2013), amplicon sequencing using the Illumina platform was applied. The same procedure was used for quantification of the wt/mutated allele in the *IDS* gene transcript.

Generation of iPSC lines

The iPSC lines were generated from mononuclear cells isolated with Histopaque (Sigma-Aldrich, St. Louis, MO) according to manufacturer's instructions from peripheral blood of the presented MPS II female patient. Isolated peripheral blood mononuclear cells (PBMC) were frozen in 10% dimethyl sulphoxide (DMSO) in inactivated foetal bovine serum (FBS, BenchMark™ Fetal Bovine Serum, Gemini Bio-Products, West Sacramento, CA) and kept in liquid nitrogen until further use. Thawed PBMCs were cultured in complete LGM medium (Lonza, Walkersville, MD) containing 0.4 µg/ml of purified no azide/low endotoxin NA/LE Mouse Anti-Human CD3 (BD Biosciences, San Jose, CA), 0.4 µg/ml of Mouse Anti-Human CD28 (BD Biosciences), and 50 ng/ml of interleukin 2 (IL2; Abbiotec, San Diego, CA) and were plated onto CD3-coated 6-well plates for five days. Reprogramming of the cells into iPSCs was performed using the CytoTune™-iPS 2.0 Sendai Reprogramming Kit (Invitrogen, Carlsbad, CA) according to manufacturer's instructions. In brief, the cells were transduced at an appropriate multiplicity of infection (MOI) with each of the three reprogramming vectors (KOS MOI = 5, hc-Myc MOI = 5, hKlf4 MOI = 3) in the complete LGM medium. The free virus was removed by replacing the medium on the second day. The cells were transferred onto the layer of feeder cells (irradiated mouse embryonic fibroblasts) in the presence of HES medium (KnockOut™ESC/iPSC Medium Kit) with 8 ng/ml basic fibroblast growth factor (bFGF; Life Technologies, New York, NY) on the 4th day after the transduction. The selected colonies were picked and placed in 12-well plates containing feeder cells and then passaged with Accutase (STEMCELL Technologies Inc., Vancouver, BC, Canada) and the StemPro EZPassage tool (Invitrogen, Carlsbad, CA, USA) until the creation of stable iPSC lines.

Expression of pluripotency markers in generated iPSC was confirmed by immunostaining as previously described (Lian et al., 2013). Primary antibodies used in this study were directed to Oct3/4 (Santa Cruz Biotechnology, Dallas, TX, cat# sc-5279), SSEA4 (Invitrogen, cat# 41-4000), anti-TRA-1-81 (Invitrogen, cat# 41-1100), Sox2 (Santa Cruz Biotechnology, cat# sc-365823), CD63 (Abcam, Cambridge, UK, cat# ab1318), heparan sulphate (Amsbio, Abingdon, UK, Cat# 370255-1) and Lin-28 (Proteintech Group, Chicago, IL, cat# 11724-1-AP). The cells were incubated with Alexa Fluor 488- and Alexa Fluor 568-conjugated secondary antibodies (Molecular Probes, Invitrogen) and the nuclei were counterstained with 4',6-diamidino-2-phenylindole (DAPI, Invitrogen).

Naïve iPSC lines were established by cultivation of generated iPSC in NHSM medium containing leukaemia inhibitory factor (LIF) and small molecule inhibition of ERK1/ERK2 and GSK3β signalling, which induce conversion of primed iPSC toward naïve pluripotency, as described previously (Gafni et al., 2013).

Determination of enzyme activities

Total leukocytes were isolated from the blood anticoagulated with EDTA within 24 h of drawing using the method described by Skoog and Beck (1956). The iPSC were re-plated onto Geltrex® (Life Technologies, Grand Island, NY)-coated 6-well plates and cultivated in mTeSR™1 medium (STEMCELL Technologies Inc.) for two passages for the removal of the feeder cells. The homogenates were prepared by sonication in water. The protein concentration was determined using the method described by Hartree (1972). Iduronate-2-sulphate sulphatase activity was assayed using fluorogenic substrate 4-methylumbelliferyl-α-L-iduronate-2-sulphate according to the method described by Voznyi et al. (2001).

Results

Clinical description

A 5-year-old girl was born in term as a first child of healthy, non-consanguineous Ukrainian parents. Postnatal adaptation and early development were uneventful. She used five words and started to walk at the age of 13 months. Snoring, hearing impairment and delayed speech were recognized at the age of two years. A mild improvement in hearing was observed with a hearing device; however, the speech problems persisted. Coarse facial features, gingival hyperplasia, mild hepatosplenomegaly, sternal protrusion, claw hands, lumbal hyperlordosis, large joint contractures and mild mental retardation were noted during the third year of life. At the age of 3.5 years, clinical and laboratory analyses revealed mild paleocerebellar symptoms, mild mitral regurgitation, and "dysostosis multiplex" on the X-ray survey.

Table 2. X-chromosome inactivation at three X-chromosome loci compared with a mutant alelle in the IDS gene

Sample	Locus			
	Methyl sensitive		Transcript analysis	
	AR (Xq12) %	*CNSKR2* (Xp22.12) %	*LAMP2* (Xq24) A:T %	*IDS* (Xq28) G:A %
Proband (leukocytes)	98:2[a]	99:1[a]	100:0[b]	0,5:99,5[b]
Proband (buccal swabs)	96:4	n.d.[c]	n.d.[c]	n.d.[c]
Mother (leukocytes)	n.i.[d]	70:30	n.d.[c]	n.d.[c]

[a] Maternal chromosome is preferentially inactivated, [b] transcript analysis using the amplicon-based deep sequencing: number of reads Q>30 *LAMP2* (c.156A>T, rs12097) A: 3910, T: 2. The A allele was inherited from the patient's father.
IDS (c.1403G>A) G: 18, A: 3668. Only the mutated allele is expressed. [c] not determined, [d] non-informative marker

No corneal clouding was present. Urinary excretion of heparan and dermatan sulphates were increased (60.5–65.7 g/mol creatinine; controls < 15.5). The IDS activity was markedly decreased in leukocytes (0.46 nmol/4 h/mg, control range: 28.1–70.4 nmol/4 h/mg) and serum (19 nmol/4 h/ml, control range: 167–475 nmol/4 h/ml). Heterozygous mutation c.1403G>A (p.Arg468Gln) was identified in the *IDS* gene. The girl is treated with enzyme replacement therapy, the glycosaminoglycan excretion decreased (19.5–22.5 g/mol creatinine), but she still has speech problems, delay of fine motor functions and a moderate delay of the gross motor development.

X-chromosome inactivation and mutation analysis in patient´s tissues

Examination of the methylation status at the *AR* locus (Xq12) showed extreme skewing in both blood leukocytes and buccal swabs; the maternal allele was almost completely inactivated. Complete inactivation of the maternal allele was also observed in *CNKSR2* and apparent homozygosity for the c.156A allele inherited from the patient's father was detected in the *LAMP2* transcript. Deep sequencing of the *IDS* gene transcript revealed exclusive expression of the mutated allele (Table 2).

As the maternal allele is completely inactivated and only the mutated *IDS* is expressed, it can be deduced that the patient inherited the mutated allele from her father. However, Sanger sequencing did not identify the mutation c.1403G>A in the patient's parents. To detect possible somatic mosaicism in the parental tissues, DNA isolated from three cell types (peripheral leukocytes, urinary sediment cells and buccal swabs) was subjected to amplicon-based deep sequencing. The number of reads corresponding to the mutated allele was below the detection limit (< 0.5%) when the total sequence depth was higher than 1300 in all analysed tissues. Thus, the somatic mosaicism was not demonstrated, while germline mosaicism could not be excluded as meiotic cells from the parents were not available for analysis.

Generation of iPSC lines

Two of the multiple generated patient's iPSC lines have been used for the study. The clones were positive for the characteristic pluripotency markers Oct3/4, SSEA4, anti-TRA-1-81, Lin28, and Sox2 (Fig. 1). The patient's iPSC lines also expressed slightly higher amounts of heparan sulphate (Fig. 2); however, the quantitative determination of GAGs in the cell lysate using dimethyl methylene blue (DMB) with spectrophotometric detection (Lopez-Marin et al., 2013) did not show significant differences. The IDS activities in two

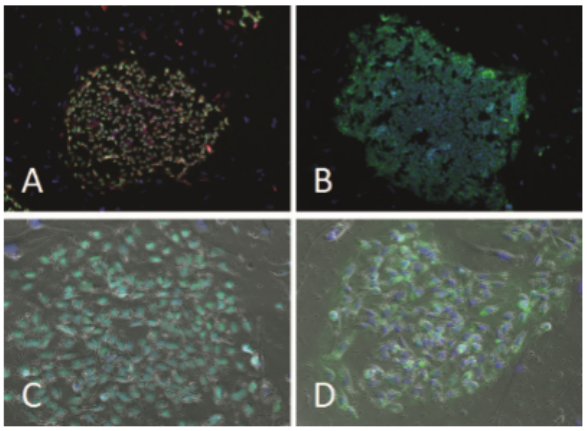

Fig 1. Characterization of iPSC colonies – pluripotency markers. **A:** Lin28 (red), Oct3/4 (green), DAPI (blue); **B:** SSEA4 (green), DAPI (blue); **C:** Sox2 (green), DAPI (blue) and **D:** anti-TRA-1-81 (green), DAPI (blue) in phase contrast image. A, B – 10× objective, C, D – 20× objective.

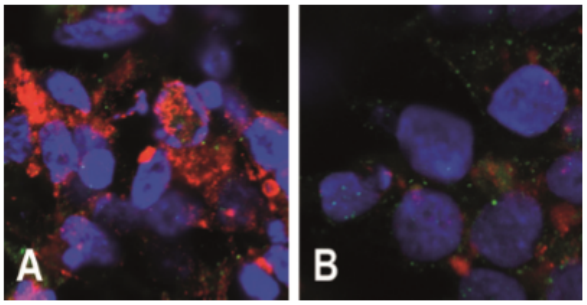

Fig 2. Detection of heparan sulphate in iPSC generated from an MPS II patient. Heparan sulphate (red), CD63 (green), DAPI (blue). **A:** MPS II patient; **B:** control; images were recorded with a laser scanning confocal microscope, 60× objective, NA 1.40

of the patient's iPSC clones were 1.49 and 2.32 nmol per mg of protein per hour, compared to 17.15 and 21.32 nmol/mg/h, respectively, in the controls. The potency to differentiate to cardiomyocytes and neuronal cells has been confirmed using previously published protocols (Stacpoole et al., 2011; Lian et al., 2013).

Analysis in two iPSC clones cultured in usual conditions showed the same XCI pattern with preferential inactivation of the maternal allele (98 : 2). Using cell culture conditions described to lead to the naïve state of iPSC with reset XCI did not result in a changed XCI ratio in the MPS II clones; however, in case of the Fabry disease heterozygote used as a control, the XCI ratio changed from 97 : 3 to 80 : 20 (Fig. 3).

Discussion

In this report we describe a 5-year-old girl with severe deficiency of IDS activity and clinical manifestation of the disease corresponding to the severe form of Hunter syndrome in boys. The disease in our patient is caused by the heterozygosity for the recurrent mutation p.Arg468Gln (Brusius-Facchin et al., 2014) in combination with highly skewed XCI resulting in exclusive expression of the mutated allele.

To reduce the risk of incorrect interpretation of the results due to chromosomal crossover or due to failure of the individual loci to correlate with XCI we performed XCI analysis using two independent methods at three X-chromosome loci. The results of methyl-sensitive methods (*AR*, *CNKSR2*) agreed well with the results of the transcription-based assay using the *LAMP2* gene polymorphism. Thus, unlike Swierczek et al. (2012), we did not observe any discrepancy among the used methods.

To date, two states of iPSC are known, referred to as primed and naïve, which differ mainly in XCI. Several attempts have been undertaken to generate a more naïve state (with two active X chromosomes in female cells) in established primed iPSC (with one inactive X chromosome) by different media formulation. In our study the XCI was analysed using the methyl-sensitive method (*AR*) in iPSC cultured in standard media and in naïve state-inducing media (Gafni et al., 2013). Cells derived from the MPS II patient did not show any change in the skewed XCI ratio in any culture conditions. There are three explanations for this finding: 1) the X chromosome remains inactive in the iPSC without going through the "reset" state when both X chromosomes in female cells are active, 2) the X chromosome is non-randomly inactivated after resetting XCI during iPSC reprogramming, or 3) a fraction of cells reached the stage of reprogramming in which both X chromosomes are active, but the used methyl-sensitive method is not able to detect these cells (Briggs and Reijo Pera, 2014). In any case, the iPSC derived from the MPS II patient differ from those derived from the Fabry disease heterozygote used as a control line, which responded to media change by partial change of the XCI ratio from 97 : 3 to 80 : 20.

Extreme skewing of XCI in favour of the mutated allele (> 95/5) is a common feature shared by symptomatic MPS II female patients (Scarpa et al., 2011). In accordance with this XCI status, symptomatic MPS II in females is associated with profound IDS deficiency comparable to affected hemizygous males, confirming the recessive nature of the disease. A similar strict correlation is not found in Fabry disease, another X-linked lysosomal storage disorder, where the overwhelming majority of heterozygotes have intermediate levels of the deficient enzyme and develop some symptoms of the disease, although later in life than the hemizygous males (Echevarria et al., 2016). According to the threshold model of Conzelman and Sandhoff, low levels of enzyme activity are compatible with normal levels of substrate degradation unless they cross a threshold, which, in lysosomal diseases, is usually lower than 10 % of the normal activity (Conzelmann and Sandhoff, 1983). It is important to note that in the tissues of heterozygotes of X-linked disorders, there are patches of deficient cells following the pattern of inactivation of the non-mutated chromosome. This illuminates the development of tissue pathology in Fabry heterozygotes, while carriers for autosomal recessive lysosomal diseases are free of it. The absence of symptoms in the majority of MPS II heterozygotes may be explained by the low threshold of the enzyme activity compatible with normal degradation of the substrate or by good uptake of the enzyme by the deficient cells from the surrounding cells. Notably, cultured fibroblasts from MPS II patients are able to cross-correct the IDS deficiency, unlike cultured skin fibroblasts from the Fabry patients (Fuller et al., 2015).

Our results and the review of the literature show that the clinical manifestation of MPS II in heterozygous females is associated with conditions leading to near monoallelic expression of the mutant allele and severe IDS deficiency, most often due to extremely skewed XCI. This suggests that girls with skewed XCI diagnosed postnatally might benefit from enzyme replacement therapy (ERT), which, if introduced early, may significantly improve further clinical course of the disease (Tylki-Szymanska et al., 2012; Tajima et al., 2013).

To our knowledge, we generated the first iPSC model from a symptomatic MPS II heterozygote and generally from any MPS II patient. These models are valuable for further research of MPS II pathogenesis and testing of therapeutic approaches in various cell types differentiated from iPSC clones and relevant to the disease. The iPSC lines from the presented case can also be used for general research of the mechanisms leading to extremely skewed XCI ratios, as the MPS II clones we have studied retained their XCI skewing under naïve state culture conditions in contrast with control clones. Hypothetically, the iPSC clones from heterozygotes of X-linked disorders with favourable XCI and thus functionally normal can serve as a source of autologous material (haematopoietic progenitors, neurons, cardiomyocytes, etc.) for cell-based therapy (Bhatnagar et al.,

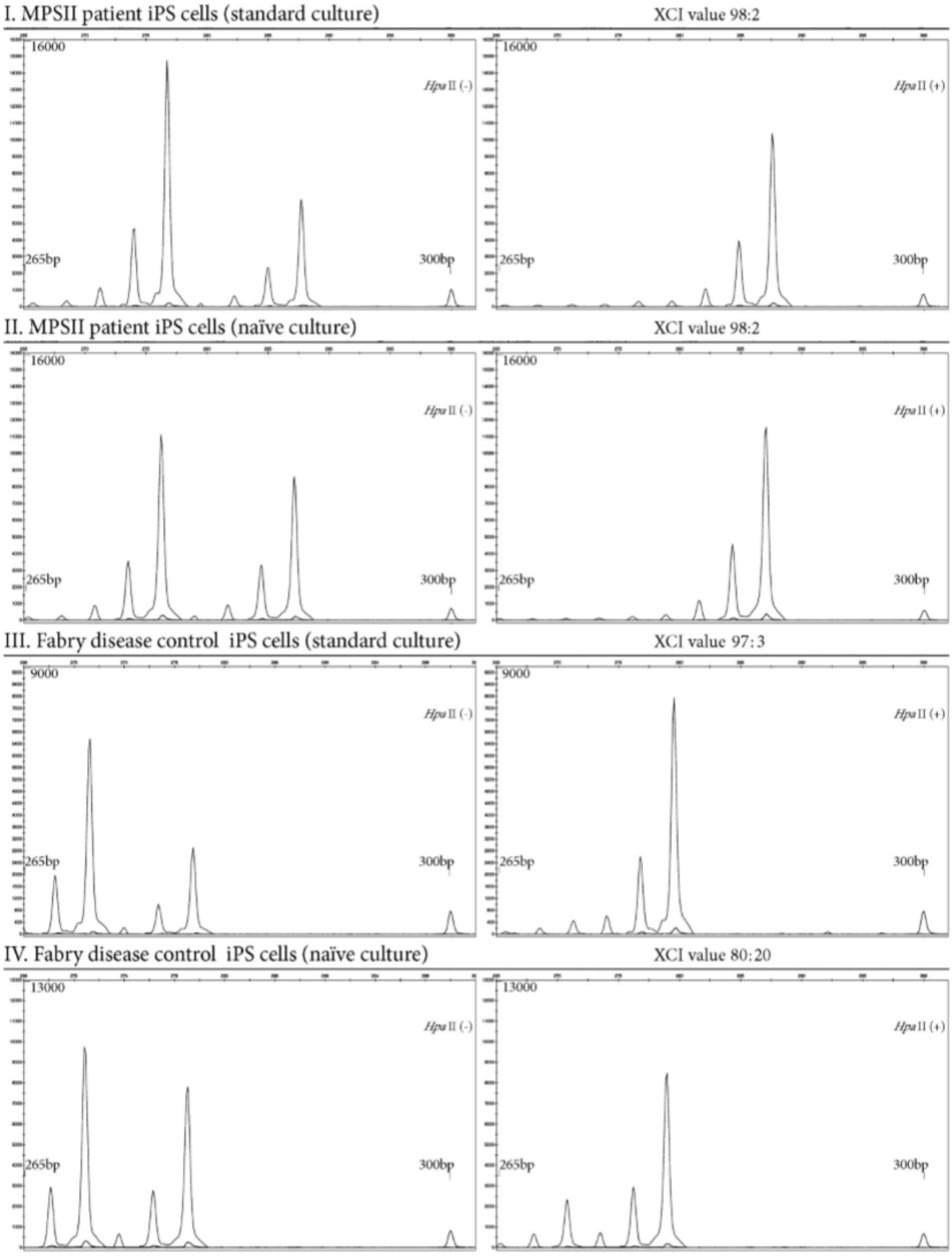

Fig 3. X-chromosome inactivation analysis in the patient's iPSC generated from the MPS II patient and a Fabry disease heterozygote serving as control. Standard and naïve culture conditions cells are compared. Methylation status analysis of the *AR* alleles before (*Hpa*II-) and after (*Hpa*II+) digestion is shown. The 300-bp peak belongs to the GeneScan 500 ROX size standard. The analysis was conducted using GeneMapper software (Applied Biosystems).

2014). These types of therapies, however, will need to await development of safe therapeutic protocols.

Acknowledgements

The authors would like to acknowledge Helena Poupětová for enzyme analysis, Hana Vlášková for constructive discussion, and Michaela Hnízdová Boučková and Larisa Stolnaja for excellent laboratory work. The authors have no conflicts of interest to disclose.

References

Bhatnagar, S., Zhu, X., Ou, J., Lin, L., Chamberlain, L., Zhu, L. J., Wajapeyee, N., Green, M. R. (2014) Genetic and pharmacological reactivation of the mammalian inactive X chromosome. *Proc. Natl. Acad. Sci. USA* **111**, 12591-12598.

Briggs, S. F., Reijo Pera, R. A. (2014) X chromosome inactivation: recent advances and a look forward. *Curr. Opin. Genet. Dev.* **28**, 78-82.

Brusius-Facchin, A. C., Schwartz, I. V., Zimmer, C., Ribeiro, M. G., Acosta, A. X., Horovitz, D., Monlleo, I. L., Fontes, M. I., Fett-Conte, A., Sobrinho, R. P., Duarte, A. R., Boy, R., Mabe, P., Ascurra, M., de Michelena, M., Tylee, K. L., Besley, G. T., Garreton, M. C., Giugliani, R., Leistner-Segal, S. (2014) Mucopolysaccharidosis type II: identification of 30 novel mutations among Latin American patients. *Mol. Genet. Metab.* **111**, 133-138.

Conzelmann, E., Sandhoff, K. (1983) Partial enzyme deficiencies: residual activities and the development of neurological disorders. *Dev. Neurosci.* **6**, 58-71.

Cotton, A. M., Ge, B., Light, N., Adoue, V., Pastinen, T., Brown, C. J. (2013) Analysis of expressed SNPs identifies variable extents of expression from the human inactive X chromosome. *Genome Biol.* **14**, R122.

Echevarria, L., Benistan, K., Toussaint, A., Dubourg, O., Hagege, A. A., Eladari, D., Jabbour, F., Beldjord, C., De Mazancourt, P., Germain, D. P. (2016) X-chromosome inactivation in female patients with Fabry disease. *Clin. Genet.* **89**, 44-54.

Fuller, M., Mellett, N., Hein, L. K., Brooks, D. A., Meikle, P. J. (2015) Absence of α-galactosidase cross-correction in Fabry heterozygote cultured skin fibroblasts. *Mol. Genet. Metab.* **114**, 268-273.

Gafni, O., Weinberger, L., Mansour, A. A., Manor, Y. S., Chomsky, E., Ben-Yosef, D., Kalma, Y., Viukov, S., Maza, I., Zviran, A., Rais, Y., Shipony, Z., Mukamel, Z., Krupalnik, V., Zerbib, M., Geula, S., Caspi, I., Schneir, D., Shwartz, T., Gilad, S., Amann-Zalcenstein, D., Benjamin, S., Amit, I., Tanay, A., Massarwa, R., Novershtern, N., Hanna, J. H. (2013) Derivation of novel human ground state naive pluripotent stem cells. *Nature* **504**, 282-286.

Hartree, E. F. (1972) Determination of protein: a modification of the Lowry method that gives a linear photometric response. *Anal. Biochem.* **48**, 422-427.

Jurecka, A., Krumina, Z., Zuber, Z., Rozdzynska-Swiatkowska, A., Kloska, A., Czartoryska, B., Tylki-Szymanska, A. (2012) Mucopolysaccharidosis type II in females and response to enzyme replacement therapy. *Am. J. Med. Genet. A* **158A**, 450-454.

Kim, D., Pertea, G., Trapnell, C., Pimentel, H., Kelley, R., Salzberg, S. L. (2013) TopHat2: accurate alignment of transcriptomes in the presence of insertions, deletions and gene fusions. *Genome Biol.* **14**, R36.

Lian, X., Zhang, J., Azarin, S. M., Zhu, K., Hazeltine, L. B., Bao, X., Hsiao, C., Kamp, T. J., Palecek, S. P. (2013) Directed cardiomyocyte differentiation from human pluripotent stem cells by modulating Wnt/β-catenin signaling under fully defined conditions. *Nat. Protoc.* **8**, 162-175.

Lonardo, F., Di Natale, P., Lualdi, S., Acquaviva, F., Cuoco, C., Scarano, F., Maioli, M., Pavone, L. M., Di Gregorio, G.,Filocamo,M.,Scarano,G.(2014)Mucopolysaccharidosis type II in a female patient with a reciprocal X;9 translocation and skewed X chromosome inactivation. *Am. J. Med. Genet. A* **164A**, 2627-2632.

Lopez-Marin, L., Gutierrez-Solana, L. G., Azuara, L. A., de Las Heras, R. S., Rodriguez, A. D., Extremera, V. C. (2013) Detection by urinary GAG testing of mucopolysaccharidosis type II in an at-risk Spanish population. *JIMD Rep.* **10**, 61-68.

Mossner, M., Nolte, F., Hutter, G., Reins, J., Klaumunzer, M., Nowak, V., Oblander, J., Ackermann, K., Will, S., Rohl, H., Neumann, U., Neumann, M., Hopfer, O., Baldus, C. D., Hofmann, W. K., Nowak, D. (2013) Skewed X-inactivation patterns in ageing healthy and myelodysplastic haematopoiesis determined by a pyrosequencing based transcriptional clonality assay. *J. Med. Genet.* **50**, 108-117.

Muenzer, J., Hendriksz, C. J., Fan, Z., Vijayaraghavan, S., Perry, V., Santra, S., Solanki, G. A., Mascelli, M. A., Pan, L., Wang, N., Sciarappa, K., Barbier, A. J. (2016) A phase I/II study of intrathecal idursulfase-IT in children with severe mucopolysaccharidosis II. *Genet. Med.* **18**, 73-81.

Musalkova, D., Minks, J., Storkanova, G., Dvorakova, L., Hrebicek, M. (2015) Identification of novel informative loci for DNA-based X-inactivation analysis. *Blood Cells Mol. Dis.* **54**, 210-216.

Neufeld, E. F., Muenzer, J. (2001) The mucopolysaccharidoses. In: *The Metabolic and Molecular Bases of Inherited Disease,* eds. Scriver, C. R., Beaudet, A. L., Sly, W. S., Valle, D., pp. 3421-3452, McGraw-Hill Co., New York

Pina-Aguilar, R. E., Zaragoza-Arevalo, G. R., Rau, I., Gal, A., Alcantara-Ortigoza, M. A., Lopez-Martinez, M. S., Santillan-Hernandez, Y. (2013) Mucopolysaccharidosis type II in a female carrying a heterozygous stop mutation of the iduronate-2-sulfatase gene and showing a skewed X chromosome inactivation. *Eur. J. Med. Genet.* **56**, 159-162.

Poupetova, H., Ledvinova, J., Berna, L., Dvorakova, L., Kozich, V., Elleder, M. (2010) The birth prevalence of lysosomal storage disorders in the Czech Republic: comparison with data in different populations. *J. Inherit. Metab. Dis.* **33**, 387-396.

Racchi, O., Mangerini, R., Rapezzi, D., Rolfo, M., Gaetani, G. F., Ferraris, A. M. (1998) X chromosome inactivation patterns in normal females. *Blood Cells Mol. Dis.* **24**, 439-447.

Scarpa, M., Almassy, Z., Beck, M., Bodamer, O., Bruce, I. A., De Meirleir, L., Guffon, N., Guillen-Navarro, E., Hensman, P., Jones, S., Kamin, W., Kampmann, C., Lampe, C., Lavery, C. A., Teles, E. L., Link, B., Lund, A. M., Malm, G., Pitz, S., Rothera, M., Stewart, C., Tylki-Szymanska, A., van der Ploeg, A., Walker, R., Zeman, J., Wraith, J. E.,

Publications in impacted journals related to the topic of this Ph.D. thesis

Supplementary publication E

Rybová J, Ledvinová J, Sikora J, Kuchař L, Dobrovolný R.: Neural cells generated from human induced pluripotent stem cells as a model of CNS involvement in mucopolysaccharidosis type II. J Inherit Metab Dis, 2018 Mar; **41**(2): p. 221-229. **IF 3.970**

J Inherit Metab Dis
https://doi.org/10.1007/s10545-017-0108-5

ORIGINAL ARTICLE

Neural cells generated from human induced pluripotent stem cells as a model of CNS involvement in mucopolysaccharidosis type II

Jitka Rybová[1] · Jana Ledvinová[1] · Jakub Sikora[1,2] · Ladislav Kuchař[1] · Robert Dobrovolný[1]

Received: 31 July 2017 / Revised: 19 October 2017 / Accepted: 22 October 2017

Abstract Mucopolysaccharidosis type II (MPSII) is a rare X-linked lysosomal storage disorder caused by mutations in the iduronate-2-sulfatase (IDS) gene (*IDS, Xq28*). MPSII is characterized by skeletal deformities, hearing loss, airway obstruction, hepatosplenomegaly, cardiac valvular disease, and progressive neurological impairment. At the cellular level, IDS deficiency leads to lysosomal storage of glycosaminoglycans (GAGs), dominated by accumulation of dermatan and heparan sulfates. Human induced pluripotent stem cells (iPSC) represent an alternative system that complements the available MPSII murine model. Herein we report on the reprogramming of peripheral white blood cells from male and female MPSII patients into iPSC using a non-integrating protocol based on the Sendai virus vector system. We differentiated the iPSC lines into IDS deficient and GAG accumulating β-Tubulin III$^+$ neurons, GFAP$^+$ astrocytes, and CNPase$^+$ oligodendrocytes. The lysosomal system in these cells displayed structural abnormalities reminiscent of those previously found in patient tissues and murine IDS deficient neuronal stem cells. Furthermore, quantitative determination of GAGs revealed a moderate increase in GAG levels in IDS deficient neurons and glia. We also tested the effects of recombinant IDS and found that the exogenous enzyme was internalized from the culture media and partially decreased the intracellular GAG levels in iPSC-derived neural cells; however, it failed to completely prevent accumulation of GAGs. In summary, we demonstrate that this human iPSC based model expresses the cellular and biochemical features of MPSII, and thus represents a useful experimental tool for further pathogenesis studies as well as therapy development and testing.

Abbreviations

ALP	alkaline phosphatase
BBB	blood brain barrier
bFGF	basic fibroblast growth factor
βTubIII	β-Tubulin III
CNPase	2′,3′-cyclic-nucleotide 3′-phosphodiesterase
EB	embryoid bodies
ERT	enzyme replacement therapy
FGF-8	fibroblast growth factor 8
GAG	glycosaminoglycans
GFAP	glial fibrillary acidic protein
HS	heparan sulfate
IDS	iduronate-2-sulfatase
iPSC	induced pluripotent stem cells
LAMP1	lysosomal-associated membrane protein 1
MAP2	microtubule-associated protein 2
MPS	mucopolysaccharidoses
NPC	neural progenitor cells
PBMC	peripheral blood mononuclear cells
P/S	Penicillin-Streptomycin
TH	tyrosine hydroxylase
XCI	X-chromosome inactivation
CDM	complete differentiation medium

Communicated by: Jaak Jaeken

Electronic supplementary material The online version of this article (https://doi.org/10.1007/s10545-017-0108-5) contains supplementary material, which is available to authorized users.

✉ Robert Dobrovolný
robert.dobrovolny@lf1.cuni.cz

[1] Rare Diseases Research Unit, Department of Pediatrics and Adolescent Medicine, Charles University, Ke Karlovu 2, Prague 12808, Czech Republic

[2] Institute of Pathology, First Faculty of Medicine, Charles University and General University Hospital, Prague, Czech Republic

Published online: 22 November 2017

Introduction

Mucopolysaccharidoses (MPSs) are caused by deficient activities of enzymes that catalyze lysosomal degradation of glycosaminoglycans (GAGs) (Neufeld and Muenzer 2001). There are seven different MPS phenotypes caused by 11 enzyme deficiencies all leading to lysosomal accumulation of GAGs and to cell, tissue, and organ dysfunction. Mucopolysaccharidosis type II (MPSII, OMIM 309900) is an X-linked disorder that presents along the entire phenotypic spectrum between two extreme clinical forms — severe and mild. Patients with severe MPSII form express coarse facial features, short stature, skeletal deformities, and cognitive defects. Neurological symptoms develop as the disease progresses and patients usually succumb by the age of 10–15 years. The mild form of MPSII is characterized by hearing impairment, carpal tunnel syndrome, joint stiffness, minimally impaired cognitive functions, and a survival into adulthood. In the peripheral and central nervous system of MPS II patients, GAG storage takes the form of vacuolar inclusion bodies with finely granular contents. Gangliosides are thought to accumulate secondarily to GAGs and form zebra- and/or granulomembranous bodies (Meier et al 1979; Wiesmann et al 1980; Neufeld and Muenzer 2001).

A MPSII diagnosis is based on clinical evaluation, identification of abnormal urine levels of GAGs, detection of the enzymatic IDS deficiency, and identification of the disease-causing mutation in the iduronate-2-sulphatase (*IDS*) gene.

Enzyme replacement therapy (ERT) has been shown to improve many of the visceral signs and symptoms of MPSII and decrease urinary levels of GAGs (Wraith et al 2008; Okuyama et al 2010; Muenzer et al 2011; Jones et al 2013). Nevertheless, the effects of ERT on the central nervous system (CNS) and neurological impairment are limited because very little of the recombinant protein crosses the blood brain barrier (BBB) (Tanaka et al 2012; Patel et al 2014).

The murine knock-out model (*Ids*-KO) phenotypically replicates the human MPSII disease (Muenzer et al 2002) and was repeatedly used to test experimental therapies (Cardone et al 2006; Polito and Cosma 2009; Polito et al 2010). The neuropathological phenotype is readily detectable in 2-4 months-old *Ids*-KO mice, is progressive and comprises wide-spread intra-neuronal lysosomal storage and neurodegeneration, aberrant ubiquitin and alpha-synuclein expression, astrogliosis and abnormalities in the morphology and number of CD68+ microglial/macrophages (Cardone et al 2006; Polito and Cosma 2009; Polito et al 2010; Motas et al 2016). Importantly, studies in the neural stem cells derived from the *Ids*-KO mice suggested impaired neurogenesis and glial-mediated neuronal demise (Fusar Poli et al 2013).

Despite its substantial utility, alternative use of human cell/tissue cultures may help overcome some of the species-specific limitations of the available rodent model. However, for a long time cell culture-based approaches remained restricted by the cell types accessible for collection and cultivation. Fortunately, human induced pluripotent stem cells (iPSC) technology (Takahashi and Yamanaka 2006) allows for selective generation of cell types specifically affected in individual disease conditions. As such, iPSCs are particularly useful for studies focused on neurological/neuronal phenotypes including lysosomal storage diseases (Meng et al 2010).

Herein we report a reprogramming of peripheral white blood cells of MPSII patients into iPSC and their differentiation into neural lineages. We then used these differentiated neuronal and glial cells to explore MPSII neural pathology and evaluate the effects of ERT. Overall, we show that this novel human-derived iPSC model could be a useful tool for studies of MPSII pathogenesis as well as therapy development.

Materials and methods

Patients

iPSC lineages were derived from one male (IDS_$\mathbf{X}^{\mathbf{mut}}$/Y) and one heterozygous female MPSII (IDS_$\mathbf{X}^{\mathbf{mut}}$/X) patient. Detailed clinical description and laboratory results of the patients are available in Supplemental Materials and Methods.

Reprogramming of peripheral blood mononuclear cells (PBMC) into iPSC

Isolated PBMC of both MPSII patients and healthy controls were reprogrammed into iPSC using a CytoTune™-iPS 2.0 kit (Life Technologies, Carlsbad, CA, USA) according to the manufacturer's instructions. The kit uses the Sendai virus for transfection of cells. Pluripotency was confirmed using immunofluorescence labeling of the cells with primary antibodies against OCT3/4, SSEA4, TRA-1-81, and LIN28. The cells were also histochemically tested for expression of alkaline phosphatase.

iPSC differentiation into neurons, astrocytes, and oligodendrocytes

iPSC were differentiated into neuronal and glial cells using the modified protocols of Stacpoole et al (2011) and All et al (2015). The neurospheres of neural progenitor cells (NPC) were frozen and cryo-sectioned according to (Gomes et al 2010). Differentiation into neurons, astrocytes, and oligodendrocytes was detected using immunostaining with primary antibodies against SOX1, nestin, β-tubulin III (βTubIII), MAP2, vimentin, synapsin I, tyrosine hydroxylase (TH), glial fibrillary acidic protein (GFAP), and 2′,3′-cyclic-nucleotide 3′-phosphodiesterase (CNPase). Antibodies targeting

lysosomal-associated membrane protein 1 (LAMP1) and cathepsin D (CatD) were used to identify lysosomes in the terminally differentiated cells. Anti-heparan sulfate (HS) was used to detect the dominant accumulated substrate.

Determination of IDS activity

Total leukocytes were isolated from peripheral EDTA blood within 24 h of collection using the method described by Skoog and Beck (1956). Water homogenates of leukocytes were prepared by indirect sonication (3 × 10 seconds) in an ice bath. Protein concentrations were determined using the method developed by Hartree (1972). IDS activity was assayed using a fluorogenic substrate (4-methylumbelliferyl-α-L-iduronate-2-sulfate) as described by Voznyi et al (2001).

To determine IDS activity in iPSC lines, the cells were plated on Geltrex® coated 6-well plates (Life Technologies, New York, USA) with two passages in mTeSR™1 medium (STEMCELL Technologies, Vancouver, Canada) to eliminate feeder cells prior to analyses. iPSC were harvested with Accutase (Life Technologies, New York, USA) and processed identically to leukocytes.

Loading of recombinant IDS into neural progenitor cells

Recombinant enzyme (Elaprase® (idursulfase), Shire Human Genetic Therapies, Inc., Lexington, MA, USA) supplemented the differentiation media, at a final concentration of 1 μg/ml, from the stage of NPC for 10 weeks.

Uptake of the recombinant enzyme was also studied in spontaneously differentiated iPSC. The recombinant enzyme in the complete DMEM/F12 medium with 10% FBS and Penicillin-Streptomycin (P/S) was used to grow iPSC in Geltrex-coated 6-well plates for 3 weeks. Control cultures without the recombinant IDS were prepared in parallel.

Light and electron microscopy

Imaging of the samples was performed using a Nikon Ti90 fluorescent microscope (Nikon, Tokyo, Japan) equipped with 10× Plan Fluor Ph1/0.30, 20× S Plan Fluor Ph1/0.45, 40× S Plan Fluor Ph2/0.60, 60× S Plan Fluor Ph2/0.70 objectives and a DS-Qi1Mc camera. The images were processed in NIS-elements software (Nikon, Tokyo, Japan).

For electron microscopy, neural and glial cells were cultivated for 6 weeks on cover slips pre-coated with Geltrex. Cells on the cover slips were fixed with 3% glutaraldehyde, dehydrated in an ethanol series, and mounted in Durcupan Epon. The tissue sections were observed and images were taken using a JEOL 1400+ (JEOL, Tokyo, Japan) transmission electron microscope equipped with an Olympus Veleta CCD camera and Radius software.

Photometric determination of GAG levels

Cell homogenates in water were prepared by sonication (3 × 10 seconds on ice) in a Cup horn sonifier 450 (Branson Ultrasonics Corporation, Danbury, Connecticut, USA). Total protein concentration was determined using Roti-Quant reagent (Carl Roth GmbH + Co. KG, Karlsruhe, Germany). The GAG assay was performed using 96-well plates with 5 μg of total protein per well. The dimethylmethylene blue assay followed a protocol previously published by de Jong et al (1992). Chondroitin-6-sulfate served as a standard. Absorbance was measured at 520 nm using a multi-mode microplate reader (Synergy2, BioTek, VT, USA). The concentration of GAGs was expressed as μg of GAGs per μg of total protein.

For additional information, see Table S1 and Supplemental Materials and Methods.

Results

MPSII iPSC are IDS deficient and can be differentiated into neurons, astrocytes, and oligodendrocytes

Activated PBMCs isolated from the peripheral blood of MPSII patients and two healthy (control) individuals were reprogrammed using non-integrating Sendai virus vectors expressing the reprogramming factors (Oct3/4, Sox2, Klf4, and c-Myc). iPSC colonies typically started forming nine days after viral infection (Fig. S1A-D). Approximately 4–6 colonies were picked from each patient and control cultures and passaged until disappearance of the non-replicating Sendai virus. After 3–5 passages, the iPSC showed a morphology similar to embryonic stem cells (Fig. S1D) and expressed the pluripotency markers OCT3/4, LIN28, SSEA4, TRA-1-81, and ALP (Fig. S1E-H). The X-chromosome inactivation (XCI) ratio was almost completely skewed leaving the mutant allele active in all isolated iPSC IDS_$\mathbf{X^{mut}}$/X clones.

Identical to results in patient leukocytes (Supplemental Materials and Methods), IDS activity in patient iPSC was either absent (IDS_$\mathbf{X^{mut}}$/Y cells (0.01 and 0.07 nmol/4 h/mg, Fig. S1) or low (IDS_$\mathbf{X^{mut}}$/X: 5.94 and 9.28 nmol/4 h/mg, control range: 68.6–85.3 nmol/4 h/mg).

iPSC lines were differentiated to NPC, neuronal, and glial cells. The differentiation protocols were initiated by generating a suspension of iPSCs to allow formation of multicellular iPSC aggregates (EBs), which later transformed into neurospheres (Fig. 1a, b). After 2 weeks in complete differentiation medium (CDM), neurospheres were positive for the NPC markers Nestin and SOX1 (Fig. 1c, d).

The capacity to form EBs was markedly different between cell lines from MPSII patients and healthy controls. Control iPSC spontaneously formed compact, spherically shaped EBs

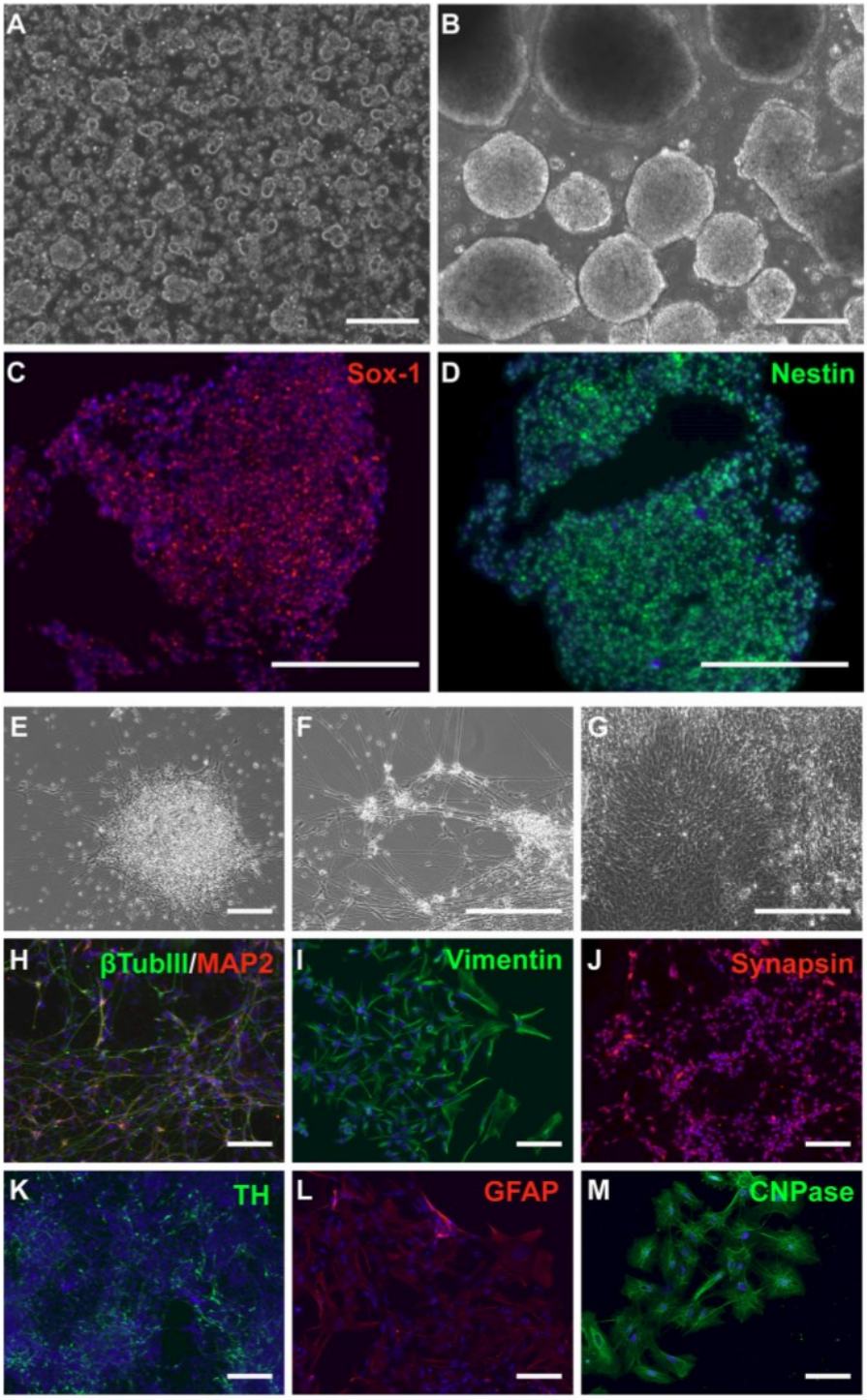

after plating a single cell suspension onto ultra-low attachment plates. Control EBs also remained spherical even after dissection into smaller pieces and could be passaged every 5–7 days for up to 3 months. However, IDS_$\mathbf{X}^{\mathbf{mut}}$/Y iPSC did not spontaneously form EBs under the same conditions as controls. To facilitate formation, we used AggreWell™800 plates (STEMCELL Technologies). Moreover, IDS_$\mathbf{X}^{\mathbf{mut}}$/Y EBs also required longer times (≈ 12–15 days) to become compact

◀ **Fig. 1** Characterization of iPSC-derived neural cells. Aggregation of single cell suspension of iPSC was observed one day after neural induction (**a**) and round, different sized spheres could be detected after 7 days of induction (**b**). Detection of neural progenitor marker SOX1 (**c**) and Nestin (**d**) in controls' and patients' EBs after 14 days of differentiation. Neuronal processes emanating from the neurospheres (**e**, **f**) and neural rosette formation (**g**) were observed after transferring the neurospheres to Geltrex-coated plates after 28 days of differentiation in the presence of a medium with GDNF and BDNF. βTubIII$^+$ (H), MAP2$^+$ (**h**) and vimentin$^+$ (**i**), TH$^+$ (**j**), and synapsin$^+$ neurons (**k**) were observed regardless of addition of RA or FGF-8. We were also able to detect the presence of GFAP$^+$ astrocytes (**l**) and CNPase$^+$ oligodendrocytes (**m**) in the cell culture after 6 weeks of differentiation. Nuclei were counterstained with DAPI (blue signal) in C, D, and H-M. Scale bars: 200 μm for all images

compared to control EBs. Formation of IDS_$\mathbf{X^{mut}}$/X EBs was initially similar to that of healthy control cells but after ≈ 6 weeks the yields decreased similarly to IDS_$\mathbf{X^{mut}}$/Y. For both IDS_$\mathbf{X^{mut}}$/Y and IDS_$\mathbf{X^{mut}}$/X, the quality of their EBs was also lower (i.e., non-spherical, non-compact) compared to controls.

To terminally differentiate neurospheres, EBs were cultured for an additional 2 weeks in CDM supplemented with retinoic acid. After adhesion and cultivation in the terminal differentiation medium for an additional 2–8 weeks, we found a heterogenous mixture of neural cells and the formation of neural rosettes (Fig. 1e–g). Immunofluorescence analyses confirmed the presence of vimentin$^+$, β-TubIII$^+$, and MAP2$^+$ neurons. Among those, we found synapsin$^+$ and TH$^+$ cells potentially indicative of spinal motor or dopaminergic neurons (Fig. 1h–k). GFAP$^+$ astrocytes and CNPase$^+$ oligodendrocytes, both of which can be distinguished from neurons by their larger nuclei (Fig. 1l, m), were present in the cultures as well.

MPSII neural cells display lysosomal abnormalities

To determine the impacts of IDS deficiency on the lysosomal compartment of the neuronal and glial cells, lysosomal membrane marker LAMP1 and lysosomal luminal marker CatD were assayed using immuno-cytofluorescence after 6 weeks of terminal differentiation. The augmented lysosomal compartment was observed in the perinuclear region of GFAP$^+$ astrocytes, CNPase$^+$ oligodendrocytes, and occasionally βTubIII$^+$ neurons of MPSII patients (Fig. 2 bottom row).

Neuronal and glial cells could be repeatedly passaged. However, we observed a decrease in number of βTubIII$^+$ cells in contrast with glial cells as well as a reduced ability to organize into regular rosette-like structures after re-seeding the cell mixture on Geltrex-coated plates.

Morphology and sub-cellular changes of the adherent neural cells were evaluated by electron microscopy after 8 weeks of differentiation on glass slides. Contrary to the heterogenous cellular population evaluated by immuno-cytofluorescence, cells with larger glia-like nuclei prevailed, suggesting relative fragility of neuronal precursors for ultrastructural.

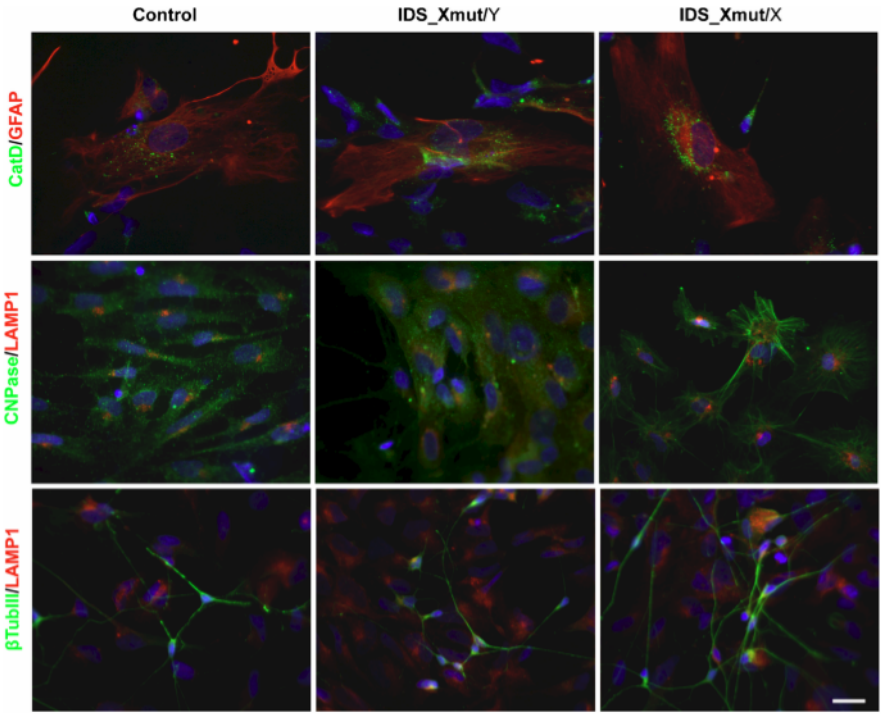

Fig. 2 Lysosomal accumulation in iPSC derived neural cells. Differentiated neural cells were cultured for six weeks and used for immunofluorescence analysis of GAG accumulation. Increased numbers of LAMP1$^+$ or CatD$^+$ lysosomes were detected mainly in GFAP positive astrocytes and CNPase positive oligodendrocytes and occasionally in βTubIII positive neurons in both hemizygous and heterozygous MPSII patients compared to control(s). Nuclei were counterstained with DAPI (blue signal). Scale bar: 20 μm for all images

Importantly, both control and patient neural cells formed complex neurosphere structures and developed thin cytoplasmic processes (Fig. 3a). In comparison to control cells (Fig. 3c), patient (Fig. 3a and b) neural cells contained numerous pleomorphic cytoplasmic vacuoles. Some of these vacuoles contained concentrically arranged lamellar material while others had a relatively electron lucent granular appearance.

GAG levels were increased in differentiated neural cells

GAG levels in the homogenates of patient iPSC and NPC cultures were not increased compared to healthy controls (Fig. 4a). However, GAG levels in terminally differentiated neuronal and glial cells, after 8 and 12 weeks of culture, were 1.5–4.3× (IDS_$\mathbf{X^{mut}}$/Y) and 1.7–4.6× (IDS_$\mathbf{X^{mut}}$/X) higher than in controls (Fig. 4a). Importantly, augmentation of GAG accumulation was more evident when comparing the 8 and 12 weeks' values in individual patients. The increase (*data not shown*) was 6.5× and 10.5× in IDS_$\mathbf{X^{mut}}$/Y and IDS_$\mathbf{X^{mut}}$/X, respectively.

Recombinant IDS reduced GAG accumulation in MPSII neural cells only partially

MPSII and healthy control neural cells were differentiated in media supplemented with recombinant IDS for 10 weeks after reaching the NPC stage, after which no increase in GAG was noticeable in patient cells. While the recombinant enzyme

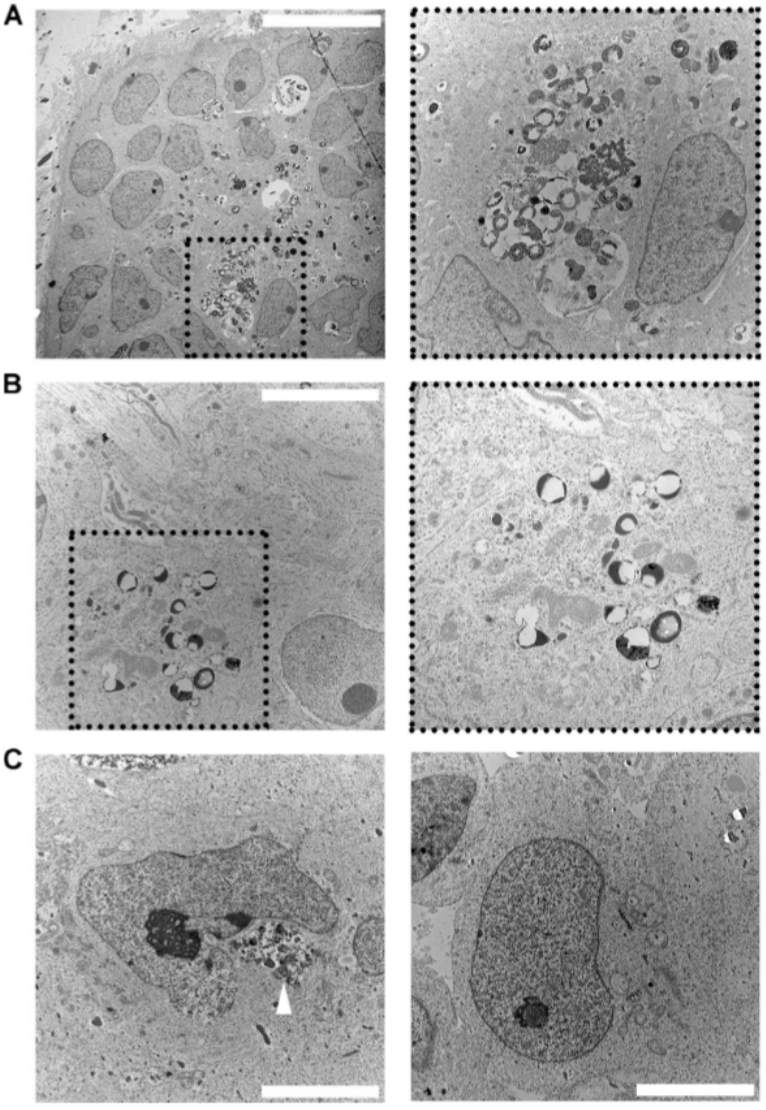

Fig. 3 Electron microscopy analysis of iPSC derived neural cells. Up to 8 weeks-old terminally differentiated neural cells were used for electron microscopy of morphology studies and potential lysosomal storage in patient cells. Similar features were observed in all studied patient samples. **a** edge of a neurosphere with emanating cellular processes and pleomorphic cytoplasmic vacuoles (IDS_$\mathbf{X^{mut}}$/X). **b** comparable cytoplasmic vacuoles in the male patient cells (IDS_$\mathbf{X^{mut}}$/Y). **c** some control cells contained autophagic-like vacuoles (white arrowhead). Scale bar: (**a**) 200 μm, (**b** and **c**) 5 μm

slightly reduced the levels of abnormally elevated GAGs in patient cells (Fig. 4a), the treatment did not prevent the increase of GAG levels in MPSII cultures, even when started before the onset of GAG accumulation. All samples cultured with the recombinant enzyme showed up to a tenfold increase in intracellular IDS activity compared to non-ERT controls (Fig. S2B. Cells differentiated spontaneously in FBS containing media had similar values as iPSC derived neural cultures (Fig. S2A).

HS accumulates preferentially in MPSII. Increased content was detected in a mixture of neural cells, of both patients. Interestingly, its co-localization with the lysosomal marker LAMP1 was not confirmed (Fig. 4b), since the HS signal was prominently observed in close vicinity to or at the cell surface.

Discussion

While CNS involvement is a hallmark of MPSII, its neuropathogenesis still remains relatively understudied. This discrepancy is partly due to the lack of representative patient tissue samples for studies comparing human (neuro)pathology with that of animal model(s). Somatic cell reprogramming technology circumvents these restrictions because patient-derived iPSC can be generated and differentiated into various cell types including neuronal and glial cells. To partly bridge this gap, we prepared and initially characterized an iPSC-based neuronal and glial model derived from peripheral blood mononuclear cells of MPSII patients.

Critical for the practical utility of the model, and unlike other monogenic diseases (Chen et al 2016), we did not observe any decline in self-renewal capacity of the MPSII patient-iPSC lines compared to controls. However, the cultures from the X-hemizygous male patient and, to some extent, from the X-heterozygous female patient expressed reduced ability to spontaneously form embryoid bodies. This observation makes our patient derived MPSII cellular model similar to previously reported impaired embryoid body formation by murine MPSVII iPSCs (Meng et al 2010).

While potentially limiting, we showed that by modifying the cultivation protocol, the MPSII iPSC lineages could be differentiated into neurospheres. These observations suggest that IDS deficiency may, similarly to other neurological diseases, partly interfere with the fitness of the neuronal and glial precursors (Russo et al 2015). Critically however, and as previously documented in IDS deficient murine neuronal stem cells (Fusar Poli et al 2013), IDS deficiency does not represent a fundamental compromise to the differentiation potential of the human MPSII iPSCs.

Studies in the fetal MPSII CNS tissues (Meier et al 1979; Wiesmann et al 1980) suggested that the extent of the storage process relates to the differentiation status of particular neural cells. The latter reports further showed that neurons and neuroblasts of the less developed fetal cerebral and cerebellar cortex were nearly devoid of the storage pathology. In

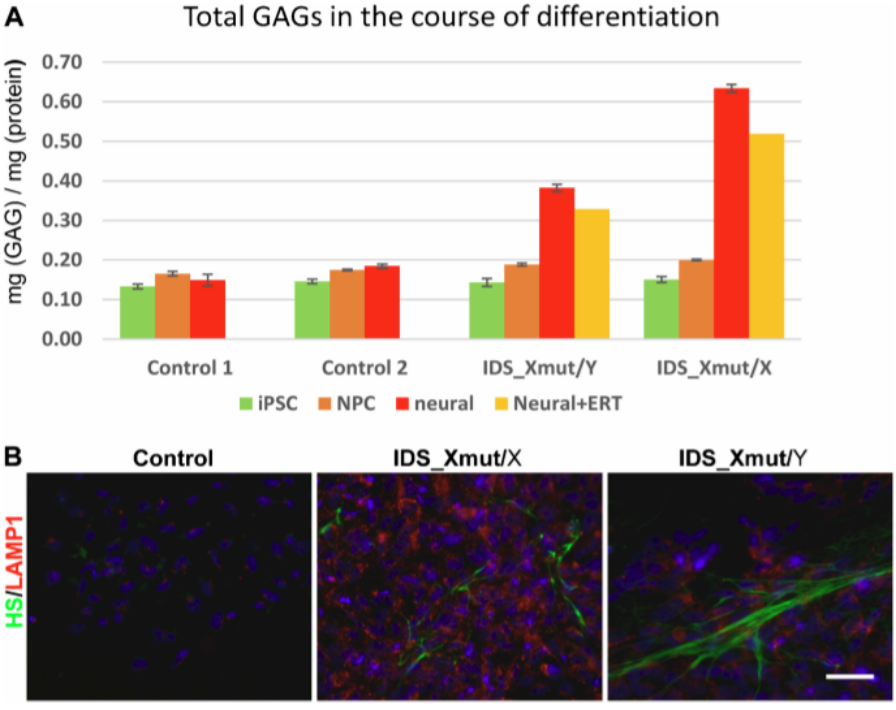

Fig. 4 Analysis of GAG accumulation in iPSC, NPC and differentiated neural cells of MPSII patients and controls using a photometric method. GAG levels were normal in patient iPSC and NPC. Maturation of neural cells was accompanied by an increase in accumulated GAGs. GAG accumulation was reduced by supplementing the deficient IDS (**a**). Co-staining of HS and LAMP1 did not shown overlap of the specific signals. HS accumulated in the cytoplasmic membranes from both patients (**b**). Scale bar:20 μm for all images

compliance with these observations in the fetal tissues are data gained in the murine MPSII progenitor neuronal cells. The extent of the subcellular storage in these cells also showed considerable dependence on their differentiation status (Fusar Poli et al 2013).

This stated, we hypothesize, that when compared to the differentiated human MPSII neural cells or CNS of *Ids-KO* mice with a fulminant neuropathology, the relative lack of the ultrastructural subcellular storage in the MPSII patient derived adherent neural cells reflects their still relatively under-differentiated status and short post-mitotic culture phase.

No significant increase in GAGs was detected in patient iPSC and NPC compared to healthy controls. As with the Fabry disease (lysosomal alpha-galactosidase deficiency) iPSC model (Itier et al 2014), this may be caused by the high proliferative rate of the cells and consecutive dilution of undegraded substrates. Abnormal and progressive accumulation of GAGs became apparent in more differentiated patient cells, which was likely caused by decreased proliferation and prolonged cultivation.

The recombinant IDS used for ERT is endocytosed and targeted to the lysosomes via mannose and mannose-6-phosphate receptors on the cell-surface (Wraith et al 2008). The effect of ERT on CNS clinical involvement is not clear. A prevalent opinion is that the recombinant enzyme is too large to cross the BBB (Boado et al 2013; Noh and Lee 2014), which prevents its transfer from the blood to the brain parenchyma. Currently, intrathecal enzyme infusion is one of the tested therapeutic approaches to overcome these limitations.

We tested ERT in our iPSC derived neural cells by administering a commercially available recombinant enzyme to the cells starting at the progenitor stage, while no significant increase in GAG was detected. However, despite high intracellular enzyme activity there was still a gradual increase in accumulated GAG in patient cells. It is known that HS as well as some other GAGs are present in the cell membrane or in the extracellular matrix where they mediate molecular interactions at the cell surface, bind growth factors, chemokines, extracellular matrix components, enzymes, and play an active role in signal transduction (Perrimon and Bernfield 2001; Gallagher 2006). HS was immunodetected at elevated levels on the cell surface, but not within lysosomes. This phenomenon was previously described in MPSIII where HS is also one of the main storage compounds (Jakobkiewicz-Banecka et al 2016). We hypothesize that increased amounts of IDS substrates in patient cells originate mainly from their presence in extracellular material with proximity to the plasma membrane. HS in these storage loci are not transported to lysosomes for degradation nor are they degraded extracellularly by IDS at a neutral pH. The lack of extracellular accumulation in parallel control cultures could be due to suboptimal intra-lysosomal IDS activity or a shift in HS type from membrane-bound to a free form that is present in the extracellular matrix that is not recycled back into neuronal cells (Sarrazin et al 2011). The second major GAG accumulated in MPSII, dermatan sulfate, is present mainly in the connective tissues and does not contribute significantly to the neuropathology (Varki 1999).

In conclusion, we created an iPS cell model of MPSII which can differentiate to various neural cell types related to the CNS pathology of the disease. The iPSC derived terminally differentiated cells accumulate increased amounts of GAG. HS, one of two substrates affected by the enzyme defect, localized mostly to the plasma membrane or extracellularly. This biochemical phenotype was not observed in proliferating cells suggesting that longer term cultivation of non-proliferated cells could further emphasize the phenotype. The established iPSC lines can be used for future screening of potential therapeutic improvements such as better targeting of recombinant enzymes to neuronal/glial cells, mainly in combination with the iPSC based model of the BBB, which was also successfully produced by others (Canfield et al 2017).

Acknowledgments The authors thank Irena Knesplova and Dr. Filip Majer for their technical assistance and Dr. Martin Magner for assistance with collection of patient samples and clinical evaluation.

Details of Funding This work was funded by a research grant of the Medical Research Agency of The Czech Republic, AZV ČR 15-33297A.

The authors confirm independence from the sponsors; the content of the article was not influenced by the sponsors.

Compliance with ethical standards

Competing interest Jitka Rybova, Robert Dobrovolny, Jana Ledvinova, Jakub Sikora and Ladislav Kuchar declare no competing interests but disclose the following: Robert Dobrovolny and Jitka Rybova have received honoraria for lectures and/or hotel/travel expenses for relevant meetings from Shire, plc.

Animal rights This article does not contain any studies with animal subjects performed by any of the authors.

Conflict of interest J. Rybova, J. Ledvinova, J. Sikora, L. Kuchar, R. Dobrovolny declare that they have no conflict of interest.

References

All AH, Gharibani P, Gupta S et al (2015) Early intervention for spinal cord injury with human induced pluripotent stem cells oligodendrocyte progenitors. PLoS One 10:e0116933

Boado RJ, Hui EK, Lu JZ, Sumbria RK, Pardridge WM (2013) Blood-brain barrier molecular trojan horse enables imaging of brain uptake of radioiodinated recombinant protein in the rhesus monkey. Bioconjug Chem 24:1741–1749

Canfield SG, Stebbins MJ, Morales BS et al (2017) An isogenic blood-brain barrier model comprising brain endothelial cells, astrocytes, and neurons derived from human induced pluripotent stem cells. J Neurochem 140:874–888

Cardone M, Polito VA, Pepe S et al (2006) Correction of hunter syndrome in the MPSII mouse model by AAV2/8-mediated gene delivery. Hum Mol Genet 15:1225–1236

Chen J, Riazifar H, Guan MX, Huang T (2016) Modeling autosomal dominant optic atrophy using induced pluripotent stem cells and identifying potential therapeutic targets. Stem Cell Res Ther 7:2

Fusar Poli E, Zalfa C, D'Avanzo F et al (2013) Murine neural stem cells model hunter disease in vitro: glial cell-mediated neurodegeneration as a possible mechanism involved. Cell Death Dis 4:e906

Gallagher JT (2006) Multiprotein signalling complexes: regional assembly on heparan sulphate. Biochem Soc Trans 34:438–441

Gomes IC, Acquarone M, Maciel Rde M, Erlich RB, Rehen SK (2010) Analysis of pluripotent stem cells by using cryosections of embryoid bodies. J Vis Exp. doi: 10.3791/2344

Hartree EF (1972) Determination of protein: a modification of the Lowry method that gives a linear photometric response. Anal Biochem 48: 422–427

Itier JM, Ret G, Viale S et al (2014) Effective clearance of GL-3 in a human iPSC-derived cardiomyocyte model of Fabry disease. J Inherit Metab Dis 37:1013–1022

Jakobkiewicz-Banecka J, Gabig-Ciminska M, Kloska A et al (2016) Glycosaminoglycans and mucopolysaccharidosis type III. Front Biosci (Landmark Ed) 21:1393–1409

Jones SA, Parini R, Harmatz P, Giugliani R, Fang J, Mendelsohn NJ (2013) The effect of idursulfase on growth in patients with hunter syndrome: data from the hunter outcome survey (HOS). Mol Genet Metab 109:41–48

de Jong JG, Wevers RA, Liebrand-van Sambeek R (1992) Measuring urinary glycosaminoglycans in the presence of protein: an improved screening procedure for mucopolysaccharidoses based on dimethylmethylene blue. Clin Chem 38:803–807

Meier C, Wismann U, Herschkowitz N, Bischoff A (1979) Morphological observations in the nervous system of prenatal mucopolysaccharidosis II (M. Hunter). Acta Neuropathol 48:139–143

Meng XL, Shen JS, Kawagoe S, Ohashi T, Brady RO, Eto Y (2010) Induced pluripotent stem cells derived from mouse models of lysosomal storage disorders. Proc Natl Acad Sci U S A 107:7886–7891

Motas S, Haurigot V, Garcia M et al (2016) CNS-directed gene therapy for the treatment of neurologic and somatic mucopolysaccharidosis type II (hunter syndrome). JCI Insight 1:e86696

Muenzer J, Lamsa JC, Garcia A, Dacosta J, Garcia J, Treco DA (2002) Enzyme replacement therapy in mucopolysaccharidosis type II (hunter syndrome): a preliminary report. Acta Paediatr Suppl 91: 98–99

Muenzer J, Beck M, Eng CM et al (2011) Long-term, open-labeled extension study of idursulfase in the treatment of hunter syndrome. Gen Med: Off J Am Coll Med Gen 13:95–101

Neufeld EF, Muenzer J (2001) The Mucopolysaccharidoses. In: Scriver CR, Beaudet AL, Sly WS (eds) The metabolic and molecular basis of inherited disease. McGraw-Hill, New York, pp 3421–3452

Noh H, Lee JI (2014) Current and potential therapeutic strategies for mucopolysaccharidoses. J Clin Pharm Ther 39:215–224

Okuyama T, Tanaka A, Suzuki Y et al (2010) Japan Elaprase treatment (JET) study: idursulfase enzyme replacement therapy in adult patients with attenuated hunter syndrome (mucopolysaccharidosis II, MPS II). Mol Genet Metab 99:18–25

Patel P, Suzuki Y, Tanaka A et al (2014) Impact of enzyme replacement therapy and hematopoietic stem cell therapy on growth in patients with hunter syndrome. Mol Gen Metab Rep 1:184–196

Perrimon N, Bernfield M (2001) Cellular functions of proteoglycans–an overview. Semin Cell Dev Biol 12:65–67

Polito VA, Cosma MP (2009) IDS crossing of the blood-brain barrier corrects CNS defects in MPSII mice. Am J Hum Genet 85:296–301

Polito VA, Abbondante S, Polishchuk RS, Nusco E, Salvia R, Cosma MP (2010) Correction of CNS defects in the MPSII mouse model via systemic enzyme replacement therapy. Hum Mol Genet 19:4871–4885

Russo FB, Cugola FR, Fernandes IR, Pignatari GC, Beltrao-Braga PC (2015) Induced pluripotent stem cells for modeling neurological disorders. World J Transplant 5:209–221

Sarrazin S, Lamanna WC, Esko JD (2011) Heparan sulfate proteoglycans. Cold Spring Harb Perspect Biol 3:a004952

Skoog WA, Beck WS (1956) Studies on the fibrinogen, dextran and phytohemagglutinin methods of isolating leukocytes. Blood 11: 436–454

Stacpoole SR, Bilican B, Webber DJ et al (2011) Efficient derivation of NPCs, spinal motor neurons and midbrain dopaminergic neurons from hESCs at 3% oxygen. Nat Protoc 6:1229–1240

Takahashi K, Yamanaka S, (2006) Induction of Pluripotent Stem Cells from Mouse Embryonic and Adult Fibroblast Cultures by Defined Factors. Cell 126 (4):663–676. https://doi.org/10.1016/j.cell.2006.07.024

Tanaka A, Okuyama T, Suzuki Y et al (2012) Long-term efficacy of hematopoietic stem cell transplantation on brain involvement in patients with mucopolysaccharidosis type II: a nationwide survey in Japan. Mol Genet Metab 107:513–520

Varki A (1999) Essentials of glycobiology, vol xvii. Cold Spring Harbor Laboratory Press, Cold Spring Harbor, NY, p 653

Voznyi YV, Keulemans JL, van Diggelen OP (2001) A fluorimetric enzyme assay for the diagnosis of MPS II (hunter disease). J Inherit Metab Dis 24:675–680

Wiesmann UN, Spycher MA, Meier C, Liebaers I, Herschkowitz N (1980) Prenatal mucopolysaccharidosis II (hunter): a pathogenetic study. Pediatr Res 14:749–756

Wraith JE, Scarpa M, Beck M et al (2008) Mucopolysaccharidosis type II (hunter syndrome): a clinical review and recommendations for treatment in the era of enzyme replacement therapy. Eur J Pediatr 167: 267–277

Supplementary Materials to the Paper edited: *Neural cells generated from human induced pluripotent stem cells as a model of CNS involvement in mucopolysaccharidosis type II.*

(J Inherit Metab Dis)

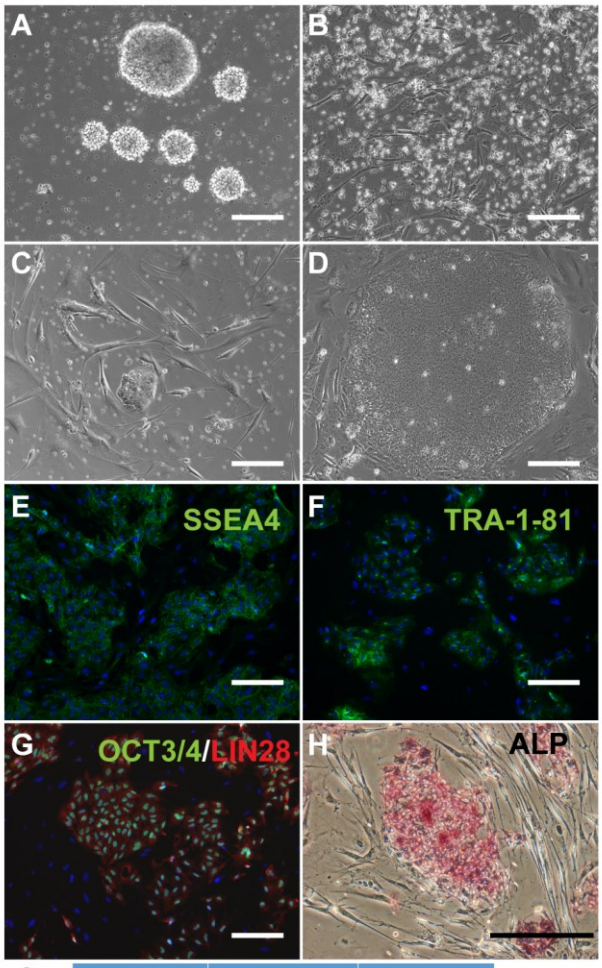

Figure S1: Generation of iPSC lines from activated mononuclear cells isolated from peripheral blood of MPSII patients and control individuals. Detection of pluripotency markers. **A-D:** Stimulated mononuclear cells (A) after infection by Sendai virus were transferred onto feeder cells at the day three (B). The formation of the iPSC colonies were observed at the day 9 (C) and compact colonies at the day 16 (D). **E-G:** Immunofluorescence analysis showing the expression of SSEA4 (E), TRA-1-81 (F), OCT3/4 and LIN28 (G) in iPSC lines. **H:** iPSC clones were positive for alkaline phosphatase. The nuclei were conterstained with DAPI (blue). The scale bars indicate 100 µm. **I:** Disease phenotype of patients' iPSC lines was verified by enzyme assay using fluorogenic substrate 4-MU-α-D-L-iduronate-2-sulphate. Two selected IDS_Xmut/X iPSC clones showed a weak residual activity of IDS, which is in accordance with the results measured in leukocytes.

I

Sample	IDS activity [nmol/mg.4hod]	β-GAL activity [nmol/mg.hod]
IDS_X^{mut}/Y_a	0.07	132.16
IDS_X^{mut}/Y_b	0.00	110.08
IDS_X^{mut}/X_a	5.94	501.25
IDS_X^{mut}/X_b	9.28	451.32
C1	68.6	222.12
C2	85.3	331.45

Table S1. The information regarding primary antibodies used for immunostaining

Markers of differentiation				
Antibody	**Host**	**Catalog number**	**Industry**	**Cell type**
OCT3/4	mouse	sc-5279	Santa Cruz Biotechnology, Dallas, TX, USA	iPSC
SSEA4	mouse	41-4000	Life Technologies, Carlsbad, CA, USA	iPSC
LIN28	rabbit	11724-1-AP	Proteintech Group, Chicago, IL, USA	iPSC
TRA-1-81	mouse	41-1100	Life Technologies, Carlsbad, CA, USA	iPSC
SOX1	rabbit	ab22572	Abcam, Cambridge, MA, USA	neural progenitors
Nestin	mouse	MAB5326	EMD Millipore, Massachusetts, USA	neural progenitors
βTubIII	mouse	T8660	Sigma-Aldrich, Saint Louis, MO, USA	neurons
MAP2	rabbit	ab32454-100	Abcam Cambridge, MA, USA	neurons
Vimentin	mouse	MU074-UC	BioGenex, Fremont, CA, USA	neurons
Synapsin I	mouse	574777	EMD Millipore, Massachusetts, USA	neurons
TH	mouse	MAB318	EMD Millipore, Massachusetts, USA	neurons
GFAP	red	Z0334	DakoCytomation, Glostrup, Denmark	astrocytes
CNPase	mouse	ab6319	Abcam, Cambridge, MA, USA	oligodendrocytes
Other markers				
Antibody	**Host**	**Catalog number**	**Industry**	**Marker of**
LAMP1	rabbit	-	gift from Dr. Carlsson; University of Umea, Sweden	lysosomes
CatD	mouse	ab6313	Abcam, Cambridge, MA, USA	lysosomes
HS	mouse	ab23418	Abcam, Cambridge, MA, USA	heparan sulfate

Patients' clinical and diagnostic description

The male patient (IDS_$\mathbf{X^{mut}}$/Y) is currently 18 years old and was diagnosed with MPSII at the age of 5 years. While born apparently healthy, the patient's psychomotor development was delayed and within first two years he started to present with organomegaly and coarse facial features. He also suffered from joint contractures, cardiac valve involvement, and hearing impairment. The patient's urine excretion of GAGs was elevated (68.1 g/mol creatinine compared to < 16.1 in controls) and IDS activity in leukocytes was reduced to 0.03 nmol/24 h/mg (control range 0.9–4.4 nmol/24 h/mg). The patient carries the c.[1181-1G>A] *IDS* mutation that leads to deletion of four nucleotides from the spliced mRNA. The patient has been receiving ERT for 8 years (Dvorakova et al 2016).

The clinical characteristics of the female MPSII patient (IDS_$\mathbf{X^{mut}}$/X) were previously described in detail by (Reboun et al 2016). The patient is currently 6 years old and was diagnosed with MPSII at 3.5 years. The patient was born at term and her postnatal adaptation and early development were uneventful. However, snoring, hearing problems and delayed speach were recognized by the age of 2 years. Coarse facial features, gingival hyperplasia, mild hepatosplenomegaly, claw hands, lumbal hyperlordosis, large joint contractures, and mild mental retardation developed during her third year of life. The patient's urine excretion of GAGs was elevated (60.5–65.7 g/mol creatinine compared to < 15.5 in controls) and IDS activity in leukocytes was markedly decreased (0.46 nmol/4 h/mg, control range: 28.1–70.4 nmol/4 h/mg). The patient is heterozygous for the c.[1403G>A] (p.Arg468Gln) *IDS* mutation. Importantly, X inactivation analysis in her leukocytes revealed preferential inactivation of the normal allele, which correlates well with her severe clinical phenotype. The patient has been receiving ERT for 3 years.

Isolation of mononuclear cells and their reprogramming into iPSC

Peripheral blood mononuclear cells (PBMC) from both patients were isolated using Histopaque (Sigma-Aldrich Inc., USA) and stored in liquid nitrogen in 10% dimethyl sulfoxide (DMSO) and 90% inactivated fetal bovine serum (BenchMark FBS, GEMINI Bio-Products, West Sacramento, USA) until further use. After thawing, the PBMCs were activated in complete LGM medium (Lonza, Walkersville, USA) containing 0.4 µg/ml of purified NA/LE mouse anti-human CD3 (BD Biosciences, San Jose, USA), 0.4 µg/ml of mouse anti-human CD28 (BD Biosciences, San Jose, USA), and 50 ng/ml of IL2 (Abbiotec, San Diego,

USA) and were grown on CD3 coated 6-well plates for 5 days (Daheron and D'Souza 2008). Activated leukocytes were reprogrammed using a CytoTune™-iPS 2.0 Sendai Reprogramming Kit (ThermoFisher Scientific Inc.). The transient expression of Oct3/4, Sox2, Klf4, and c-Myc factors were performed according to the manufacturer's instructions and with the recommended multiplicity of infection (MOI) for each vector (KOS MOI = 5, hc-Myc MOI = 5, hKlf4 MOI = 3) in complete LGM medium. The medium was replaced on the second day to remove the virus and the cells were further grown on irradiated mouse embryonic fibroblasts, which served as feeder cells. HES medium (KnockOut™ ESC/iPSC Medium Kit: DMEM/F12 with GlutaMAX and KnockOut Serum Replacement) with bFGF (8 ng/ml) was used from the 4th day. Individual colonies were transferred to 12-well plates containing feeder cells and then passaged with Accutase and EZPassage™ tool (all from ThermoFisher Scientific Inc.) until stable iPSC lines were generated.

Differentiation of iPSC into neuronal and glial lineages

Differentiations of iPSC into neuronal and glial cells were based on previously published protocols (Stacpoole et al 2011; All et al 2015). In brief, iPSC maintained in feeder-free conditions on Geltrex-coated plates (ThermoFisher Scientific Inc.) and in mTeSR™1 medium (STEMCELL Technologies Inc., Vancouver, BC, Canada) were dissociated to single cells suspension using Accutase (ThermoFisher Scientific Inc.). Embryoid bodies (EBs) were formed using AggreWell™800 plates (STEMCELL Technologies Inc.) according to the manufacturer's instructions, in a 1:1 mixture of mTeSR1 medium and complete differentiation medium (CDM). CDM consisted of IMDM/F12 medium (1:1) supplemented with 1% Chemically Defined Lipid Concentrate, Penicillin-Streptomycin (P/S), 7.5% BSA (all from ThermoFisher Scientific Inc.) 7µg/ml insulin, 15 µg/ml transferrin, and 450 µM monothioglycerol (all from Sigma-Aldrich, Inc., USA), and 10 µM Y27632 (Tocris Bioscience, UK). On the second day, the medium was changed to complete CDM. On the third day, EBs were transferred to ultra-low attachment plates and cultivated for another 10 days. The medium was exchanged every 2–3 days. Neural progenitor cells (NPCs) were generated by supplementing the medium with bFGF2 (20 ng/ml) and Heparin (5 µg/ml; Sigma-Aldrich Inc., USA) for 3 days. EBs were passaged using EZPassage™ tool (ThermoFisher Scientific Inc.) when the spheres were large and darkened in the center. NPC cultures were maintained under the same conditions for up to three months.

Neurons were prepared in CDM supplemented with 0.1 µM of retinoic acid (RA, Sigma-Aldrich Inc., USA) and 1 µM purmorphamine (Tocris bioscience) from day 14 to 28. Terminal differentiation was completed by plating EBs or single cells onto Geltrex-coated tissue culture plates and grown in terminal differentiation medium, which consisted of DMEM medium (Biochrom Ltd., UK) supplemented with B-27 Supplement, P/S (all from ThermoFisher Scientific Inc., USA), GDNF (10 ng/ml), and BDNF (10 ng/ml; all from PeproTech Inc., USA). Oligodendrocytes were differentiated by plating single cells onto Geltrex-coated adherent plates and culturing the cells in DMEM medium supplemented with EGF (10 ng/ml) for 7 days, and with EGF (20 ng/ml) and PDGF-AA (PeproTech Inc., USA) for another 25 days. All procedures involving neuronal and glial differentiation were performed at 37 °C, 5% CO_2, and 5% oxygen atmosphere.

Preparation of neurosphere cryo-sections

The preparation of cryo-sections was based on the modified protocol by (Gomes et al 2010). The neurospheres were washed in PBS (2x 5min), then transferred into PCR tubes, fixed in 4% paraformaldehyde in PBS (30min), washed in PBS (1x 5min), and sequentially placed for 30 minutes in 10%, 20%, and 30% PBS-buffered sucrose. After the last wash, EBs were transferred (using a pipette tip) into a cup made from aluminum foil. To keep the EBs at the bottom of the cup, tissue freezing medium (Leica Microsystems GmbH, Wetzlar, Germany) was slowly added. The samples were frozen on dry ice and 10 µm sections were cut using a cryostat microtome (Leica Biosystems, Nussloch GmbH) and transferred onto poly-L-lysine (Sigma-Aldrich Inc., USA) coated cover slips. All sections were air-dried and stored at −80 °C until further use.

Characterization of iPSC and neural cells by immunostaining and ALP staining

The cells were fixed in 4% paraformaldehyde in PBS for 15 min, permeabilized with 0.2% Triton-X100 in PBS for 5 min, and blocked in 10% FBS in PBS for 1 hour, all at room temperature (RT). The cells were incubated overnight at 4 °C with primary antibodies (Table S1) in blocking buffer. On the following day the samples were washed with PBS (5x 5 min) and the cells were labeled with Alexa Fluor 488- and Alexa Fluor 568-conjugated species-specific secondary antibodies (ThermoScientific Fisher Inc., USA) for 1 hour at 37 °C. The cells were then washed with PBS (5x 5 min) and nuclei were counterstained using 4',6-diamidino-2-phenylindole (DAPI, ThermoScientific Fisher Inc., USA) for 15 min at 37 °C.

The sections were mounted on slides using Immu-Mount medium (ThermoScientific Fisher Inc., USA). Images were taken using either a Nikon Ti80 (Nikon Instruments Europe BV, Netherlands) or a Leica SP8X confocal microscope (Leica Microsystems GmbH, Wetzlar, Germany).

For alkaline phosphatase (ALP) staining, the cells, in 24-well plate with feeder cells, were fixed in 4% paraformaldehyde in PBS for 2 min at RT. The cells were then washed with PBS (2x 5 min) and water (1x 5 min) and allowed to air dry for several minutes. ALP solution (86R Phosphatase Alkaline Kit, Sigma-Aldrich Inc., USA) was prepared according to the manufacturer's instructions and the cells were incubated with 0.5 ml of this substrate solution for 15 min at RT, in the dark. After a final wash with PBS (2x 5 min), sections were mounted on slides using Immu-Mount medium.

Determination of IDS activity

Total leukocytes were isolated from EDTA blood within 24 hours of its collection using the method describe by (Skoog and Beck 1956). Water homogenates of leukocytes were prepared by indirect sonication (3x 10 seconds) in an ice bath. The protein concentrations were determined using the method describe by (Hartree 1972). IDS activity was assayed using the fluorogenic substrate 4-methylumbelliferyl-α-L-iduronate-2-sulphate as described by (Voznyi et al 2001). Enzyme assay is a two-step procedure in which the substrate is first desulphated by endogenous IDS to produce a substrate for α-L-iduronidase. In the second step, partially purified α-L-iduronidase was added to the reaction mixture to release the 4-methylumbelliferone (MU). The reaction was stopped with 0.2 M glycine/NaOH buffer (pH 10.6) and the fluorescence of 4-methylumbelliferone was measured on a spectrofluorometer at excitation/emission wavelengths of 365 nm/448 nm (Perkin Elmer LS50B, Wellesley, USA). IDS specific activity is typically expressed in nmol of MU released per mg of protein per 4 hours.

Electron microscopy

The neural cells were cultivated for 6 weeks on cover slips pre-coated with Geltrex, fixed with 3% Glutaraldehyde in phosphate buffer (pH 7.2–7.4, 30 min, at RT), washed with phosphate buffer (2x 10 min, at RT) and contrasted overnight at 8 °C with 2% OsO_4 in phosphate buffer. On the following day the samples were washed with phosphate buffer (3x

10 min, at RT) and dehydrated using an ethanol (EtOH) series: 50% EtOH (2x 10 min, at RT), 70% EtOH (2x 10 min, at RT), 90% EtOH (2x 10 min, at RT), 100% EtOH (2x 30 min, at RT), and propylene oxide (2x 15 min, at RT).

Dehydrated samples were sequentially placed in polymerization mixtures (1:1 for 1.5 hour and 3:1 overnight, at RT) of Durcupan Epon (Fluka, Hatfield, PA, USA; prepared according to manufacturer's instructions) and Propylene oxide, respectively. The following day the samples were placed in a clear Durcupan medium for an additional 4 hours. Gelatin capsules were filled with fresh medium, placed on the specimens, and kept two days at 60–70 °C for polymerization. Ultrathin sections (60 nm) were cut on an ultramicrotome and placed on copper grids. The samples on grids were contrasted in a 5% water solution of uranyl acetate (10 min, at RT), washed in distilled water, and lastly in Reynolds solutions for 10 min, at RT. After further washes in distilled water, the samples were air dried at RT.

References

All AH, Gharibani P, Gupta S, et al (2015) Early intervention for spinal cord injury with human induced pluripotent stem cells oligodendrocyte progenitors. *PloS one* 10: e0116933.

Daheron L, D'Souza S (2008) Blood - SeV derived fibroblast generated iPSCs. In *StemBook* Cambridge (MA).

Dvorakova L, Vlaskova H, Sarajlija A, et al (2016) Genotype-phenotype correlation in 44 Czech, Slovak, Croatian and Serbian patients with mucopolysaccharidosis type II. *Clin Genet*.

Gomes IC, Acquarone M, Maciel Rde M, Erlich RB, Rehen SK (2010) Analysis of pluripotent stem cells by using cryosections of embryoid bodies. *Journal of visualized experiments : JoVE*.

Hartree EF (1972) Determination of protein: a modification of the Lowry method that gives a linear photometric response. *Analytical biochemistry* 48: 422-427.

Reboun M, Rybova J, Dobrovolny R, et al (2016) X-Chromosome Inactivation Analysis in Different Cell Types and Induced Pluripotent Stem Cells Elucidates the Disease Mechanism in a Rare Case of Mucopolysaccharidosis Type II in a Female. *Folia Biol (Praha)* 62: 82-89.

Skoog WA, Beck WS (1956) Studies on the fibrinogen, dextran and phytohemagglutinin methods of isolating leukocytes. *Blood* 11: 436-454.

Stacpoole SR, Bilican B, Webber DJ, et al (2011) Efficient derivation of NPCs, spinal motor neurons and midbrain dopaminergic neurons from hESCs at 3% oxygen. *Nat Protoc* 6: 1229-1240.

Voznyi YV, Keulemans JL, van Diggelen OP (2001) A fluorimetric enzyme assay for the diagnosis of MPS II (Hunter disease). *Journal of inherited metabolic disease* 24: 675-680.

7.2. Non impacted publications related to topic of this PhD thesis

Supplementary material F

Conference abstract and poster:

December 2014 – poster presentation: The 2014 ascb/ifcb meeting, Philadelphia, Pennsylvania; USA: Rybová J, Dobrovolný R, Asfaw B, Sládková J, Hyliš M, Ledvinová J: Fabry cardiomyocytes generated from induced pluripotent stem cells as a human model for morphology and pathobiochemistry studies.

Fabry cardiomyocytes generated from induced pluripotent stem cells as a human model for morphology and pathobiochemistry studies

Rybová J[1], Dobrovolný R[1],Asfaw B[1], Sládková J[2], Hyliš M[3], Ledvinová J[1]

[1]Institute of Inherited Metabolic Disorders, First Faculty of Medicine, Charles University in Prague and General University Hospital in Prague, Czech Republic
[2]Department of Pediatrics and Adolescent Medicine, 1st Faculty of Medicine, Charles University in Prague and General University Hospital in Prague, Czech Republic
[3]Laboratory of Electron Microscopy, Faculty of Science, Charles University in Prague

Lysosomal storage disorders is a group of more than 60 genetic disease caused by functional defects in lysosomal enzymatic or non-enzymatic proteins. Fabry disease, an example of one enzymopathie, is caused by-deficiency of lysosomal alpha-galactosidase A (EC 3.2.1.22). This defect leads to progressive accumulation of glycosphingolipids with terminal alpha-galactosyl moiety, dominantly globotriaosylceramide (Gb3Cer) and smaller amounts of galabiosylceramide (Ga2Cer) and blood group B antigens in lysosomes of most non-neuronal tissues (mainly heart, kidney and liver) and body fluids [1].

In 2006, Takahashi and Yamanaka first described generation of induced pluripotent stem cells from mouse embryonic fibroblast by retroviral transduction of four transcription factors Oct3/4, Sox2, c-Myc and Klf4 [2]. These cells provide an excellent opportunity to produce disease-relevant cell types for pathophysiology studies and development of new therapeutic approaches.

We prepared transgene-free human iPS cells from urine cells isolated from Fabry patients by transduction with Sendai virus expressing reprogramming factors. Derived iPS cell lines were positive for pluripotent markers Lin-28, SSEA-4, Oct3/4 and alkaline phosphatase activity. Fabry disease phenotype was confirmed by determining deficient alpha-galactosidase activity.

Cardiomyocytes (CM) are one of the major cell types affected in Fabry disease and therefore, we decided to differentiate generated iPS cells into cardiac cells. We performed differentiation based on the work of Lian et al [3]. Generated Fabry-CM and control-CM were positive for cardiac markers Troponin I and Nkx2.5. The efficiency of differentiation, tested by flow cytometry, was significantly smaller for Fabry-CM compared to control probably due to Fabry phenotype.

Morphology of cultivated CM was determined via electron microscope. Ultrastructure analysis of Fabry-CM revealed abnormally sized and shaped mitochondria, almost regularly associated with aberrant and sparse cristae, dilated endoplasmatic reticulum and membranous cytoplasmic body structures in comparison with controls. We suggest that observed damages of intracellular architectures of Fabry-CM are tightly associated with their functional pathology followed by clinical phenotype of the heart of Fabry patients, predisposed to storage. Further studies are needed to elucidate the cascade of molecular events connected with etiopathogenesis FD.

Recently, it was described effective clearance of Gb3Cer by the recombinant enzyme in Fabry disease iPS cell [4]. Trafficking of supplied enzyme within the compartments highly loaded with storage compounds will be the subject of our further studies.

1. Elleder M. in: Fabry Disease, Eds.Elstein D, Altarescu G and Beck M, Springer 2010, pp.39-79
2. Takahashi K, Yamanaka S.: Cell. 2006 Aug 25;126(4):663-76. Epub 2006 Aug 10
3. Lian, X., et al.: Nature Protocols, 2012. 8(1): p. 162-175.ISSN
4. Iltier, J.M., et al.: J Inherit Metab Dis, 2014.ISSN

This work was supported by Grant IGA MZ NT14015-3/2013 and project RVO-VFN64165 from the Ministry of Health, project PRVOUK-P24/LF1/3 from the Ministry of Education, Grant SVV 266 504 from the Charles University in Prague, Czech Republic and Grant GA UK 56214 from the Charles University in Prague, Czech Republic

Fabry cardiomyocytes generated from induced pluripotent stem cells as a human model for morphology and pathobiochemistry studies

ABSTRACT
LYSOSOMAL STORAGE DISORDERS IS A GROUP OF MORE THAN 60 GENETIC DISEASE CAUSED BY FUNCTIONAL DEFECTS IN LYSOSOMAL ENZYMATIC OR NON-ENZYMATIC PROTEINS. FABRY DISEASE, AN EXAMPLE OF ONE ENZYMOPATHIE, IS CAUSED BY DEFICIENCY OF LYSOSOMAL ALPHA-GALACTOSIDASE A (EC 3.2.1.22). THIS DEFECT LEADS TO PROGRESSIVE ACCUMULATION OF GLYCOSPHINGOLIPIDS WITH TERMINAL ALPHA-GALACTOSYL MOIETY, DOMINANTLY GLOBOTRIAOSYLCERAMIDE (GB3CER) AND SMALLER AMOUNTS OF GALABIOSYLCERAMIDE (GA2CER) AND BLOOD GROUP B ANTIGENS IN LYSOSOMES OF MOST NON-NEURONAL TISSUES (MAINLY HEART, KIDNEY AND LIVER) AND BODY FLUIDS [1].
IN 2006, TAKAHASHI AND YAMANAKA FIRST DESCRIBED GENERATION OF INDUCED PLURIPOTENT STEM CELLS FROM MOUSE EMBRYONIC FIBROBLAST BY RETROVIRAL TRANSDUCTION OF FOUR TRANSCRIPTION FACTORS OCT3/4, SOX2, C-MYC AND KLF4 [2]. THESE CELLS PROVIDE AN EXCELLENT OPPORTUNITY TO PRODUCE DISEASE-RELEVANT CELL TYPES FOR PATHOPHYSIOLOGY STUDIES AND DEVELOPMENT OF NEW THERAPEUTIC APPROACHES.
WE PREPARED TRANSGENE-FREE HUMAN IPS CELLS FROM URINE CELLS ISOLATED FROM FABRY PATIENTS BY TRANSDUCTION WITH SENDAI VIRUS EXPRESSING REPROGRAMMING FACTORS. DERIVED IPS CELL LINES WERE POSITIVE FOR PLURIPOTENT MARKERS LIN28, SSEA-4, OCT3/4 AND ALKALINE PHOSPHATASE ACTIVITY. FABRY DISEASE PHENOTYPE WAS CONFIRMED BY DETERMINING DEFICIENT ALPHA-GALACTOSIDASE ACTIVITY.
CARDIOMYOCYTES (CM) ARE ONE OF THE MAJOR CELL TYPES AFFECTED IN FABRY DISEASE AND THEREFORE WE DECIDED TO DIFFERENTIATE GENERATED IPS CELLS INTO CARDIAC CELLS. WE PERFORMED DIFFERENTIATION BASED ON THE WORK OF LIAN ET AL [3]. GENERATED FABRY-CM AND CONTROL-CM WERE POSITIVE FOR CARDIAC MARKERS TROPONIN I AND NKX2.5. THE EFFICIENCY OF DIFFERENTIATION, TESTED BY FLOW CYTOMETRY, WAS SIGNIFICANTLY SMALLER FOR FABRY-CM COMPARED TO CONTROL PROBABLY DUE TO FABRY PHENOTYPE.
MORPHOLOGY OF CULTIVATED CM WAS DETERMINED VIA ELECTRON MICROSCOPE. ULTRASTRUCTURE ANALYSIS OF FABRY-CM REVEALED ABNORMALLY SIZED AND SHAPED MITOCHONDRIA, ALMOST REGULARLY ASSOCIATED WITH ABERRANT AND SPARSE CRISTAE, DILATED ENDOPLASMATIC RETICULUM AND MEMBRANOUS CYTOPLASMIC BODY STRUCTURES IN COMPARISON WITH CONTROLS. WE SUGGEST THAT OBSERVED DAMAGES OF INTRACELLULAR ARCHITECTURES OF FABRY-CM ARE TIGHTLY ASSOCIATED WITH THEIR FUNCTIONAL PATHOLOGY FOLLOWED BY CLINICAL PHENOTYPE OF THE HEART OF FABRY PATIENTS, PREDISPOSED TO STORAGE. FURTHER STUDIES ARE NEEDED TO ELUCIDATE THE CASCADE OF MOLECULAR EVENTS CONNECTED WITH ETIOPATHOGENESIS FD.

Rybová J[1], Dobrovolný R[1], Asfaw B[1], Sládková J[2], Hyliš M[3], Ledvinová J[1]

[1]Institute of Inherited Metabolic Disorders, First Faculty of Medicine, Charles University in Prague and General University Hospital in Prague, Czech Republic; [2]Department of Pediatrics and Adolescent Medicine, 1st Faculty of Medicine, Charles University in Prague and General University Hospital in Prague, Czech Republic; [3]Laboratory of Electron Microscopy, Faculty of Science, Charles University in Prague

Introduction:

Lysosomal storage disorders (LSD) is a group of more than 60 genetic diseases caused by functional defects in lysosomal enzymatic or non-enzymatic proteins. Fabry disease, an example of LSD enzymopathy, is caused by deficiency of lysosomal alpha-galactosidase A (EC 3.2.1.22). This defect leads to progressive accumulation of glycosphingolipids with terminal alpha-galactosyl moiety, dominantly globotriaosylceramide (Gb_3Cer) and smaller amounts of galabiosylceramide (Ga_2Cer) and blood group B antigens in lysosomes of most non-neuronal tissues (mainly heart, kidney and liver) and body fluids [1].

In 2006, Takahashi and Yamanaka first described generation of induced pluripotent stem cells from mouse embryonic fibroblast by retroviral transduction of four transcription factors Oct3/4, Sox2, c-Myc and Klf4 [2]. These cells provide an excellent opportunity to produce disease-relevant cell types for pathophysiology studies and development of new therapeutic approaches.

Aims:

- Generation of transgene-free human iPS cells from urine cells isolated from Fabry patients and their characterization.
- Differentiation of established iPS cells into cardiomyocytes, their characterization, description of the Fabry phenotype and morphological studies.

Conclusions:

We generated transgene-free hiPS cells as a cellular model of Fabry disease. Their pluripotent state was confirmed by detection of Sox2, Lin28, SSEA4 and Oct3/4 and Fabry phenotype by demonstrating deficient alpha-galactosidase aktivity.

We were able to prepared cardiomyocytes (CM) from generated iPS cells which were positive for cardiac markers - Troponin I and Nkx2.5. In Fabry-CM was proven the presence of accumulated Gb_3Cer as well as disorganized contracting fibrils and abnormally sized and shaped mitochondria.

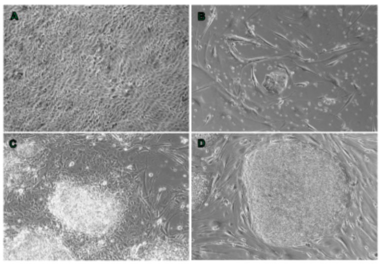

Fig.1: Generation of iPS cells from human model of Fabry disease
The formation of the iPS colony after infection of urinary cells (A) by Sendai virus was observed at the day 9 (B). Example of partially differentiated (C) and undifferentiated (D) colonies after several passage of the iPS cells. All images taken with 10x objective.

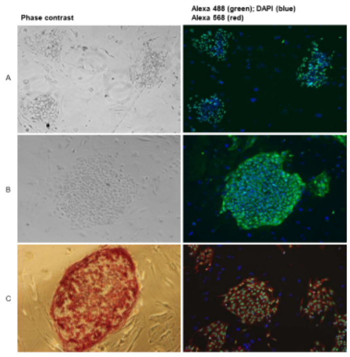

Fig.2: Characterization of generated Fabry-iPS cells using pluripotency markers
Immunofluorescence analysis showing the expression of Sox-2 (A), SSEA-4 (B), Oct3/4 (green) and Lin-28 (red) (C) in iPSc lines (10x objective). Analyzed iPS clones were also positive for alkaline phosphatase (D; 20x objective).

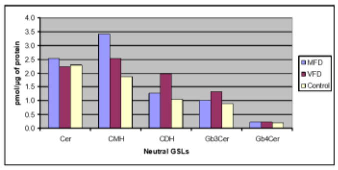

Fig.3: MS/MS analysis of neutral glycosphingolipids in control and Fabry iPS cells

The MS/MS does not differentiate between the glucosyl and galactosyl moieties because of the same mass. Therefore, glucosylceramide and galactosylceramide, lactosylceramide and digalactosylceramide are quantified as monohexosylceramides (CMH) and dihexosylceramides (CDH). Samples were measured in duplicates.
MFD, VFD – Fabry-iPS cells generated from urine cells from two male Fabry patients

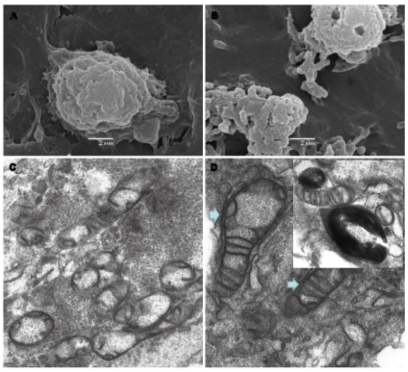

Fig.5: Scanning and transmission electron microscope analysis of control and Fabry cardiomyocytes.
SEM images of control-CM (A) and generated Fabry-CM (B) Bar: 2 micro. Surface of Fabry-CM revealed broken with polymorphous irregular microvilli in contrast to control-CM. TEM images of control-CM (A) and generated Fabry-CM (B) at 25,000x original magnification. Enlarged mitochondria (blue arrow), dilated endoplasmatic reticulum formations and membrane enveloped dense bodies (at the upper right side of picture D) were observed in comparison with control cells (C).

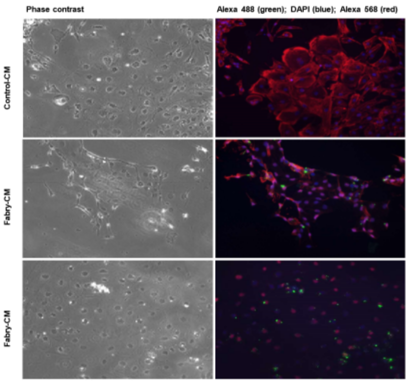

Fig.4: Fabry and control cardiomyocytes generated from human iPS cells (10x objective)
Positivity of beating control and Fabry-CM for cardiac markers Troponin I and Nkx2.5 (A-C, Alexa 568). Functionally organized contractile proteins into fibers in control-CM (A) versus less numerous and disorganized fibers in Fabry-CM (B, Alexa 568) and their significant accumulation of Gb3Cer (B, C, Alexa 488) compared to undetectable one in the control (A, Alexa 488).

Results and Discussion:

The transgene-free human iPS cells were produced from urine cells by CytoTune®-iPS Sendai Virus Reprogramming Kit. The urine cells were selected because of a minimal invasiveness of the primary material collection. The formation of iPS cell colonies started typically nine days after infection (**Fig.1**). The selected colonies were picked from Fabry hemizygous and control cells and passaged until creation of stable iPS cell lines and disappearance of nonreplicating Sendai virus from cultures. Derived iPS cell lines were positive for pluripotent markers Lin28, Sox2 SSEA4, Oct3/4 and alkaline phosphatase activity (**Fig.2**). Interestingly, although Fabry disease phenotype was confirmed by determining deficient alpha-galactosidase activity, significant accumulation of Gb3Cer was not observed in IPS cells (**Fig.3**). This is probably due to rapid proliferation of the cells leading to the dilution of undegraded substrates and overall decreased demand on catabolic pathways.

Cardiomyocytes (CM) are one of the major cell types affected in Fabry disease and therefore we decided to differentiate generated iPS cells into cardiac cells. We performed differentiation based on the work of Lian et al [3] using serum-free defined medium, small molecule inhibitors of glycogen synthase kinase 3 (CHIR99021) and canonical Wnt signal pathway (IWP2). Generated Fabry-CM and control-CM were positive for cardiac markers Troponin I and Nkx2.5 (**Fig.4**). The efficiency of differentiation, tested by flow cytometry, was significantly smaller for Fabry-CM compared to control probably due to Fabry phenotype which was also confirmed by the presence of accumulated Gb_3Cer and less numerous and disorganized fibers (**Fig.4**). Accumulation of Gb_3Cer was not detected in control cells and thus may lead to an inability to generate functional fibers in Fabry-CM as previously described [4] .

Morphology of cultivated CM was determined via transmission and scanning electron microscope. Surface of Fabry-CM revealed broken with polymorphous tips in contrast to control-CM (**Fig.5 A-B**) Undifferentiated pluripotent control cells were covered by multiple projections (philopodia) of different lengths, while in Fabry–CM these processes were observed in substantially less amount.(data not shown). When compared to the mitochondria of control CM , greater heterogeneity in size and shape of individual mitochondria and diverse amount of aberrant mitochondria with poorly developed or disoriented cristae were observed with TEM (**Fig.5 D**). Further, dilated endoplasmatic reticulum formations, occurrence of autophagosomes and membrane enveloped granular dense bodies (possible aggregates of phospholipids) have been recorded in Fabry-CM (**Fig.5** at the upper right side of picture **D**) in contrast to control-CM (**Fig.5 C**).

Recently, an effective clearance of Gb_3Cer by the recombinant enzyme in Fabry disease iPS cells has been reported [4]. Trafficking of supplied enzyme within the compartments highly loaded with storage compounds will be the subject of our further studies.

Materials and methods:

Isolation of urine cells and their reprogramming into iPS cells

Urine cells were isolated for two male patients with confirmed diagnosis of Fabry disease. For clone VFD and MFD, the patients are hemizygous for c.277G > A (D93N) and c.511G > C (G171R) changes. The urine cells were isolated based on the work of Zhou et al [5]. In breaf, after centrifugation (400g, 10 min, RT) of urine samples, the cell pellets were washed with PBS, centrifuged (200g, 10 min, RT) and resuspended in 1 ml of Primary medium and transferred into single well of 12-well plate. 1 ml of Primary medium was added each day for an additional four days. 96 hours after plating, the Primary medium was replaced with RE proliferation medium which was changed daily. Small colonies were observed after 5 days and were passaged with Accutase (Invitrogen) when they reached 70-80% confluency.

The urine cells of 3rd passage were used for reprogramming by transduction with CytoTune™-iPS 2.0 Sendai Reprogramming Kit (Invitrogen) according to manufacturing instructions. In brief, the cells were infected with an appropriate MOI of each titter contained in HES medium with bFGF (KnockOut™ESC/iPSC Medium Kit, Invitrogen). The medium was replaced with fresh one without virus on the second day and the cells were transferred on the layer of feeder cells (irradiated WT MEFs) on the 4th day. Selected colonies were picked to 12well plates containing feeder cells and then propagated to create a stable iPS cell lines.

Characterization of iPSc

Immunostaining: IPS cell colonies in 24well plate with feeder cells were fixed in 4% paraformaldehyde in PBS for 15 min at room temperature and permeabilized in 0.2% Triton-X100 in PBS for 5 min at room temperature, then blocked in 5% FBS in PBS for 1 hour at room temperature. After washing with PBS (3 x 5 min), the cells were incubated with primary antibody to Oct3/4 (mouse monoclonal, Santa Cruz), SSEA4 (mouse monoclonal, Invitrogen), Sox2 (mouse monoclonal, Sanat Cruz) and Lin-28 (rabbit polyclonal, Proteintech) at 4°C overnight. After washing with PBS (3 x 5 min), cells were labeled with Alexa Fluor 488 and Alexa Fluor 568-conjugated secondary antibodies for 1 hour at 37°C. Cells were then washed with PBS and nuclei were counterstained with DAPI in PBS for 15 min at 37°C. After final washing with PBS (2 x 5 min), specimens were analyzed using a fluorescence microscope (Nikon).
Alkaline phosphatase (ALP) staining: Cells in 24well plate with feeder cells were fixed in 4% paraformaldehyde in PBS for 2 min at room temperature. The cells were then washed with PBS (2 x 5 min) and with milliQ water (1x 5 min) and allowed to air dry for a few minutes. ALP solution (86R Phosphatase Alkaline Kit, Sigma-Aldrich) were prepared according to the manufacturer's instructions and cells were incubated with 0,5 ml of this dye solution for 15 min at room temperature in dark. After final washing with PBS (2 x 5 min), specimens were mounted with Immu-Mount (Shandon, Pittsburg, Pa.).
Tandem mass spectrometry (FIA-ESI-MS/MS analysis): Selected lipid isoforms (C16-C26; non-hydroxy and hydroxy) were measured in cell lipid extracts by flow injection analysis and multiple reaction monitoring in positive ion mode using ceramide specific product ion with m/z 264 [6].

Non impacted publications related to topic of this PhD thesis

Supplementary material G

Conference abstract and poster:

October 2015 – poster presentation: ESGLD, Pozzuoly, Italy: Rybova J, Asfaw B, Poupetova H, Kuchar L, Ledvinova J, Dobrovolny R: Crispr/Cas9 Generation Of iPSC Models Of Fabry And Schindler Disease

Crispr/Cas9 Generation Of iPSC Models Of Fabry And Schindler Disease

Rybova J., Asfaw B., Poupetova H., Kuchar L., Ledvinova J. ., Dobrovolny R

Institute of Inherited Metabolic Disorders, First Faculty of Medicine, Charles University in Prague and General University Hospital in Prague, Czech Republic

Human pluripotent stem cells (iPSc) generated from various cell types of patients offer a unique opportunity to produce disease-relevant cell types for pathophysiology studies and development of new therapeutic approaches as they possess unlimited self-renewal capacity and potential to generate all adult cell types, including rare or inaccessible human cell population. However, due to rarity of many genetic disorders, the opportunity to obtain biological samples is often exclusive.

Recently, an efficient genome manipulation technology using the RNA-guided DNase Cas9, the clustered regularly interspaced short palindromic repeats (CRISPR) system, has become widely used for rapid and highly efficient generation of knockout human iPSC used in modeling of disease conditions. CRISPR/Cas9 system induce double strand breaks (DSBs) at desired genomic loci, triggering the endogenous DNA repair machinery. Processing of DSBs by the error-prone nonhomologous end-joining (NHES) pathway leads to small insertions and deletions (indels) useful for generating loss-of-function mutations.

In our study, knockouts in two lysosomal hydrolases, alpha-galactosidase A gene (GLA, Fabry disease) and alpha-N-acetylgalactosaminidase gene (NAGA, Schindler disease) were made by this technology. Moreover, to help elucidate biological significance of substrate specificity overlap of GLA and NAGA, double knockouts of both genes were produces. The successful generation of the models were confirmed by demonstration of deficient activities in the iPSC lines and sequencing of the GLA and NAGA genes. The cells were used for initial experiments including study of natural substrates degradation (B-6-2, Gb3Cer, A-6-2) in GLA, NAGA and double knockout differentiated cells.

This work was supported by Grant IGA MZ NT14015-3/2013; project RVO-VFN64165 from the Ministry of Health; Grant SVV 266 504 from the Charles University in Prague, Czech Republic; Grant GA UK 56214 from the Charles University in Prague, Czech Republic and AZV 15-33297A, Czech Republic

CRISPR/Cas9 Generation of iPS Cells Models of Fabry and Schindler Diseases

Rybova J., Asfaw B., Poupetova H., Kuchar L., Ledvinova J Dobrovolny R.

Institute of Inherited Metabolic Disorders; Charles University in Prague and General Teaching Hospital in Prague, Czech Republic

Introduction:

Human pluripotent stem cells (iPSc) generated from various cell types of patients offer a unique opportunity to produce disease-relevant cell types for pathophysiology studies and development of new therapeutic approaches as they possess unlimited self-renewal capacity and potential to generate all adult cell types, including rare or inaccessible human cell populations.

Recently, an efficient genome manipulation technology using the RNA-guided DNase Cas9, the clustered regularly interspaced short palindromic repeats (CRISPR) system, has become widely used for rapid and highly efficient generation of knockout human iPSC used in modeling of disease conditions. CRISPR/Cas9 system induce double strand breaks (DSBs) at desired genomic loci, triggering the endogenous DNA repair machinery. Processing of DSBs by the error-prone nonhomologous end-joining (NHES) pathway leads to small insertions and deletions (indels) useful for generating loss-of-function mutations.

Aims:

Preparation of human cellular iPS models of Fabry disease (knockout of α-galactosidase A gene), Schindler disease (knockout of α-N-acetylgalactosaminidase gene) and model of both diseases (double knockout) by CRISPR/Cas9 System and their characterization.

Loading experiments with radiolabeled glycolipids Gb_4Cer, A-6-2 and B-6-2 in differentiated control and enzyme deficient cells.

Conclusions:

We generated transgene-free hiPS model of Fabry and Scindler disease and model of both diseases. Their pluripotent state was confirmed by detection of Sox2, Lin28, TRA-1-81 and Oct3/4 and disease phenotype by demonstrating relevant deficient enzyme activity.

In all three models deficiency was confirmed by significant block of *in situ* degradation of glycolipid substrate(s) of missing enzyme.

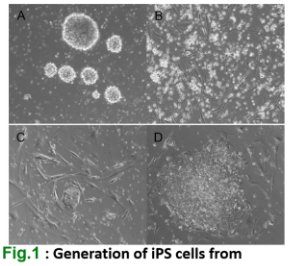

Fig.1 : Generation of iPS cells from stimulated mononuclear cells isolated from peripheral blood

Stimulated mononuclear cells (A) after infection by Sendai virus were transferred onto feeder cells at the day three (B). The formation of the iPS colonies were observed at the day 9 (B) and compact colonies at the day 16 (D). All images taken with 10x objective.

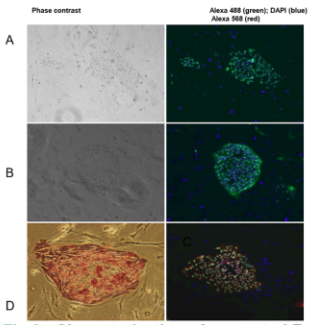

Fig.2 : Characterization of generated Fabry-iPS cells using pluripotency markers

Immunofluorescence analysis showing the expression of Sox-2 (A), TRA-1-81 (B), Oct3/4 (green) and Lin-28 (red) (C) in iPSc lines (10x objective). Analyzed iPS clones were also positive for alkaline phosphatase (D; 20x objective).

Tab.1 : Values of enzyme activities in iPS cells after genome editing by CRISPR/Cas9 System

Sample	α-NAGA activity [nmol/mg.hod]	α-GALA activity [nmol/mg.hod]	β-GAL activity [nmol/mg.hod]
GALA1	23.82	0.32	220.67
GALA2	27.44	0.51	314.50
NAGA1	0.19	36.544	223.87
NAGA2	0.19	46.78	300.29
DKO1	0.19	0.19	353.66
DKO2	0.19	0.32	271.87
CO1(control)	25.74	38.40	346.37
CO2 (control)	25.78	34.56	271.872

References:

1. Takahashi K., et al. Cell 2006 Aug 25;126(4):663-76. Epub 2006 Aug 10
2. Ran F. A., et al. 2013 Nov;8(11):2281-308. doi: 10.1038/nprot.2013.143. Epub 2013 Oct 24
3. Asfaw B., at al. J Lipid Res. 2002 Jul;43(7):1096-104
4. Lian X., et al.: Nature Protocols, 2012; 8(1): p. 162-175.ISSN
5 Ilker J.M., et al. : J Inherit Metab Dis, 2014.ISSN
6. Keslová-Veselíková J.: Virchows Arch. 2008 Jun; 452(6). 651–665.

Results and Discussion:

The transgene-free human iPS cells were produced from stimulated mononuclear cells isolated from peripheral blood by CytoTune®-iPS Sendai Virus Reprogramming Kit. The formation of iPS cell colonies started typically ninth day after infection (**Fig.1**) and derived control iPS cells were positive for pluripotent markers Lin28, Sox2 TRA-1-81, Oct3/4 and alkaline phosphatase activity (**Fig.2**).

We successfully applied CRISPR/Cas9 System for efficient genome modification in human iPS cells based on the work of Ran F.A. et al [2] to generate knockout in two lysosomal hydrolases, alpha-galactosidase A gene (GLA, Fabry disease) and alpha-N-acetylgalactosaminidase gene (NAGA, Schindler disease). Moreover, to help elucidate biological significance of substrate specificity overlap of GLA and NAGA, double knockouts of both genes were produces. Confirmation of both enzyme deficiencies were made by enzyme assay by fluorogenic substrates **(Tab.1)**.

We also performed *in situ* loading experiments of tritium-labeled glycolipids Gb4Cer, A-6-2 and B-6-2 by spontaneously differentiated control and disease-iPS cells. As expected, in all models significant block on degradation of glycolipid substrate(s) of deficient enzyme(s) was evident (Fig.3). It was described that relatively high residual activity of α-GLA toward glycolipid B-6-2 compared to A-6-2 (probably also to Gb3Cer) in culture of patient fibroblasts probably due to α-NAGA [3]. These two enzymes have a high degree of structural and biochemical similarity due to their common ancesteral origin. In these initial experiments we didn't observe a clear-cut contribution of α-NAGA to degrade natural substrate of α-GLA (especially B-6-2) as hypothesised in previous study with Fabry disease and Schindler disease fibroblast cultures.

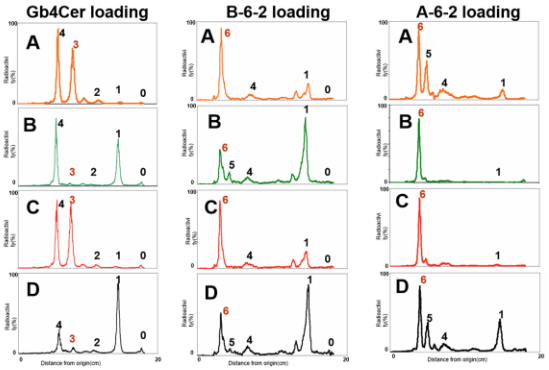

Fig.3: Degradation of tritium-labeled glycolipids Gb4Cer, B-6-2 and A-6-2 by spontaneously differentiated iPS cells with knockout of α-GLA, α-NAGA gene and double knockouts of both genes (DKO) produced by CRISPR/cas9 System

Lipid pattern of α-GLA (**A**), α-NAGA(**B**), both enzymes (**C**) deficient cells and (**D**) control cells. The chromatographic positions of substrate and various products are indicated by number of monosacchide residues on the glycolipid: e.g **1** (glucosyl ceramide), **4** (Gb_4Cer, globotetraosyl ceramide). In the cells with α-GLA deficiency was a significant block in degradation of glycoplipids B-6-2 and Gb_3Cer(globotriosyl ceramide), whereas α-NAGA deficient cells degradation of A-6-2 was blocked. In double knockout cells none of the three glycolipid substrates was degraded.

Materials and methods:

Reprogramming into iPS cells

The iPS cells were generated from stimulated mononuclear cells isolated from peripheral blood with Histopaque (Sigma) with CytoTune™-iPS 2.0 Sendai Reprogramming Kit (Invitrogen) according to manufacturing instructions. In brief, the cells kept in LGM media (Lonza) containing 0,4 μg/ml of CD3 and CD28 antibodies and 50ng/ml of IL2. The cells were kept in CD3 coated plates. After proliferation started the cells were tested for subtype by FACS and infected with an appropriate MOI of each titter contained in complete LGM medium. The medium was replaced with fresh one without virus on the second day and the cells were transferred on the layer of feeder cells (irradiated WT MEFs) in the presence of HES medium with bFGF (KnockOut™SESC/iPSC Medium Kit, Invitrogen) on the 4th day. Selected colonies were picked to 12well plates containing feeder cells and then propagated to create a stable iPS cell lines.

Genome editing in human iPS cells with the CRISPR/Cas9 system

Target genomic sequences were designed by an online CRISPR Design Tool (http://tools.genome-engineering.org). sgRNAs for each target were clonned into the pSpCas9(BB)-2A-Puro (PX459) plasmid (Addgene, Cambridge, USA) and finished plasmids were transformed into a competent E. coli strain: Library Efficiency® DH5α™(LifeTechnologies,) according to the protocol supplied with the cells. The sequence of each colony was verified by sequencing from the U6 promoter using a U6-Fwd primer.

Control iPS cells (15th passage) were cultivated onto GelTrex in the presence of mTESR1 medium (STEMCELL Technologies) for two passage before transfection. For transfection by electroporation (1.05 V; 2x30 ms) was used $1x10^6$ of the cells. A 2.5 μg/ml puromycin (SigmaAldrich,) was added to the cells after 24 hours of electroporation for overnight and new feeder cells were added after 48 hours in the presence of HES medium + bFGF. Colonies of iPS cells began to form after one week. Some of these colonies were picked up from α-GALA, α-NAGA and DKO cells to 24well plates containing feeder cells and then propagated to create a stable iPS cell lines. Deficit of the enzymes was confirmed by determination of enzyme activities with synthetic fluorogenic substrates in cell homogenate.

Characterization of iPSc

Immunostaining: iPS cell colonies in 24well plate with feeder cells were fixed in 4% paraformaldehyde in PBS for 15 min at room temperature and permeabilized in 0.2% Triton-X100 in PBS for 5 min at room temperature, then blocked in 5% FBS in PBS for 1 hour at room temperature. After washing with PBS (3 x 5 min), the cells were incubated with primary antibody to Oct3/4 (mouse monoclonal, Santa Cruz), SSEA4 (mouse monoclonal, Invitrogen), Sox2 (mouse monoclonal, Sanat Cruz) and Lin-28 (rabbit polyclonal, Proteintech) at 4°C overnight. After washing with PBS (3 x 5 min), cells were labeled with Alexa Fluor 488 and Alexa Fluor 568-conjugated secondary antibodies for 1 hour at 37°C. Cells were then washed with PBS and nuclei were counterstained with DAPI in PBS for 15 min at 37°C. After final washing with PBS (2 x 5 min), specimens were analyzed using a fluorescence microscope (Nikon).

Alkaline phosphatase (ALP) staining: Cells in 24well plate with feeder cells were fixed in 4% paraformaldehyde in PBS for 2 min at room temperature. The cells were then washed with PBS (2 x 5 min) and with milliQ water (1x 5 min) and allowed to air dry for a few minutes. ALP solution (86R Phosphatase Alkaline Kit, Sigma-Aldrich) were prepared according to the manufacturer's instructions and cells were incubated with 0,5 ml of this dye solution for 15 min at room temperature in dark. After final washing with PBS (2 x 5 min), specimens were mounted with Immu-Mount (Shandon, Pittsburg, Pa.).

Loading assays and analysis of degradation products

10^7 dpm of [^{3}H] glycolipid substrates were applied per 25 cm^2 flask, feeding time was 3 days. To limit resynthesis and production of soluble radioactive products, 80 μg/ml conduritol B-epoxide was added to the cell culture medium (DMEM with 10% FBS). Harvested cells were homogenized, and lipids were extracted with chloroform-methanol (2:1; v/v) and separated on HPTLC plates (Silica gel Merck, Germany). Chromatograms were evaluated by TLC-Linear Radioactivity Analyzer (Raytest, Germany)

Acknowledgement:

This work was supported by Grant IGA MZ NT14015-3/2013 and project RVO-VFN64165 from the Ministry of Health, AZV ČR 15-33297A, project PRVOUK-P24/LF1/3 from the Ministry of Education, Grant SVV 266 504 from the Charles University in Prague, Czech Republic and Grant GA UK 56214 from the Charles University in Prague, Czech Republic

Univerzita Karlova v Praze, 1. lékařská fakulta

Kateřinská 32, Praha 2

Prohlášení zájemce o nahlédnutí do závěrečné práce absolventa studijního programu uskutečňovaného na 1. lékařské fakultě Univerzity Karlovy v Praze

Jsem si vědom/a, že závěrečná práce je autorským dílem a že informace získané nahlédnutím do zpřístupněné závěrečné práce nemohou být použity k výdělečným účelům, ani nemohou být vydávány za studijní, vědeckou nebo jinou tvůrčí činnost jiné osoby než autora.

Byl/a jsem seznámen/a se skutečností, že si mohu pořizovat výpisy, opisy nebo kopie závěrečné práce, jsem však povinen/a s nimi nakládat jako s autorským dílem a zachovávat pravidla uvedená v předchozím odstavci.

Příjmení, jméno (hůlkovým písmem)	Číslo dokladu totožnosti vypůjčitele (např. OP, cestovní pas)	Signatura závěrečné práce	Datum	Podpis